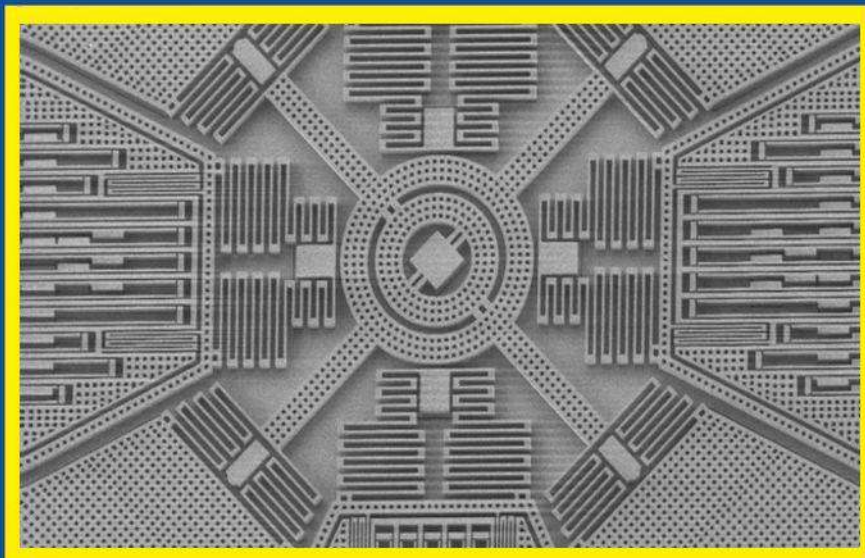




WYDAWNICTWO POLSKIEJ AKADEMII NAUK  
MONOGRAFIE KOMITETU INŻYNIERII ŚRODOWISKA

vol.181



## HIGHLY LINEAR MICROELECTRONIC SENSOR SIGNAL CONVERTERS BASED ON PUSH-PULL AMPLIFIER CIRCUITS

**Edited by Waldemar Wójcik and Sergii V. Pavlov**

W. Wójcik, S.V. Pavlov, O.D. Azarov, S. Smailova,  
R.L. Golyaka, S.V. Bohomolov, T. Ławicki, S.S. Kulenko

LUBLIN 2022

**WYDAWNICTWO POLSKIEJ AKADEMII NAUK  
KOMITET INŻYNIERII ŚRODOWISKA**

**MONOGRAFIE  
NR 181**

**HIGHLY LINEAR MICROELECTRONIC  
SENSOR SIGNAL CONVERTERS BASED  
ON PUSH-PULL AMPLIFIER CIRCUITS**

**By edited Waldemar Wojcik and Sergey V. Pavlov**

**W. Wójcik, S.V. Pavlov, O.D. Azarov, S. Smailova,  
R.L. Golyaka, S.V. Bohomolov, T. Ławicki, S.S. Kulenko**

Lublin 2022

## Wydawnictwo Polskiej Akademii Nauk 2022

© Komitet Inżynierii Środowiska PAN

ISBN 978-83-63714-80-2

### *Komitet Redakcyjny*

prof. Anna Anielak	dr hab.inż. Agnieszka Kaczmarczyk
prof. Kazimierz Banasik	dr hab. inż. Piotr Koszelnik
prof. <span style="border: 1px solid black; padding: 0 2px;">January Bień</span>	dr hab. inż. Leszek Książek
prof. Ryszard Błażejowski	prof. Hanna Obarska-Pempkowiak
prof. Michał Bodzek	prof. Małgorzata Pawłowska
dr hab. inż. Andrzej Bogdał	prof. Krzysztof Pulikowski
dr hab. Klaudia Borowiak	prof. Czesława Rosik-Dulewska
prof. Tadeusz Chmielniak	dr hab. inż. Stanisław Rybicki
dr hab. inż. Tomasz Ciesielczyk	prof. Mariusz Sojka
dr hab. Lidia Dąbek	dr hab. inż. Izabela Sówka
dr hab. inż. Wojciech Dąbrowski	prof. Kazimierz Szymański
dr hab. inż. Magdalena Gajewska	dr hab. inż. Tomasz Tymiński
dr hab. inż. Marta Gmurek – Członek AMU	prof. Józefa Wiater
prof. Marek Gromiec	prof. Mirosław Wiatkowski
dr hab. inż. Katarzyna Ignatowicz	prof. Tomasz Winnicki
prof. Krzysztof Józwiakowski	prof. Maria Włodarczyk-Makuła
prof. Katarzyna Juda-Rezler	dr hab.inż. Ewa Wojciechowska
prof. Radosław Juszcak	prof. Irena Wojnowska-Baryła
dr hab. inż. Tomasz Kałuża	

### *Redaktor Naczelny*

Prof. dr hab. Lucjan Pawłowski

### *Recenzent wydawniczy*

Dr hab. inż. Konrad Gromaszek

Dr hab. inż. Roman Kvyetnyy

© Copyright Komitet Inżynierii Środowiska PAN

### *Zdjęcie na okładce*

Materiały PSEW

### *Skład i łamanie*

Tomasz Ławicki

**Abstract:** Monograph considers scientific problems dealing with the development of the integral signal converters for microelectronic sensors of biomedical designation, in particular, in the devices, intended for measurement of the parameters of the respiratory system, biochemical analysis, technological processes in pharmacology, etc. New approaches to their electrothermal modeling are proposed, a number of signal converters of flow thermal sensors, based on newest microelectronic element base are suggested. Monograph is intended for the specialists working in the sphere of microelectronics, it also can be useful for the students and postgraduates of the corresponding fields of study.

**Streszczenie:** Monografia rozpatruje problemy naukowe związane z rozwojem integralnych konwerterów sygnałów dla mikroelektronicznych czujników o przeznaczeniu biomedycznym, w szczególności w urządzeniach przeznaczonych do pomiaru parametrów układu oddechowego, analizy biochemicznej, procesów technologicznych w farmakologii itp. Zaproponowano nowe podejście do ich modelowania elektrotermicznego, zaproponowano szereg konwerterów sygnału przepływowych czujników termicznych, opartych na najnowszej bazie elementów mikroelektronicznych. Monografia jest przeznaczona dla specjalistów zajmujących się mikroelektroniką, może być również przydatna dla studentów i doktorantów odpowiednich kierunków studiów.

## CONTENT

1. Analysis and substantiation of the problem, dealing with the development of high linear converters of the thermal flow sensors of general and biomedical designation .....	9
1.1. Analysis of the state – of-art of the development of the thermal flow sensors of general and biomedical designation .....	9
1.2. Characteristic features of the thermal calculation of the thermal flow sensors of general and biomedical designation .....	24
1.3. Trends of development of the integral signal converters of the sensor devices .....	33
1.4. Analysis of the integral signal transducers of the microelectronic thermal flow sensors of general and biomedical designation .....	35
1.5. Characteristics of the temperature distribution in biomedical objects ....	46
2. Analysis of the existing methods of the construction of the highlinear analog devices for signal converters .....	50
2.1. Survey of the methods of the construction of the analog converting devices for multiple – digit systems of measurement, registration and processing of signals.....	50
2.2. Analysis of the static and dynamic errors of the analog devices in the converting paths of the analog-to-digital systems .....	68
2.3. Circuit organization and the errors of the existing push-pull current amplifiers .....	74
2.3.1. Push-pull current amplifiers with the parametric setting of the working points .....	74
2.3.2. Push-pull current amplifiers with the autobalancing of the working points .....	79
2.4. Push pull buffer voltage devices .....	82
3. Development of mathematical models and electric thermal modeling of the measuring primary circuits of the thermal flow sensors converters...85	
3.1. Mathematical model of the integral structure thermal field.....	85
3.2. Electrothermal modeling of measuring converters in pulse operation modes.....	94
3.3. Electric thermal modeling of temperature-dependent volt-ampere characteristics of the resistive converters .....	106
3.4. Electric thermal modeling of the temperature-dependent VAC of the diode-type converters .....	120
3.5. Electric thermal modeling of temperature-dependent VAC of the transistor-type converters .....	125

4. Mathematical models of static and dynamic characteristics of the input transistor stages of the push-pull dc amplifiers.....	132
4.1. Static transfer characteristics of the input stages of the push-pull dc amplifiers .....	132
4.2. Determination and minimization of the static errors of the push-pull direct currents amplifiers input stages .....	140
4.2.1. Compensation of the zero shift.....	140
4.2.2. Definition and minimization of the non-linearity of the transfer characteristic.....	142
4.3. Nonlinear distortions of the transfer characteristic of the input stages in the frequency zone .....	146
4.4. Models of AFC and PFC of the input stages .....	154
5. Methods of circuit-functional organization of the highlinear analog devices on the base of the push-pull structures.....	165
5.1. Methods of circuit organization of the highlinear buffer devices on the base of the push-pull structures .....	165
5.1.1. Circuit organization and models of the transfer characteristics of the cores of the push-pull buffer devices .....	165
5.1.2. Methods of linearity error decrease, zero shift and loading capacity increase of the buffer devices.....	172
5.2. Methods of circuit organization of current-voltage and voltage voltage-current converters, based on push-pull current amplifiers.....	178
5.3. Minimization of the linearity errors and zero shift of current-voltage and voltage-voltage converters.....	187
6. Circuit engineering realization of signal converters of the thermal sensors and high-linear analog devices of biomedical designation.....	191
6.1. Recommendations regarding the construction of temperature mode controllers .....	191
6.2. Circuit engineering realization of the differential thermometer .....	216
6.3. Practical realization of the signal converters of the thermal flow sensors of the biomedical designation .....	223
6.4. Circuit functional organization of the push-pull d.c. amplifiers, characteristics of which correspond to system requirements.....	235
6.5. High-linear current-voltage and voltage-voltage converters with the parametric correction of the zero-shift .....	239
6.6. High linear fast acting buffer voltage devices with push-pull organization .....	244
6.7. Amplifier of the difference currents for high sensitive comparators ....	247
7. References.....	250

## LIST OF ABBREVIATIONS

A/D	–	analog-digital;
ACU	–	autocorrection unit;
ADC	–	analog-digital converter;
AFC	–	amplitude-frequency characteristic;
APS	–	amplifier phase splitter;
AS	–	analog switch;
ASTP	–	analyzer of the sound tracks parameters;
BCM	–	bidirectional current mirror;
BI	–	biomedical information;
CC	–	current compensator;
CC	–	current conveyor;
CCC	–	code-current converter;
CCG	–	controlled current generator;
CM	–	current mirror;
CVC	–	current-voltage converter;
DA	–	digital-analog;
DAC	–	digital-analog converter;
DCA	–	direct current amplifier;
FB	–	feedback;
FBC	–	feedback channel;
FS	–	flow sensor;
IAS	–	intermediate amplifying stage;
IFC	–	information form converter;
IMS	–	information-measuring system;
IPPS	–	input push-pull stage;
MC	–	measuring converter;
NLDC	–	nonlinear distortions coefficient;
OA	–	operation amplifier;
PFC	–	phase-frequency characteristic;
PPDCA	–	push-pull direct current amplifier;
PPOS	–	push-pull output stage;
TA	–	thermoanemometer;
VB	–	voltage buffer;
VCU	–	voltage shift unit;
VVC	–	voltage-voltage converter.

## INTRODUCTION

The development of modern diagnostic devices of biomedical designation is characterized by the rapid widening of physical methods of measuring transformation of functional possibilities, improvement of technical characteristics, wide introduction of microelectronic technologies and microprocessor engineering. These trends are vividly manifested in one of the most important classes of diagnostic equipment – devices for measurement of gasses and fluids flow speed (flow sensors), used for measurement of the respiratory system parameters (in particular, in case of asthmatic diseases), artificial respiration systems, means of biochemical analysis. Besides, flow sensors find wide application in the technological processes of pharmacology and devices used for ecological monitoring.

From the point of view of biochemical compatibility of the materials, high operation reliability, minimal impact on the parameters of the studied flow and the possibility to measure both small and large flows of fluids and gasses thermal flow sensor (hot-wire anemometer) – devices, measuring ability of which is based on the determination of the temperature field in locally heated substance of the flow have the priority in biomedical equipment [1,2,139].

Great contribution in the development of the signal converters of thermal flow sensors of the general and biomedical designation was made, first of all, by the prominent scientists of the well-known domestic and foreign schools: O. D. Azarov, Z. Yu. Gotra, R. L. Golyaka, V. S. Gutnikov as well as Allen B. Holmes, Richard Miller, David W. Spitzer, N. T. Nguyen, D. Lee and others.

The importance of the development of new generation of the integrated signal converters for microelectronic thermal flow sensors is stipulated by several factors. First, structural-circuit solutions, used in the conventional signal converters, in particular, for measuring circuits of thermal resistive type, do not meet the requirements regarding the minimization of energy consumption of microelectronic thermal flow sensors. Secondly, with the transition to low voltage energy supply sources, the minimization of the parasitic impact on the result of the measurement of signal transmission lines resistances becomes very important. Thirdly, in the process of the development of the sensor devices for the flow measurement all the requirements regarding their compliance with modern directions of microelectronic sensors development, in particular, interface compatibility, possibility of program control of the measuring process, enhanced functional possibilities, compliance with the standard for the intelligent sensors IEEE1451.2, compliance with the requirements to the equipment of biomedical designations, etc, must be taken into account.



That is why, the realization of the approaches on the modern element base, obtained in the research, in particular, integrated high precision CMOS rail-to-rail operation amplifiers, bidirectional multiplexers of ADG type, microconverters of ADuC type, powerful D-MOS HEX FET transistors, etc., is of paramount importance. Thus, the problems of development of modern integrated high linear converters of microelectronic thermal flow sensors and construction of high linear analog devices on the base of push-pull structures is beyond the limits of the engineering practices and requires new approaches and studies.

We shall be grateful for all critical remarks and wishes concerning further development of the studies.

# 1. Analysis and substantiation of the problem, dealing with the development of high linear converters of the thermal flow sensors of general and biomedical designation

## 1.1. Analysis of the state – of-art of the development of the thermal flow sensors of general and biomedical designation

Thermal flow sensor is a device for measurement of liquid or gas flow rate, based on the principle of measurement of the temperature field of the locally heated substance of the flow [40-43].

Several basic methods of signal formation, stipulated by the flow rate are distinguished. In the simplest method the temperature of the heater, located in the flow is measured – the temperature of the heater decreases with the increase of the flow rate, as a result of heat exchange. More progressive methods imply the local heating of the flow environment and measurement of the temperature difference in the flow in the areas prior to (S1) and after (S2) the heater in the direction of the flow propagation (Fig. 1.1). This enables, first, to measure not only the flow rate but also its direction and, secondly, minimize the impact of the temperature of the flow substance on the result of the measurement.

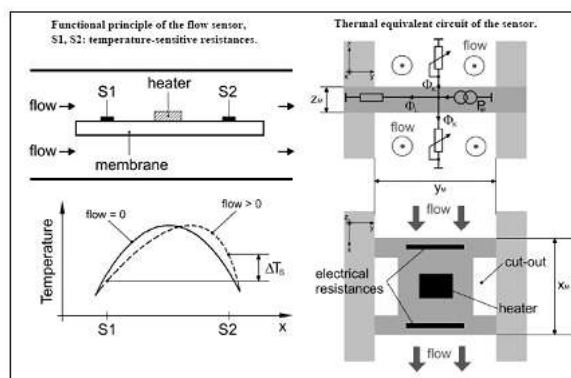


Fig. 1.1. Structure and the functional principle of microelectronic thermal flow sensors operation

Static and dynamic (Thermal Time-of-Flight Mode Transducers) information signal formation circuits, in particular, as it is shown on the example of

biomedical thermal flow sensor with integrated signal converter, are distinguished (Fig. 1.2) [44-47].

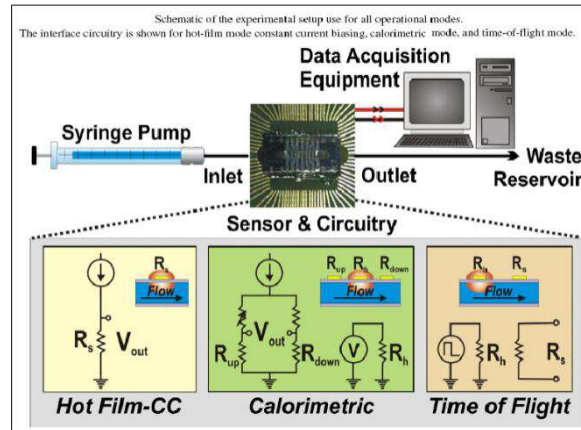


Fig. 1.2. Principles of signal formation in thermal flow sensors

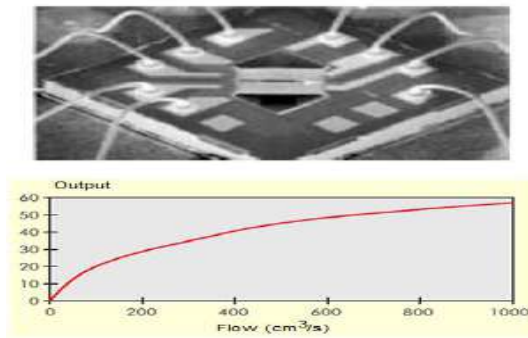
If it is necessary to measure the large volumes of flows in the main line of a large diameter, the bypass pipe of small diameter (connected in parallel to the main) is formed in it, the flow in this bypass pipe is proportional to the flow in the main line. Measuring the flow rate only in the bypass pipe and approximating the obtained result of the measurement by the flow rate in the main line, the reduction of energy losses for flow heating is achieved and the temperature impact of thermal flowmeter on the flow on the whole.

In various functional-structural realizations of the thermal flow sensors their sensors of the temperature difference are combined with the heaters. In such a case, a flow sensor consists of two functionally integrated elements, each of them is heated and, characterized by the known value of the temperature resistance coefficient, provides the possibility of temperature signal formation.

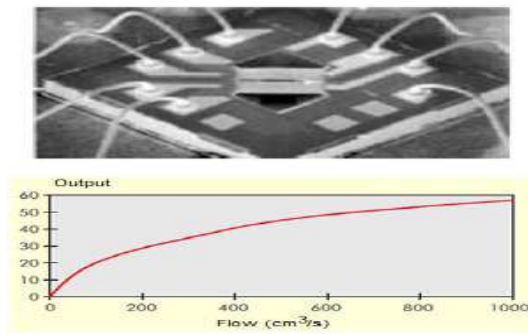
The temperature of the first in the direction of the propagation flow of the functionally integrated element is smaller relative to the second, similar to the dimensions and heating energy element that is stipulated by the heat transfer between these elements of the flow medium. The example of the realization of the microelectronic flow sensor, based on the functionally integrated elements of the thermoresistive type, in particular, model AWP 2100 V – of the world leader in the field of microelectronic sensor electronics, Honeywell company, is shown in Fig. 1.3 [48].

Membrane structure of the sensor, that provides minimal value of heat transfer between functionally integrated elements and the chip of the integrated circuit, is formed by the technology of the silicon MEMS (Micro-Electromechanical – Systems) structures. The dimensions of the flow sensor,

based on MEMS structure, typically do not exceed several millimeters whereas the dimensions of the sensing elements (in particular, functionally integrated elements) are of the order 100 microns. Important role in thermal flow sensors Heating mode and mutual location of temperature difference sensors relative to the heater play an important role in thermal flow sensors, this is discussed in [49].



a)



b)

Fig. 1.3. Microelectronic MEMS structure of: a) thermal flow sensor; b) typical characteristics

New direction in the development of thermal flow sensors is presented by the multiband MEMS flow sensor, based on the matrix of functionally integrated elements [50]. The construction of such a sensor is shown in Fig. 1.4., distribution of the temperature in the elements is shown in Fig. 1.5 and its exterior view – in Fig. 1.6.

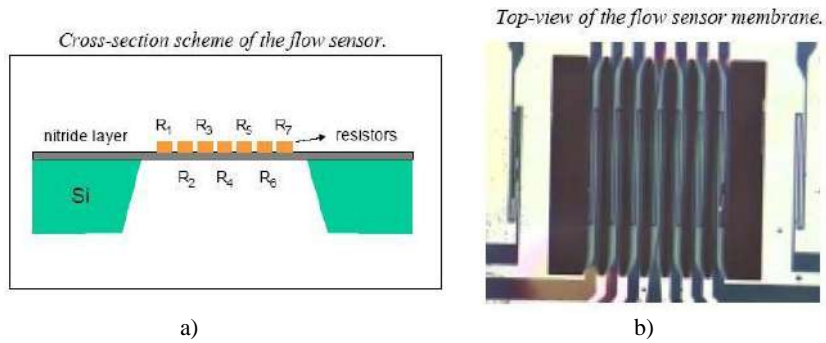


Fig. 1.4. Construction of the thermal matrix MEMS flow sensor: a) cross-section scheme; b) photograph

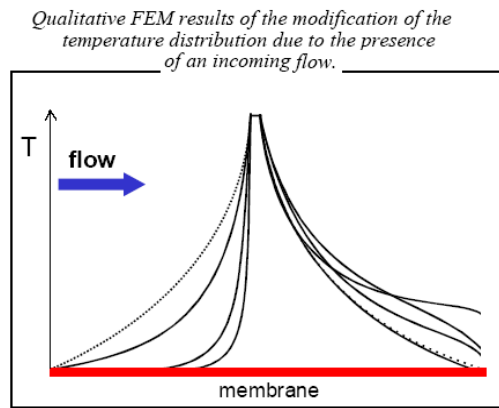


Fig. 1.5. Temperature distribution in the thermal matrix flow sensor

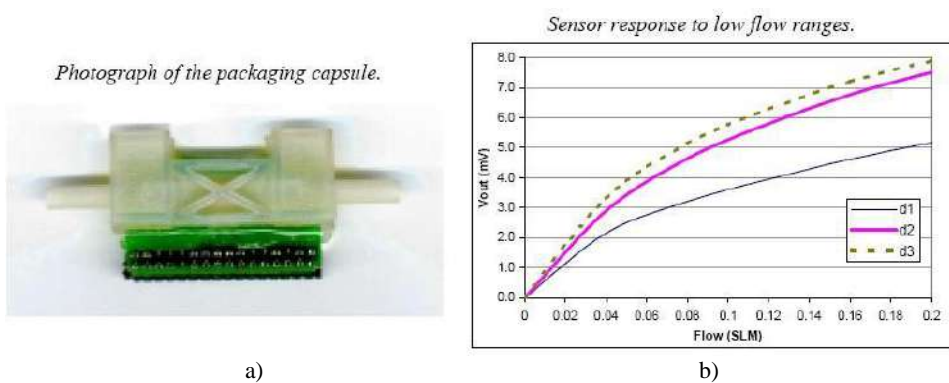


Fig. 1.6. Thermal matrix flow sensor: a) photograph; b) example of the functional characteristics

Construction, principle of signal formation and functional characteristics of matrix flow sensors, based on thermal-time-of-flight mode are shown in Fig. 1.7, 1.8, correspondingly [51]. Such method provides further decrease of energy consumption and the possibility of microprocessors signal conversion without the usage of the analog-to-digital converters.

Greater part of the thermal flow sensors, considered above, did not get industrial introduction – the given publications demonstrate only the realization of the laboratory prototypes. That is why, to give a more comprehensive vision of the state of art of thermal flow sensors development, we will suggest several examples of the mass production and commercially available devices of such type. They are, in particular, thermal flow sensors, manufactured by the company ELDRIGE PRODUCTS Inc. (Fig. 1.5), hot-wire anemometers A-477 (Fig. 1.10), Testo 405 (Fig. 1.11) and Testo 425 (Fig. 1.12), presented at the market of Ukraine by the Association " Industry-Ukraine" [52, 53]. Sphere of the application – monitoring of the labor conditions in industry, ecology, etc.

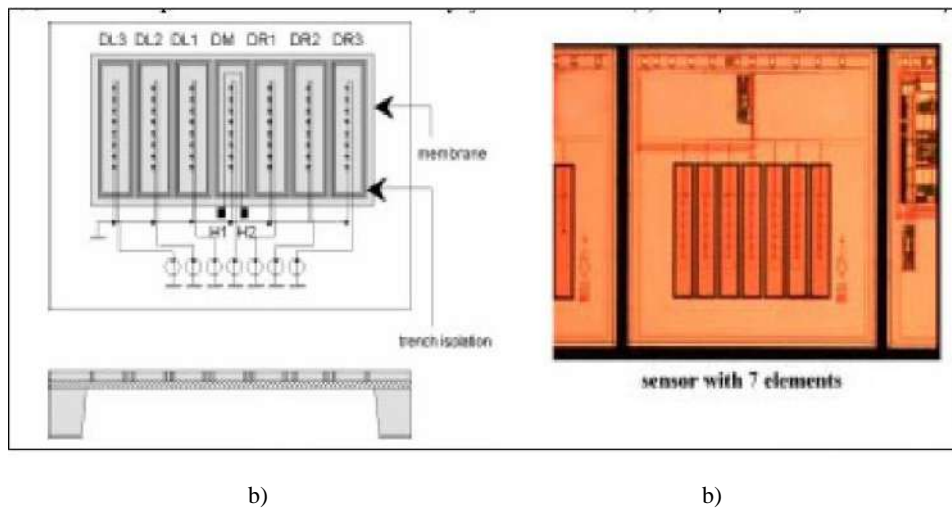


Fig. 1.7. Matrix thermal Time-of-flight mode flow sensor: a) construction; b) exterior view

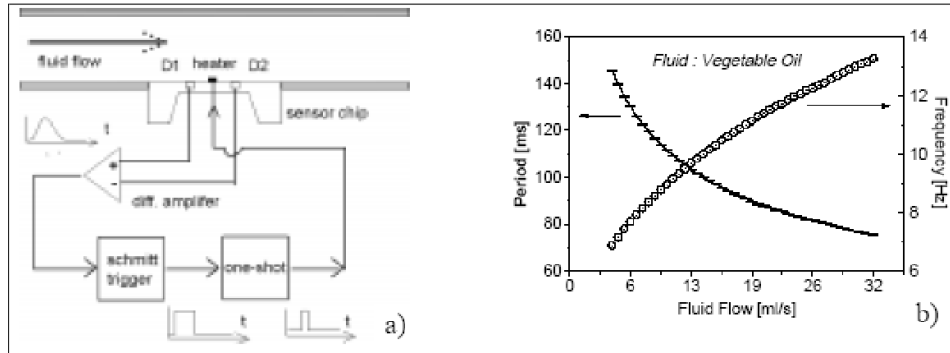


Fig. 1.8. Matrix Thermal-Time-of-Flight Mode flow sensor: a) functional scheme of signal formation; b) characteristics of the conversion

We will consider thermal flow sensors, developed for biomedical application. The required information can be found at numerous information resources, they describe, in particular, characteristic features of the devices of biomedical designation, scientific research, devoted to the development of the flow sensor for biomedical application, carried out in Bio-MEMS & Microsystems Laboratories of University of South Florida (Fig. 1.13) [54] and State of Utah Center of Excellence for Biomedical Microfluidics (Fig. 1.14) [55].


Figure 1.9 is a collage of various flow meters and sensors. Below the collage is a detailed advertisement for Eldridge Products, Inc. The advertisement includes the company name, logo, and text describing their thermal gas mass flow measurement and control instrumentation. The text reads: "ELDRIDGE PRODUCTS INC - Thermal Gas Mass Flow Measurement and Control Instrumentation". "Eldridge Products Inc - Abbreviated as EPI, has more than 20 years experience in the design and production of thermal mass flow meters and flow switches." "The Eldridge Master-Touch flowmeters include microprocessor technology and remains at the forefront of thermal gas mass flow instrumentation." "Eldridge manufactures a range of in-line and insertion style thermal mass flow meters with integral and remote electronics options. Single point and multipoint units as well as the new Thermal Flow Averaging tube is unique to Eldridge Products Inc." The advertisement also features an image of a flow meter installation in a pipe.

Fig. 1.9. Information materials of the Company ELDRIDGE PRODUCTS Inc

## А-471 Цифровой термо-анемометр

### А-471 Цифровой термо-анемометр

**Четыре выбираемых при эксплуатации диапазона от 500 до 15000 футов/мин**



Цифровые термо-анемометры серии 471 представляют собой универсальные приборы с двумя функциями, которые быстро и легко определяют скорость воздушного потока, либо в футах в минуту, либо метрах в секунду, а также температуру воздуха в F или C. Высококонтрастный ЖК дисплей показывает, как выбранный диапазон, так и текущую скорость.

В условиях плохой освещенности хорошая видимость обеспечивается достаточной задней подсветкой. Для экономии батареи через 2-1/2 минуты подсветка автоматически выключается. Есть предупреждения о низкой емкости батареи. В модели 471 на зонде из нержавеющей стали с удобной ручкой выгравирована маркировка глубины погружения для 0-8 дюймов и 0-20 см. В полностью

#### Модели

Номер диапазона	Скорость, футов/мин (FPM)	Скорость, м/сек (MPS)	Точность
1	0-800	0-3,0	±3% F.S.
2	0-1500	0-7,0	±3% F.S.
3	0-5000	0-30	±4% F.S.
4	0-15000	0-75	±5% F.S.

Номера модели

Модель 471-1

Модель 471-2

Модель 471-3

Цифровой термо-анемометр включает батарею, антистатический браслет, 8-ступенчатое сверло, сумку для переноски и инструкции.

Цифровой термо-анемометр с телескопическим зондом включает батарею, антистатический браслет, 8-ступенчатое сверло, сумку для переноски и инструкции.

Цифровой термо-анемометр с телескопическим зондом и наконечником включает батарею, антистатический браслет, 8-ступенчатое сверло, сумку для переноски и инструкции.

Fig. 1.10. Brief characteristics of the hot-wire anemometer A-471

### Компактный термоанемометр testo 405 с поворотной головкой

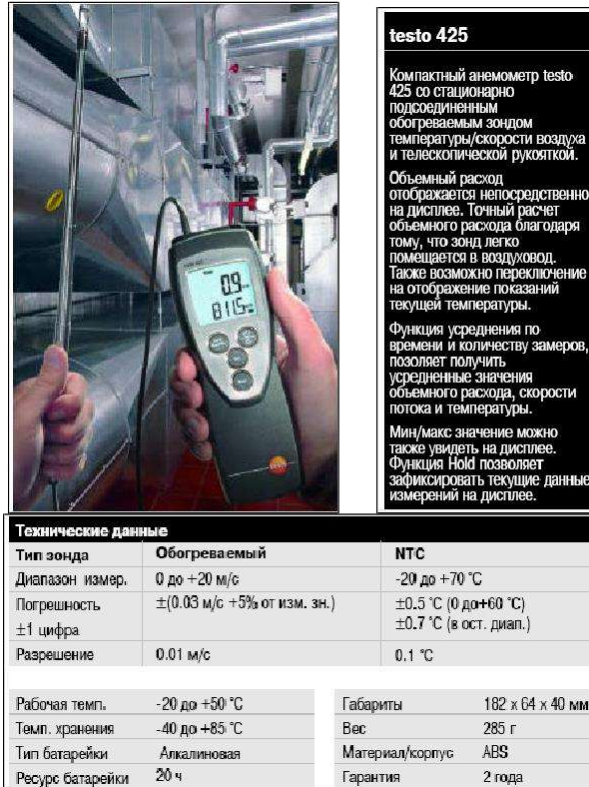


- Дисплей на гибком шарнире с фиксатором.
- Точные "профессиональные сенсоры" впервые применяемые в недорогих приборах Стик-Класса.
- Управление при помощи одной кнопки.
- Большой и удобный для считывания данных дисплей.
- Встроенный колпачок для защиты датчиков влажности и скорости.
- Пользователь может легко заменить батарейки.
- Многофункциональный держатель (только для Стиков м/с, % ОВ и °C).
- Фиксатор для газосходов (только для Стиков % ОВ и м/с).

<b>Диапазон изм.:</b>	0...5 м/с при -20...0 °C 0...10 м/с при 0...+50 °C 0...99990 м³/ч -20...+50 °C
<b>Разрешение:</b>	±0,01 м/с / ±0,1 °C
<b>Погрешность:</b>	±5 % от изм. знач. ±0,10 м/с (до 2 м/с) ±0,30 м/с (свыше 2 м/с) ± 0,5 °C
<b>Рабочая темп.:</b>	0...+50 °C
<b>Темп. хранения:</b>	-20...+70 °C
<b>Тип батарейки:</b>	3 шт. размер AAA
<b>Ресурс батарейки:</b>	Около 25 ч.
<b>Зонд:</b>	Ø 12/16 мм, Длина: около 300 мм
<b>Самоотключение:</b>	Через 5 мин.
<b>Гарантия:</b>	1 год

Fig. 1.11. Brief information about the hot-wire anemometer Testo 405





**testo 425**

Компактный анемометр testo 425 со стационарно подсоединенным обогреваемым зондом температуры/скорости воздуха и телескопической ручкой.

Объемный расход отображается непосредственно на дисплее. Точный расчет объемного расхода благодаря тому, что зонд легко помещается в воздуховод. Также возможно переключение на отображение показаний текущей температуры.

Функция усреднения по времени и количеству замеров, позволяет получить усредненные значения объемного расхода, скорости потока и температуры.

Мин/макс значение можно также увидеть на дисплее. Функция Hold позволяет зафиксировать текущие данные измерений на дисплее.

Технические данные		
Тип зонда	Обогреваемый	NTC
Диапазон измер.	0 до +20 м/с	-20 до +70 °C
Погрешность	±(0.03 м/с +5% от изм. зн.)	±0.5 °C (0 до+60 °C)
±1 цифра		±0.7 °C (в ост. диап.)
Разрешение	0.01 м/с	0.1 °C
Рабочая темп.	-20 до +50 °C	Габариты
Темп. хранения	-40 до +85 °C	182 x 64 x 40 мм
Тип батарейки	Алкалиновая	Вес
Ресурс батарейки	20 ч	285 г
		Материал/корпус
		ABS
		Гарантия
		2 года


Fig. 1.12. Brief information about the hot-wire anemometer Testo 425

Main requirements to the flow sensors of biomedical designation are the following: biomedical compatibility of the materials and the ability to measure small values of the velocity (mass transfer) of the studied fluid or gas flow.

If these sensors are used for studying the parameters of the respiration system the main requirement is minimal inertia and ergonomic indices. Sensors for biomedical in-situ studies must be characterized by minimal dimensions and energy consumption.

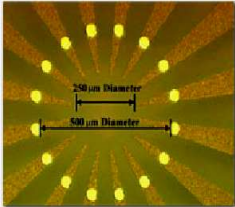
In particular, Fig. 1.15 shows the construction and functional characteristics of microelectronic flow sensors of biomedical designation [47]. The sensor is manufactured in the base of LTCC (Low Temperature Coffered Ceramics) using the elements of thick-film technology, that provides biomedical compatibility with the investigated fluids.

**BIO-MEMS & MICROSYSTEMS**      **BIG IDEAS | SMALL DEVICES**      **USF** UNIVERSITY OF SOUTH FLORIDA COLLEGE OF ENGINEERING



*Welcome to the  
Bio-MEMS & Microsystems Laboratory*

**Bio-Sensors and Micro-fluidics**



The research objectives of this proposal are: (a) Development of novel MEMS sensors and techniques to reliably and repeatedly image individual cells/organisms using bio-impedance measurements, (b) Integration of micro fluidic sensors into flow-through system to develop a generic identification technique and (c) Understand and analyze the challenges in signal processing enabling differential detection. Research outcomes of this proposal would facilitate the fundamental understanding and optimizing of the science and technology of bio-impedance at a micro scale. The research will establish the fundamental science required to enable the development of a single generic sensor that would be capable to identify cells based on their bio-impedance maps.

Fig. 1.13. Information resource Bio-MEMS & Microsystems Laboratory of University of South Florida

Address <http://www.memc.utah.edu/>      Go      Un

**U** **State of Utah Center of Excellence for Biomedical Microfluidics** **U**

Home      Research      Publications      Personnel      Education

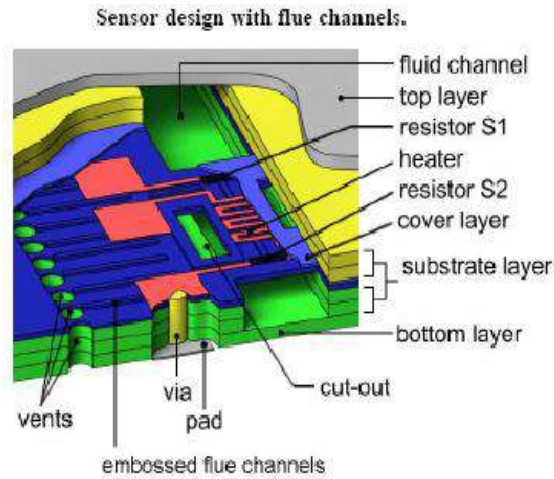
Research: [Our Mission](#)   [Research Profile](#)   [Fabrication Capabilities](#)   [Collaboration](#)   [Director Info](#)   [Contact](#)  
 Publications: [Info](#)  
 Personnel:  
 Education:  
 Foundry Services:

**Welcome**

Welcome to the Home Page for the [State of Utah Center of Excellence](#) for Biomedical Microfluidics at the [University of Utah](#). The Center is dedicated to the discovery, understanding, development and commercialization of microscale and MEMS devices for application to biological, biomedical, and medical problems. Work in this field is sometimes referred to as BioMEMS. The Center is directed by [Bruce Gale](#), an associate professor in the [Department of Mechanical Engineering](#). Typically about 15-20 graduate and undergraduate students are employed in the Center.



Fig. 1.14. Information resource of State of Excellence for Biomedical Microfluidics



**Sensor characteristics as a function of the applied flow for water: resistance difference S1 –S2**

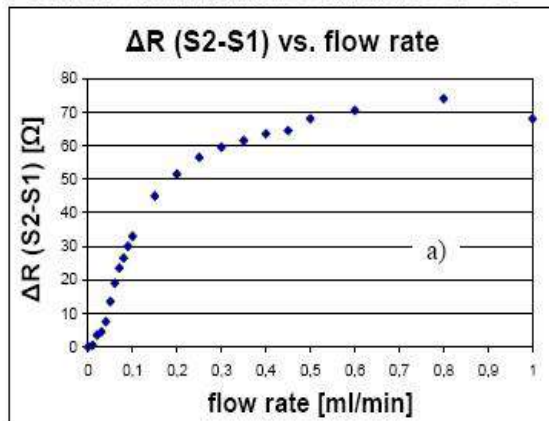


Fig. 1.15. LTCC – based microelectronic flow sensor of biomedical designation: a) construction; b) functional characteristics

Another typical example of the flow sensor of biomedical designation is the microelectronic module of the base of biocompatible MEMS matrix [46]. Matrix of the sensor is realized on the base of biocompatible Parylene C Membrane with platinum sensor electrodes. In order to improve the heat insulation of the thermal flow sensor its membrane is "suspended" above the beamed micromechanical channel made of silicon. Principle of the functioning and the design of the sensor are shown in Fig. 1.16, succession of its structure formation – in Fig. 1.17, exterior view – in Fig. 1.18. Wide range of functional

characteristics of the given flow sensor in various operation modes can be seen in Figs. 1.19 – 1.22.

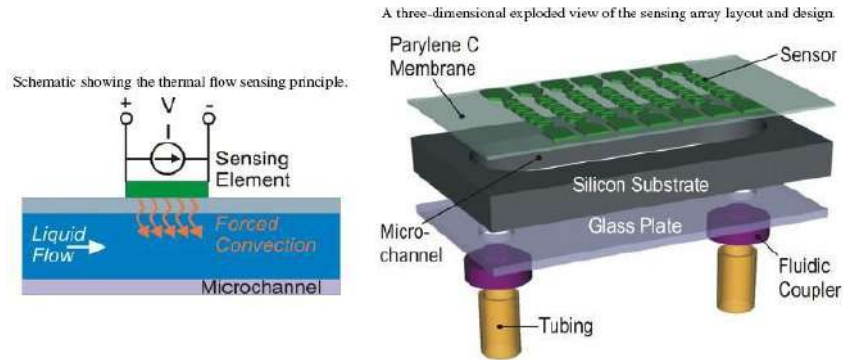


Fig. 1.16. Microelectronic flow sensor of biomedical designation on the base of Parylene C membrane [46]: a) functional principle; b) design

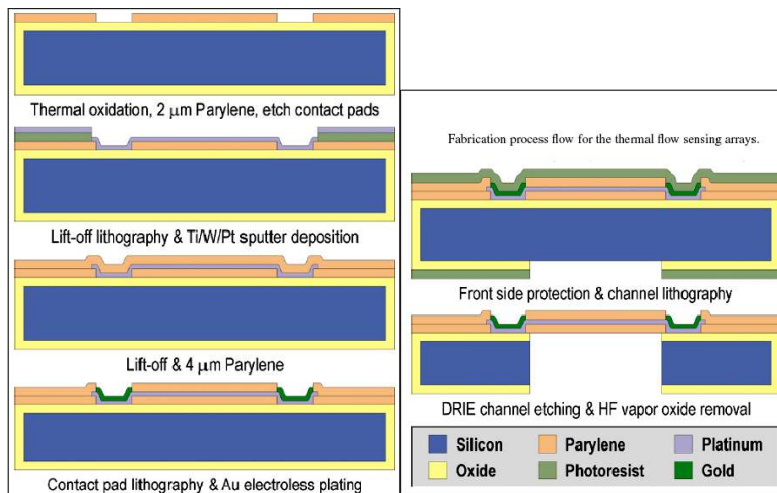


Fig. 1.17. Succession of flow sensor structure formation [46]

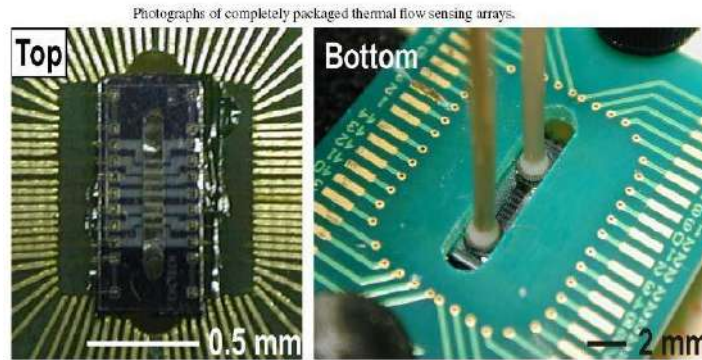


Fig. 1.18. Exterior view of the flow sensor [46]

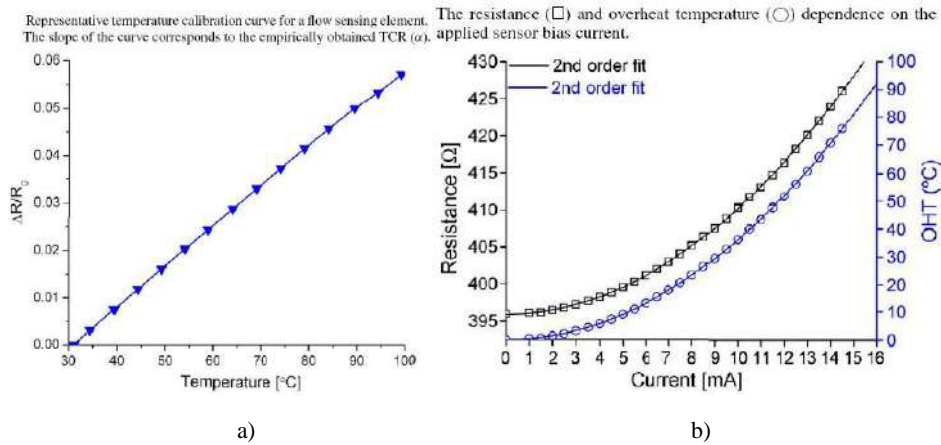
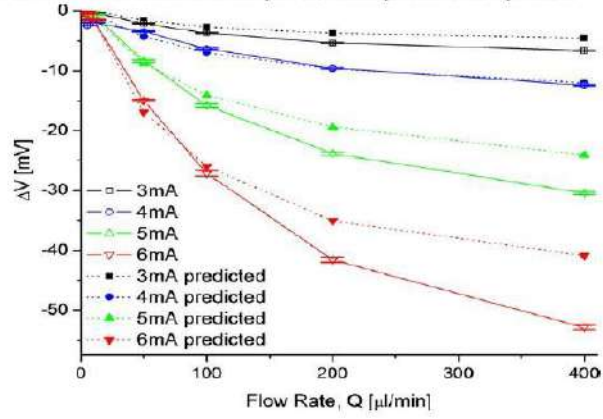


Fig. 1.19. Characteristics of the thermoresistive elements of the flow sensor [46]: a) temperature; b) current

Analysis of the characteristics of the considered sensors enables us to make a number of important conclusions.

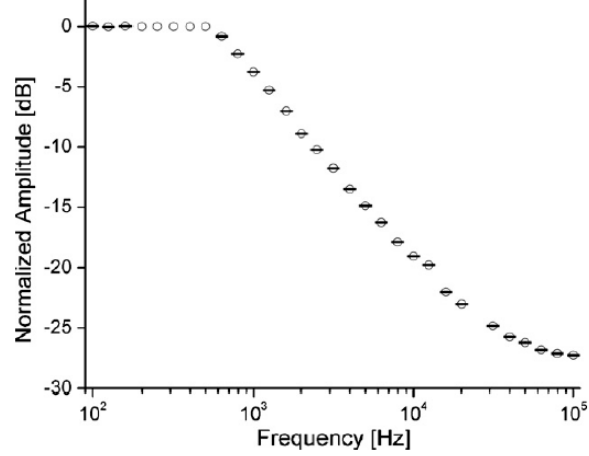
First, modern microelectronic flow sensors, in particular, sensors of biomedical designation, are characterized by a great variety of signal formation principles – from the elementary linear converters, based on one sensitive element to non-linear (generation, time-dependent) converters, based on the matrices of the functionally integrated elements. Realization of these principles puts forward the problem of the development of the corresponding signal converters that meet the requirements of modern microelectronics.

Response of three sensors connected in series for constant current biasing and hot-film mode operation at four different overheat ratios and over the flow rate range of 0–400  $\mu\text{L}/\text{min}$  (mean  $\pm$  S.E. with  $n = 60$ ). The predicted response, or sum of the individual sensor responses, is also plotted for comparison.



a)

Frequency response for constant current biasing with a sinusoidal input (mean  $\pm$  S.E. with  $n = 4$ ). The cutoff frequency is 890 Hz and after which the output drops off at 15 dB/decade.



b)

Fig. 1.20. Characteristics of the thermoresistive elements of the flow sensor [46]: a) functional; b) frequency

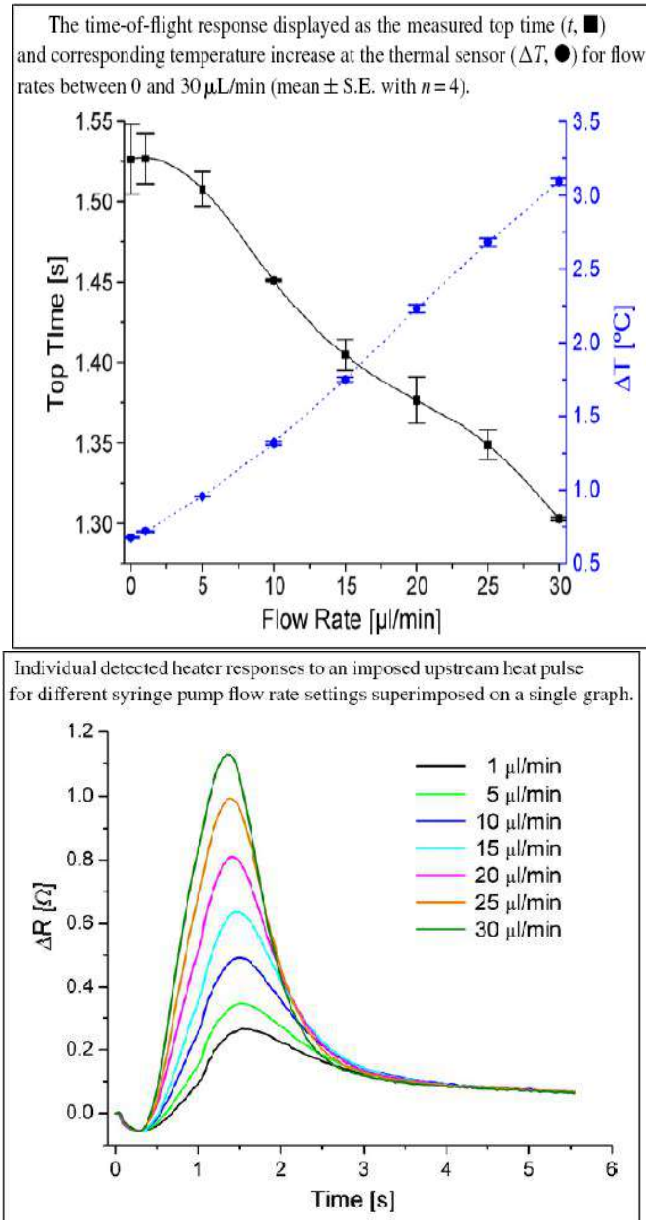


Fig. 1.21. Temporal functional characteristics of the flow sensor [46]

Secondly, the expansion of the range of flow rates measurement causes certain problems – the characteristics of the sensor's conversion which enable it to measure small flows becomes non-linear at the increase of the flow rate. At

certain critical values of the velocity the extremum of the transformation function is observed, it makes impossible the measurement of both small and great velocities. The solution of this problem requires the corresponding control over the thermal power of the sensor heaters and a number of other circuit engineering solutions. Thirdly, the problem of energy supply of thermal flow sensors remains actual. It is especially typical for the supply of the sensors of biomedical designation from autonomous, small-size low power, low voltage electric chemical elements. The heating of the flow substances as compared with the energy supply of modern micro power CMUS of the integrated circuits requires greater energy. Besides, with the decrease of the supply voltage (for the small-size, self-contained supply sources it is typically not more than 3V), it is necessary to decrease the resistance of the heating elements. Applying functionally integrated elements used both for heating and the measurement of the temperature, the decrease of the resistance (as a rule, to the values of less than 100 ohm) leads to parasitic impact on the result of signal lines measurement. Thus, the decrease of energy consumption (power and heating temperature) leads to the advent of the parasitic impact of signal lines resistances and, as a result, to worsening of the functional characteristics, in particular, decrease of the accuracy of flow rate measurement.

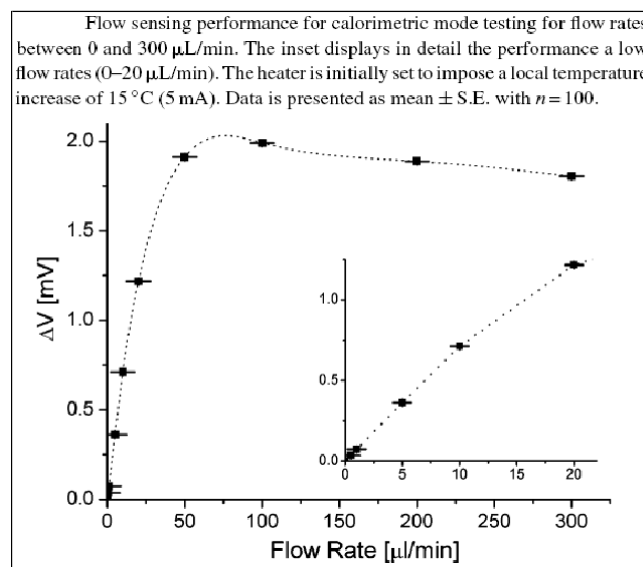


Fig. 1.22. Functional flow sensor performance for high and low flow rates [46]

The solution of these problems, along with other problems, which will be mentioned below, became the main aim of the given study.



## 1.2. Characteristic features of the thermal calculation of the thermal flow sensors of general and biomedical designation

In general case the dependence between the temperature parameters of the thermoanemometer primary transducer and flow parameters can be written in the form of Newton-Richmann equation [1-5]:

$$P_H = K_1 \cdot \alpha \cdot F \cdot \Delta t, \quad (1.1)$$

where  $K_1$  – is the coefficient, which is introduced, as in greater part of cases not the difference of temperatures of the heat exchange surface and fluid that is measured but another value  $\Delta t$ ;  $\alpha$  – is the heat transfer coefficient;  $F$  – is heat exchange surface;  $\Delta t$ - is temperatures difference.

In general form the heat transfer coefficient is determined by the criterial dependence:

$$N_u = A \cdot Re^n \cdot Pr^b \cdot Gr^b \left( \frac{Pr_c}{Pr_c} \right)^d, \quad (1.2)$$

where  $Nu$ - is Nusselt criterion, it characterizes the heat exchange between the surface of the wall and the fluid (gas);  $Re$  – is Reynolds criterion, it characterizes the relation of inertial forces and viscosity and determines the character of fluid (gas) flow;  $Pr$  – is Prandtl number, it characterizes the physical properties of the fluid (gas);  $Gr$  – is Grashof number, it characterizes the lifting force, occurring in the fluid (gas) as a result of densities difference.

Prandtl similarity criterion  $Pr$ - is purely physical parameter; it characterizes the property of the flow. Grashof number  $Gr$  also does not contain the velocities of the flow and only characterizes the interaction of the molecular friction and lifting force, stipulated by the densities difference in separate points of the flow due to its non-isothermality. Only Reynolds criterion  $Re$  contains the velocity of the flow we are interested in that is why, in general case, the connection (1.2) between the Nusselt criterion  $Nu$ , that contains heat transfer coefficient and Reynolds criterion, that contains the velocity of the flow  $v$ , can be written in the form:

$$N_u = C \cdot Re^n, \quad (1.3)$$

where  $C$  – is specific heat of the measuring environment; or:

$$\frac{\alpha \cdot d}{\lambda} = C \cdot \left( \frac{v \cdot d \cdot p}{\mu} \right)^n, \quad (1.4)$$

it follows:

$$\alpha = C \cdot \frac{\lambda \cdot d^{n-1} \cdot \rho^n}{\mu^n} = C \cdot \frac{\lambda \cdot d^{n-1}}{\mu^n} \cdot G_m^n, \quad (1.5)$$

where  $d$  - is the diameter of the pipe, where the flow rate is measured;  $v$  - is the flow rate;  $p$ ,  $\mu$  - are density, viscosity, thermal conductivity of the measuring environment, correspondingly,  $G_m$  - is mass rate.

Taking into account the equation (1.5) and combining all the values, characterizing the properties of the flow and the construction of the primary converter, instead of the equation (1.1), the equation for the flow meters of the thermal layer and thermoanemometric flow meters can be written in the form:

$$P_H = K \cdot G_m^n \cdot \Delta t, \quad (1.6)$$

For the calorimetric flow meters, where the information value is the amount of heat, taken by the flow, if the thermal losses are not present and thermal physical properties of the flow are constant, the heat balance equation for the unit of the cross-section area is valid:

$$P_H = G_m \cdot c_p \cdot \Delta t, \quad (1.7)$$

where  $c_p$  - is the isobaric specific heat of the flow;  $\Delta t$  - is the temperature difference before and after the heater.

The process of the temperature field change can be presented by two components:

heat take-off from the heater by the flow without violating the symmetry of primary temperature field;

temperature increases on the surface of the wall in the direction of the flow motion.

The result of the first component of the process is temperature decrease in all the points of the field, the result of the second - is a certain temperature increase in all the points, according to the linear law in the direction of the flow. Temperature field, created by the heater on the surface, if the flow is missing, is one-dimensional; the temperature changes only along the axis:  $t=f(x)$ .

Temperature reading is carried out from the flow temperature (gas or fluid)  $t_p$  before the heater, temperature of which is  $t_h$ , and after it:

$$\vartheta_H = t_H - t_p.$$

At the distance  $x$  from the heater we allocate the element of  $dx$  length with the cross-section area  $F$ . Thermal balance equation for the considered element, can be written as (Fig. 1.23)

$$Q_1 - Q_2 = dQ, \quad (1.8)$$

where  $Q_1$  – is the amount of heat, entering the elements of the ring;  $Q_2$  – is the amount of heat, leaving the element;  $dQ$  – is the amount of heat, released by the internal surface of the element of the flow cross-section, located in the pipe of the thermoammeter.

According to the Fourier's law:

$$Q_1 = \lambda \cdot \frac{d\vartheta}{dx} \cdot F; Q_2 = -\lambda \cdot \frac{d}{dx} \left( \vartheta + \frac{\vartheta}{dx} \right) \cdot F,$$

where  $\vartheta$  – is the excess temperature near the heater;  $\lambda$  – is the thermal conductivity of the measured environment;  $F$  – is heat exchange surface.

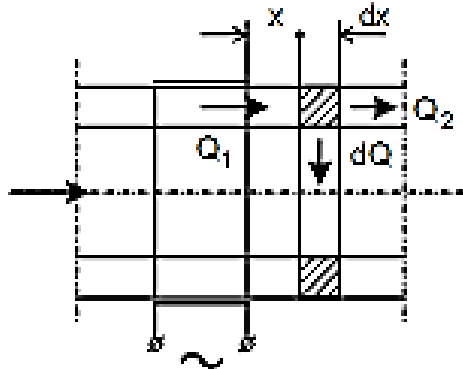


Fig. 1.23. Before the calculation of the temperature field of the thermal flow sensor

The equation follows:

$$dQ = \lambda \cdot F \cdot \frac{d^2\vartheta}{dx^2} dx, \quad (1.9)$$

At the same time, according to Newton-Richmann law this heat can be expressed by the equation:

$$dQ = \alpha \cdot \vartheta \cdot \Pi dx, \quad (1.10)$$

where  $\Pi$  – is the internal diameter of the thermoanemometer pipe.

Having compared the equations (1.9) and (1.10) we obtain differential equation that describes the temperature change of the pipe wall:

$$\frac{d^2 \vartheta}{dx^2} = \frac{\alpha \cdot \Pi}{\lambda \cdot F} \vartheta = m^2 \vartheta, \quad (1.11)$$

where  $m = \sqrt{\frac{\alpha \cdot \Pi}{\lambda \cdot F}}$ .

General integral of the equation (1.11) has the form:

$$\vartheta = C_1 \cdot e^{mx} + C_2 \cdot e^{-mx}. \quad (1.12)$$

Constants  $C1$  and  $C2$  are determined from boundary conditions, namely: if  $x = 0, v = v_H$  if the pipe length  $l = \infty$  all the heat, supplied to the pipe, is released in the fluid if  $x = \infty, v = 0$ . Substituting the boundary conditions in the equation (1.12) we obtain of  $x=0$ :

$$\vartheta_y = C_1 + C_2,$$

and if  $x=\infty: C_1 \cdot e^{\infty} = 0$

Having substituted  $C1$  and  $C2$  in the equation (1.12), we obtain:

$$\vartheta = \vartheta_H \cdot e^{-mx}, \quad (1.13)$$

In the dimensionless form this equation has the form:

$$\Theta \cdot \frac{\vartheta}{\vartheta_H} = e^{-mx}, \quad (1.14)$$

It follows from the expression  $m = \sqrt{\frac{\alpha \cdot \Pi}{\lambda \cdot F}}$  that the value of  $m$  parameter is proportional to the convective heat transfer from the internal surface of the pipe and inversely proportional to  $\sqrt{\lambda \cdot F}$  – factor that determines the heat transfer, thermal conductivity along the pipe. Fig. 1.24 shows the dependence of the dimensionless temperature  $\Theta$  on the length of the pipe at various values of  $m$  parameter.

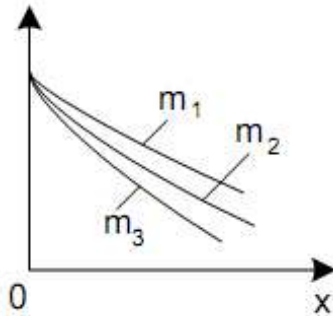


Fig. 1.24. Change of the dimensionless temperature if the flow is missing for various values of  $m$  ( $m_1 < m_2 < m_3$ )

The greater is the value of  $m$ , the greater is the decrease of the dimensionless temperature  $\Theta$ . If  $x \rightarrow \infty$  all the curves asymptotically approach to  $\Theta=0$ .

For the measurement of the consumption it is necessary to measure the temperature field on the surface of the primary converter, determined by the heat exchange processes of the flow rate, these processes are described by the system of four differential equations: equation of the motion:

$$-\frac{dp}{dx} + \mu \left( \frac{d^2 v}{dr^2} + \frac{1}{r} \cdot \frac{dv}{dr} \right) = 0; \quad (1.15)$$

equation of the through flow:

$$\frac{dv}{dx} = 0; \quad (1.16)$$

equation of the energy in the cylindrical coordinates:

$$p \cdot c_p \left( v_r \frac{dt}{dr} + v \frac{dt}{dx} \right) = \lambda \left( \frac{d^2 t}{dr^2} + \frac{1}{r} \cdot \frac{dv}{dr} + \frac{d^2 t}{dx^2} \right); \quad (1.17)$$

equation of the heat transfer:

$$\left( \frac{dt}{dn} \right)_c = -\frac{\alpha}{\lambda} (t_c - t_p), \quad (1.18)$$

where  $p$  - is the pressure of the flow;  $r$  is the radius of the pipeline;  $v_r$  is the velocity in the radial direction;  $\frac{dt}{dn}$  - is the temperature gradient;  $\mu$  - is the viscosity of the measuring environment.

The last equation is the main condition or single – valuedness condition. It combines the temperature gradient near the separation surface of wall and fluid with the conditions of the heat transfer to the flow in the thermoanemometer.

It is rather complicated to solve this system of equations (1.15) – (1.18) analytically. That is why, for the solution of heat exchange problems the experimental method, involving similarity theory is used. In this case, the equation is reduced to the dimensionless form. The values of these equations will be either similarity criteria or the relation of the homogeneous values.

Instead of the velocity  $v_x$  in the considered point of the radius  $r$ , the flow temperature  $t_p$  and coordinate  $x$  along the axis of the pipe (in the direction of the flow) the dimensionless values will be used in the equation:

$$\bar{V} = \frac{v}{\bar{v}}; R = \frac{r}{r_0}; \Theta = \frac{t_p}{t_e}; X = \frac{x}{l_0},$$

where  $\bar{v}$  – is average velocity of the flow;  $r_0$  – is the radius of the pipe;  $l_0$  – are the coordinates along the pipe of the thermoanemometer;  $t_e$  – is the temperature of the environment.

Equation of the convective heat transfer and energy in the dimensionless form will have the form:

$$N_u = - \left( \frac{d\Theta}{dR} \right)_{r=0}; \quad (1.19)$$

$$P_e \left( v \frac{d\Theta}{dX} + v_r \frac{d\Theta}{dR} \right) = \frac{d^2\Theta}{dR^2} + \frac{1}{R} \frac{dX}{dR} + \frac{d^2\Theta}{dX^2}. \quad (1.20)$$

Equations of motion and of through flow also get the corresponding form. For practical application, as a rule, criterial equations, obtained as a result of experimental studies, are used. It should be noted, that with the reduction of the size of microelectronic flow sensors, that is typical in biomedical devices, the problem of the theoretical description of the flow behavior, with the account of the boundary conditions, fluctuations and fluid tension becomes actual. These areas of research, as well as the problems of mathematical modeling, calculation of parameters and methods of thermal flow sensors calibration are presented in numerous publications, in particular, in the papers of the recent years [54-63].

Fig. 1.25 shows the results of the experimental acoustic research of the flow front distribution in case of its contact with the surface and the dependence of pressure distribution in the flow on the parameters of the criterial equations. A number of other examples of the experimental research of the dependence of microelectronic flow sensors signal on the parameters of the latter, based on the

combination of the thermal and manometric methods of measuring conversion are shown in Figs. 1.26 and 1.27 [61].

The problem of mathematical modeling of the thermal flow sensors is directly connected with the calculation of temperature distribution in the structure of the sensor. Methods of the thermal calculation nowadays are generally known, and for their realization wide range of the software products, in particular, Simulink (library Sim Power System) of the Matlab environment of the company Math Web Inc., Comsol or Semisel is used [64, 65].

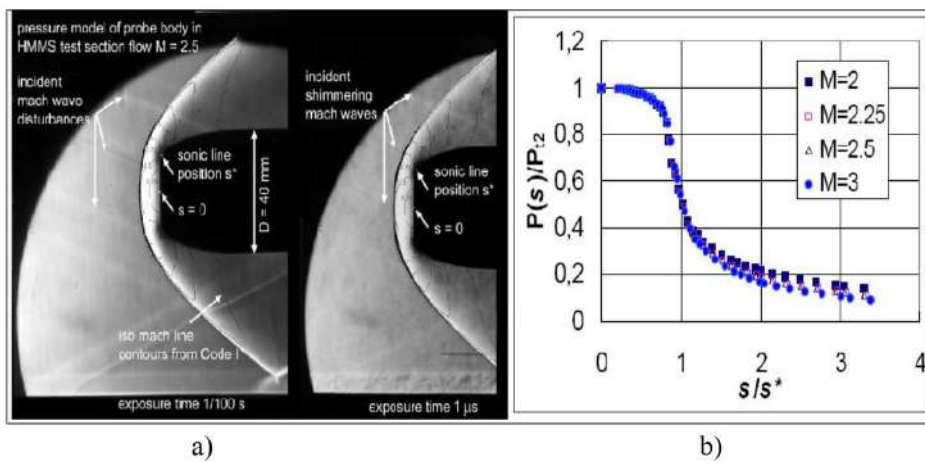


Fig. 1.25. Distribution dependence: a) of the flow front at its contact with the surface; b) pressure in the flow on the parameters of the criterial equations

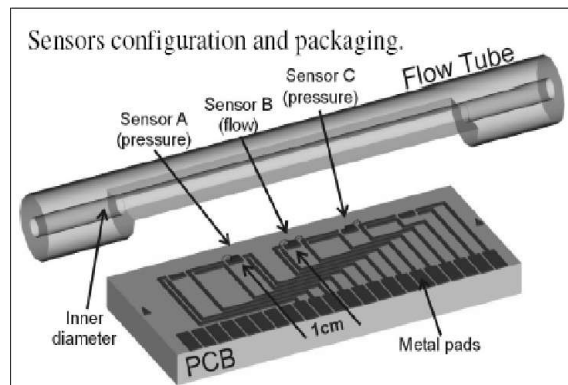


Fig. 1.26. Structural diagram of the microelectronic flow sensor that combines thermal and manometric methods of measuring transformation

The example of the comparison of the results of the model and experimental studies of the microelectronic heater temperature field is shown in Fig. 1.28. Model studies were carried out, using COMSOLTM script language, experimental studies – by means of video devices of the infrared range.

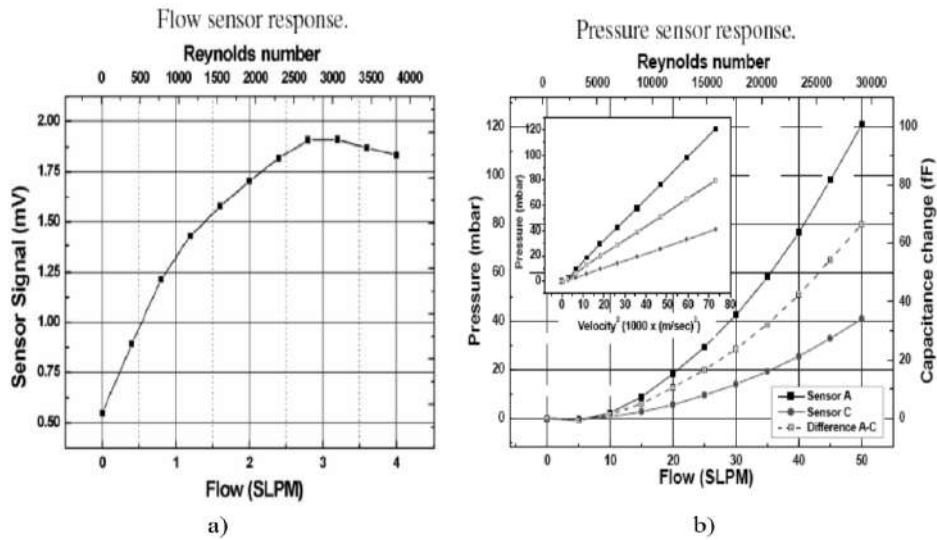


Fig. 1.27. Dependence of the output signal of the flow sensors on the value of Reynold's number: a) thermal; b) manometric

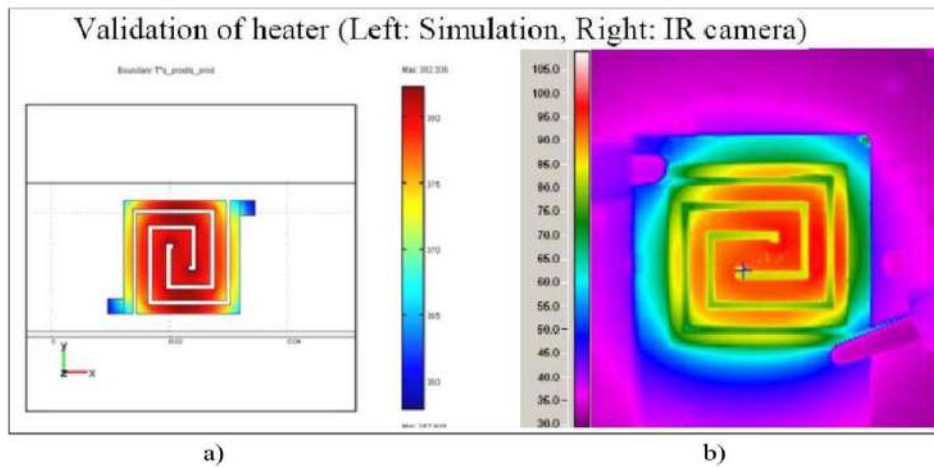


Fig. 1.28. Results of the studies of microelectronic heater temperature field: a) model; b) experimental



If dynamic thermal processes are to be calculated, the application of the software products of SEMISEL type is rather efficient, these products use electric thermal analogy – thermal processes in separate sections of the structure are replaced by the corresponding  $RC$  links. The example of such calculations is shown in Fig. 1.29.

But, in spite of the large volume of information and variety of the commercially available software products, designed for thermal modeling, the analysis, carried out, showed that the methods of mathematical modeling of thermal flow sensors operation modes require further development. In the first place, it is connected with the necessity to combine thermal and electrical modeling in a single system, that would enable to perform the optimization of structural- circuit engineering solutions of the operation modes of the primary converters of the thermal flow sensors with the dynamic thermal modulation of volt-ampere characteristic of these converters by their own heating current.

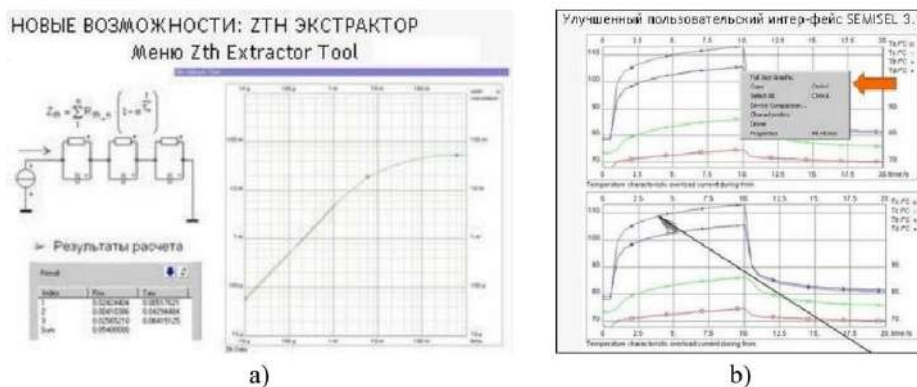


Fig. 1.29. Principle and the results of : a) electro thermal analogy; b) model calculation of the dynamic thermal processes

It should be noted that the problem of combining the thermal and electrical modeling has already been partially solved, in particular, in the last versions of the software for the circuit simulation PCPICE and MicroCap [66, 67]. However, as we have already shown, application of the above-mentioned software products for the problems of the dynamic electric thermal modeling of the thermal flow sensors requires the solution of the problem of the synthesis of electric thermal models of thermoresistive, diode and transistor structures of the primary converters, volt-ampere characteristic of which is modulated by the operating current.

### 1.3. Trends of development of the integral signal converters of the sensor devices

Modern state-of-art of sensor electronics is greatly determined by the microprocessor engineering. Wide introduction of modern microprocessors enables to improve substantially technical characteristics of microelectronic sensors, broaden their functional possibilities, provide mutual compatibility and the possibility of the formation of measuring-diagnostic system [68–72]. Future – oriented direction – smart sensors are formed [73–78]. Criteria and parameters of the intellectualization of the process of physical environment parameters measurement and requirements to microelectronic facilities, providing this process are determined by the International Standard IEEE 1451 – networked smart transducer interface standard [79–80]. High-efficient and convenient interfaces by means of which sensors are connected to the computer – based systems of data mining, are developed [81–84]. Much attention is paid to the reduction of energy consumption of the devices and provision of the possibility of their operation, using low voltage power supply sources [85–91].

For example, Fig. 1.30 shows the generalized functional diagram of the smart MEMS device that contains; MEMS sensor, as it is shown in Fig. 1.30 they may be light sensors, sound sensors, pressure sensors, chemicals sensors or temperature sensors; Input analog signal processing unit; Digital Signal Processing unit; Output analog signal processing unit; MEMS actuators, i.e., inverse relatively the sensor by the functional action transducer, that provides mechanics, display, electrical power or other devices; Optical or electrical communication.

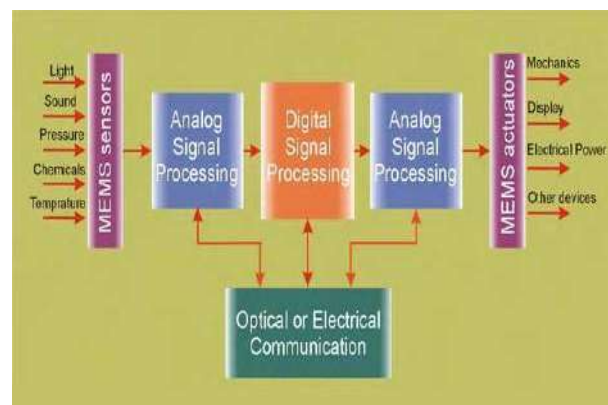


Fig. 1.30. Functional scheme of the Smart MEMS device

Unlike sensor devices of temperature, magnetic field, mechanical stress, humidity, etc, flow measuring sensors still are at the initial stage of the development of the methods and means of their intellectualization. Although the process of electric signal measurement, for instance, of thermoanemometric flow sensor of the bridge type is rather simple, the provision of all the requirements to modern smart electronics is far more complicated problem. We will consider this problem from the point of view of the methods, realized by the signal transducers of the thermal flow sensors. The following principle methods and approaches, providing intellectualization of flow measurement sensor can be formulated:

- increase of measuring conversion accuracy on the base on special circuit engineering solutions;
- adaptation of the transducer operation modes according to the flow parameters and measuring conditions;
- minimization of the energy consumption and provision of the possibility of operation from low voltage small power supply sources;
- interface with modern operating systems (OS) of the computer equipment, collection and visualization of the measurements results.

Generalized structure of the flow sensor, the components of which are primary transducer, signal analog transducer (secondary transducer), analog-to-digital converter, microcontroller and interface, is shown in Fig. 1.31

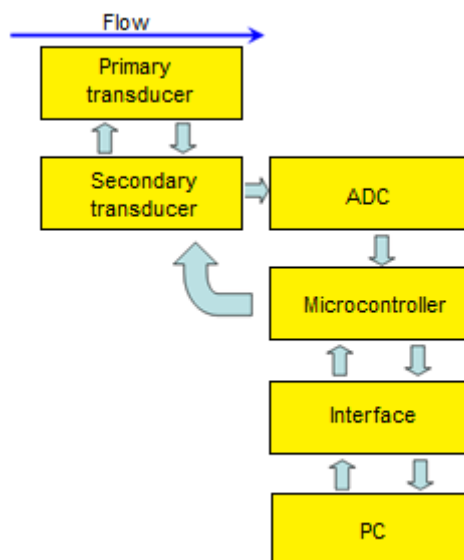


Fig. 1.31. Functional diagram of the Smart flow sensor

#### **1.4. Analysis of the integral signal transducers of the microelectronic thermal flow sensors of general and biomedical designation**

In recent years rapid development is observed in the sphere of the construction of signal transducers of microelectronic sensors, element base of new generation is created, projects, aimed at interfaces and supply parameters unification are realized, such a notion as the art of circuit engineering has appeared. These developments are highlighted in the monographs [92–101] and papers [102–107]. Latest achievements in the sphere of analog-to-digital converters (ADC) are presented in [108,109].

It should be noted that sometimes there exists a misperception that microprocessors have completely ousted the means of analog processing of signals. In fact, this is true only for simple sensor devices, which do not possess high metrological characteristics. As the surrounding world is analog by its nature (obviously, that is not a question of the dual nature of the microworld) signal converters of the analog signal are and will remain the determinative components of highly precision and functionally complex sensor devices. Numerous studies on this subject, published in the editions of IEEE [110–116] and the process of the constant renovation of analog integrated amplifiers prove this statement [117,118].

New direction of the development of signal converters is their integration directly in the structure of solid-state integrated circuits of the smart sensor, in particular, in biomedical catheter CMOS blood flow sensor [119].

However, as we determined in the process of the analysis of the available literature sources, a greater part of signal converters of thermal flow sensors do not meet the requirements of modern electronics. This can be shown on the example of the circuit of the signal converter of thermal flow sensor, developed for biomedical application, presented in in Fig. 1.32. [46] (it should be noted, that the cited paper is published in the scientific community journal of microelectronic sensors Sensor and Actuator of the Elsevier Publishing House in 2008). As it is seen, the circuit of the signal converter requires bipolar  $\pm 15$  V supply source, that does not meet the requirements of modern electronics (as it was already mentioned, modern microelectronic sensor devices must provide normal operation at 3V single pole supply), signal converter does not provide compensation of the parasitic impact of the signal lines, a number of nonoptimal circuit engineering solutions is also available.

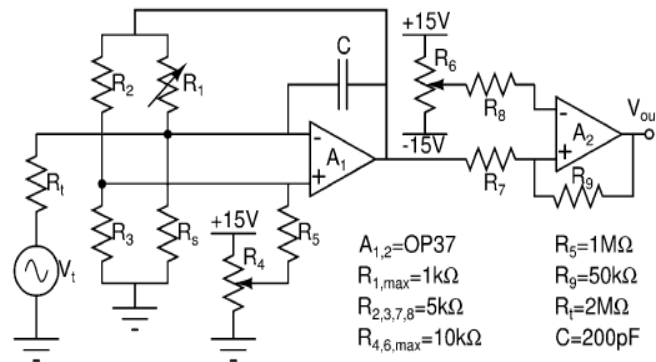


Fig. 1.32. Signal converter connection of the thermal flow sensor [46]

It is important to note, that the problem of the transition on the small power low voltage supply source is one of the most complex as only in the recent years low voltage high precision analog integrated circuit became available ( this class of circuits got the name of vLow Voltage Rail-to-Rail Circuits), the correct usage of low voltage analog circuits requires new circuit engineering solutions and regarding the thermal flow sensors, the determining problem is the decrease of the supply voltage of the circuit of the functionally integrated elements “heating – temperature measurement”.

We will consider this problem in detail. Then, taking into account the requirement to modern energy-efficient electronic equipment, the resistance of the heater of the thermal sensor to the flow must be rather low, in particular, if the supply voltage is  $3\text{V}$  and heating power is  $0.1\text{W}$ , the resistance of the heater must not exceed  $100\ \text{ohm}$ . The resistance of the line of signal transmission may be several ohms. That stipulates the considerable error (several percent) of the heater resistance measurement. On the other hand, the accuracy of the temperature sensor resistance measurement must be several orders higher (typical error of the resistance measurement must not exceed  $0.03\%$ ). Thus, thermal flow sensors with functionally integrated elements “heating – temperature measurement” require special circuit engineering solutions regarding signal conversion.

The decrease of signal line resistance impact on the result of measurement, is provided by the usage of the three-wired line. The examples of such converters are presented in Fig. 1.33 [94–97, 101].

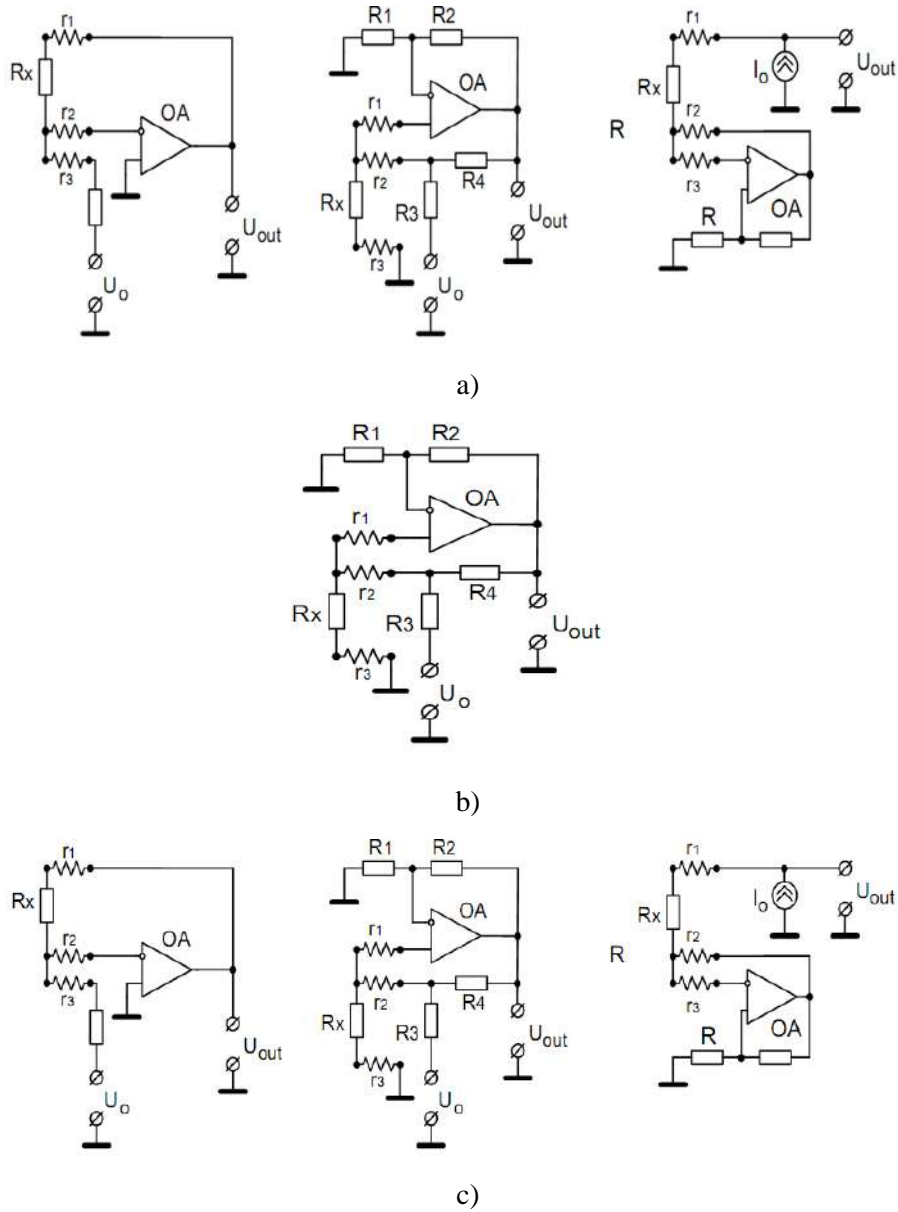


Fig. 1.33. Diagrams of the three-wired converters of active resistance

The first diagram (Fig. 1.33a) is based on the elementary inverting amplifier. If the resistances of the line are neglected, the output voltage of the converter is  $U_{out} = -U_0 \cdot R_x / R_0$ . The impact of the signal line in the converter decreases

due to the connection of one of the outputs ( $r_1$ ) in series with the measuring resistor  $R_x$ , the second output ( $r_2$ ) in series with  $R_0$  and the third ( $r_3$ ) in series with high input resistance of the operational amplifier (OA). Taking into account the resistances of the outputs and having met the conditions  $r_1 \ll R_x$ ,  $r_2 \ll R_0$  determine:

$$U_{out} = -U_0 \cdot \frac{R_x + r_1}{R_0 + r_2} \approx -U_0 \cdot \frac{R_x}{R_0} \left( 1 + \frac{r_1}{R_x} - \frac{r_2}{R_0} \right).$$

Further, having assumed  $r_1 / R_x \approx r_2 / R_0$  we obtain:

$$1 + \frac{r_1}{R_x} - \frac{r_2}{R_0} \approx 1,$$

Thus, the impact of transmission lines resistances on the output voltage becomes minimal. We should also pay attention to the problems of the accurate provision of the necessary relations – the resistance of the signal line can change in time and the change of the measuring resistor  $R_x$ . that is the base of the measuring process, in its turn, also changes the preset relation.

The following circuit of the converter (Fig. 1.33b) provides the realization of the relation  $R_1 R_4 = R_2 R_3$ , in this case the current across  $R_x$  does not depend on the change of this resistor. The output voltage is determined by the expression:

$$U_{out} = U_0 \cdot \frac{R_x}{R_3} \left( \frac{R_2}{R_1} + 1 \right) \frac{1 + r_3 / R_x}{1 + r_2 (R_3 \parallel R_4)}.$$

The error of the line resistance decrease if  $r_2 \approx r_3$  and at the change of  $R_x$  in relatively narrow limits  $R_x \approx R_3 \parallel R_4 = R_3 R_4 / (R_3 + R_4)$ .

One more scheme with the tree-wire signal line is shown in Fig. 1.33c. Its positive feature is the independence of the condition of mutual compensation of the line resistance on the change of measuring resistor  $R_x$  resistance.

Operation amplifier (OA) is connected across  $r_2$ ,  $r_3$  by the negative feedback with the coefficient  $\beta_+ = 0.5$ . That is why, at the inputs of OA and at low potential output  $R_x$ , the voltage  $U = -I_0 r_2$  is maintained. This is explained by the fact that if positive feedback is missing the output voltage of OA is  $-I_0 r_2$ , and at the inputs zero potential is observed.

Taking into account the positive feedback, at the output of OA the doubled voltage  $-2I_0 r_2$  is obtained. Half of this voltage across the resistive divider is sent to the non-inverting input of OA. It is obvious, that the same voltage will be formed at the inverting input. The stability of the circuit is provided by the

advantage of the negative feedback over the positive  $\beta^- > \beta^+$ . Thus, the output voltage of the converter is:

$$U_{out} = I_0 \cdot (R_x + r_1 - r_2),$$

if  $r_1 = r_2$  stipulates the absence of the impact on the output signal of the signal line resistance. Accuracy of balancing does not depend on the change of  $R_x$ . Four-wire communication lines provide considerable decrease of the errors, caused by the impact of line resistances. Typical circuits of such converters are shown in Fig. 1.34.

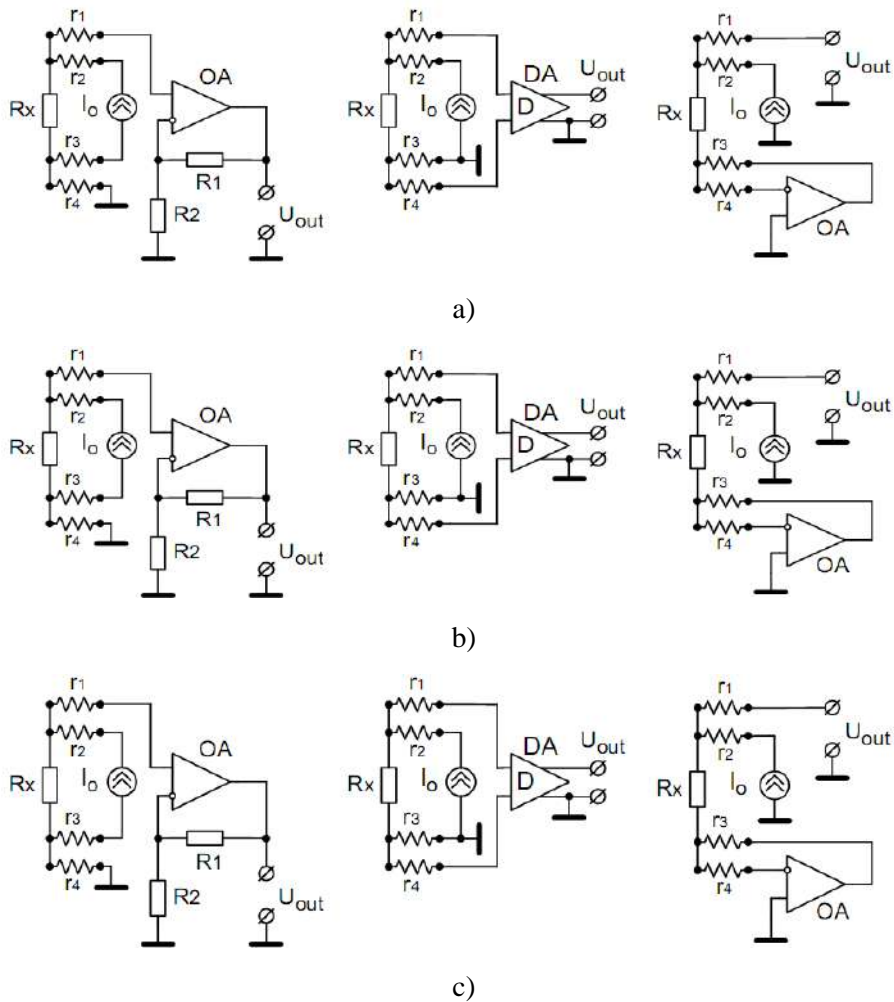


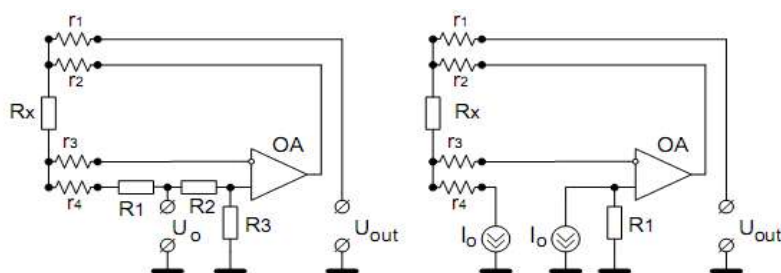
Fig. 1.34. Circuits of the four-wire converters of the active resistance



The first circuit (see Fig. 1.34a) contains a galvanic source of current and four-wire communication line. Such source of current (without connection with the “earth”) enables to simplify the amplification circuit. Having selected the amplifier with the input resistance  $R_{in}$ , far greater than the resistances of the signal line  $R_{in} \gg r_1, r_4$ , the latter can be neglected. The resistances of the signal line  $r_2, r_3$  are not the part of the output voltage formation circuit, that is why, they do not influence the result of measuring.

The requirement of the galvanic decoupling of the current source is eliminated if the differential amplifiers with high input resistance are used (Fig. 1.34b). As in the first circuit, the resistances of the signal line do not influence the result of measurement. The alternative variant of the converter circuit, which does not require either galvanic decoupling of the current source or differential amplifier, is shown in Fig. 1.34c. Voltage repeater on OA maintains zero potential at the low output of the measuring resistor  $R_x$ . As a result, the dependence of the output voltage of the converter on voltage drop at the output  $r_3$  disappears. The resistances of the line  $r_1, r_2, r_4$  do not influence the result of measurements, as  $r_2, r_3$  are connected in series with high output resistance of the current source and  $r_1$  - with the input resistance of OA of the signal circuit (it is not shown on the circuit). However, this variant requires additional OA for decreasing the output resistance of the converter.

The converters of the active resistance of the direct measurement have an essential drawback, stipulated by the dependence of the output voltage on the absolute value of the measuring resistor and not on its change. As it will be shown below, this drawback is eliminated by the bridge type converter. However, the formation of the voltage, value of which is proportional to the change of  $R_x$  increment relatively certain initial value  $R_{x0}$  can be performed by means of direct measurement converters. Basic methods of their realization are shown in Fig. 1.35



a)

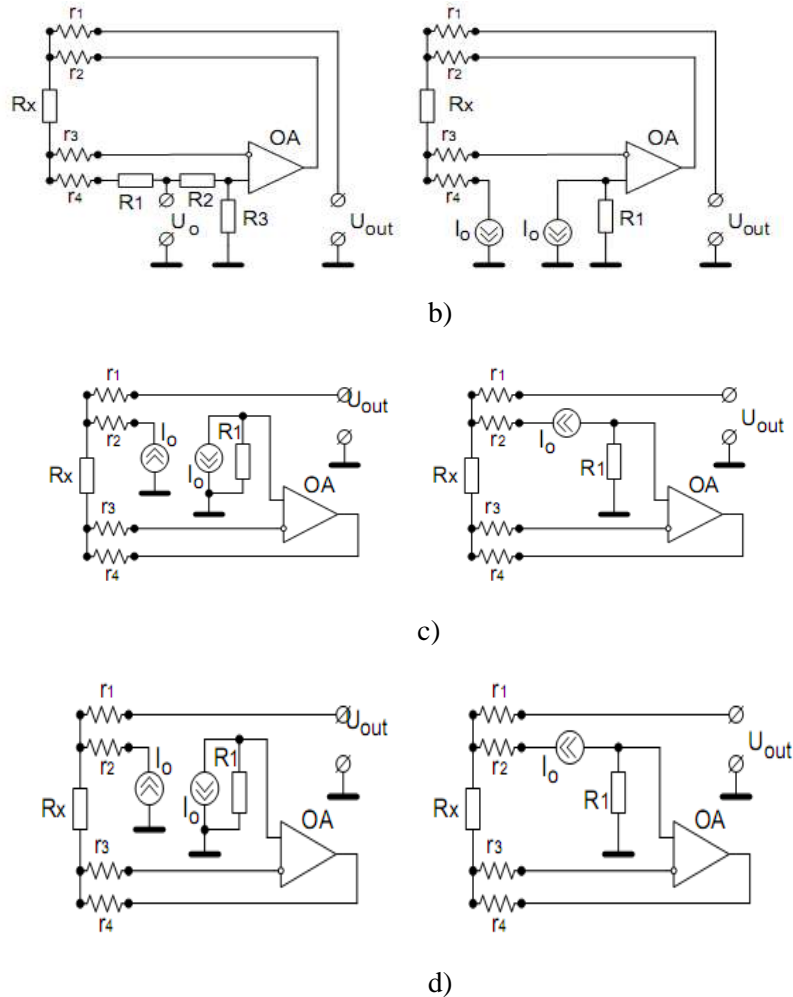


Fig. 1.35. Circuits of the converters with the proportionality to the increment of the resistance

The first circuit is built on the base of the converter, considered above. However, this circuit uses a four-wire line and the part of the reference voltage  $U_o$  is applied to the non-inverting input of OA (Fig. 1.35a). Resistances of the outputs  $r_2$  and  $r_3$  make the part of the deep feedback circuit that is why their impact on the output voltage is minimal. Resistance  $r_1$  increases to some extent the output resistance of the converter but in case of provision of the high input resistance of the next amplifier, this circumstance is unessential. The resistance of the output  $r_4$  is connected in series with  $R_1$  and directly influences the output voltage:

$$U_{out} = \frac{U_0}{1 + R_3 / R_2} \left( \frac{R_3}{R_2} - \frac{R_x}{R_1 + r_4} \right).$$

This impact is decreased by increasing  $R_1$ , providing the condition  $R_1 \gg r_4$ , and the preset value of working current of the measuring resistor  $R_x$  is formed by the corresponding change of the reference voltage  $U_0$ . The relation of the resistors  $R_2$  and  $R_3$  is established proceeding from the condition of the equality to zero of the output voltage at the preset initial value of measuring resistor  $R_x = R_{x0}$ .

In the circuit, shown in Fig. 1.35b, two mutually equal sources are used. Output voltage of the converter is:

$$U_{out} = I_0 \cdot (R_x + r_1 - r_2).$$

Sources of mutually equal current are manufactured as single-crystal current mirrors. The accuracy of mutual equality of currents in this case is high, which makes this circuit competitive with bridge type converters. Another modification of this type of converter is shown in Fig. 1.34c. The same functional dependence of the output voltage is formed as a result of using two sources of current, values of which are mutually equal and signs are different. The variant of the converter with the formation of the output voltage, proportional to the change of measuring resistor, based on galvanically insulated sources of current, is given in Fig. 1.35d.

In the thermal flow sensors with the structure of the half-bridge converter circuits, shown in Fig. 1.36c can be used. In the first circuit (see F 1.36a) the bridge is supplied from two symmetric voltages  $+U_0$  and  $-U_0$ . To decrease the error, caused by voltage drop in the supply circuits, voltages  $+U_0$ ,  $-U_0$  are supplied to measuring resistors across voltage repeaters on  $OAI$ ,  $OA2$ . Output voltage across the output  $r_3$  in general case- five output half-bridge, is amplified by means of non-differential amplifier with high input resistance (in the circuit this OA is not shown). Output voltage is determined in the following away:

$$U_{out} = U_0 \frac{R_2 - R_1}{R_1 + R_2}.$$

The drawback of the given circuit is high requirements to the symmetry of half-bridge supply voltages – non-equality of their modules directly influences the measurement results.

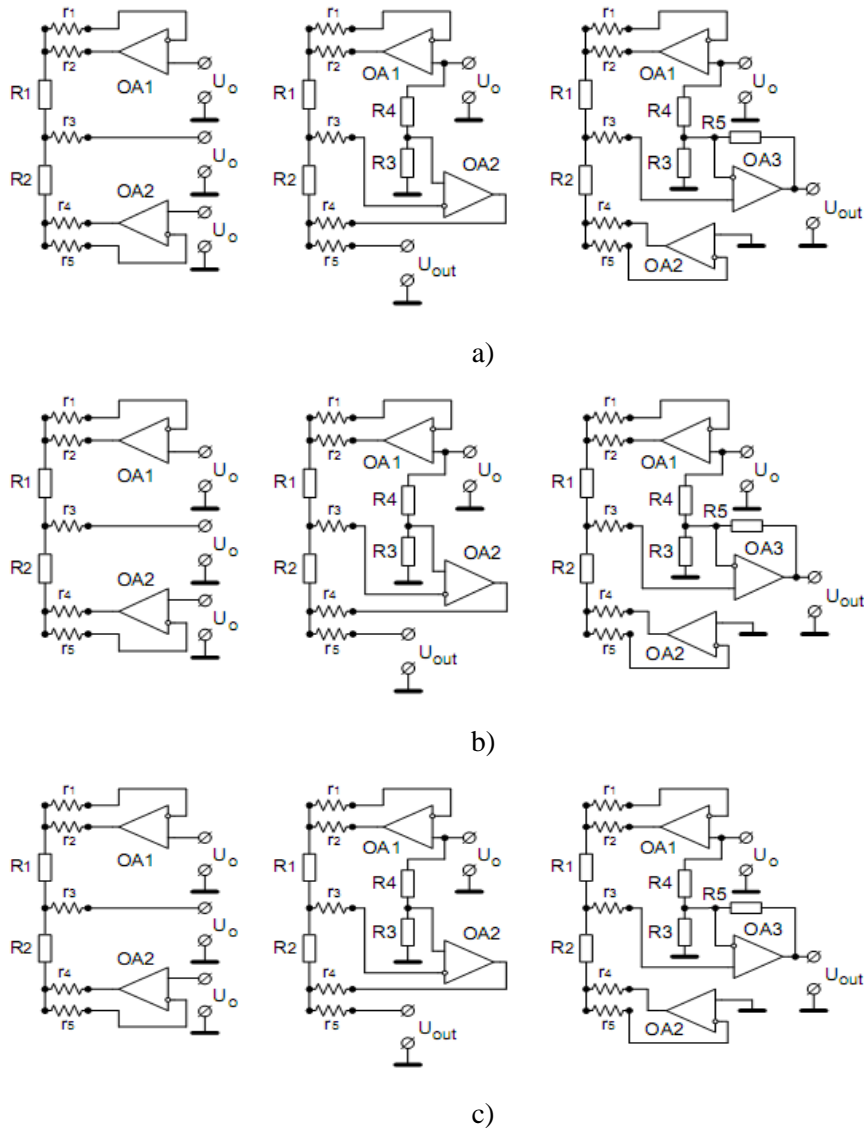


Fig. 1.36. Circuits of the half-bridge converters

In the second circuit (see FIG. 1.26b) five-output half-bridge is also used, but its supply is provided only by one voltage  $U_o$ . Operational amplifier (OA1) maintains this voltage at the upper output of the half-bridge. OA2 forms at the low output of the half-bridge the voltage at which the potentials are equalized in the middle point of the half-bridge and at the output of the divider from the resistor  $R_3, R_4$ . As a result the current flows across the half-bridge:

$$I = U_0 \frac{R_4}{R_1(R_3 + R_4)},$$

and the output voltage, formed at low output of the half-bridge, is:

$$U_{out} = U_0 \frac{R_3}{R_3 + R_4} - IR_2 = U_0 \frac{R_1 R_3 - R_2 R_4}{R_1(R_3 + R_4)}.$$

In separate case, if  $R_3=R_4$ , we have:

$$U_{out} = U_0 \frac{R_1 - R_2}{2R_1}.$$

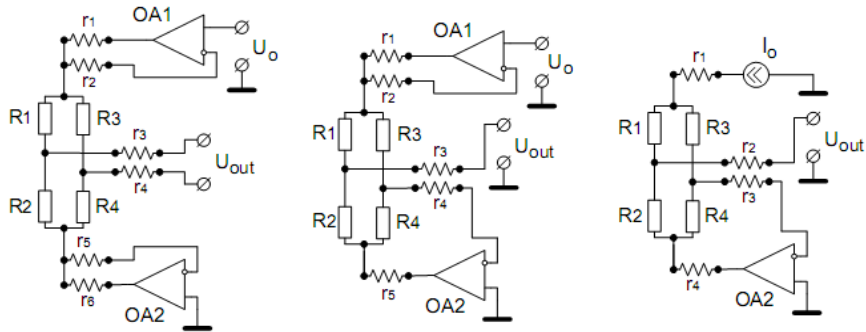
The circuit of the converter, shown in FIG. 1.36c, comprises three operational amplifiers and this, besides minimal error of line resistances, enables to amplify the output voltage:

$$U_{out} = U_0 \frac{R_2}{R_1 + R_2} \left( \frac{R_5}{R_3} + \frac{R_5}{R_4} + 1 \right) - U_0 \frac{R_5}{R_3} = U_0 \frac{R_2 R_3 (R_4 + R_5) - R_1 R_4 R_5}{(R_1 + R_2) R_3 R_4}.$$

If the condition is provided, the output voltage is:

$$U_{out} = U_0 \frac{R_2 - R_1 R_5}{R_2 + R_1 R_3}.$$

Typical construction schemes of the bridge resistive converters of the thermoanemometric sensors are shown in Fig. 1.37.



a)

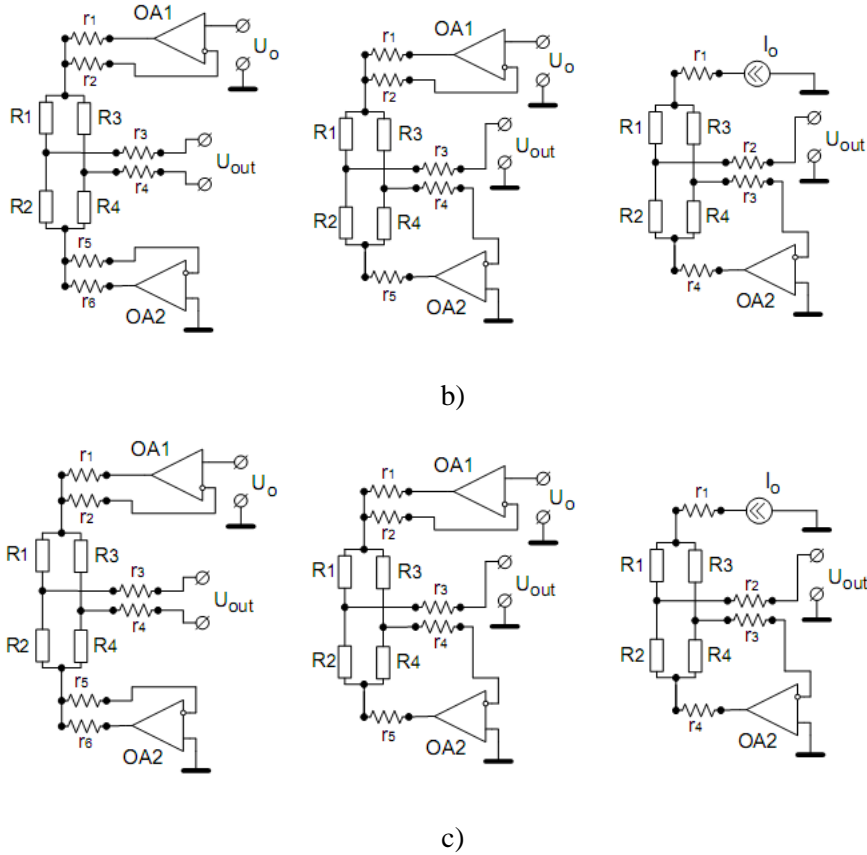


Fig. 1.37. Circuits of the bridge converters

The first of them (see Fig. 1.37a) – six output bridge – for the amplification of the output signal provides differential amplifier with large output resistance, output voltage equals:

$$U_{out} = U_0 \frac{R_1 R_4 - R_2 R_3}{(R_1 + R_2)(R_3 + R_4)}.$$

The improved version of the converter is shown in Fig. 1.37b. The advantage of the circuit is a five-output bridge and the possibility of using a non-differential amplifier. At the upper peak (in the circuit) of the bridge the voltage  $U_0$  is supplied by means of  $A1$ . At the low peak of the bridge the voltage is formed, at this voltage the potential on the left peak equals zero. This condition is satisfied if the voltage at the low peak is  $U = -U_0 R_2 / R_1$ .

The third version of the converter, the circuit of which is shown in FIG. 1.37c, provides the compensation of the signal lines resistances only at four

outputs of the bridge, The bridge is supplied by the stable current  $I_0$ , it is divided into two components:  $I_1$  - across the resistor  $R_1 + R_2$  and  $I_2$  - across the resistors  $R_3 + R_4$ :

$$I_1 = I_0 \frac{R_3 + R_4}{R_1 + R_2 + R_3 + R_4}; \quad I_2 = I_0 \frac{R_1 + R_2}{R_1 + R_2 + R_3 + R_4}.$$

By means of OA the voltage between the resistor  $R_1$  and  $R_2$  is maintained at zero level that determines the output voltage:

$$U_{out} = I_1 R_1 - I_2 R_2 = I_0 \frac{R_1 R_4 - R_2 R_3}{R_1 + R_2 + R_3 + R_4}.$$

The above-mentioned analysis of the circuits of the half-bridge and bridge measuring converters shows that the problems of the compensation of the parasitic impact of the transmission lines, as a rule, have rather efficient solutions. However, this conclusion cannot be applied to the full extent to measuring converters of thermal flow sensors.

At least, there are two reasons. First, in the most typical thermal flow sensors with functionally integrated elements "heating - temperature measurement" the release of heat takes place not only on these elements (a useful part of energy consumption) but also on the control elements of the output transistors of OA. This stipulates the excessive energy consumption and, in case of the monolithic integration of the primary converter circuit with the signal converter of the sensor device, parasitic heating of the sensor structure in the areas of the control transistors location. In their turn, such areas of the parasitic heating distort the temperature field of the primary converters, which leads to the increase of flow measurement error. Secondly, in the process of the transition to the small-size, low power, low voltage supply sources the voltage drop at the control transistors of the heating circuit could be comparable with the voltage at the primary functionally integrated converter, that considerably decreases the efficiency of energy consumption and the accuracy of sensor device operation.

Concerning the problems of the digital signal conversion, interfaces, software, etc., in the authors' opinion, the latter completely meet the requirements to the units of modern sensor devices and are rather universal.

## 1.5. Characteristics of the temperature distribution in biomedical objects

Accumulation of the heat in a biomedical environment that consists of tiny particles in the middle of optically uniform surroundings can be divided into two components: accumulation of heat in the singular particles which absorb and

heat accumulation in the environment (for instance, biotissue) that surrounds these particles.

In case of the therapeutic impact the processes of the transformation of the electromagnetic energy of laser beam into heat energy take place. This transformation of the radiation energy into heat can be performed in the case if the laser radiation is absorbed by the specific chromophore tissues [100].

The density of the heat source energy  $q$  (W/m<sup>3</sup>) in the volume of the tissue, being radiated, is the functional of the absorption coefficient  $\alpha$  and general density of radiation  $L$ , that consists of the slope part of the optical beam  $L_C$  and the part of the radiation from the surrounding tissue, that scatters:

$$q(r, t) = \alpha [L_C(r, t) + L_S(r, t)],$$

where  $r$  – is radius – vector of the observation point,  $t$  – is time.

Energy of light, converted into the heat causes in the volume, being radiated, local temperature increase. If phase transitions do not occur, then the temperature  $T$  increases proportionally to the density of energy  $q$ . Part of the heat is released, depending on the temperature gradient, by means of heat conduction in the colder surrounding area. As a result, the maximum achievable temperature area being radiated, is limited, at the full intensity of radiation, i.e., for the pressed intensity of the radiation a certain maximum temperature exists. For each tissue there exists a specific threshold of the intensity that must be overcome to achieve necessary local temperature [100].

In view of the fact that the part of energy as a result of the heat conductivity and other processes is transported into neighboring sections, not only the volume, being radiated, is heated but also the neighboring sections. By local blood flow *in vivo* the heat is removed from the tissue, being radiated. Thermal properties of living tissue are determined, on the whole, by three processes: heat conductivity, heat accumulation; heat removal by the vascular system.

*Heat conductivity.* The heat passes from the warmer sections to colder sections of the tissue. Heat flow  $dQ/dt$  is directly proportional to the temperature gradient, i.e, in 1-D case in the ideal uniform specimen of the tissue of  $S$  length and the cross-section  $A$  to the location with lower temperature  $T_2$  according to the formula [100]:

$$\frac{dQ}{dt} = \gamma A(T_1 - T_2) / S, \quad (1.20)$$

where  $\gamma$  – is the coefficient of the proportionality (it characterizes heat conductivity).

Heat conductivity of fluids and solids practically does not depend on the temperature. It increases, for instance, in water from 0,62 W/mK at 37 °C only to 0,64 W/mK in 57 °C. Concerning the biotissue, these values are 0,3÷0,5



W/mK, depending on the water concentration . For this case such relation is valid:

$$\gamma = (0,06 \div 0,057 \omega / \rho),$$

where  $\rho$  – is the density of the tissue ( $\text{kg/m}^3$ );  $\omega$  – is the content of water in the tissue ( $\text{kg/m}^3$ ) . Values of heat conductivity for the biological substances are shown in Table 1.1.

Table 1.1. Values of heat conductivity for the biological substances

Substance	$\gamma$ [W/m·K]
Ethanol	0,17
Adipose tissue	$\approx 0,3$
Tissue , containing the air	$\approx 0,5$
Blood	0,62

In the process of the conversion of light energy into thermal energy the chaotic motion of atoms and molecules increases. Energy transfer by means of heat conduction is carried out in the direction of lower temperature and more rapid molecules in the warm area transfer the kinetic energy by means of the collisions of slow molecules in the colder part of the tissue.

*Heat accumulation.* The property of the tissue to accept and accumulate heat is described by the specific heat  $c$  ( $\text{kJ/kg.K}$ ). This value equals the amount of heat  $Q$  that leads to temperature increase of the unit of mass by  $1\text{K}$ :

$$c = (1,55 \div 2,8 \omega / \rho).$$

The value of the specific heat for the fat – 1.930, blood – 3.22. In the process of phase transition all heat energy is used to overcome intermolecular forces, the temperature of the investigated volume, when the temperature of phase transition is achieved, remains stable, until the phase change is over. General space and time characteristics of the temperature distribution in the volume of the issue, being radiated, is described by general heat transfer equation [100]:

$$\frac{dT}{dt} = (q / \rho c) + (\gamma \nabla^2 T / c), \quad (1.21)$$

where  $\nabla^2 = (d^2 / dx^2 + d^2 / dy^2 + d^2 / dz^2)$  – is the Laplace operator,  $q / \rho c$  – is temperature change in the volume, connected with the absorption of the radiation,  $\gamma \nabla^2 T / c$  – corresponds to temperature change, connected with the release of heat in the environment.

Temperature distribution at the moment of time  $t'$  in the point  $x'$  at the release of heat quantity  $Q$  is described:

$$T_0(x, t) = \frac{Q \cdot \exp\left\{-\frac{(x-x')^2}{4\gamma(t-t')}\right\}}{2\rho c(\pi\gamma(t-t'))^{1/2}} = \frac{Q \cdot e^{-\frac{(x-x')^2}{4\gamma(t-t')}}}{2\rho c\sqrt{\pi\gamma(t-t')}}. \quad (1.22)$$

For the radiation field with space and time changes, at the density of heat distribution  $q(x', t')$  we obtain:

$$T(x, t) = \frac{1}{\rho c\sqrt{\pi\gamma}} \int_0^t \int_{-\infty}^{\infty} \frac{q(x', t')}{\sqrt{t-t'}} e^{-\frac{(x-x')^2}{4\gamma(t-t')}} dx' dt'. \quad (1.23)$$

For practical calculation of time characteristics of local heating distribution the time of thermal relaxation is introduced:

$$\tau = \left[ d^2 \rho c \right] / \gamma = d^2 / \chi, \quad (1.24)$$

where  $d$  – is the depth of the biotissue. That is, if the short pulse of heat is applied to the surface of the tissue, then the time  $\tau$  passes until the substantial heating starts in the depth.

*Heat removal by the blood flow and other mechanisms.* Heat energy from the area, being radiated, is removed not only due to the heat conductivity but also across the vascular system. The blood arrives in the volume, being radiated at normal arterial temperature and is immediately heated to local temperature in the capillary region [100].

For the assessment of the temperature distribution under the impact of the vessels, perfusion time  $t_b$ , i.e., the time, during which the blood is changed in the unit of the tissue volume, is introduced. Transfer of heat by blood flow can become the dominant factor, when establishing stationary temperature distribution, especially, in case of the continuous radiation.

The impact of blood flow on stationary temperature distribution occurs only in the case, when the area of the tissue radiation section is greater than the depth of thermal penetration. If the area of radiation is smaller, then heat transfer is determined by the thermal conductivity. Also the heat can be removed by means of metabolic processes, evaporation of the water from the surface and convection.

## **2. Analysis of the existing methods of the construction of the highlinear analog devices for signal converters**

### **2.1. Survey of the methods of the construction of the analog converting devices for multiple – digit systems of measurement, registration and processing of signals**

Multi-digit analog-to-digital systems, as the variety of information systems comprise the systems of measurement, registration and processing of signals that is one of the spheres of engineering activity, where by means of electronic facilities registration, processing, accumulation, measurement and dissemination of information in the form of electric signals is realized [120]:

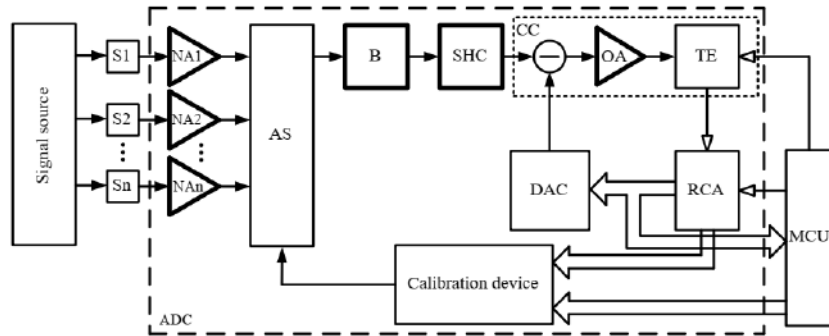
At the same time, the above-mentioned systems include [121]:

- automated control-measuring technological units;
- information-registration systems with digital recording and signals processing;
- measuring complexes and devices for the analysis of the parameters and characteristics of the signals and paths.

Structural diagrams of these systems are shown in Fig. 2.1, where – S1, S2, ..., S<sub>n</sub> – sensors; NA1, NA2, ..., NA<sub>n</sub> – normalizing amplifiers; F1, F2, ..., F<sub>n</sub> – filters; B – buffer device; AS – analog switch; DA – difference amplifier; TE – threshold element; CC – comparison circuit; CCC – code-current converter; RSA – register of serial approximation; CU (MCU) – control unit (microprocessor).

Nowadays the above-mentioned systems of measurement, registration and processing of signals require analog-to-digital devices with rather high characteristics: dynamic range up to 100-140 dB; signal/noise ratio – 96/120 dB; coefficient of non-linear distortions – 0, 001-0,002 %, spectrum of input signal frequencies – 16-20000 Hz, binary exit code length is 14-20 bits and sampling rate 44.1 kHz [121].

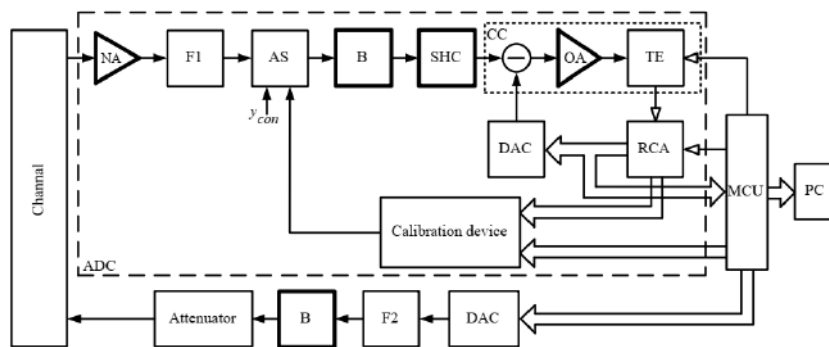
The most widely-spread devices in such systems are: ADC, DAC, buffer devices CVC, and VVC, sample-and-hold circuits(S/H circuits), etc. [122].



a)



b)



c)

Fig. 2.1. Systems of measurement, registration and processing of signals with the calibration of the conversion characteristic: a) automated control-measuring technological unit; b) information – registration system of data collection and processing; c) analyzer of sound tracks parameters

Achievements in the sphere of digital technologies enabled the signals processing. One of the ways of the development of this priority direction both abroad and in our country is the construction and application of high-linear, multiple-digit ADC and DAC with weight redundancy [121-125]. However, in spite of the high performance of the existing ADC and DAC, their application in the systems of measurement, registration and signals processing remains current, as the element base in the form of analog devices with corresponding characteristics must be created. That is why, it is expedient to consider the system ADC and DAC not as functionally completed units but as a set of analog linear devices [121]. There exist such types of the above-mentioned devices:

- normalizing amplifiers;
- buffer voltage devices;
- current-voltage converters;
- voltage-voltage converters;
- analog signals sample-and-hold circuits;
- signals difference amplifiers for high sensitive comparators;
- filters of low and high-frequency signals;
- analog signals switches;
- alternative current signals amplifiers.

Almost in all modern high linear converters the elements of autocalibration and autocorrection are available, these elements provide efficient metrological characteristics due to the possibility to compensate for the primary errors of the element base. The correction is performed in a special mode, called self calibration and enables to determine real characteristics of the analog devices, as a result of applying the structural solutions with available feedback.

The advantage of such approach is the possibility to provide high technical characteristics at the reduced requirements to the element base of the analog devices and technologies of their manufacture. The correction of static errors allows the application of circuit engineering solutions, providing high operation rate [121].

On the other hand, a high level of accuracy, achieved by means of self calibration can be provided only in case of low level of non correctable errors of the analog devices, ADC and DAC consist of. And this, in its turn, requires such an approach to the design, where along with structural solutions special circuit engineering methods, aimed at provision of high accuracy and operation rate, are used. As a result the analog devices of multiple digit ADC and DAC possess a number of features, enabling to distinguish their study in an independent branch.

It is known that ADC and DAC within IMS are used in combination with other analog devices. Provision of the corresponding characteristics of these

devices and their coordination with ADC and DAC is a rather complex problem [121, 122, 126]. Also it is known that, for the most part, there is no possibility to correct certain errors of such nodes, in spite of the inclusion of such nodes in the correction contour.

Thus, having considered the specific features of the systems of measurement and processing of the signals, we make a conclusion that in the process of practical realization of ADC and DAC with self calibration, there exists a number of problems that require separate studies of the analog devices regarding their metrological characteristics, structural and circuit engineering solutions, methods of correction. Special attention should be paid to such analog devices as: AS, NA, OA VB, CVC, VVC and others, main requirements to these devices are given in Table 2.1. In its turn, the classification of the analog devices for the analog-to-digital systems is given in Fig. 2.2.

Table 2.1. Requirements, regarding static and dynamic characteristics of the analog devices. Specific features of the structure

Linear devices	Operation rate	Linearity	Symmetry of the transient characteristics	Availability of OA
Analog switches	+	+	–	–
Buffer devices	+	+	+	+
Sample-and-hold circuits	+	+	–	–
Current-voltage converters	+	+	+	+
Voltage-voltage converters	+	+	+	+
Difference amplifiers	+	+	+	+



Fig. 2.2. Classification of the analog devices for the analog-to-digital systems

Conventionally, such analog devices are constructed on the base of the universal OA, using the corresponding connection circuits, shown in Fig. 2.3 [127, 128].

As a rule, single-step DCA, conventionally constructed according to the three-stage structure, shown in Fig. 2.4a, are used for such purposes.

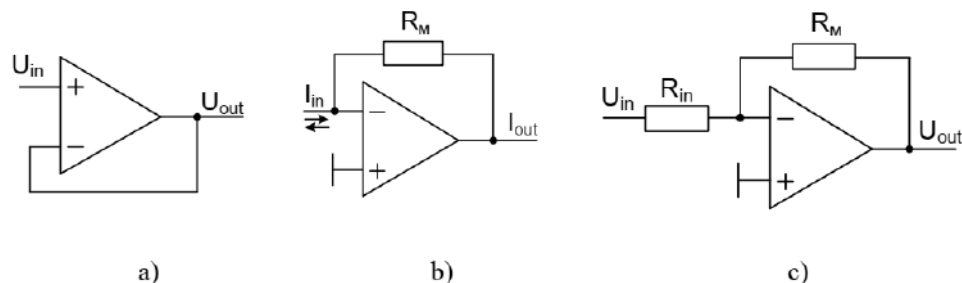


Fig. 2.3 Analog devices on the base of universal OA: a) voltage buffer; b) current-voltage converter; c) voltage-voltage converter

The basis of the greater part of modern amplifiers is the input differential stage [129–131], which allocates the difference of voltages and amplifies it. Intermediate and push-pull output stage provides the amplification of the input signal. Special attention should be paid to the fact that in single-step DCA the output stage is a push-pull one and this, in its turn, enables to increase the carrying capacity and linearity of the transfer characteristic [129–133].

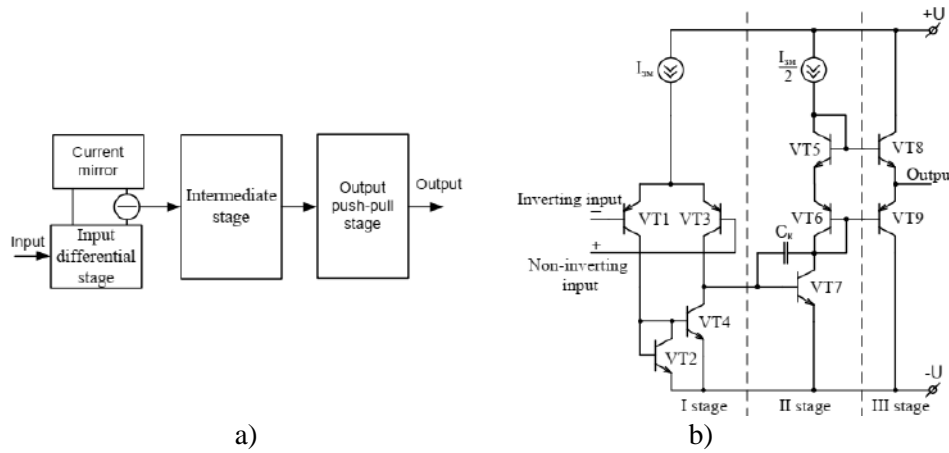


Fig. 2.4. Single-step DCA with differential input stage: a) structural diagram; b) simplified three stage flow diagram

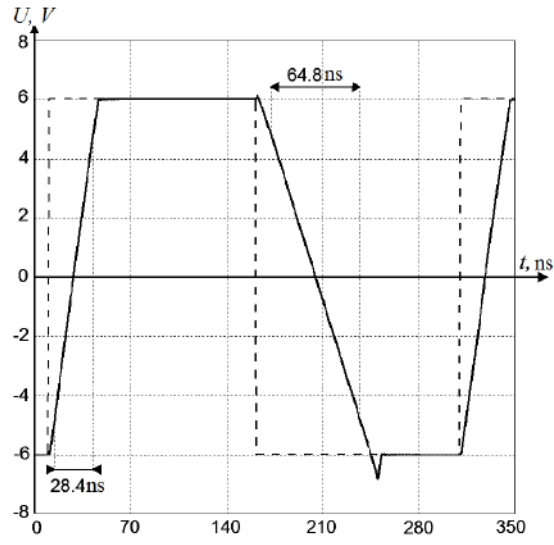
However, the application of the single-stage DCA is not very advantageous because such circuits introduce considerable distortions in the form of the signal being processed. The drawback is also different duration of the leading edge and trailing edge of the pulse signal and narrow band of the complete non-distorted power [134], as it is shown in Fig. 2.5. Recently for the construction of the analog devices with the wide bandwidth the so-called current conveyors, with the corresponding switching circuits such as DCA, VB, CVC, VVC, shown in Fig. 2.6 [135–142] are used.

The characteristics of such devices are described by the relations:

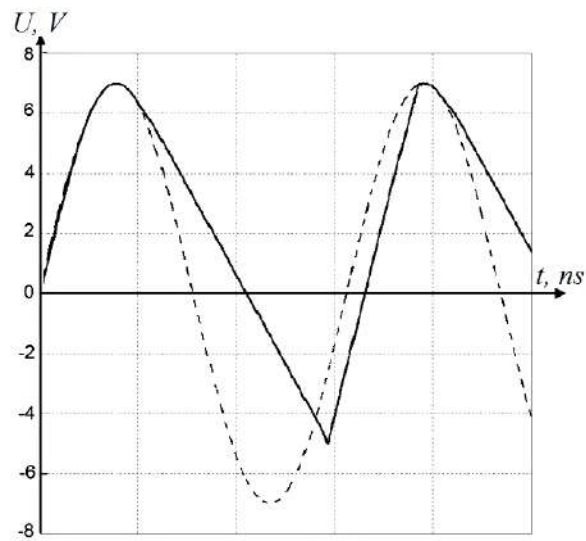
$$\begin{aligned}
 \text{DCC: } I_{out} &= I_{in} \cdot \frac{R_1}{R_2}; & \text{VB: } U_{out} &= U_{out} \cdot \frac{R_{load}}{R_1}; \\
 \text{VCC: } U_{out} &= -I_{in} \cdot R_1; & \text{VVC: } U_{out} &= U_{in} \cdot \frac{R_{load}}{R_1}.
 \end{aligned}$$

As it is known, frequency operation range of OA-based circuits is limited by FBC. The increase of the dynamic and frequency ranges of the analog devices can be realized in the process of transition to signal processing in the current basis [134, 143]. Circuit, operating in the current basis, has smaller resistance values in the nodes. Thus, maximum voltage values in the internal nodes of the circuits are smaller than signal processing in the voltage basis.





a)



b)

Fig. 2.5. Limitations of the dynamic characteristics of the single-stage DCA: a) symmetry of the transient characteristics; b) distortion of the sinusoidal output signal

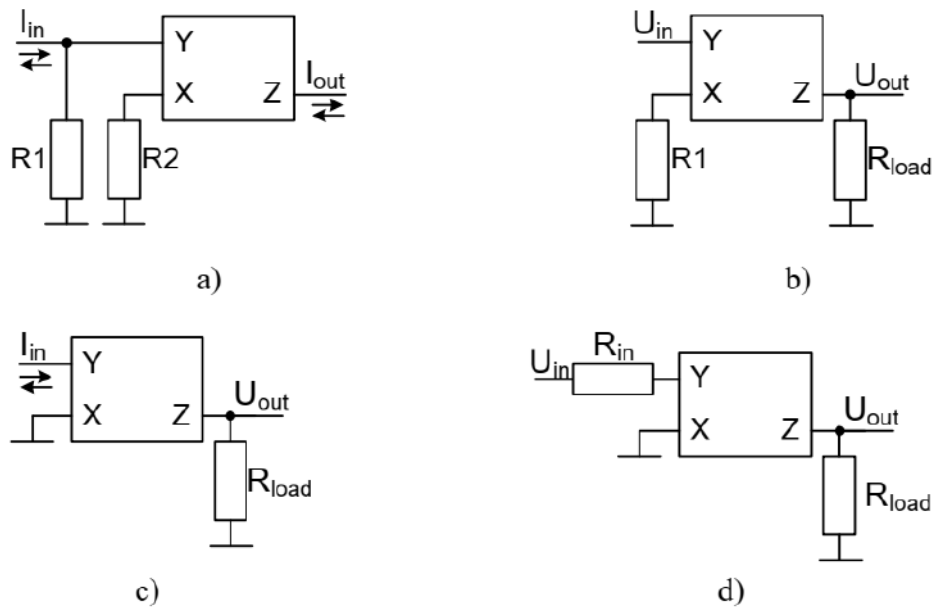


Fig. 2.6. Analog devices on the base of CC : a) direct current amplifier; b) voltage buffer; c) current –voltage converter; d) voltage- voltage converter

This leads to the decrease of non-linear distortions and increase of the dynamic range. Besides, as the parasitic capacitances are charged to smaller voltage values, the signal processing rate increases and the operation frequency range also increases.

CC (current converters) of the first generation (CCI) was suggested for the first time in 1968, however as an independent element it did not gain wide usage. In 1970 the CC of the second generation was realized (CCII) [136]. Such CCII are constructed according to the pull-push structure (Fig. 2.7a) both on bipolar (Fig. 2.7b) and field-effect transistors (Fig. 2.7c).

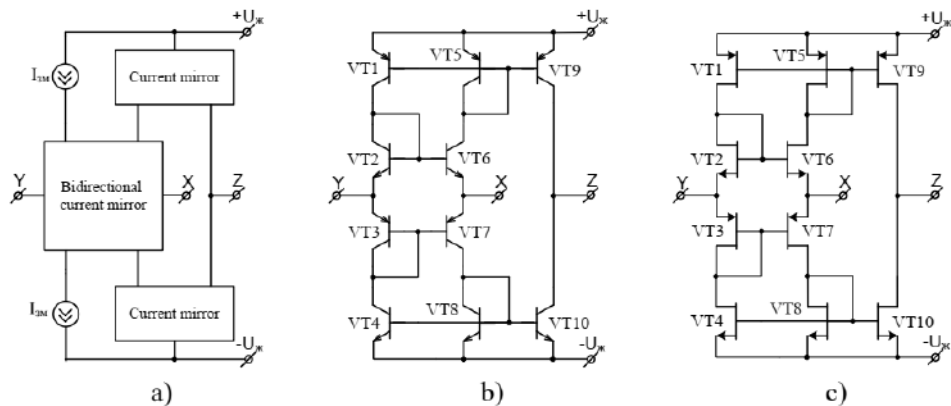


Fig. 2.7. Current converter II: a) generalized structural diagram; b) on bipolar transistors; c) on field-effect transistors

CCII operates according to the relations:

$$U_X = k \cdot U_Y; I_Y = 0; I_Z = \pm a \cdot I_X,$$

where  $U_x, U_y$  – are voltages at the inputs X and Y, correspondingly;  $I_x, I_y, I_z$  – are currents at the inputs X, Y, Z correspondingly;  $k$  and  $a$  – are the coefficients of voltage and current transfer.

The parameters, characterizing CC are the coefficients of voltage and current transfer  $k$  and  $a$  (in an ideal case they equal unit) and the resistances at the outputs X and Y (in an ideal case, the resistance at the output X approaches infinity, the resistance at the output X – tends to zero).

Sign “+” or “-” in the expression for current  $I_z$  defines the type of the current conveyer – non-inverting (CCII+) or inverting (CCII-), correspondingly. Non Inverting is a conveyer where the currents at the outputs X and Z are directed simultaneously in the conveyer or “from” the conveyer.

As the current repeater in current conveyer II+ (CCII<sup>+</sup>) the CR is used. For the realization of CCII<sup>-</sup> the CCII<sup>+</sup> with the simplest CR, connected to the output Z, is used.

However, the introduction of this element in the circuit results in the worsening of CCII characteristics – as compared with the output circuit of CCII<sup>+</sup> without the additional current mirror. Thus, for the realization of the precision CCII<sup>-</sup> it is necessary to use more complex circuits of current repeaters with the inversion.

In 1995 CC of the third generation (CCIII) was suggested [142]. CCIII are constructed on the base of four CCII and are mainly used for the currents measurements (Fig. 2.8).

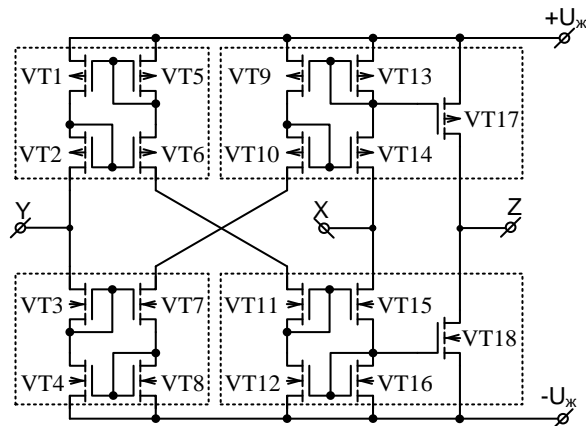


Fig. 2.8. Current conveyor III of field-effect transistors

CC possesses the bands of operating frequencies of the order of hundreds of megahertz that substantially exceeds bands of operating frequencies of OA. This is explained by the absence of stages with large gain factors. At the same time, there is no need to connect the correction circuit that considerably decreases the band of OA operating frequencies .

The conclusion can be drawn that the realization of the circuits on the base of CC enables to increase the frequency range of the amplifiers and devices on their base to tens-hundreds megahertz if the consumed power does not exceed the consumed power of OA. The following drawbacks of CC should be mentioned:

- transfer factor on the current is close to the unit;
- introduction of the additional phase shifts ;
- worsening of the amplification on the stage of the operation system.

Another approach to the construction of DCA is the usage of the push-pull structures. It should be noted that the first PDCA were constructed as far back as in the 1970s [144–145]. However, they were imperfect as they had limited number (1-2) of the amplifying stages and small gain factor. One of the reasons was that in the above-mentioned circuits with multistage structure (2–3) it is difficult to set the needed mode on the direct current. Thus, it was impossible to make use of the advantages provided by PDCA with the symmetrical structure. The alternative approach is the construction of PDCA with loop-through amplification channels [122, 127, 143], its structural diagram is shown in Fig. 2.9, that enables it to achieve the symmetry of the leading edge and trailing edge of the output signal.

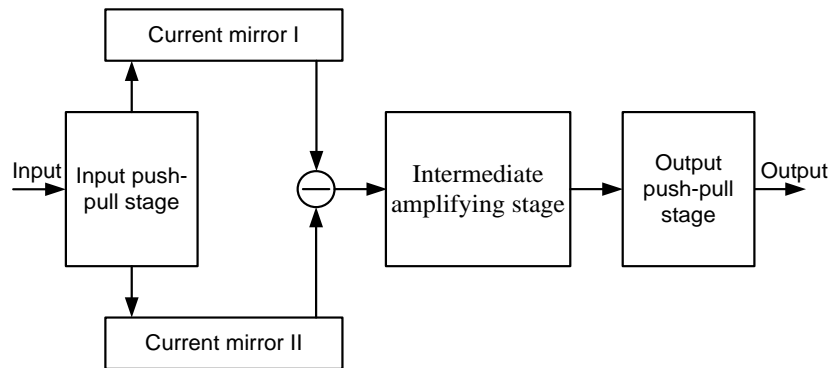


Fig. 2.9. Structural diagram of modern PDCA with the loop-through amplification channel

Characteristic feature of the given approach is the usage of CR, which determines the increment of the current flowing across the input stage.

The construction of such types of the devices started as far back as in the 1980s and became popular due to the simplicity and cheapness of IAS working point setting and the possibility of the balancing of the leading edge and trailing edge of the output signal at the reaction on the bipolar rectangular input pulse.

It is known, that Analog Devices company manufactures PDCA AD810–AD815, Intersil – EL5160–5165, ON Semiconductor – NCS2501, NCS2510, NCS2511, NCS2530 and NCS2535 [146–159]. Their basic characteristics are shown in Table 2.2.

Table 2.2 – Characteristics of the modern PDCA with the loop-through amplification channels

Model	Bandwidth, MHz	Slew rate, V/ms	Input offset voltage, mV	Input offset current, mA	Distortion/Frequency, dB/ MHz.
AD810	80	1000	1.5	2	-61/5
AD811	140	2500	0,5	2	-74/5
AD812	145	425	2	0,3	-90/1
AD813	100	250	2	0,5	-90/1
AD815	120	900	10	2	-66/1
EL5160	200	1700	5	-	-50/5
EL5161	200	1700	5	-	-50/5
EL5162	500	4000	5	-	-50/5
EL5163	500	4000	5	-	-50/5
EL5164	600	4700	5	-	-73/5
EL5165	600	4700	5	-	-73/5

Model	Bandwidth, MHz	Slew rate, V/ms	Input offset voltage, mV	Input offset current, mA	Distortion/Frequency, dB/ MHz.
NCS2501	200	450	4	4	-55/5
NCS2502	110	230	4	20	-49/5
NCS2510	1400	2500	4	35	-69/5
NCS2511	1000	2500	10	35	-67/5
NCS2530	200	450	4	5	-55/5
NCS2535	1400	2500	10	35	-69/5

Analyzing the Table we make a conclusion that PDCA, constructed according to the considered structure, possesses good dynamic characteristics. At the same time, it is worth mentioning that the general gain factor determines IAS and PPOS, as CR has the transfer coefficients close to unit and OPPOS –  $\frac{1}{2}$  [131]. The enhancement of the gain factor is possible by means of increasing the amount of the amplifying stages, but the usage of the great quantity of IAS leads to great phase shifts, the correction of these shifts P will result in the reduction of PDCA operation rate [160–164]. The drawback of such circuits is the possibility of operation only with low ohmic loading and great dependence of the gain factor on the loading resistance [122, 127, 143]. The corresponding AFC is shown in Fig. 2.10.

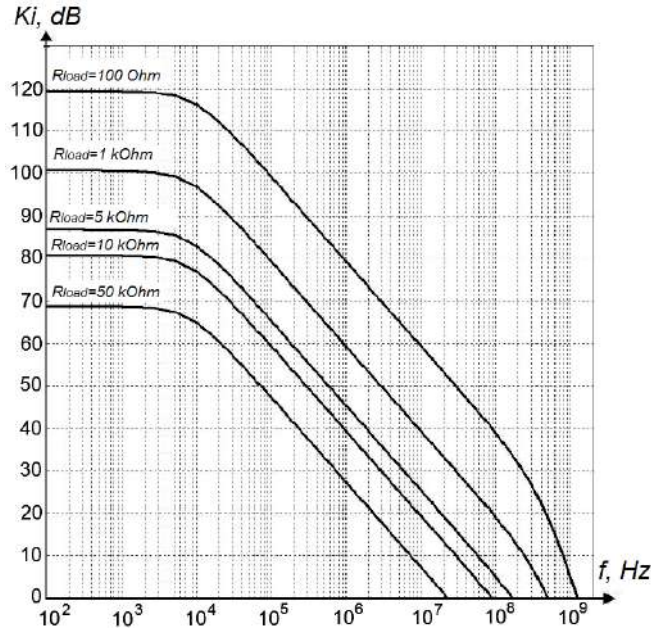


Fig. 2.10. AFC of PDCA with the loop-through amplification channel at the change of the load resistance

The solution of the problem of direct current mode setting was suggested in the scientific school of the professor Olexiy Azarov by means of introduction in the circuit current compensators(CC), which provide identical operation modes of DCA stages [134, 165]. This enabled the construction of PODCA with the separated amplification channels, characteristic feature of these channels is the available auto balancing of the operating points of the intermediate transistor stages.

Structural organization of such PDCA is shown in Fig. 2.11 [166].

For the construction of PDCA with average gain factor, structural diagram, shown in Fig. 2.11a, is used. It contains: IPS, two symmetrical IAS on the bipolar p-n-p and n-p-n transistors, BDCR and POS. Gain factor will be determined by the formula [166]:

$$K_i = K_{iinp} \cdot K_{iis} \cdot K_{iout} = \frac{2 \cdot \beta_{p-n-p}^2 \cdot \beta_{n-p-n}^2}{\beta_{p-n-p} + \beta_{n-p-n}},$$

where  $K_{inp}$ ,  $K_{is}$ ,  $K_{iout}$  – are current gains of the input, intermediate and output stages, correspondingly;  $\beta_{p-n-p}$ ,  $\beta_{n-p-n}$  – are current gains of the bipolar p-n-p and n-p-n transistors, correspondingly.

For the construction of PDCA with high gain factor, structural diagram, shown in Fig. 2.11b is used. It contains: IPS, two symmetrical IAS on bipolar p-n-p and n-p-n transistors, several BDCR and POS.

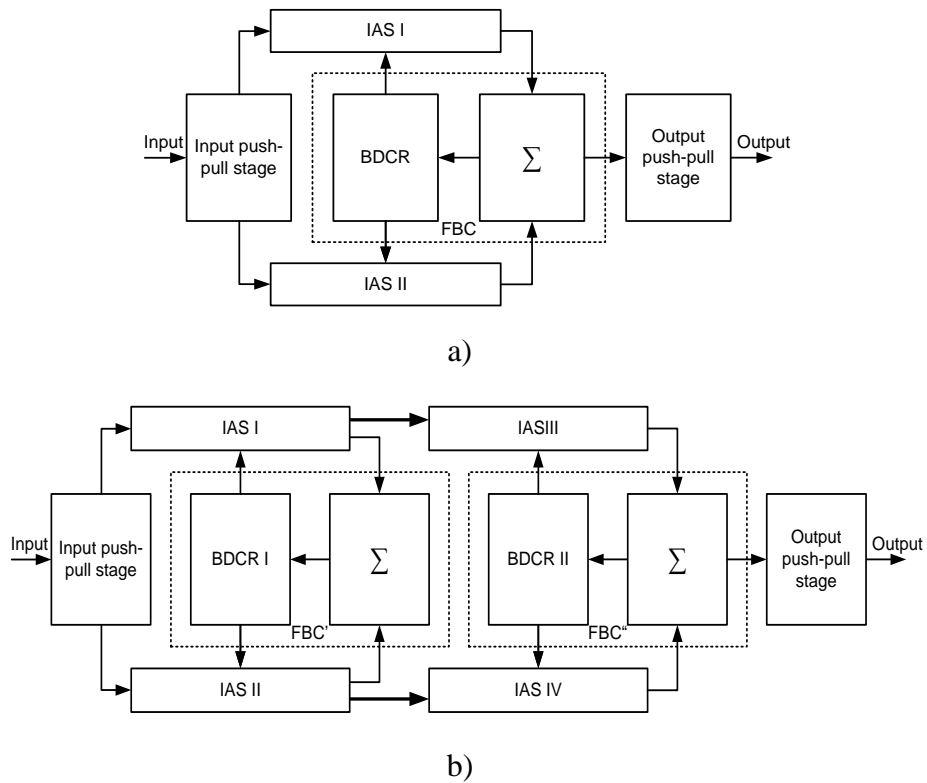


Fig. 2.11. Structural diagram of PDCA with separated amplification channels: a) with average gain factor; b) with high gain factor

Gain factor is determined by the formula [166]:

$$K = K_{iin} \cdot K_{is_{\Sigma}} \cdot K_{iout} = \frac{2 \cdot \beta_{p-n-p}^2 \cdot \beta_{n-p-n}^2 \cdot \beta_1' \cdot \beta_2' \cdot \beta_1'' \cdot \beta_2''}{\beta_{p-n-p} + \beta_{n-p-n} \cdot (\beta_1' \cdot \beta_2' + \beta_1'' \cdot \beta_2'')},$$



where  $K_{i\Sigma}$  – is total current gain of the intermediate stages;  $\beta_1', \beta_2'$  – are current gains of the bipolar transistors of the first stage;  $\beta_1'', \beta_2''$  – are current gains of the bipolar transistors of the second stage.

Increasing the number of the amplifying stages and, correspondingly, increasing  $K_i$ , application of the symmetrical structure and BDCR in the amplifying stages enables the construction of DCA with high gain factors. [165,166]. However, multistage circuits have worse dynamic characteristics, in particular, greater number of the poles of AFC and considerable phase shifts of the output signal [134]. That is why, the design of the multistage PDCA with the above-mentioned gain factor should be performed with a minimal amount of stages.

At the same time, it is worth mentioning the advantages that could be achieved constructing DCA, using push-pull structures:

- high operation speed;
- symmetrical transient characteristic at the reaction on the input bipolar pulse;
- high Slew rate;
- large bandwidth;
- maximum usage of the frequency properties of the transistors up to boundary frequency  $f_t$ .

The developers of the analog-to-digital systems often face the problem, dealing with the choice of the amplifier, which operates with low errors of constant level transmission. The problem of signal matching also remains in the focus of the developers' attention, as the current DAC the circuit of OA switching is used as CVC, whereas for DAC with voltage output VB and VVC switching circuits are used (see Fig. 2.3).

Efficient approach to the construction of such kinds of analog devices is the usage of the transimpedance amplifiers [167]. They combine both high linear direct current parameters and excellent characteristics of alternating signal amplification.

The advantages of the transimpedance amplifier of the resistances as compared with the conventional OA are determined by the character of the basic structures of these devices. Transimpedance amplifier (Fig. 2.12a) is the controlled source of voltage with asymmetric output, controlled by the current, passing across asymmetric input. It should be mentioned that the inverting and non-inverting inputs of such amplifiers are nodes with small and large resistance, correspondingly. Input resistance  $R_{inp}$  determines the gain factor of

the circuit with closed feedback. The transfer function in the form of Laplace transform of such amplifier is:

$$G(s) = \frac{-\frac{R_m}{R_{in}}}{1 + C_c \cdot \left[ R_m + \left(1 + \frac{R_m}{R_{in}}\right) \cdot r_{in} \right] \cdot s},$$

where  $R_m$  – is the resistance of the feedback resistor;  $r_{in}$  - is the internal input resistance;  $C_c$  – is the internal capacitance of the correction. Gain factor of the device is determined by the set  $\left(1 + \frac{R_m}{R_{in}}\right) \cdot r_{in}$  of the denominator.

Conventional OA (Fig. 2.1b) is a device with a symmetrical input and asymmetrical output. Inverting and non-inverting inputs are identical and have high resistance. Gain factor with the closed feedback depends both on  $R_{inp}$  and  $R_m$ . Transfer function in the form of the Laplace. Transform of such amplifier is:

$$G(s) = \frac{-\frac{R_m}{R_{in}}}{1 + \frac{C_c}{g_{in}} \cdot \left[ 1 + \frac{R_m}{R_{in}} \right] \cdot s}.$$

In this expression the main impact on the gain factor is performed by the multiplier of  $1 + \frac{R_m}{R_{in}}$ . The circuit, set by the gain factor, also influences the frequency characteristic of the amplifier.

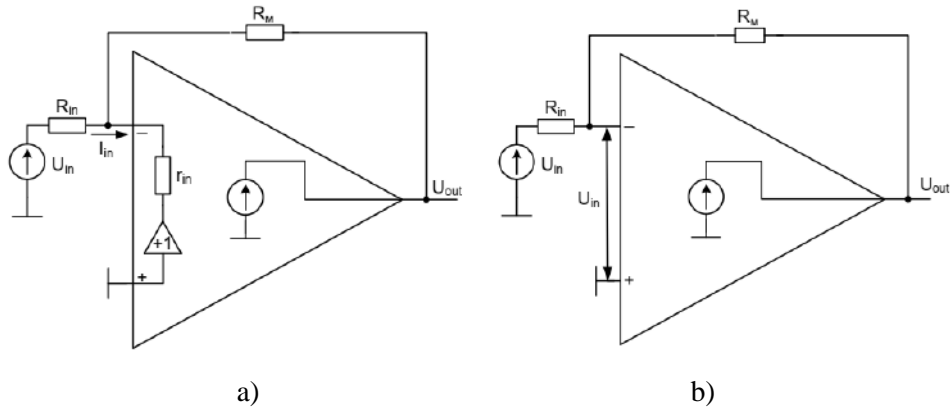


Fig. 2.12. Equivalent circuits of the DCA in the modes of : a) transimpedance amplifier; b) operation amplifier

In the conventional OA with the closed feedback at the increase of amplification the bandwidth proportionally decreases. Transimpedance amplifiers, on the contrary, provide relative independence of the values of the bandwidth and amplification when the feedback circuit is closed at low values of amplification, nearly 20-30. When the gain factor starts to grow, then the frequency characteristic of the transimpedance amplifier behaves as the characteristic of OA.

Characteristics of these circuits on the changing signal have differences in the circuit configurations. In OA (see Fig. 2.4b) the first stage transforms the differential input voltage between the inverting and non-inverting inputs into the asymmetric output voltage. The second stage amplifies this voltage, and the third – forms the preset current in the external loading circuits. High resistance input stage worsens certain parameters of OA at the amplification of the changing signals. Incompliance between the resistance of the signal source and the input resistance of the first stage of the amplifier creates a parasitic pole, which causes the distortion of the output signal. This influences the bandwidth and worsens the linearity and distorts the form of the output signal.

Besides, negative feedback in the ordinary OA creates quasizero potential at the inverting input, which enables us to consider this point to be virtual earth. For the stability of the amplifier with the negative feedback phase-correcting circuits are to be introduced, for instance, the circuit with feed forward high frequency components. The feed forward correction breaks the linearity of the phase characteristic of the amplifier.

Unlike OA transimpedance amplifiers (Fig. 2.13) has different inputs: inverting input, connected to the emitter of two complementary transistors VT4 and VT5, which form the point with low resistance, non-inverting input – between two serially connected transistors VT1 and VT2 in the diode connection. This input

is characterized by the high resistance and by its parameters is analogous to the inputs of OA.

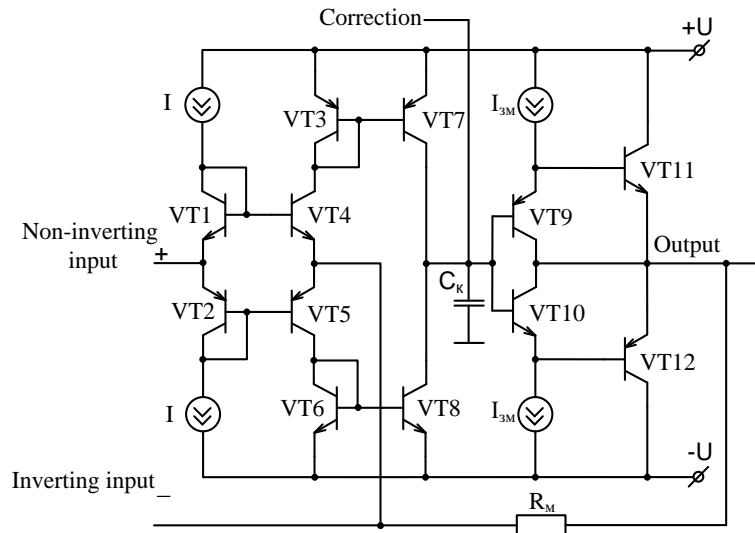


Fig. 2.13. Schematic organization of the transimpedance amplifier

In the process of the amplifier operation the error current across the resistance  $R_m$  arrives at the inverting input. Transistors VT4 and VT5 deliver it to CR, constructed on the transistors VT3, VT6, VT7 and VT8. Complementary currents, set by the transistors VT7 and VT8, charge the capacitor  $C_c$ . Finally, the output stage on the transistors VT9, VT10, VT11 and VT12 performs the functions of buffer amplifiers between  $C_c$  and the load. Besides converting the current into the voltage the capacitor  $C_c$  maintains the stability of the amplifier, preventing self-excitation at high frequencies.

Current feedback in the transimpedance amplifier gives a number of important advantages, providing the stability of the bandwidth, increasing the linearity of the phase characteristics, increasing the growth rate and providing the symmetry of the output signal fronts.

The stability of the bandwidth is one of the most important advantages of the given circuit for numerous spheres of application. As the error signal, which is formed by the resistor  $R_m$ , arrives at the input of the circuit in the form of the current but not voltage, then the transimpedance amplifier does not require the negative feedback for the creation of virtual earth on the inverting input. As a result, there is no need to have the correction circuits, which can influence the bandwidth. What is more, if the resistance of the resistor  $R_m$  is maintained constant, the bandwidth of the amplifier with the closed feedback will be fixed,

regardless of the value of the gain factor. Besides, transimpedance amplifiers provide the linearity of the phase characteristic in a wide range of frequencies.

The circuit with the current feedback provides the symmetry of the leading and trailing edges of the transient characteristic. The growth of the output signal of the transimpedance amplifier rapidly increases at the advent of the input current. The rapid growth of the input level will lead to the initiation of one part of the amplifier and disconnection of another part, i.e., causing the switching of two identical sources of current. As a result, for any preset amplitude of the output voltage the hours of rise and fall turn out to be practically equal.

Another advantage of the transimpedance amplifier is small non-linear distortions. This is explained by the fact that the transistors of such a scheme perform the functions of the current amplifiers but not voltage. As the bipolar transistors according to their operation principle are current devices, they operate in a linear mode with minimal harmonic and intermodulation distortions.

Thus, as compared with the existing OA, transimpedance amplifiers have smaller levels of distortions, large bandwidth and symmetry of the reaction on the bipolar rectangular input pulse. The advantages of the transimpedance amplifiers are determined namely by the push-pull structure of such devices. CVC and VVC, constructed on the basis of devices exceeding by their characteristics CVC and VVC, constructed on the basis of OA.

Generalizing the material, considered in the given section, it is expedient to note that the promising direction in the construction of high linear analog devices for the systems of measurement, registration and processing of signals is the application of the push-pull structures. At the same time, in spite of the variety of the existing models of high linear devices, manufactured by leading world-known companies, in particular Analog Devices, National Semiconductor, Texas Instruments, Linear Technology, ON Semiconductor, Philips, Inetrstil [122, 128], there exist possibilities of the further improvement of their characteristics.

## **2.2. Analysis of the static and dynamic errors of the analog devices in the converting paths of the analog-to-digital systems**

The basis of the multi digital analog-to-digital systems is highlinear, system ADC and DAC, which, in their turn, contain analog devices. The latter greatly influence the static and analog characteristics of the analog-to-digital systems on the whole.

Considering the structures of the systems of measurement, registration and processing of signals, shown in Fig. 2.1, we can distinguish AD and DA channels [168], generalized structure of which is shown in Fig. 2.14.

At the same time, any AD channel can be presented in such a way that various errors are imposed at the input signal  $A_{inp}$  under the impact of the internal factors and the factors of the environmental character [129, 130, 169, 170]:

- for AS:  $\Delta_{0AS}$  – zero,  $\Delta_{LIN AS}$  – integral linearity;
- for B:  $\Delta_{0B}$  – zero,  $\Delta_{LIN B}$  - integral linearity;
- for IA:  $\Delta_{0IA}$  – zero,  $\Delta_{LIN IA}$  - integral linearity,  $\Delta_{S IA}$  – scale;
- for ADC:  $\Delta_0$  – zero,  $\Delta_{INT}$  - integral linearity,
- $\Delta_{DIF}$  - differential linearity,  $\Delta_S$  – scale.

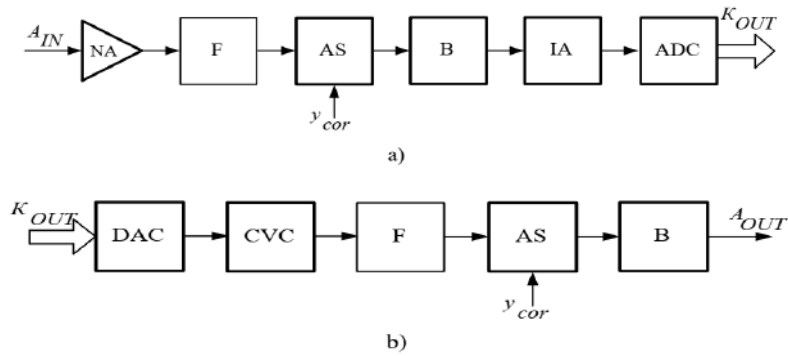


Fig. 2.14. Generalized structure of the channels of the multidigital systems of measurement, registration and processing of self-calibrated signals: a) AD-conversion; b) DA-conversion

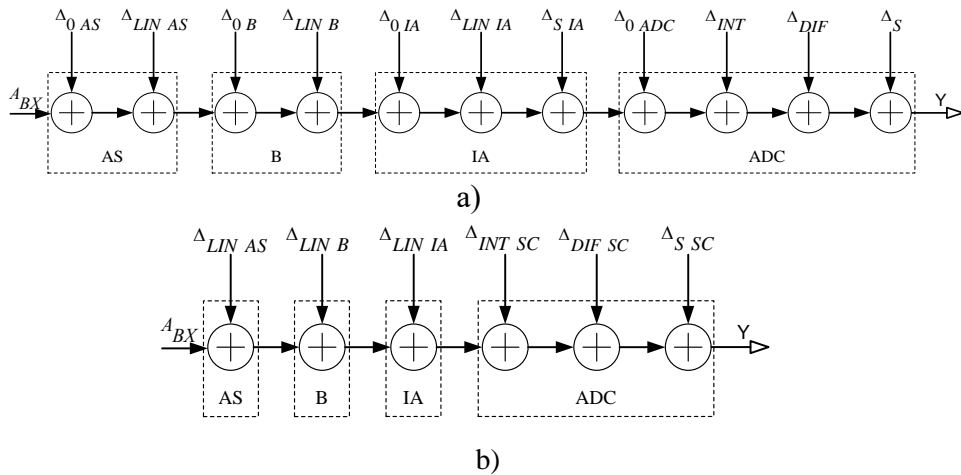


Fig. 2.15. Model of error components of the loop-through channel of AD-conversion: a) prior the calibration; b) after the calibration

For the account of these statistical errors, the model of the error components of the loop-through channel of AD-conversion can be built, the model is shown in Fig. 2.15a.

At the output of AD-conversion channel prior the calibration the signal contains the errors of the analog nodes, each separate analog node introduces such components [171]:

$$\Delta_{\Sigma AS} = \sqrt{\Delta_{0AS}^2 + \Delta_{LIN AS}^2} \text{ – for the analog switch;}$$

$$\Delta_{\Sigma B} = \sqrt{\Delta_{0B}^2 + \Delta_{LIN B}^2} \text{ – for the buffer;}$$

$$\Delta_{\Sigma IA} = \sqrt{\Delta_{0IA}^2 + \Delta_{LIN IA}^2 + \Delta_{S IA}^2} \text{ – for program amplifier;}$$

$$\Delta_{\Sigma ADC} = \sqrt{\Delta_{0ADC}^2 + \Delta_{INT}^2 + \Delta_{DIF}^2 + \Delta_S^2} \text{ – for the ADC.}$$

Total error consists of the sum of errors, added by each separate node of the channel and is determined as [171]

$$\Delta_{\Sigma} = \sqrt{\Delta_{\Sigma AS}^2 + \Delta_{\Sigma B}^2 + \Delta_{\Sigma IA}^2 + \Delta_{\Sigma ADC}^2} .$$

This can lead to considerable distortion of the input signal  $A_{inp}$ . For the correction of AD conversion error self-calibration can be used. However, when this procedure is used only so-called correction errors are eliminated.

At the same time, additional methodical errors can appear (Fig. 2.15b).

In DA-channel as a result of available primary errors of analog nodes elements as well as in the process of operation under the impact of the internal environment factors such error components appear:

- for code – current converter (CCC):
- $\Delta_{dig}$  – superpositions of digit weights,
- $\Delta_{qun DAC}$  – quantization,  $\Delta_{inj}$  – integral linearity,
- $\Delta_{DIF}$  - differential linearity,  $\Delta_{O DAC}$  – zero,
- for CVC:  $\Delta_{O CVC}$  – zero,  $\Delta_{LIN CVC}$  - integral linearity,
- for AS:  $\Delta_{OAS}$  – zero,  $\Delta_{LIN AS}$  - integral linearity,
- for B:  $\Delta_{OB}$  – zero,  $\Delta_{LIN B}$  - integral linearity.

The model of the error components of the loop-through channel of DA-conversion is shown in Fig. 2.16a.

At the output of DA-conversion channel prior to calibration signal  $A_{out}$  contains errors of the analog nodes of DA-conversion channel and each separate analog node introduces such error [171]:

$$\Delta_{\Sigma DAC} = \sqrt{\Delta_{dig}^2 + \Delta_{qun DAC}^2 + \Delta_{INT}^2 + \Delta_{DIF}^2 + \Delta_{0 DAC}^2}$$
 – for code-current converter;

$$\Delta_{\Sigma CVC} = \sqrt{\Delta_{0 CVC}^2 + \Delta_{LIN CVC}^2}$$
 – for current-voltage converter;

$$\Delta_{\Sigma AS} = \sqrt{\Delta_{0 AS}^2 + \Delta_{LIN AS}^2}$$
 – for analog switch;

$$\Delta_{\Sigma B} = \sqrt{\Delta_{0 B}^2 + \Delta_{LIN B}^2}$$
 – for buffer.

Thus, total error consists of the sum of errors, added by each separate node of the channel and is determined as [171]

$$\Delta_{\Sigma} = \sqrt{\Delta_{\Sigma CCC}^2 + \Delta_{\Sigma CVC}^2 + \Delta_{\Sigma AS}^2 + \Delta_{\Sigma B}^2}.$$

For their correction self-correction can be used (see Fig. 2.16b).

Analyzing the models of the static errors of the loop-through channels of the AD and DA conversion (see Fig. 2.15 and Fig. 2.16) main types of errors of the analog devices can be distinguished: scale, zero shift and linearity.

At the same time, all the static errors, emerging in AD and DA-converting channels may be divided into the categories, shown in Table 2.3 [121, 127, 169]:

- correctable – i.e., those, that could be considerably decreased;
- partially correctable – these are errors, which could be corrected to certain acceptable level;
- non-correctable – those, which cannot be decreased or compensated, by means of self-calibration. Simultaneously, they can be decreased, applying circuit engineering solutions or structurally.

To eliminate the correctable errors the procedure of self-calibration can be applied. This operation can efficiently be performed in CIF on the base of calculus systems with weight redundancy [127,169]. It is worth mentioning that when the self-calibration is applied, these errors become apparent mainly in the form of partially correctable errors. But they are of minor importance as compared with the errors, emerging as a result of the parameters change of analog unit's elements.



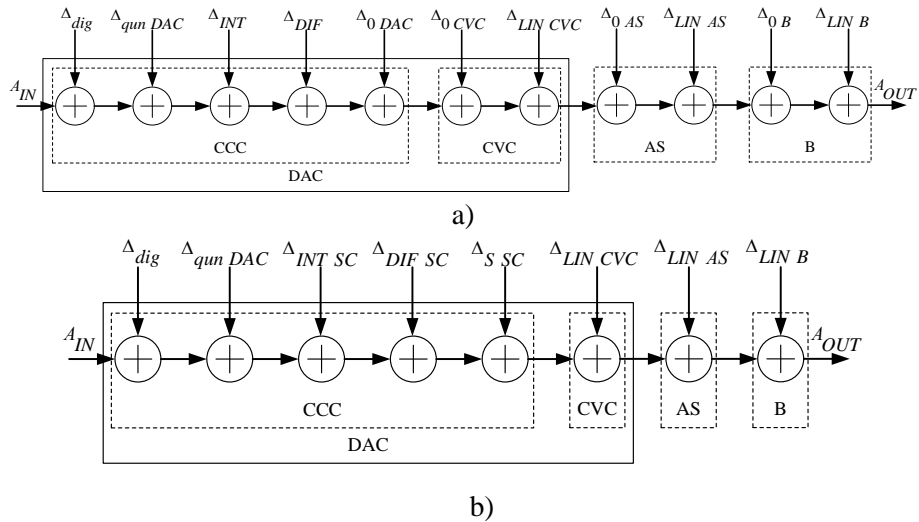


Fig. 2.16. Model of loop-through channel of DA-conversion error components

At the same time the advantage of self-calibration as compared with other methods of correction, namely, the lack of the necessity to perform self-calibration separately for each analog node, should be underlined. As all the above-mentioned nodes are covered by the general FBC, the procedure takes place for the whole system.

It is worth mentioning that the error of the integral linearity hypothetically is possible to correct, but the process requires considerable software-hardware expenditures, in its turn, this leads to complication of the self-calibration path and increase of the end product price [121]. This is the reason why this kind of error for the greater part of cases is referred to as non-correctable.

Dynamic characteristics of the analog-to-digital systems are greatly determined by the parameters of the analog devices, which are the components of these systems. That is why it is expedient to analyze their characteristics.

As it is known, a greater part of the analog nodes is constructed on the base of the single-stage DCA, connected according to the circuits, shown in Fig. 2.3 DCA, themselves possess their specific static errors, shown in Fig. 2.17.

Table 2.3. Static errors of the converting channels

Correctable errors	Non-correctable errors	Partially correctable errors
1. Zero shift: $\Delta_{0AS}$ , $\Delta_{0B}$ , $\Delta_{0IA}$ $\Delta_{0ADC}$ , $\Delta_{0DAC}$ , $\Delta_{0CVC}$ . 2. Scale: $\Delta_{SIA}$ , $\Delta_S$ , $\Delta_{SSC}$ . 3. Differential linearity: $\Delta_{DIF}$ .	1. Integral linearity: $\Delta_{LINAS}$ , $\Delta_{LINB}$ , $\Delta_{LINIA}$ , $\Delta_{LINCVC}$ . 2. Quantizing DAC: $\Delta_{qunDAC}$ . 3. Superposition of digits weights $\Delta_{dig}$ . 4. Integral non-linearity of self-calibration $\Delta_{INTSC}$ .	1. Integral linearity DAC: $\Delta_{INT}$ . 2. Differential non-linearity of self-calibration: $\Delta_{DIFSC}$ .

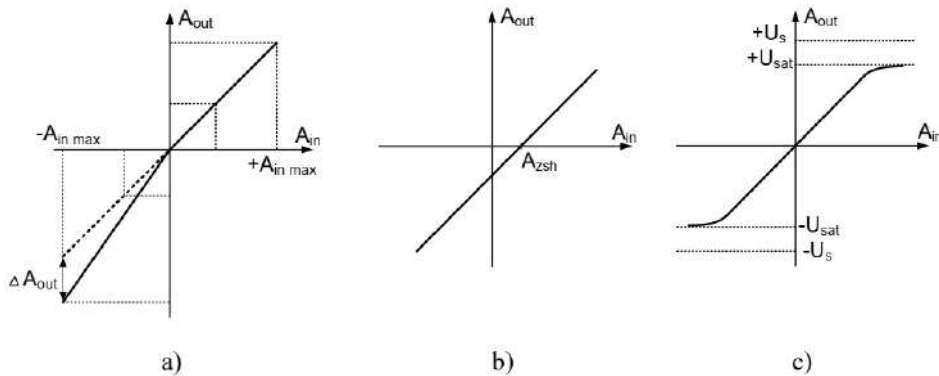


Fig. 2.17. Types of distortions of the transfer characteristic of DCA: a) asymmetry  $K_i$ , if the polarity of  $A_{inp}$  changes; b) zero shift; b)  $A_{out}$  range limitation

In this case the equalities occur:

$$\Delta A_{out} = A_{out}(+A_{in\ max}) - A_{out}(-A_{in\ max});$$

$$\Delta A_{zsh} = A_{out} - A_{in};$$

$$\Delta U_{out} = A_{out}(+U_{sat}) - A_{out}(-U_{sat}).$$

As a rule, achieving the high level of accuracy is provided by the increase of the FB depth that requires AFC and PFC correction and, correspondingly, results in the decrease of operation speed and the bandwidth. Better indices possess PDCA with the loop-through amplification channels, which are characterized by the symmetry of the output signal fronts and the simplicity of setting the amplifying stages modes. However, the drawback of such circuits is great dependence of the gain factor on the resistance of the load [122,128,143]. The best indices for the construction of high linear analog devices possess the PDCA with the distributed amplification channels, where the level of non-correctable errors decreases but the usage of the existing PDCA requires precise setting of the working point current of the amplifying stages but it is problematic.

### **2.3. Circuit organization and the errors of the existing push-pull current amplifiers**

#### **2.3.1. Push-pull current amplifiers with the parametric setting of the working points**

Taking into account the fact that the promising direction in the construction of high linear analog devices is the usage of the push-pull structures, it is expedient to perform the analysis of the possibilities of the construction of such devices on the base of PDCA. We will analyze the electric parameters of the simplest functional circuit of PDCA, shown in Fig. 2.18.

It contains IPPS, constructed in the form of a self-complementing circuit with the general base on the transistors VT1 and VT2. On the bases of these transistors the bias voltages  $-U_{bv}$  and  $+U_{bv}$  are supplied for setting the working point mode. The point of connection of the transistors VT1 and VT2 emitters serves as the input of the circuit. Sources of the currents  $I_3$  and  $I_4$  set the bias current in the collectors and emitters of the input transistors VT1 and VT2 correspondingly. DCA also contains the distributed IAS, constructed on the transistors VT3 and VT4. The connection point of the collectors of these transistors serves as the output of the amplifier. The circuit is connected to two sources of the supply voltage  $+U_s$  and  $-U_s$ , correspondingly [165].

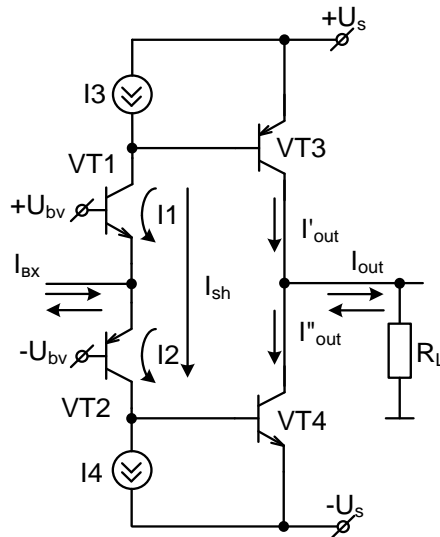


Fig. 2.18. Simplified functional diagram of PDCA with the distributed intermediate stages

It is known that the transfer characteristics of the first stage will have the form [165].

$$I_1 = -\frac{1}{2}I_{in} + \sqrt{\frac{I_{in}^2}{4} + I_0^2}. \quad (2.1)$$

Similarly

$$I_2 = \frac{1}{2}I_{in} + \sqrt{\frac{I_{in}^2}{4} + I_0^2}. \quad (2.2)$$

Fig. 2.19 presents the graph of  $I_1$  and  $I_2$  dependence on  $I_{in}$ . It illustrates how the current at the input of the amplifier is divided into the components, which is branched into the collectors VT1 and VT2. The values of  $I_1$  and  $I_2$  are determined by the volt-ampere characteristic of the transistors and depend on their power [165].

For the increments of the currents  $\Delta I_2 \approx I_2 - I_0$  and  $\Delta I_1 \approx I_1 - I_0$ , the dependence, shown in Fig. 2.20, takes place. It should be noted that the functions  $\Delta I_1 = f(I_{in})$  and  $\Delta I_2 = f(I_{in})$  have two zones:

1)  $|I_{in}| \leq 2I_0$  - small signal; 2)  $|I_{in}| > 2I_0$  - zone of a large signal.

In the first zone:  $\Delta I_2 \approx \frac{1}{2}I_{in}$ . In the second  $\Delta I_2 \approx I_{in} - I_0$ .

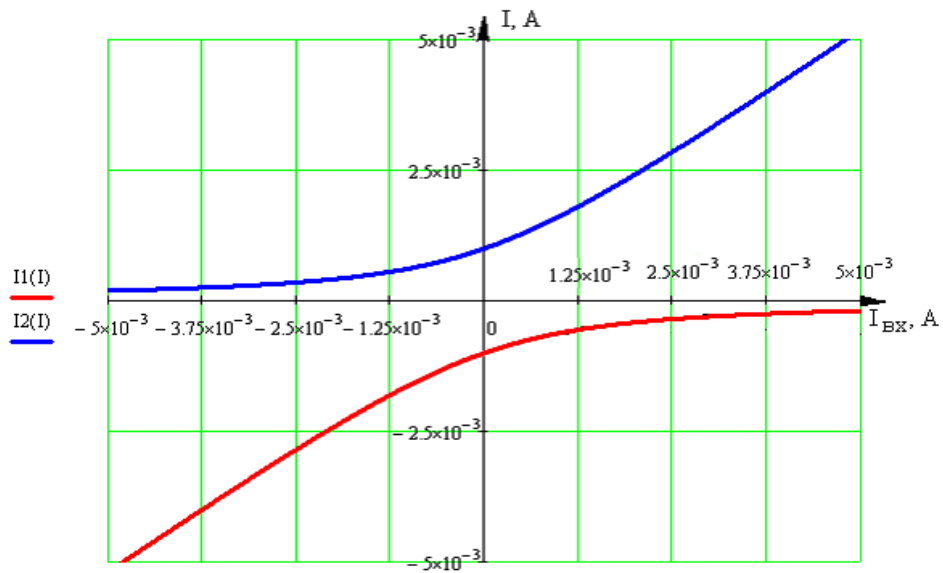


Fig. 2.19. Dependence  $I_1$  and  $I_2$  on  $I_{\text{inp}}$

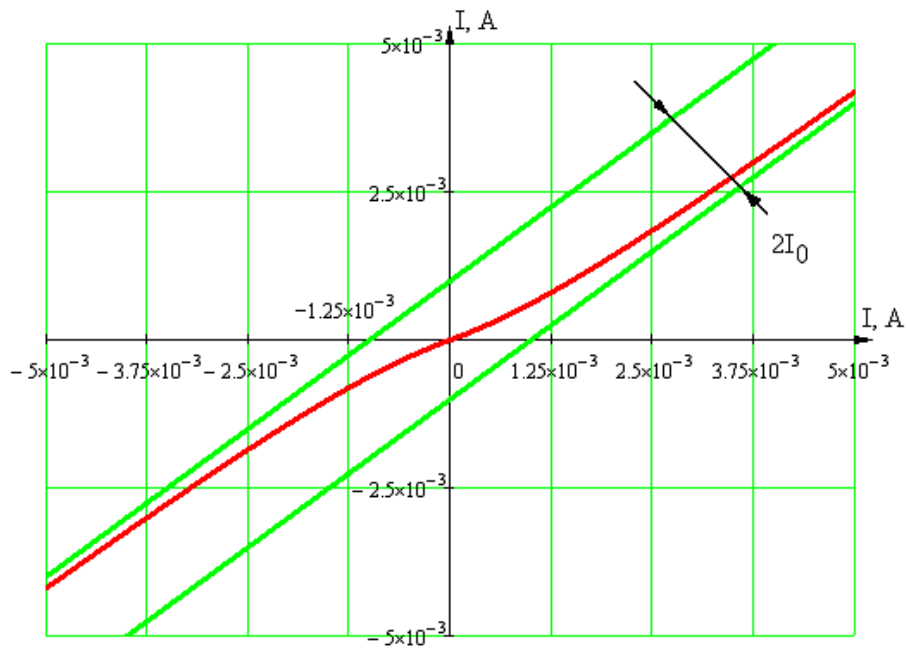


Fig. 2.20. Dependence of the currents increments  $\Delta I_1$  and  $\Delta I_2$

We will consider the branching of  $I_{imp}$  into the components and its further motion along the amplification channels. We obtain:

$$I_{B3} \approx \frac{\beta_1}{\beta_1 + 1} \cdot I_1 - I_3; \quad I_{B4} \approx \frac{\beta_2}{\beta_2 + 1} \cdot I_2 - I_4;$$

$$I'_{out} \approx \beta_3 \cdot I_{B3}; \quad I''_{out} \approx \beta_4 \cdot I_{B4},$$

where  $\beta_1 - \beta_4$  – are current gain factor.

Loading current is formed as the difference of two components

$$I_L = I''_{out} - I'_{out}.$$

With the account of (2.1) and (1.2) we obtain

$$I_L = \frac{1}{2} \cdot \left( \frac{\beta_4 \cdot \beta_2}{\beta_2 + 1} + \frac{\beta_3 \cdot \beta_1}{\beta_1 + 1} \right) \cdot I_{in} + \left( \frac{\beta_4 \cdot \beta_2}{\beta_2 + 1} - \frac{\beta_3 \cdot \beta_1}{\beta_1 + 1} \right) \cdot \sqrt{\frac{I_{in}^2}{4} + I_0^2}. \quad (2.3)$$

The expression (2.3) shows that non-linearity of the first stage is transferred to the output across the asymmetry of the amplifier “arms”. In case of zero current we have:

$$I_L = \left( \frac{\beta_4 \cdot \beta_2}{\beta_2 + 1} - \frac{\beta_3 \cdot \beta_1}{\beta_1 + 1} \right) \cdot I_0 \Bigg|_{I_{in} = 0}$$

That is why, the increment of the output current, that equals

$$\Delta I_L = I_L(I_{in}) - I'_L(I_{in}),$$

where  $I'_L(I_{in})$  – is the value of  $I_L$  at  $I_{in} = 0$ , is determined in the form

[165]:

$$I_L = \frac{1}{2} \cdot \left( \frac{\beta_4 \cdot \beta_2}{\beta_2 + 1} + \frac{\beta_3 \cdot \beta_1}{\beta_1 + 1} \right) \cdot I_{in} + \left( \frac{\beta_4 \cdot \beta_2}{\beta_2 + 1} - \frac{\beta_3 \cdot \beta_1}{\beta_1 + 1} \right) \cdot \left( \sqrt{\frac{I_{in}^2}{4} + I_0^2} - I_0 \right).$$

Function  $\Delta I_L = f(I_{in})$  is shown in Fig. 2.21.

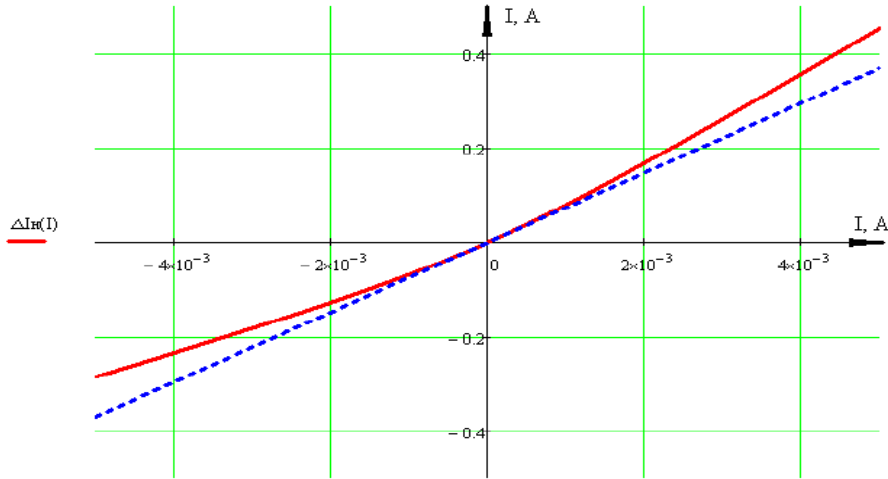


Fig. 2.21. Dependence of the output current increment  $\Delta I_L = f(I_{in})$

Dashed line shows the linear component, and the increment  $\Delta I_L$  from  $I_{in}$  is shown by a solid line:

$$\Delta I_L = \frac{1}{2} \cdot \left( \frac{\beta_4 \cdot \beta_2}{\beta_2 + 1} + \frac{\beta_3 \cdot \beta_1}{\beta_1 + 1} \right) \cdot I_{in} \cdot$$

This equality occurs under the condition  $|I_{in}| \leq 2I_0$  if  $|I_{in}| \ll I_0$ . In this case:

$$\Delta I_L \approx \frac{\beta_4 \cdot \beta_2}{\beta_2 + 1} \cdot I_{in} + \left( \frac{\beta_4 \cdot \beta_2}{\beta_2 + 1} - \frac{\beta_3 \cdot \beta_1}{\beta_1 + 1} \right) \cdot I_0,$$

and if  $|I_{in}| \ll I_0$ :

$$\Delta I_L \approx \frac{\beta_3 \cdot \beta_1}{\beta_1 + 1} \cdot I_{in} + \left( \frac{\beta_4 \cdot \beta_2}{\beta_2 + 1} - \frac{\beta_3 \cdot \beta_1}{\beta_1 + 1} \right) \cdot I_0.$$

If we assume  $\frac{\beta_4 \cdot \beta_2}{\beta_2 + 1} > \frac{\beta_3 \cdot \beta_1}{\beta_1 + 1}$ , then graphically this will be shown as the

growth of the gain factor in the zone of large positive currents and, correspondingly, its decrease in the zone of large, by absolute values, negative currents. All this is accompanied by the manifestation of the small constant component of the output current [165].

It should be noted, that the additional bias currents  $I_3$  and  $I_4$  in the circuits of the bases of the third and fourth transistors can compensate only the static part of the constant component of the load current:

$$\beta_3 I_{B3} - \beta_4 I_{B4} = \left( \frac{\beta_4 \cdot \beta_2}{\beta_2 + 1} - \frac{\beta_3 \cdot \beta_1}{\beta_1 + 1} \right) \cdot I_0.$$

Non-linear part of the constant component cannot be compensated in this way. That is, the compensation at the expense of the shifting of the second stage is possible only separately or for the zone of the small signal or only for the zone of large signal [165]. At the same time, it is easy to see that the value of the linearity error of the transfer characteristic of PDCA depends only on the non-identity of  $\beta$  values for p-n-p and n-p-n transistors and their change in the range of the input and output signals.

### **2.3.2. Push-pull current amplifiers with the autobalancing of the working points**

Circuit realization of PDCA with the parametric setting of the working points is only possible if precision current generators  $I_3$  and  $I_4$  (see Fig. 2.18) are available, but it is problematic.

In the scientific school of Professor Olexiy Azarov for the first time the approach that consists in the introduction to the circuit current compensators (CC) which provide the similar operation mode of DSA stages was suggested. This enabled the construction of PDCA with the distributed amplification channels, their characteristic feature is the autobalance of the working points of the intermediate transistor stages [134]. Generalized structural scheme of PDCA with the autobalancing of the working points is shown in Fig. 2.22.



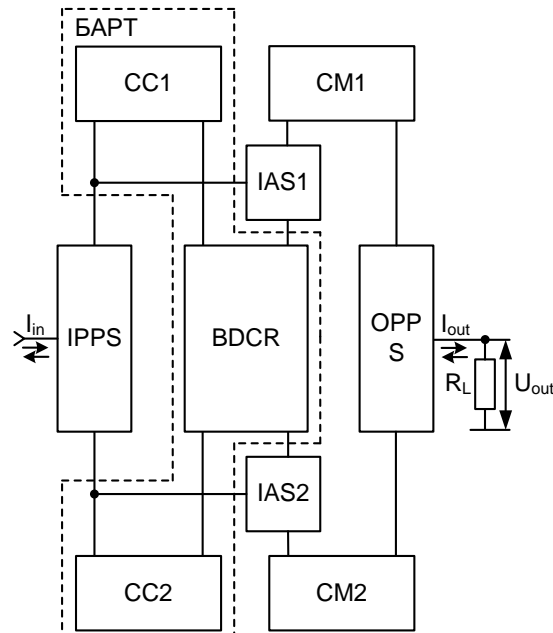


Fig. 2.22. Generalized structural scheme of PDCA with the autobalancing of the working points

PDCA with auto balancing of the working points consists of IPPS, IAS: IAS1 and IAS2, which are constructed on the bipolar transistors of different conductivity and OPPS.

Simultaneously BDCR, CC1 and CC2 form the auto balancing unit of the working point (UAWP) which provides the setting of direct current mode of IAS.

Simplified practical functional scheme of PDCA with auto balancing of the working points [127] is shown in Fig. 2.23. The amplifier contains IPPS, constructed in the form of self-complementary circuit with the common base on the transistors VT4 and VT5. Working point of this stage is set by the voltage drop on the transistors VT1 and VT2 in the diode connection, the level of which is provided by the values of the currents of current generators I1 and I2. The circuit also contains two symmetrical amplifying channels on the transistors VT11 and VT14. Working points of these transistors are set by introducing BDCR in the circuit and also CC: upper – on the transistors VT3 and VT7 and lower – on the transistors VT6 and VT10. The above – mentioned principle of the working point setting, considered in [134], is provided by the self – balancing of the collector currents of the transistors VT11, VT14 and VT7,

VT10 in the diode connection and VT3 and VT4. So, on condition  $I_{in} = 0$

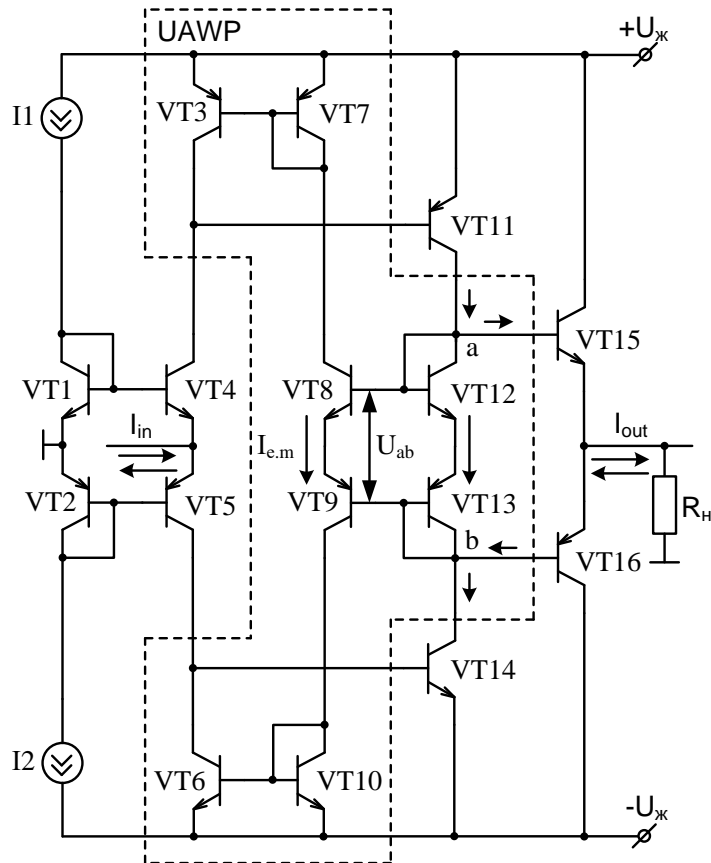
$$I_{C4} \approx I_{C5} \approx I_{C11} \approx I_{C14} \approx I_{C8} \approx I_{C9} \approx I_{C3} \approx I_{C6} \approx I_1 \approx I_2 \cdot$$


Fig. 2.23. Simplified principle scheme of PDCA with auto balancing of working points

Proceeding from the latter relation it should be noted, that the working points of the transistors, both of the upper and lower channels are set by the current levels of the generators  $I_1$  and  $I_2$ .

Availability of the BDCR in the circuit on the transistors VT8, VT9, VT12, VT13 provides constant total difference of the potentials  $U_{ab}$  on the base-emitter junctions VT12 and VT13 not only on the condition  $I_{inp} = 0$  but when  $I_{in} \neq 0$  and  $I_{C11} \neq I_{C14}$ . It should be noted that the through current  $I_{e.m.}$  across the

collector – emitter junctions of the transistors VT15 and VT16 approximately equals  $I_{c8}$  and  $I_{c9}$ .

Increment  $\Delta I_{out}$  ( $I_{in} \neq 0$ ) appears on condition that  $I_{in} \neq 0$  and  $I_{c11} \neq I_{c14}$  and  $I_{c15} \neq I_{c16}$ , at the output the difference current  $\Delta I_L$  appears that creates non – zero voltage drop  $U_{out}$  [165,166].

Current amplification factor of the above – mentioned circuit for small signal zone is determined by the formula [166] :

$$K_i = \beta_{p-n-p} \cdot \beta_{n-p-n}$$

By constructing PDCA in accordance with the suggested structural scheme, shown in Fig. 2.11 and increasing the number of the amplifying stages it is possible to increase the gain factor, at the same time it is necessary to take into account that the increase of the number of stages leads to the worsening of the dynamic characteristics.

## 2.4. Push pull buffer voltage devices

Besides the construction of the analog devices on the base of PDCA, there exist approaches, regarding their construction on the base of the push – pull structures. Many variations of the buffer devices both regarding circuit engineering organization and their designation are known. The most widely spread is the construction of the buffer devices on the base of the operation amplifiers. [122,143,170]. However, such an approach limits their operation rate.

Nowadays special attention is paid to push – pull circuits of the buffer devices. They are able to provide high linearity of the transfer characteristic and the necessary operation rate [170]. It should be mentioned that the known circuit engineering solutions of the construction of buffer devices with push-pull structure, which provide high operation rate and minor linearity, are non-balanced, have high error of zero shift and high temperature drift.

Certain advantage has the application for the construction of the core of the buffer device of the push – pull complex emitter repeaters on the bipolar transistors or push – pull structures on the base of field effect transistors. We will consider the circuit of the known buffer device with the self – balancing of the working points of the input stage [170], shown in Fig. 2.24.

It consists of the supply source I1 and I2, which set circuit stages direct current mode and bridge repeater on the transistors VT2, VT3, VT6 and VT7 with the floating supply source on the transistors VT5 and VT8.

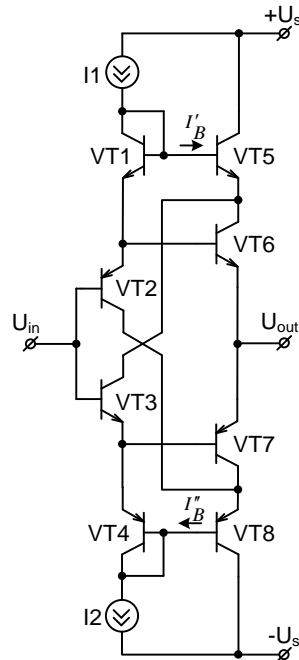


Fig. 2.24. Push-pull buffer device with the self – balancing of the working points of the input stage

Transistors VT1 and VT4 create the necessary bias. Buffer device of the push – pull structure, as compared with the circuit on the base the single – stage DCA, has low linearity error and the rate of the input signal growth for various half – periods is practically the same. However, the circuit has low linearity error but high error of zero shift.

However, in spite of the high linearity and operation speed, the above-mentioned buffer device has high zero shift error, that emerges due to the different values of the base-emitter voltages of the transistors VT2 and VT3, that automatically is transferred at the output of the circuit and causes the advent of error of zero shift error which is determined in the form of  $\Delta U_{out} = U_{out} - U_{in}$ , :

$$\begin{cases} I'_B = f(U_{out}); \\ I''_B = f(U_{out}); \end{cases} \quad \begin{cases} (U_{BE})_{VT1} = f(U_{out}); \\ (U_{BE})_{VT4} = f(U_{out}). \end{cases}$$

This is the additional source of the transfer characteristic non-linearity.

Also the approach to the construction of the buffer devices with the setting of the workings points by the external generators is known. The generalized structure and block diagram are shown in Fig. 2.25.

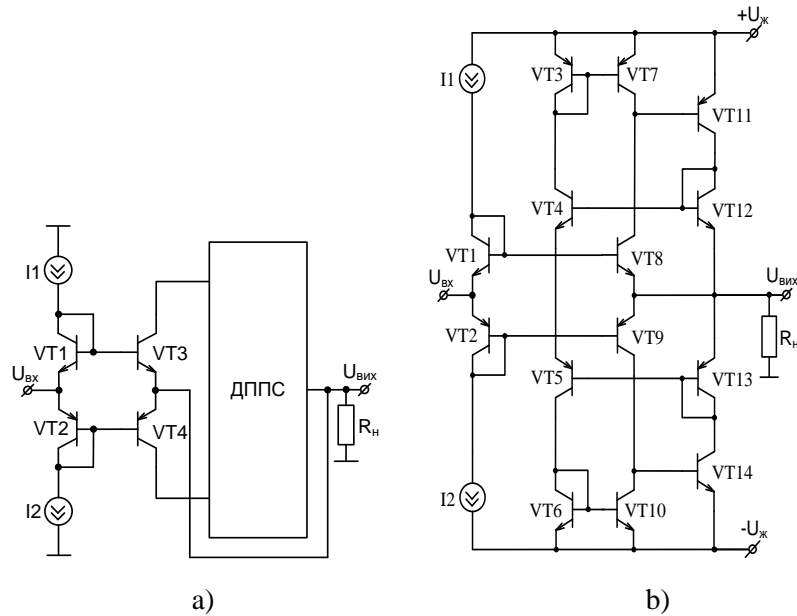


Fig. 2.25. Push – pull buffer device with the setting of the working points by the external generators; a) structural diagram; b) block diagram

It is known that non-zero value of the output resistance leads to the change of the scale and worsening of the transfer characteristic linearity. Application of PDCA enables to increase the loading capacity and maintain the set level of the linearity. The output resistance  $r_{out}$  decreases  $K_i$  times. At the same time, in spite of the improved characteristics, the problem of setting the working point of the input transistors VT1 and VT2 remains unresolved; this requires the usage of precision current generators I1 and I2.

### **3. Development of mathematical models and electric thermal modeling of the measuring primary circuits of the thermal flow sensors converters**

Information signal of the primary thermal flow sensors converters is their temperature that depends on the intensity of the heat exchange between the structure of the converter and the flow medium (gas or fluid). Modeling studies of the circuits of the above-mentioned measuring converters, carried out for the optimization of their structure and supply modes, require the combination of the analysis of the electric and thermal processes in a single complex.

Unfortunately, known packages of circuit modeling, in particular, PSpice and MicroCAP, do not allow combining electric and thermal analysis - in the course of such modeling studies the temperature of the elements cannot change if the electric power, released in these elements, varies. That is why, the problem of the development of the adaptation method of the circuit modeling procedure in the given packages for the realization of the possibility of the complex analysis of electric and thermal processes in the circuits of primary thermal flow sensors converters, was put forward. The realization of this task requires the creation of the model (equivalent circuit) of the elements, volt-ampere characteristic of which is influenced in the process of self-heating of these elements.

In the given section complex technique of the electric thermal modeling of the measuring converters of thermal flow sensors, is presented; it contains the synthesis of the equivalent circuit of the pulse temperature relaxation and the method of formation of converters VAC in the self heating mode by the supply current. Problems of the iteration process instability in the process of VAC analysis of the measuring converters with negative differential resistance, caused by self-heating, are considered.

Method of the synthesis of electric thermal models of thermoresistive, diode and transistor structures of the primary thermal flow sensors converters was suggested. Unlike the known packages of circuit modeling this method enables one to obtain VAC during one cycle of DC analysis, taking into account the self-heating of the above-mentioned converters.

#### **3.1. Mathematical model of the integral structure thermal field**

Techniques and models of calculation of the temperature fields of the electronic equipment and, in particular, solid-state and hybrid integrated circuits have already been adequately discussed in numerous publications. A number of specialized programming products are available, namely: WinTherm (developer

ANALYSIS TECH; [www.analysisstech.com](http://www.analysisstech.com)), T3Step and Thermodel (developer MICRED; [www.micred.com](http://www.micred.com)), BETAsoft Board (developer DYNAMIC SOFT ANALYSIS; [www.betasoft-thermal.com](http://www.betasoft-thermal.com)), etc. [54-65]. Taking into consideration, that the scientific aspects of the greater part of thermal calculations are comprehensive, at least, from the point of view of the tasks, put forward in the given research, further we will suggest only the description of the thermal model in general form and partial examples of the results of thermal fields of the integrated structures of the thermal hot-wire anemometers calculations. The material of the given subsection should be considered only as the initial data for the developed new approaches of the electric thermal modeling, presented in the next parts of the monograph, where the dynamic, thermal and circuit calculations of elements, the temperature of which is the informative value of the signal converter of the thermal flow are combined.

In the process of the thermal calculation of the integral structures, they are divided into the sections; in particular, into layers and parallelograms, each of them is described by the independent system of parameters - thermal conductivity factor, heat capacity, heat release power, etc. The system of heat conduction equations in the Cartesian coordinate system  $x, y, z$  for the  $i$ -th layer of the multilayer structure (assuming that the bottom boundary of the  $i$ -th layer corresponds to the coordinate  $z_i = 0$ , and the upper -  $z_i = \delta_i$ , where  $\delta_i$  - is the thickness of the  $i$ -th layer) has the form [172, 173]:

$$\frac{\partial^2 T_i}{\partial x^2} + \frac{\partial^2 T_i}{\partial y^2} + \frac{\partial^2 T_i}{\partial z^2} = 0$$

Boundary conditions are:

on lateral edges if  $x = 0, x = L_x, y = 0, y = L_y$ :

$$\frac{\partial T_i}{\partial x} = 0; \quad \frac{\partial T_i}{\partial y} = 0;$$

on the boundary of the  $i$ -th and  $(i+1)$ -th layers if  $z_i = \delta_i, z_{i+1} = 0$ :

$$T_i = T_{i+1}; \quad \lambda_i \left( \frac{\partial T_i}{\partial z_i} \right) = \lambda_{i+1} \left( \frac{\partial T_{i+1}}{\partial z_{i+1}} \right);$$

on the surface  $S$  if  $z_1 = 0$

$$\frac{\partial T_i}{\partial z_i} = -\frac{1}{\lambda_i} \sum_{j=1}^k \frac{P_j}{a_j b_j} h_j(x) h_j(y) h_j(z) + \frac{\alpha_0}{\lambda_1} T_1;$$

on the surface  $S_N$  if  $z_N = \delta_N$ :

$$\frac{\partial T_N}{\partial z_N} = -\frac{1}{\lambda_N} \sum_{j=1}^k \frac{P_j}{a_j b_j} h_j(x) h_j(y) h_j(z) + \frac{\alpha_N}{\lambda_N} T_N,$$

where  $T_i$  – is the excessive temperature (temperature of overheating) of the  $i$ -th layer over the ambient temperature ( $i = 1, 2, 3 \dots N$ );  $N$  – is a number of layers;  $\lambda_i$  – is the thermal conductivity of the  $i$ -th layer;  $P_j$  – is the power of the  $j$ -th source of heat ( $j = 1, 2, 3 \dots k$ );  $k$  – is the number of heat sources;  $a_j, b_j$  – are dimensions of the heat sources with the number  $j$  on axes  $x$  and  $y$ , correspondingly;  $h_j(x), h_j(y)$  – are coordinate-dependent functions which take the value of 1 in the area of the source and 0 outside the area of the  $j$ -th source of heat;  $h_j(z)$  – are coordinate-dependent functions, which take the value of 1 on the surface  $S_N$  and 0 - on the surface  $S_0$ , correspondingly;  $\alpha_0, \alpha_N$  – are heat transfer coefficients from the surfaces  $S_0, S_N$ .

Calculation of the temperature field, stipulated by the location of the source of heat on the surface  $S_N$ , can be performed by means of numerical methods, applying series:

$$\begin{aligned} \frac{T_{ij}}{P_j} = & \frac{(1-k_i)Z_c a_0 + 1}{Z_c a_0 a_N + a_0 + a_N} \frac{1}{L_x L_y} + \\ & + \frac{8L_x}{\pi^2 a_i a_j L_y} \sum_{n=1}^{\infty} \frac{W(n,0,k_i)}{n^2} \cos n\pi \frac{\phi_i}{L_x} \cos n\pi \frac{\phi_j}{L_x} \sin n\pi \frac{a_i}{2L_x} \sin n\pi \frac{a_j}{2L_x} + \\ & + \frac{8L_y}{\pi^2 b_i b_j L_x} \sum_{m=1}^{\infty} \frac{W(0,m,k_i)}{m^2} \cos m\pi \frac{\psi_i}{L_y} \cos m\pi \frac{\psi_j}{L_y} \sin m\pi \frac{b_i}{2L_y} \sin m\pi \frac{b_j}{2L_y} + \\ & + \frac{64L_x L_y}{\pi^4 a_i a_j b_i b_j} \sum_{n=1}^{\infty} \sum_{m=1}^{\infty} \frac{W(n,m,k_i)}{n^2 m^2} \cos n\pi \frac{\phi_i}{L_x} \cos n\pi \frac{\phi_j}{L_x} \sin n\pi \frac{a_i}{2L_x} \sin n\pi \frac{a_j}{2L_x} \times \\ & \times \cos m\pi \frac{\psi_i}{L_y} \cos m\pi \frac{\psi_j}{L_y} \sin m\pi \frac{b_i}{2L_y} \sin m\pi \frac{b_j}{2L_y} \end{aligned},$$

where  $T_{ij}$  – is the average temperature of the  $i$ -th section, heated by the  $j$ -th source of heat;  $a_i, a_j, b_i, b_j$  – are dimensions of the sections;  $\phi_i, \phi_j$  – are the coordinates of the centers of sections on the axis  $x$ ;  $\psi_i, \psi_j$  – are the coordinates of the centers of sections on the axis  $y$ ;  $L_x, L_y$  – are the

$$Z_c = \sum_{l=1}^N \frac{\delta_l}{\lambda_l}$$

dimensions of the structure on the axes  $x$  and  $y$ ; – is thermal resistance;  $\delta_l, \lambda_l$  – thickness and thermal resistance of the  $l$ -th layer ( $l = 1, 2, 3, \dots N$ );  $N$  – is a number of the structure layers;



$$W(n, m, k_i) = (G_N(1 - k_i) + k_i) \frac{Z_N}{Z_N \alpha_N + 1}$$

Variable  $k_i$  takes the value 1 in the point, located on the surface  $S_N$ , and 0 – on the surface  $S_n$ . Functions  $G$  and  $S_N$  are calculated in the consecutive order, passing the layers of the structure, starting from the first and ending with  $N = m$ , using the recurrent expressions:

$$Z_i = \frac{v\lambda_i Z_{i-1} + 1 + (v\lambda_i Z_{i-1} - 1)e^{-2v\delta_i}}{v\lambda_i Z_{i-1} + 1 - (v\lambda_i Z_{i-1} - 1)e^{-2v\delta_i}}; \quad G_i = Z_i = \frac{G_{i-1} 2v\lambda_i Z_{i-1} e^{-2v\delta_i}}{v\lambda_i Z_{i-1} + 1 + (v\lambda_i Z_{i-1} - 1)e^{-2v\delta_i}},$$

$$v = \sqrt{\frac{n^2 \pi^2}{L_x^2} + \frac{m^2 \pi^2}{L_y^2}}$$

where  $i$  – is the number of the layer.

In addition to the above-mentioned equations systems of mathematical description of the temperature fields, in the thermal flow sensors it is necessary to calculate the interaction of the heated structure of the primary converter of the flow sensor. In general case the dependence between the temperature parameters of thermoanemometric primary converter and parameters of the flow can be written in the form of the equation [1-5]:

$$P_H = K_1 \cdot \alpha \cdot F \cdot \Delta t,$$

where  $K_1$  – is the coefficient, which is introduced, as in greater part of cases it is not the difference of the temperature of the heat exchange surface and the fluid that is measured but another value  $\Delta t$ ;  $\alpha$  – is the coefficient of the convective heat transfer;  $F$  – is heat exchange surface;  $\Delta t$  – is the temperatures difference.

Main parameter of the thermal model is Nusselt criterion  $Nu$ , which characterizes the heat exchange between the surface of the heater and flow medium:

$$Nu = A \cdot Re^n \cdot Pr^b \cdot Gr^c \left( \frac{Pr_s}{Pr_c} \right)^d,$$

where  $Re$  – is Reynolds criterion, which characterizes the ratio of the inertia and viscosity forces and determines the character of fluid (gas);  $Pr$  – is Prandtl number, which characterizes the physical properties of the fluid (gas);  $Gr$  – is Grashof number, which characterizes the lifting force, which appears in the fluid (gas) as a result of densities difference.

Prandtl similarity criterion is a physical parameter, which characterizes the properties of the flow. Grashof number also does not contain the velocity of the flow and only characterizes the interaction of the molecular friction and lifting

force, this is stipulated by the densities difference in separate points of the flow due to its non-isothermality. Only Reynolds criterion  $Re$  contains the flow velocity we are interested in. That is why, in general case the connection between Nusselt criterion, which contains the coefficient of the convective heat transfer and Reynolds criterion, which contains flow velocity  $V$ , can be written in the form:

$$N_u = C \cdot Re^n,$$

where  $C$  – is specific heat of the measuring environment; or:

$$\frac{\alpha \cdot d}{\lambda} = C \cdot \left( \frac{v \cdot d \cdot \rho}{\mu} \right)^n,$$

It follows:

$$\alpha = C \cdot \frac{\lambda \cdot d^{n-1} \cdot \rho^n}{\mu^n} = C \cdot \frac{\lambda \cdot d^{n-1}}{\mu^n} \cdot G_M^n,$$

where  $d$  – is the diameter of the tube, where the flow velocity is measured;  $v$  – is the flow velocity,  $\rho$ ,  $\mu$ ,  $\lambda$  – is the density, viscosity, heat conduction of the measured medium;  $G_M$  – is a mass flow rate.

It should be noted, that for practical realization, as a rule, criterion equations, obtained as a result of the experimental research, are used.

A number of the results of the thermal calculations of two typical constructive solutions of the integral structures of the thermal flow sensors, carried out by us, are given below. The first of them (Fig 3.1a) - it is the crystal (B) of the silicon integrated circuit, in the center of which on the membrane (M) one heater (H) is formed, and on the periphery - two or four sensors (S1, S2) of the difference temperature  $\Delta T = T_{S2} - T_{S1}$ . To minimize the heat transfer from the heater to the sensors the thermal resistance of the membrane must be as high as possible - in ideal case the heat transfer must be performed only through the medium (gas or fluid) of the measuring flow. That is why; the thickness of the membrane is minimal, typically - not more than 0.05 mm.

The sensors of the different temperature must also have maximum heat resistance relative to the structure of the integrated circuit that is why, they are formed with dielectric sublayer with low thermal conductivity. Instead the thermal resistance of the integrated circuit structure on the whole must have minimal thermal resistance with the heat sink on which this circuit is mounted. It provides the fixed temperature of the structure and the lack of the temperature gradients, stipulated by the direct heat transfer across the membrane to the sensors.

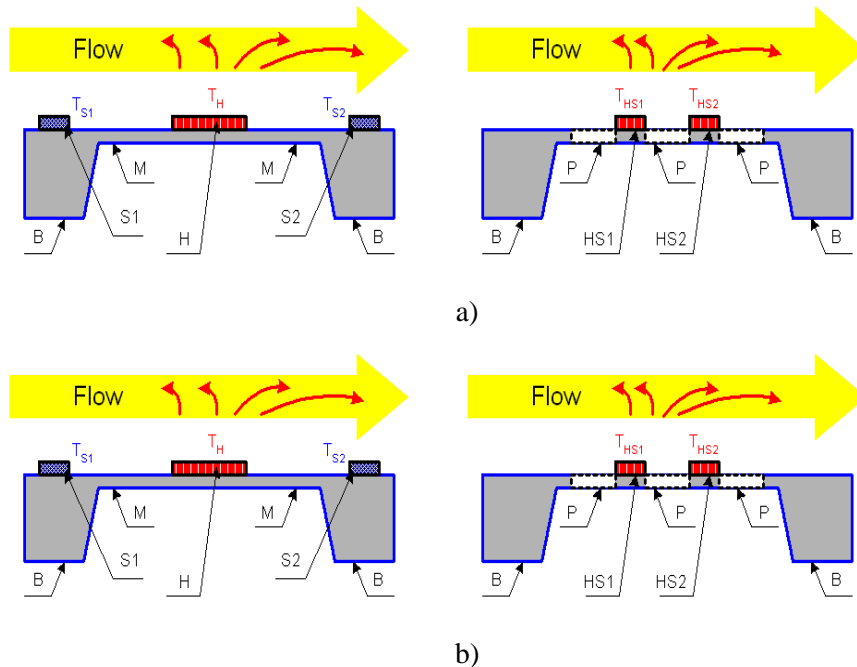


Fig 3.1. Typical constructive solutions of the thermal flow sensors

The realization of the above-mentioned requirement is not a problem as the thermal conductivity coefficient  $\lambda_{Si}$  of the silicon (basic semiconductor of the solid-state integrated circuits) and eutectic alloy gold-silicon  $\lambda_{Si-Au}$  (the layer that connects the crystal of the integrated circuit with the radiator) is rather high –  $\lambda_{Si} = 120 \text{ W/(m}\cdot\text{K)}$ ,  $\lambda_{Si-Au} = 150 \text{ W/(m}\cdot\text{K)}$ , correspondingly. Instead, thermal conductivity coefficient of the majority of the dielectric layers, on which temperature sensors are formed (oxide or silicon nitride) is several tens of times less that provides good thermal insulation of the temperature sensors from the crystal of the integrated circuit of the primary converter of the flow sensor.

The examples of the calculation results of the temperature field of the flow sensor structure without the available flow are shown in Fig 3.2a in the process of heat transfer across the flow (at various values of the normalized flow rate 1 ... 4) - in Fig 3.3. Temperature field has three characteristic sections: B - crystal of the integrated circuit, temperature of which is practically stable, M - peripheral part of the membrane and H - central part of the membrane, where the heater is located.

At very small flow rates (Flow 1) the temperature field remains practically unchanged and temperature difference between the sections of temperature Sensors 1 and Sensor 2 location is small. Increase of flow rate 2 and flow rate 3 leads to the transfer of heat in the direction of its motion and corresponding

increase of temperature difference  $\Delta T = T_{s2} - T_{s1}$ . The temperature of the heater decreases; this stipulates nonlinearity of the flow sensor conversion function.

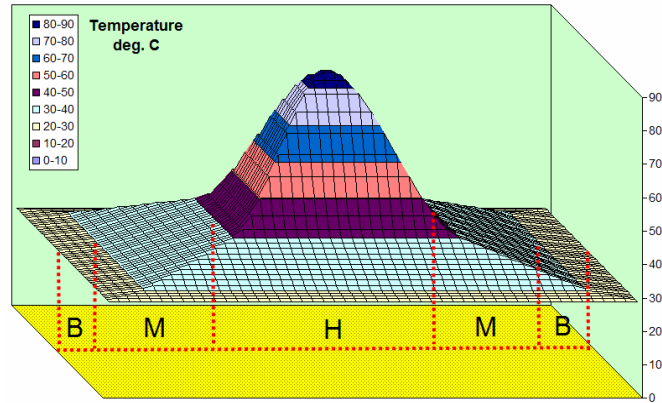


Fig 3.2. Temperature field of the integrated structure (Fig 3.1a) without the impact of the heat transfer across the flow

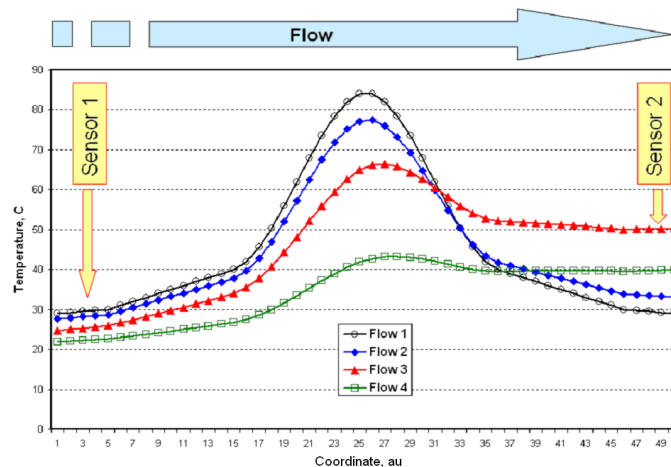


Fig 3.3. Temperature field of the integrated circuit (see Fig 3.1a) at different flow rates (in normalized units – Flow 1...4)

Further increase of the flow rate (Flow 4) leads to considerable cooling of the heater at non-sufficient heating of the flow medium, this stipulates the decrease of the structure heating in the section where temperature Sensor 2 is located and the decrease of temperature difference  $\Delta T$ . Fig 3.4 shows typical dependence of the temperature difference  $\Delta T$  on the flow rate. This dependence is the determining factor for the development of the structure of the primary flow

sensor converter and determines the linearity of the conversion function and admissible measurement range.

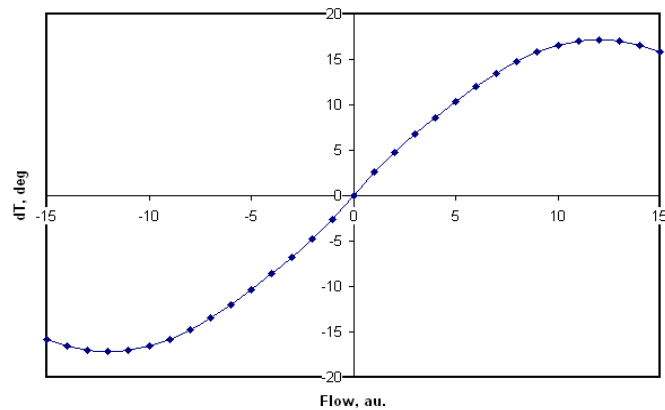


Fig 3.4. Dependence of temperatures difference  $\Delta T = T_{s2} - T_{s1}$  on the flow rate

Similar calculations were carried out also for the second typical construction of the primary converter of the thermal flow sensor structure (see Fig 3.1b), which contains two integrated elements (HS1, HS2), each of these elements serves both as a heater and temperature sensor. In order to minimize the heat transfer these elements are made in the form of bridges, contacting with the structure of the crystal only in two points. Lateral sides of the elements are suspended, i.e., heat exchange is carried out only across the medium (P) of the flow.

Typical picture of the temperature field of such a structure without the impact of the heat transfer across the flow is shown in Fig 3.5.

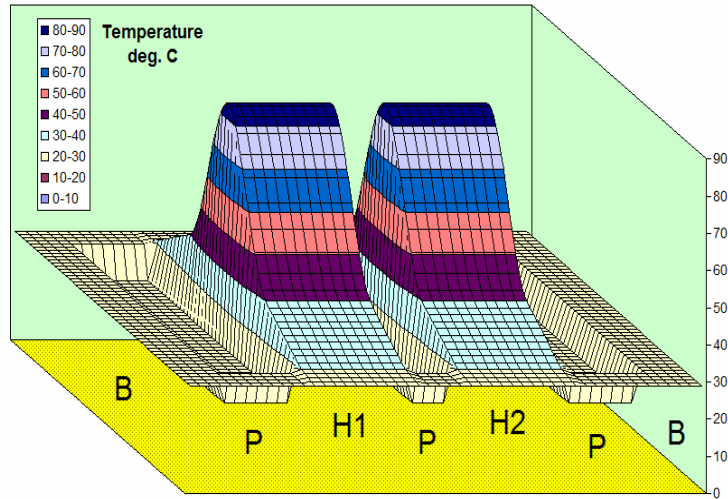


Fig 3.5. Temperature field of the integral structure (see Fig 3.1b) without the impact of the heat transfer across the flow

The temperature of the medium between the integrated elements (HS1, HS2) we assume to be a stable value (in the Fig. it is represented by the lowered sections P). Information value of the primary converter of the flow sensor is the temperature difference of the integrated elements  $\Delta T = T_{HS2} - T_{HS1}$ .

The example of the calculation of the temperature field of the structure with two integrated elements at a certain flow rate is shown in Fig 3.6. Similarly to the above-mentioned calculations the increase of temperatures difference

$\Delta T = T_{HS2} - T_{HS1}$ , is observed in case of flow rate increase, it is stipulated by the decrease of the convective heat exchange between the heaters and the flow in the direction of its propagation. In the given case it is stipulated by the increase of the medium temperature of the flow while its passage above the heaters (taking into account the large gradients of the temperatures in the flow, its temperature is not presented in the Figure- it is assumed to be the fixed value  $T_A = 20^\circ\text{C}$ ). As in the previous case with one heater at a certain critical rate of the flow the function of temperature difference takes the extreme value, after that the temperature difference decreases. This limits the range of the flow rate measurement.

The analysis, carried out, confirms the data, published in literature [1-5], that the function of thermal flow sensors conversion is nonlinear and at certain value of the flow rate there comes the mode at which the gradient of the temperatures ceases to increase and starts to decrease at the increase of the flow rate.

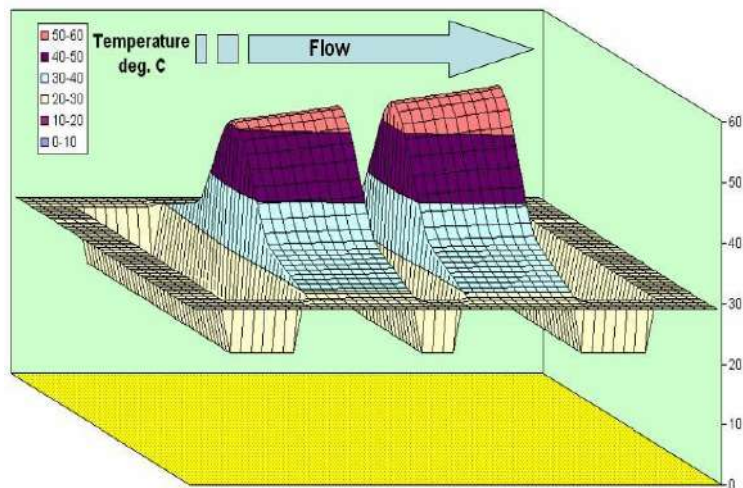


Fig 3.6. Temperature field of the integrated circuit (see Fig 3.1b) at a certain flow rate

In the next sections we will demonstrate the possibility to minimize this negative effect by means of the thermostabilization of the heater temperature. As it will be shown further, the novelty of the solution, suggested by us, is the method of thermostabilization at which high sensitivity and minimal losses of thermal energy in the control circuits of the heating process are combined.

### 3.2. **Electrothermal modeling of measuring converters in pulse operation modes**

The basis of the efficient stabilization of the heater temperature that allows to minimize losses of thermal energy on the control elements (mainly transistors) is pulse operation mode. Unlike linear control circuits, where the power of heating changes by means of corresponding change of the voltage on the heater, in pulse control circuits the power of heating changes by means of the corresponding modulation of the heating pulses duration or the period of their occurring. The amplitude of the voltage pulse on the heater practically equals the supply voltage, i.e., the voltage drop and heat release on the control element is minimal.

Especially efficient operation of the pulse heating system can be achieved, applying modern MIS - transistors, manufactured according to DMOS and V-MOS (HEXFET) technologies, which provide practically ideal key characteristics - high operation speed and minimal resistance in the conducting state  $R_{ON}$  (typically  $R_{ON} < 0,1$  Ohm). The discussion, concerning further development of pulse control systems, from the point of view of their application

for the temperature stabilization of the thermal flow sensors heater will be held in the next section.

We will consider main approaches to the circuit modeling of the given pulse circuits. The task to develop the method of the analysis of the pulse heating of the elements in the environment of PSpice and MicroCAP is put forward. It should be noted that the above-mentioned packages do not allow performing the electric and temperature modeling in a single cycle of the analysis.

We will apply the electric thermal analogy, its essence will be considered on the example of one-dimensional thermal flow in the solid state body. Assuming in the first approximation the independence of the thermal conductivity of the body on the temperature, the system of equations of the thermal flow can be written in the form:

$$\begin{cases} \frac{dT}{dx} = \frac{P}{\lambda S} \\ \frac{d^2T}{dx^2} = \frac{j\omega c \rho T}{\lambda} \end{cases},$$

where  $\lambda$  – is thermal conductivity coefficient ;  $S$  – is the area of the isothermic surface;  $P$  – is thermal flow;  $c$  – is the specific heat;  $\rho$  – is the specific density of the substance.

Instead, the system of equations, that characterizes passive RC line with the distributed parameters at the established sinusoid mode, can be written in the form:

$$\begin{cases} -\frac{dV}{dx} = R_i I \\ \frac{d^2V}{dx^2} = j\omega R_i C_i V \end{cases},$$

where  $V$ ,  $I$  – are complex amplitudes of voltage and current;  $R_i$ ,  $C_i$  – is the resistance and capacitance per unit of the line length.

Comparing these two systems of equations, the formal analogy between the thermal and electrical values can be established: the amount of heat in the thermal model corresponds to the electrical charge in the electric model; temperature difference corresponds to the potentials difference; thermal flow corresponds to the electric current; the density of the thermal flow – corresponds to the current density; thermal resistance - to electric resistance; thermal conductivity coefficient – to electric conductivity; heat capacity – electric capacitance. Spatial and time parameters of both models are identical.

It is known that time dependence of the temperature  $T(t)$  in the pulse mode of heating-cooling can be presented by the expression:



$$T(t) = T_A + PZ_Q(t),$$

$$Z_Q(t) = \sum_{i=1}^N Z_{Q_i} \left( 1 - \exp\left(-\frac{t}{\tau_i}\right) \right)$$

where  $Z_Q(t)$  – is thermal resistance ; – at heating;  $Z_Q(t) = \sum_{i=1}^N Z_{Q_i} \exp\left(-\frac{t}{\tau_i}\right)$  – at cooling;  $Z_{Q_i}$  – are time -independent thermal resistances of the parametric sections of the structure in the constant heating mode;  $\tau_1, \tau_2, \dots, \tau_N$  – are thermal constants of these sections of the structure;  $\tau_i = Z_{Q_i} \cdot C_{\tau i}$ ;  $C_{\tau i}$  – is heat capacity of the i-th section of the structure.

For the thermal analysis of the structure of thermal flow-meter integrated circuit it is sufficient to allocate, at least two parametric areas, describe each area by the typical values of  $Z_{\tau i}, C_{Q_i}$ . The first area corresponds to the membrane, thermal resistance of which is the highest and the thermal constant is the smallest. The second area corresponds to the crystal of the integrated circuit. If necessary, the heating of the radiator and the adjacent environment can be considered, introducing the third and the fourth parametric areas.

Method of the model synthesis and analysis of the pulse heating of the elements in PSpice and MicroCAP environment, developed by us, consists of two stages – at the first stage, the value, that is numerically equal to the temperature of the studied element, is formed, at the second stage – taking into account this temperature, temperature relaxation of the parameters of this element, in particular, its temperature change of the resistance, current or voltage drop is calculated.

Using electric thermal analogy, the process of heating is represented by the electric equivalent circuit (Fig 3.7), where the pulse source of current  $I_0$  forms the transient process in the link of the parallelly connected electric resistance (resistor R1), value of which numerically equals thermal resistance in constant heating mode and capacitance ( capacitor C1), value of which numerically equals heat capacity of the structure. For convenience's sake, the scaling coefficient of these values can be introduced, putting into operation the corresponding coefficient between the current and thermal flow.

As it was mentioned above, thermal analysis of the integral structure of the thermal flow sensor requires the usage of at least two parametric areas. The example of the transient process of a two-element electric thermal model is shown in Fig 3.8.

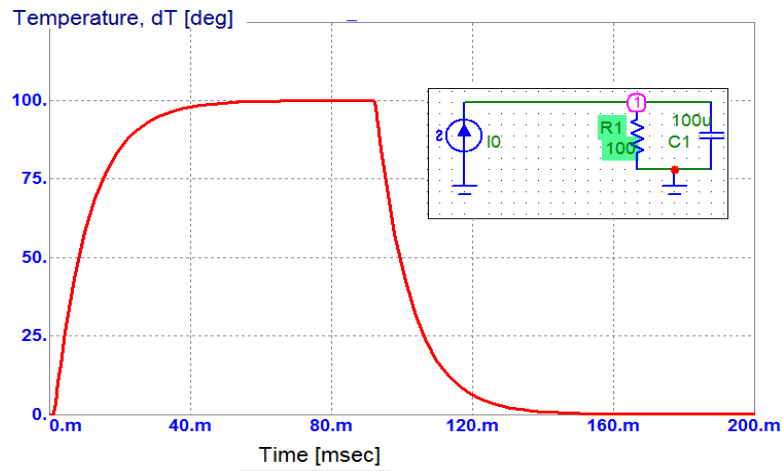
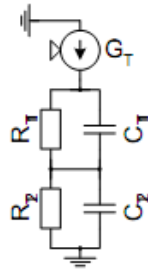


Fig 3.7. Transient process of a single-element electric thermal model

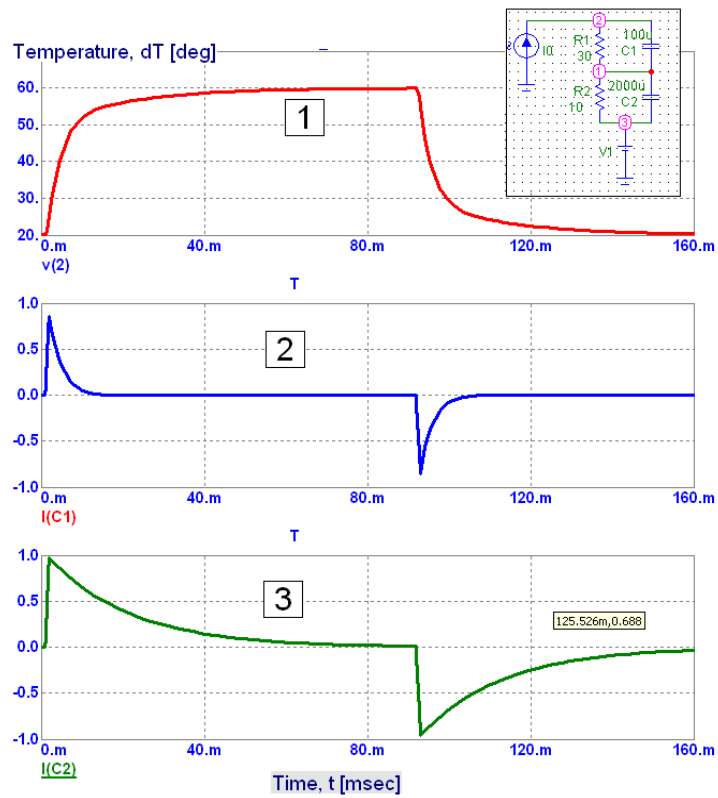
Thermal relaxation of the membrane and the crystal is presented by the "charge" of heat capacity of the first 2 and second 3 parametric areas of the integrated circuit of the primary converter of the thermal flow sensor structure.

For the description of the ambient temperature  $T_A$  the source of the constant voltage is introduced in the equivalent circuit, its value numerically equals  $V_1 \equiv T_A$ . Transient process of the two-element electric thermal model  $T_s$  with the account of the ambient temperature  $T_A$  is shown in Fig 3.9, where 1 – is the total value of the temperature  $T_s$  of the heater; 2 – is the ambient temperature  $T_A$ ; 3 – is the increment of the temperature on the membrane  $\Delta T_1$  relatively the temperature of the crystal; 4 – is the increment of the temperature of the integrated circuit crystal  $\Delta T_2$  relatively the ambient temperature.

The examples of the result of the heater temperature analysis at the short heating pulses, when the process of heating-cooling of the structure occurs during several periods, are shown in Fig 3.10.



a)



b)

Fig 3.8. Two-element electric thermal model: a) circuit; b) transient process: 1 – temperature (voltage); 2, 3 – "charge" of heat capacity, correspondingly, of the first and the second parametric areas

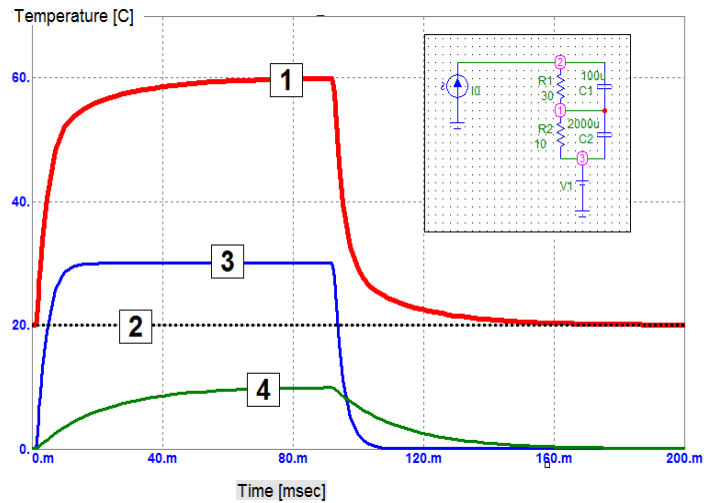


Fig 3.9. Transient process of the two-element electric thermal model  $T_s$  with the account of the ambient temperature  $T_A$

It is obvious that the heating temperature depends on the power, released on the heater and the above-mentioned model does not contain information about this power. That is why, as it will be shown below, in the process of synthesis of the thermal relaxation model, the voltage at RC circuits must be not the value of the temperature but only time-dependent index, in particular, the function of the thermal resistance  $Z_{Q(t)}$ .

In the process of the model synthesis verification of its parameters, relatively experimentally determined parameters of heating and cooling of real structures is carried out. In the process of such verification two basic approaches are used. The first approach provides the graphic identification of the parametric areas, for this purpose the input data regarding the course of heating of the studied element  $T(t)$  are presented in the form of the logarithmic graph  $\text{Log}[T(t)_{MAX} - T(t)]$ , in particular, as it is shown in Fig 3.11.

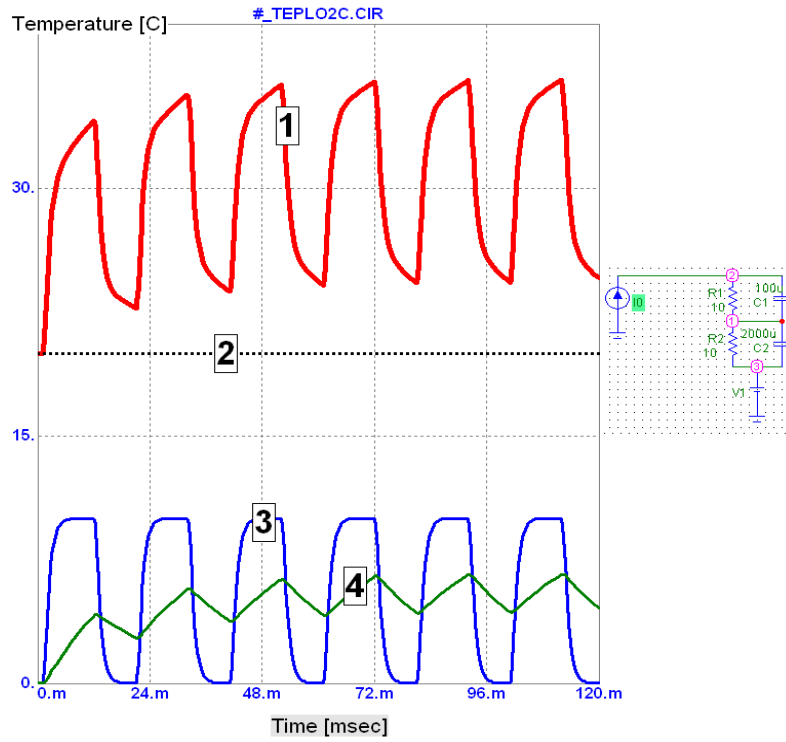


Fig 3.10. Transient process of the model at short heating pulses: 1 – temperature (voltage); 2 , 3 – "charge" of heat capacity, correspondingly, of the first and second parametric areas

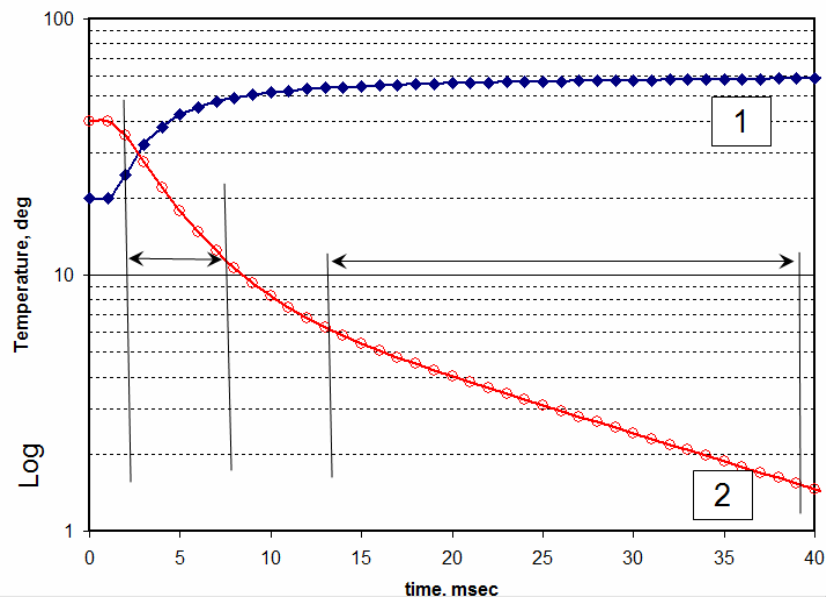


Fig 3.11. Analysis of the experimental data: 1 –  $\text{Log}(T(t))$ ; 2 –  $\text{Log} [T(t)_{\text{MAX}} - T(t)]$

Analysis of the data in the logarithmic scale enables us to determine linear sections, which correspond to the parametric areas of the structure. The second approach provides the stepping of the model parameters, for this purpose in the process of modeling analysis a certain step or the list of stepping parameters is set, in particular, as it is shown in Fig 3.12. In the process of such stepping the numerical parameters of the model, which correspond to the results of the experimental research are determined.

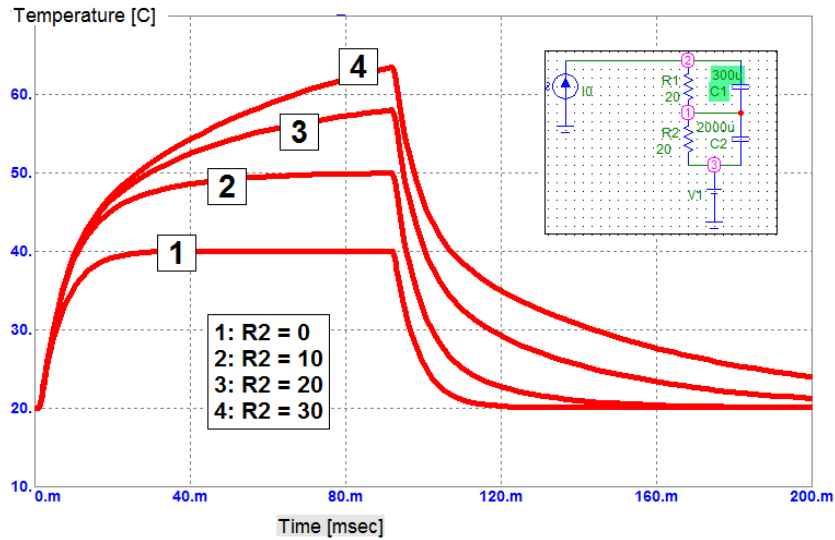


Fig 3.12. Transient process of the two-element electric thermal model at the sleeping of the thermal resistance  $Z_2 \equiv R_2$

At the second stage of the model synthesis the equivalent circuit of the studied heater is formed, the voltage at which in the process of thermal flow sensor analysis serves as the information value about its temperature. For this purpose the heater is presented by the link of two serially connected elements (Fig 3.13) - resistor (in the circuit R4) and the controlled voltage source (in the circuit E1).

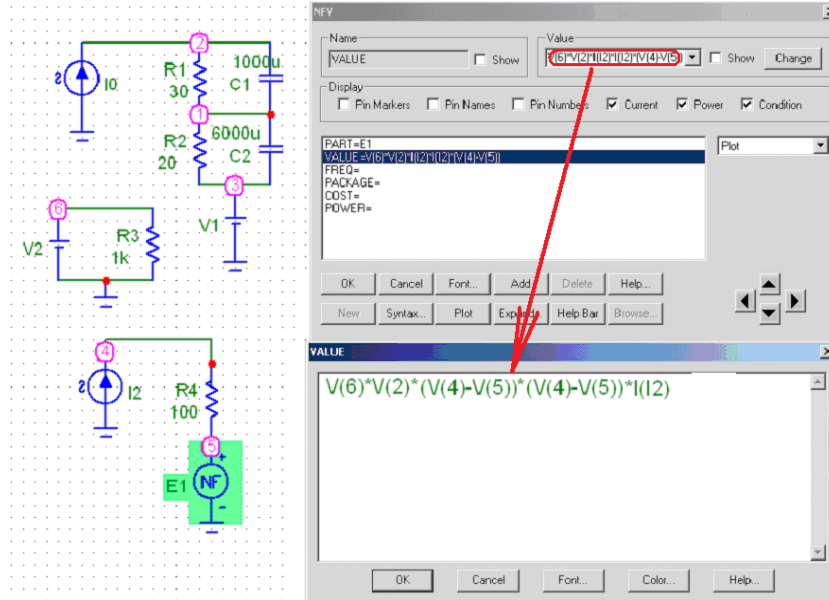


Fig 3.13. Model of electric thermal analysis and recording of the function of the controlled voltage source of NFV type

In the libraries PSpice and MicroCAP there are several types of the controlled voltage and current sources (VofV, VofI, IofV, IofI, NFV etc.), syntax of which allows tabular or analytically to set the dependence of the output value of the source on certain voltage or currents of the circuit. Having performed the analysis of the possibilities of the above-mentioned sources for the synthesis of temperature-dependent relaxation of the resistance of the resistive heater, we determined that the controlled source of NFV type as the most suitable.

Fig 3.13 shows the model of electric thermal analysis of the heater, using the controlled source of voltage of NFV type and the example of its function recording. To perform such recording we will use the information about the time dependence of the thermal relaxation of the heater, obtained at the first stage of model synthesis – in accordance with the given example – this is the value, numerically equal the voltage in the node  $V_2(t)$ . Further, having written the equation of the temperature dependence of the voltage on the heater:

$$V_{OUT}(t) = V_{OUT0} (1 + \alpha \Delta T(t)),$$

$$\Delta T(t) = P_Q Z_Q(t) = I_R V_{OUT}(t) Z_Q(t) \approx I_{R0} V_{OUT0}(t) Z_Q(t),$$

we find:

$$V_{OUT}(t) = V_{OUT0} + V_{OUT0}^2 I_{R0} \alpha Z_Q(t).$$



The first item of the obtained expression is the voltage at nominal (temperature independent) value of the heater resistance  $V_{OUT0}$ . In the model this resistance is represented by the resistor R4. The second item, modeled by the controlled voltage source of NFV type and in the model presented by the element E1, we will write in the form:

$$V(E1) = V_{OUT0}^2 I_{R0} \alpha Z_Q(t) = V(R4)^2 I(R4) K_V V_2(t),$$

$$K_V = \frac{\alpha Z_Q(t)}{V_2(t)}$$

where  $K_V$  – is the proportionality coefficient, which in the model is presented by the additionally introduced voltage source V2 (this means only the presentation of its numerical value and not dimensionality).

The example of the modeling results of the thermal relaxation of the resistive heater of the thermal flow sensor where the electro thermal model, developed by us, is used is shown in Fig. 3.14.

We can see that when the current pulse 1 is sent, the heating 2 and resistance change takes place, it is shown by the voltage drop at the fixed amplitude of the current pulse 3. For visual clarity, the temperature coefficient of the heater resistance is chosen greater than it is in reality.

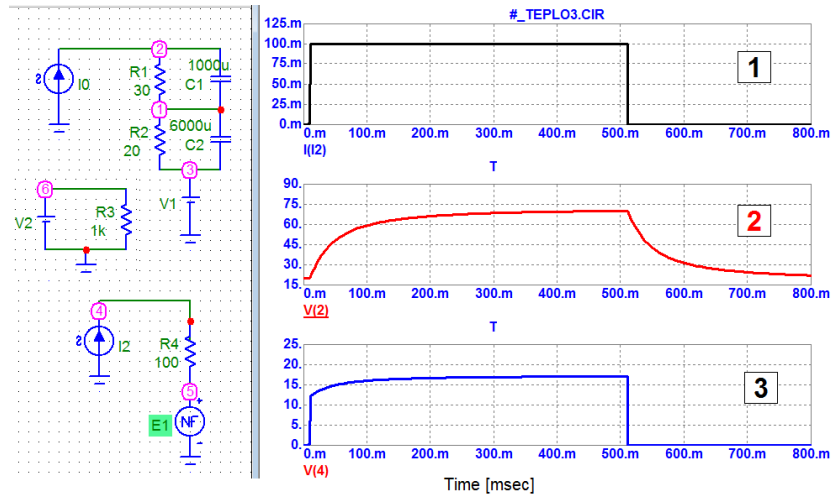


Fig 3.14. Result of the electric thermal modeling of the resistive heater:  $\alpha < 0$ : 1 – pulse of the heating current; 2 – temperature; 3 – voltage on the heater

The examples of such iteration modeling are given in Fig. 3.15 (at positive temperature coefficient of the resistance  $\alpha > 0$ ) and in Fig 3.16 (at  $\alpha < 0$ ).

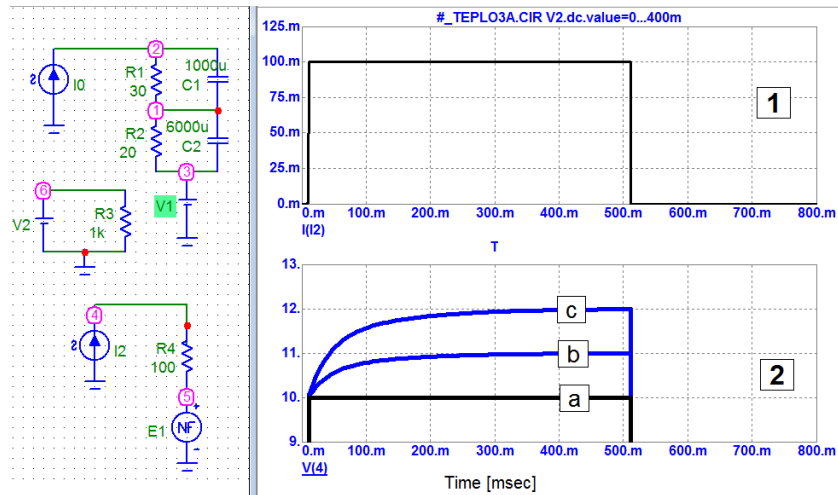


Fig 3.15. Result of the electric thermal modeling of the resistive heater at iteration  $\alpha > 0$ : 1 – pulse of the heating current; 2 – voltage on the heater

It is obvious that the proportionality coefficient  $K_v$  can be directly set by the numerical value in the formula that describes the function of the controlled source of NFV type. However, the representation of this coefficient by the voltage source V2 has the advantage in case of the iteration modeling, when the task is set to determine the change of the output voltage at the heater when its temperature coefficient of the resistance or thermal resistance changes.

Graphs with the designation *a* are obtained at  $\alpha = 0$ , it corresponds to typical result of circuits modeling in PSpice or MicroCAP, in which it is impossible to perform electrical and thermal calculations in a single cycle of the analysis. Graphs with designations *b* and *c* allow to determine thermal relaxation of the temperature-dependent resistor, for the graph *c* module  $\alpha$  is greater than for the graph *b*.

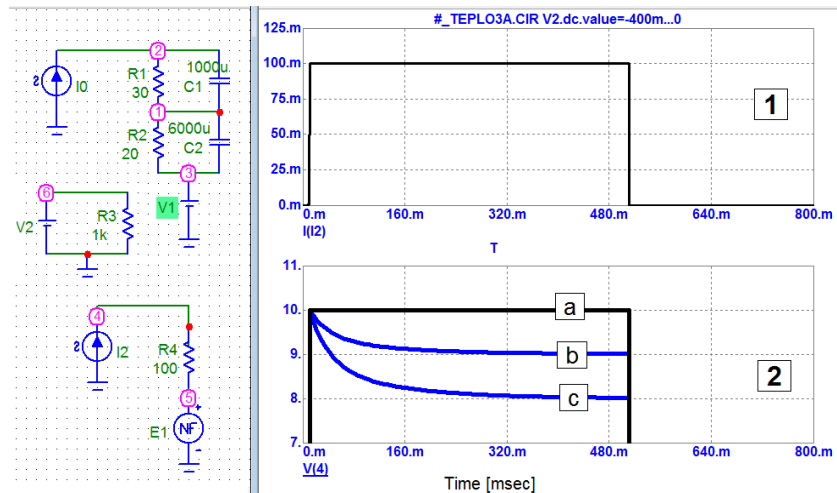


Fig 3.16. Result of electric thermal modeling of the resistive heater at iteration  $\alpha < 0$ : 1 – pulse of the heating current; 2 – voltage on the heater

### 3.3. Electric thermal modeling of temperature-dependent volt-ampere characteristics of the resistive converters

In the given subsection the problem of DC analysis (Direct Current Analysis) of VAC of thermoresistive measuring converters of thermal flow sensors is considered, the aim of the analysis is the determination of the output signal change of such converters under the impact of the electric power, stipulated by their supply current. The heating of the thermoresistive converter under the impact of the supply current leads to the change of its resistance, and this, in its turn, changes the parameters of the measuring circle. As it was mentioned above, conventional programs of circuit modeling do not allow combining in a single cycle the electric and temperature analysis. The latter can be carried out only independently on each other - typically it is realized by means of electrical DC analysis at setting of fixed temperatures. Unfortunately, such analysis does not allow obtaining real VAC of the thermoresistive converters in the process of their heating. For the sake of the example we will consider the analysis of VAC of the semiconductor thermoresistors, their temperature dependence resistance is determined by the typical

$$R(T) = A \cdot \exp\left(\frac{B}{T}\right)$$

dependence, where A, B - are the coefficients of the exponential function (with the increase of the temperature the resistance drops exponentially). VAC

of such thermoresistors is linear only at small supply currents, when the temperature of their self heating is small. However, if the supply current is from several milliamperes and higher the resistance of the semiconductor thermoresistors starts to drop, it is stipulated by the increase of their temperature. The example of VAC analysis of such thermoresistors in the mode of stationary self-heating is shown in Fig. 3.17 [174, 175]. Such analysis is a rather labor-consuming process, especially when the supply current of the thermoresistor depends on its resistance.

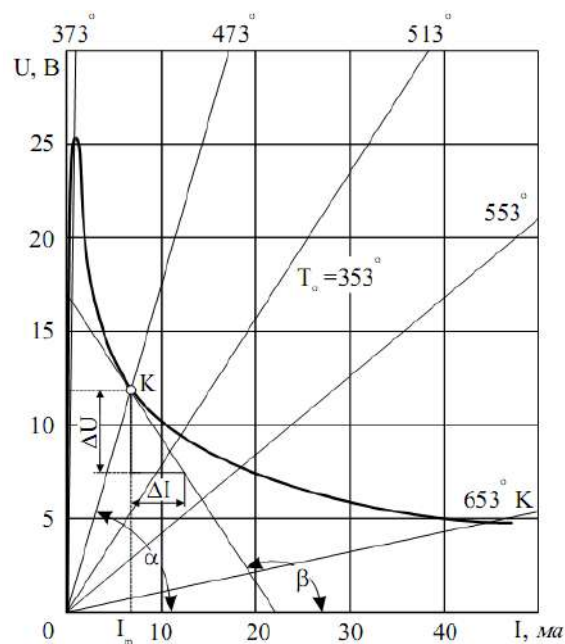


Fig 3.17. Analysis of VAC of the semiconductor thermoresistor in the mode of stationary self-heating

It should be noted that the given problem was already the subject of the detailed study, and the models (equivalent circuits) of certain thermal resistors were developed. In particular, Fig. 3.18 contains a mathematical description of the thermoresistor model C619\_10000, developed by the company Siemens (this and other similar construction principal models of the thermoresistors are shown in the library NTC.LIB). The basis of NTC.LIB type models is functionally controlled source of current - in the given example these are the sources  $G_{them}$ ,  $G_{tmp}$  and  $G_{par}$ . The examples of the thermoresistor C619\_10000 VAC modeling are shown in Fig. 3.19; variant (a) corresponds to the supply by the current source, and variant (b) - to the supply by the voltage source with serially connected resistor  $R1 = 1 \text{ k}\Omega$ . In both examples the

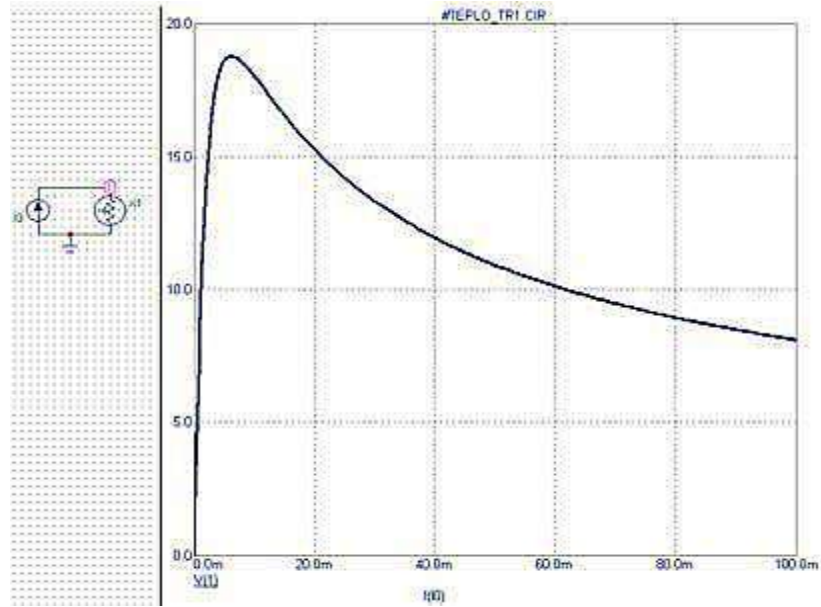
section of VAC with negative differential resistance, stipulated by the heating of the thermoresistors, is observed, which proves the correctness of the modeling result at least from the qualitative point of view.

```

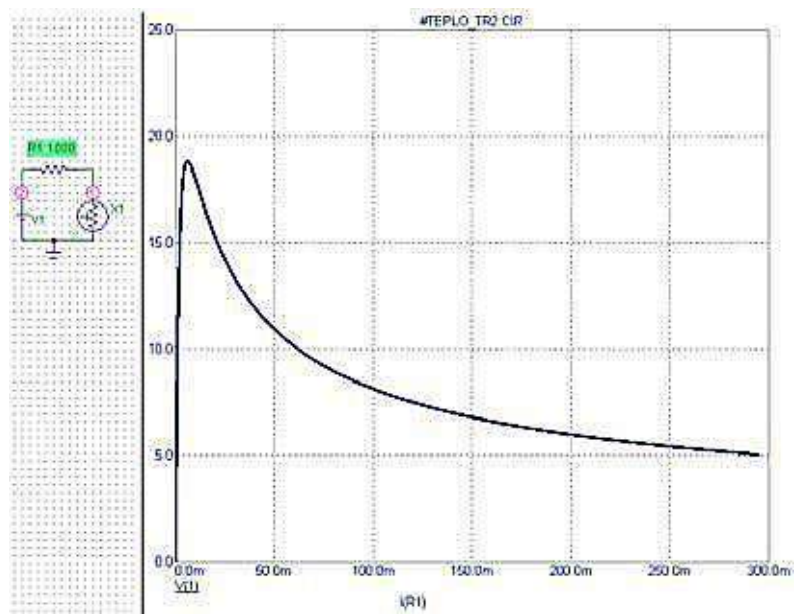
*PSPICE-SIMULATIONS MODELL FR HEISSLEITER
*SIEMENS MATSUSHITA COMPONENTS OHG DEUTSCHLANDSBERG
*"NTC.LIB" Model
*****
.subckt NTC 1 2 Params:B0=1 B1=1 B2=1 B3=0 B4=0 R25=10
+ CTH=1 GTH0=1 GTH1=1 T=1 TK = 273.15
*****
Gthem      1      4      Value      =
+ {V(1,4)/(R25*(T)*exp(((B4/(V(3)+TK+TEMP)+B3)/
+ (V(3)+TK+TEMP)+B2)/(V(3)+TK+TEMP)+B1)/(V(3)+TK+TEMP
+B0)))}
RP 1 4 1T
RS 4 2 1n
Gtmp1      0      3      Value      =
+ {V(1,4)*V(1,4)/(R25*(T)*exp(((B4/(V(3)+TK+TEMP)+B3
)
+ (V(3)+TK+TEMP)+B2)/(V(3)+TK+TEMP)+B1)/(V(3)+TK+TEMP
+B0)))}
C_par 3 0 {CTH}
R_par 3 0 1T
Gpar 3 0 Value={V(3)*(GTH0+(GTH1*(V(3)+TEMP))}
.ends

```

Fig 3.18. Mathematical description of the thermoresistor C619\_10000 model



a)



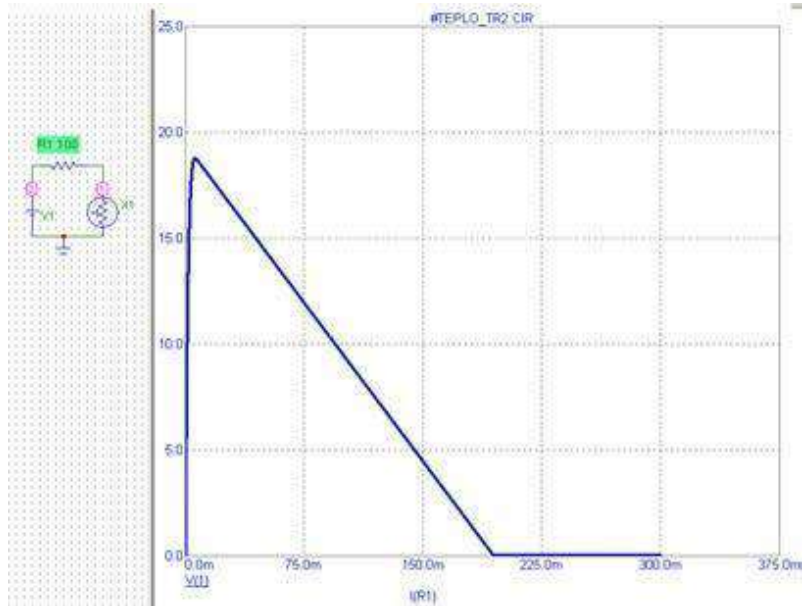
b)

Fig 3.19. Result of thermoresistor C619\_10000 VAC analysis

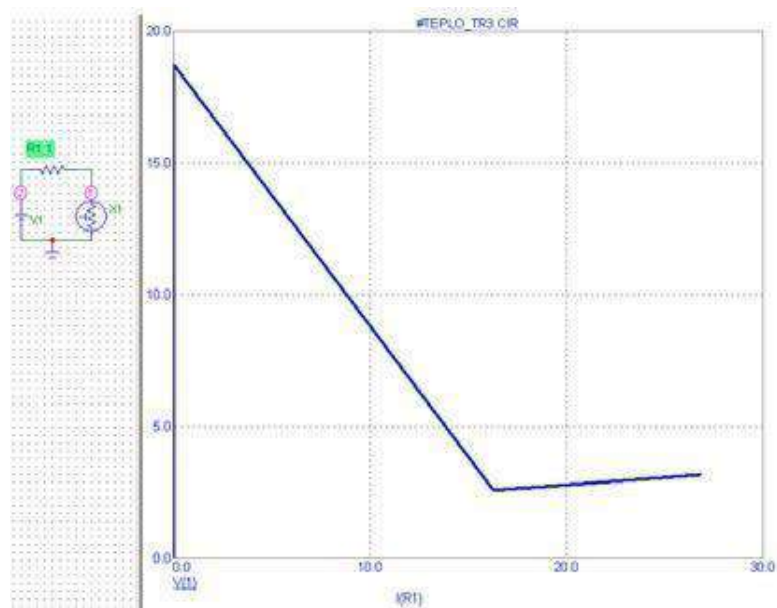
However, in the process of the detailed study of the above-mentioned model of the thermoresistor as well as in other existing models of such type, we revealed the following: first, in many cases the process of the analysis is "disrupted", i.e., programming environment of the circuit analysis issues the mistake of the iteration search of the working point and, secondly, in the existing models the possibility of the thermal resistance change (heat transfer) of the thermal resistor is not provided, it is very actual in case of modeling of the thermal flow sensors (output signal of such sensors is the function of its heat transfer).

Besides, we revealed that even when the iteration process was completed successfully (without releasing the warning about the mistake by MicroCAP program), in a number of problems the results of the VAC analysis of the thermoresistor, using NTC.LIB models, were not correct. Typical examples of such incorrect analysis are given in Fig 3.20. The essence of the incorrectness is that at the section of VAC with the negative differential resistance is approximated by the straight line, exactly; the jump of the model function of VAC takes place from the maximum value into the point of minimal value - without the intermediate points. After such a jump the model VAC function is reset or linearly grows, which does not correspond to the real VAC of the thermoresistor.

Detailed studies showed that NTC.LIB models function correctly only when the thermoresistor circuit is supplied from the current supply source, i.e., the current of the thermoresistor in the process of the analysis remains unchanged. Instead, failure of the iteration process occurs in case when the thermoresistor circuit is supplied from the of the voltage source at certain relations between the resistances of the circuit - in the given case at  $R_0 < K_x R_T$ , where  $R_0$  – is the resistance of the fixed value resistor, serially connected with thermoresistor  $R_T$ ,  $K_x$  – is the proportionality factor, that depends on the specific type of the thermoresistor.



a)



b)

Fig 3.20. Examples of the incorrect result of the thermoresistor VAC analysis using the NTC.LIB model

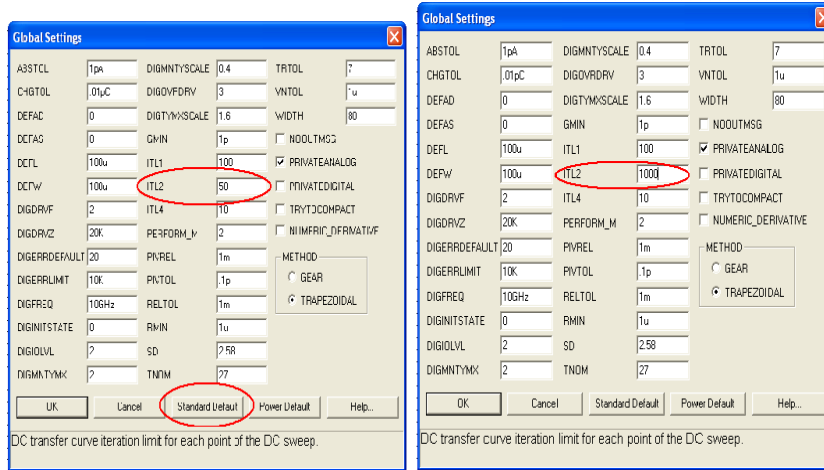


Thus, it was shown that the models of NTC.LIB type do not allow carrying out electric thermal modeling of the measuring circuits of the thermal flow sensors. We will give a more detailed analysis of the reasons for the failure of the iteration processes of the thermoresistors VAC calculation and possible methods of its elimination.

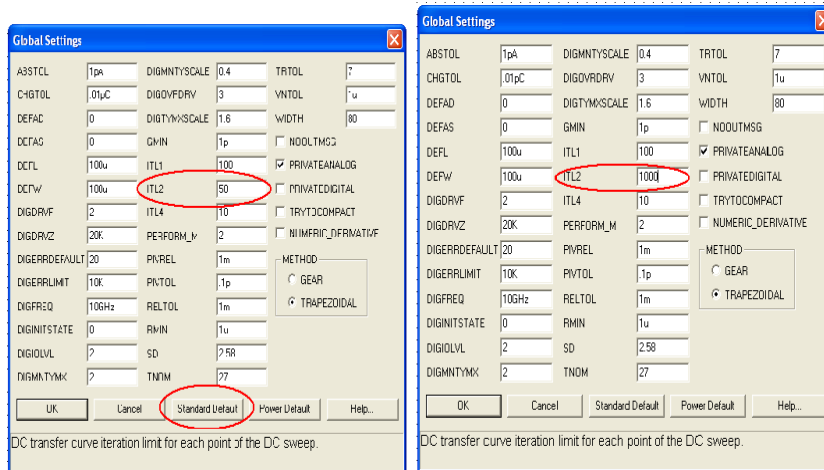
First and the most important reason for the iteration process failure is the emergence in the circuit of the thermoresistor auto oscillations, which typically occur of the VAC section with the negative differentiation resistance is available. In the given case, it is referred to as thermal auto-oscillations. It is obvious that the presence of such auto-oscillations is not a problem of circuit engineering modeling, as it is, but it is the objective parasitic phenomenon in the linear systems of the signal conversion. It is necessary to solve this problem, applying corresponding circuit solutions, in particular, as it will be shown in the next section, by the voltage sources of the thermoresistive measuring converters of the thermal flow sensors by the corresponding current sources.

The second possible reason for the incorrect analysis is not accurate determination of quantitative characteristics of the iteration processes which could be changed by Global Settings parameters. In particular, as it is shown in Fig 3.21a, the limiting number of the iteration cycles at DC analysis of VAC, set by ITL2 parameter, by default, is established  $ITL2=50$ .

Such limited number of the iteration cycles in a number of cases may lead to a large computation error as it occurs in electric thermal DC analysis of the thermoresistor VAC on the base of the temperature-dependent circuit, functionally controlled voltage source and other components of the above-mentioned equivalent circuit (Fig 3.22). As it can be seen, the result of circuit modeling is not correct – voltages at the functionally controlled sources ET and ERT have uncontrolled oscillation.



a)



b)

Fig 3.21. Parameters of the Global Settings window

Partial solution of this problem is the increase of the number of iteration cycles, for instance to  $ITL2 = 1000$  (see Fig 3.21b), this, on one hand, using modern high efficient computing equipment, does not lead to the increase of the time of analysis, and, on the other hand – it considerably improves the accuracy of the analysis. As we have already demonstrated in the course of numerous research, temperature of which is determined by the amount of Joule heat and conditions of the heat transfer, modeling of VAC of the thermoresistors with

positive temperature resistance coefficient (metal resistance thermometers) at  $ITL2 = 1000$  provides sufficiently stable iteration process.

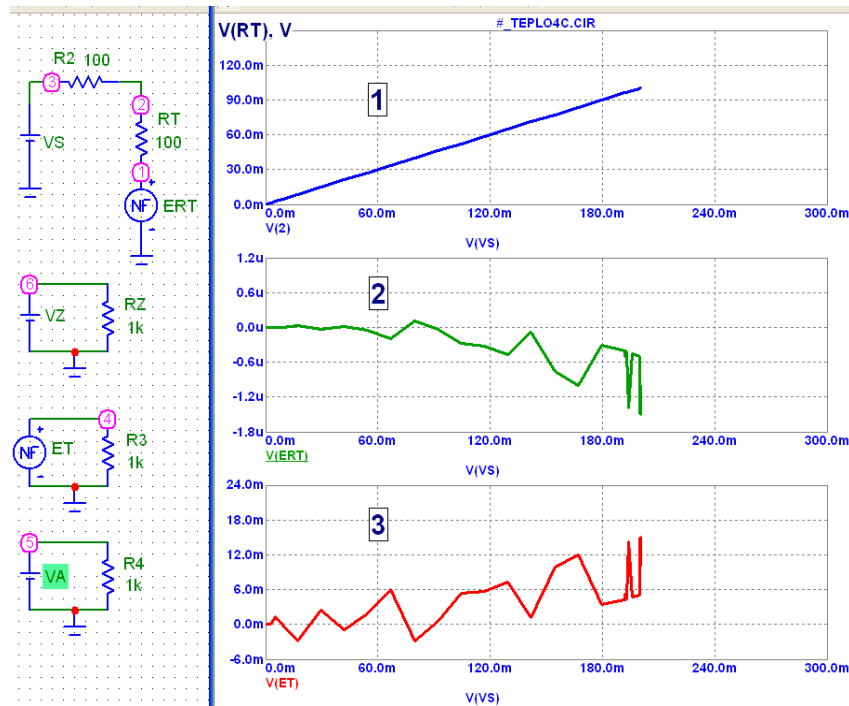


Fig 3.22. Example of the calculation inaccuracy at  $ITL2 = 50$  (Standard Default)

The third reason for the iteration process failure is incorrectly set parameters of the thermoresistors model or the analysis conditions. As the mathematical functions of the controlled current sources  $G_{them}$  and  $G_{tmp}$  models of thermoresistors NTC.LIB (see Fig. 3.18) are rather complex for determination of the reasons of the iteration failure, for the analysis of the reason we will use the circuit with the controlled current source  $G_1$ , it is connected to the voltage source  $V_1$  across the resistor  $R_1$  (Fig. 3.23).

As it can be seen, the attempt to model VAC characteristic of the thermoresistor with the extremal functional characteristic leads to the curtailing of the iteration process. Dotted line shows the theoretical functional characteristic and solid line, passing from the extremum point downwards – the result of modeling. Another example of the incorrect iteration process can be seen in Fig. 3.24, where the result of modeling of the above-considered equivalent circuit of the thermoresistor with the extremal functional characteristic on the base of the controlled voltage sources is presented.

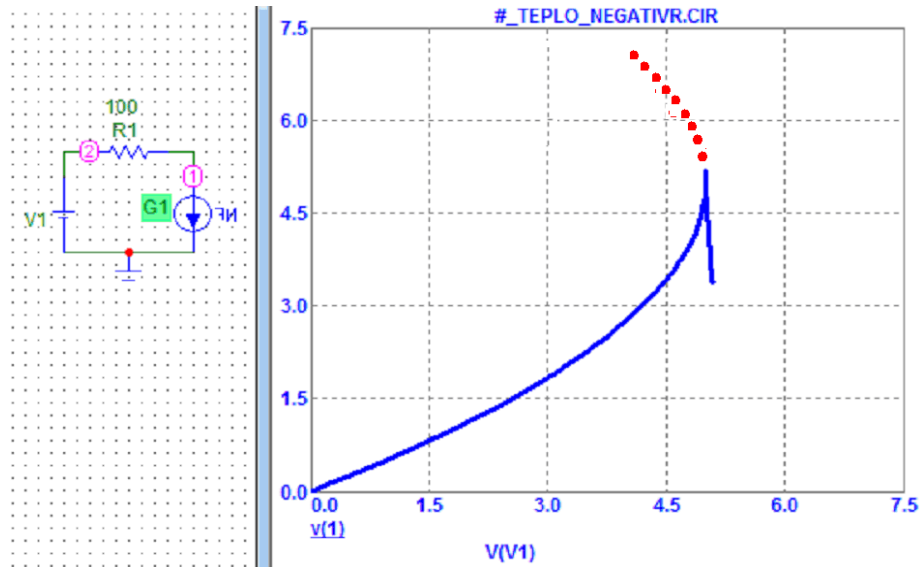


Fig. 3.23. Example of the calculation iteration process failure of the controlled current source VAC with the extremal functional characteristic

Thus, the problem of the development of the express-method for the determination of the boundaries within which the correct DC analysis of VAC of the thermoresistive measuring converters of thermal flow sensors is provided, was solved and solved.

The suggested method of the express-analysis of the stability of model study of the bridge or half bridge circuits of primary converters of the flow sensors is based on iteration process:

$$\Delta T[n+1] = P_Q[n] Z_Q = \frac{V_E^2 R_{QT}[n] Z_Q}{(R_0 + R_{QT}[n])^2}; R_{QT}[n+1] = R_{QT0}(1 + \alpha \Delta T[n+1]);$$

where  $P[n]$  and  $R_{QT}[n]$  – is thermal power, released in thermoresistive converter and its resistance in  $[n]$ -th iteration, correspondingly;

$\Delta T[n+1]$  – is the overheating of the converter in  $[n+1]$  iteration.

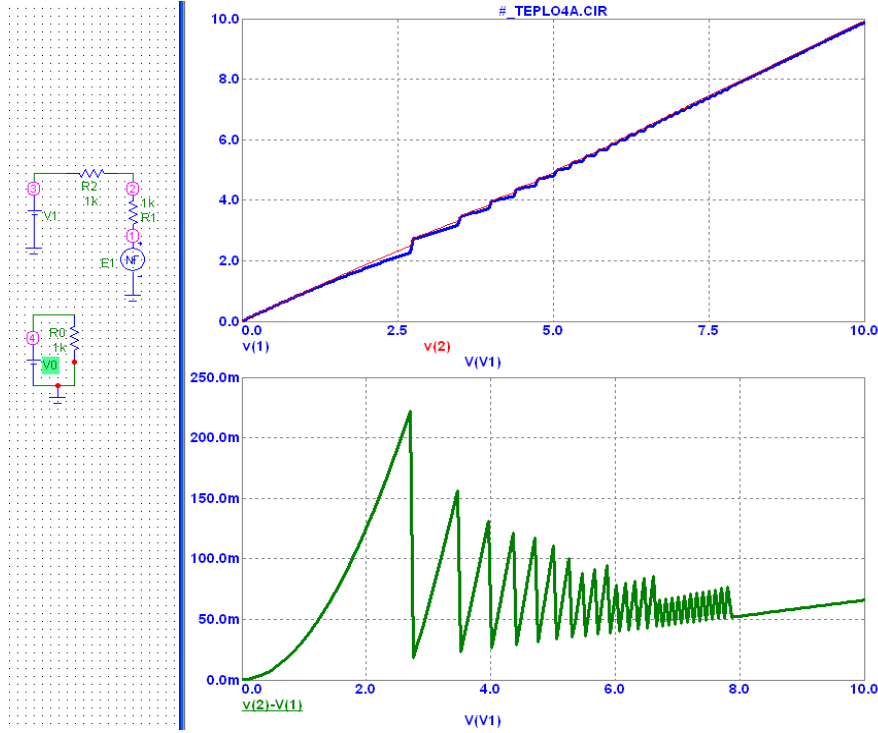


Fig. 3.24. Example of the incorrect iteration process

In particular, for the first iteration computation we have:

$$\Delta T[1] = P_Q[n]Z_Q = \frac{V_E^2 R_{QT0} Z_Q}{(R_0 + R_{QT0})^2}; \quad R_{QT}[1] = R_{QT0}(1 + \alpha \Delta T[1]),$$

for the second:

$$\Delta T[2] = P_Q[n]Z_Q = \frac{V_E^2 R_{QT}[1] Z_Q}{(R_0 + R_{QT}[1])^2}; \quad R_{QT}[2] = R_{QT0}(1 + \alpha \Delta T[2]).$$

At each stage of the calculation relative deviation factor  $D$ , which qualitatively describes the convergence of the iteration process, is determined:

$$D[n+1] = ABS \left( 1 - \frac{R_{QT}[n+1]}{R_{QT}[n]} \right)$$

Realization of the condition  $D[n \rightarrow \infty] \rightarrow 0$ , which proves the correct course of the iteration process, allows to perform the successful electric thermal model study of the circuit of the primary convertor of the flow sensor in packages PSpice and MicroCAP. Instead, if the given condition for the electric

model study is not realized, it is necessary to restrict the boundaries of DC analysis, indicating the initial point of the iteration by the option NODESET.

Several typical examples of the suggested method of the express-analysis of the stability application are given in Fig. 3.25-3.27. The left graphs show the course of the iteration  $R_{QT}[n]$ , and the right hand graphs –  $D[n]$ .

In particular, if  $V_E=10$  V;  $R_0 = 100$  Ohm;  $R_{QT0} = 100$  Ohm;  $Z_Q = 100$  grad/W;  $\alpha = 0,1$  grad $^{-1}$  (see Fig. 3.25) the iteration process is successful - already at the tenth cycle deviation coefficient is  $D = 10^{-5}$  [10].

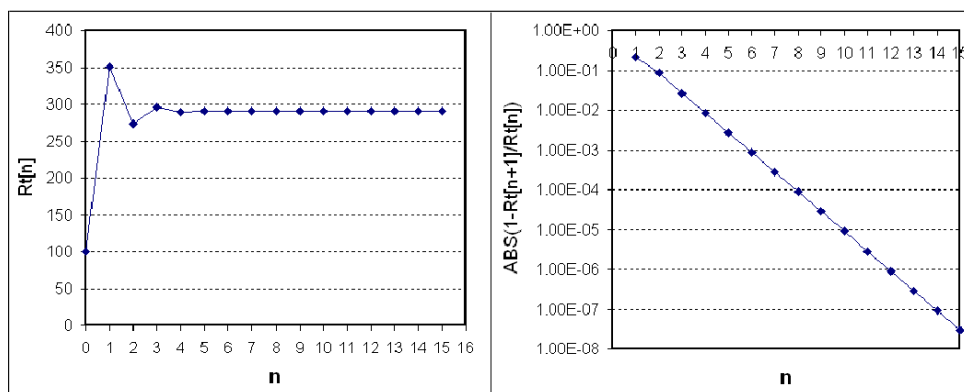


Fig 3.25. Course of the iteration process at:  $V_E=10$  V;  $R_0 = 100$  Ohm;  $R_{QT0} = 100$  Ohm;  $Z_Q = 100$  grad/W;  $\alpha = 0,1$  grad $^{-1}$

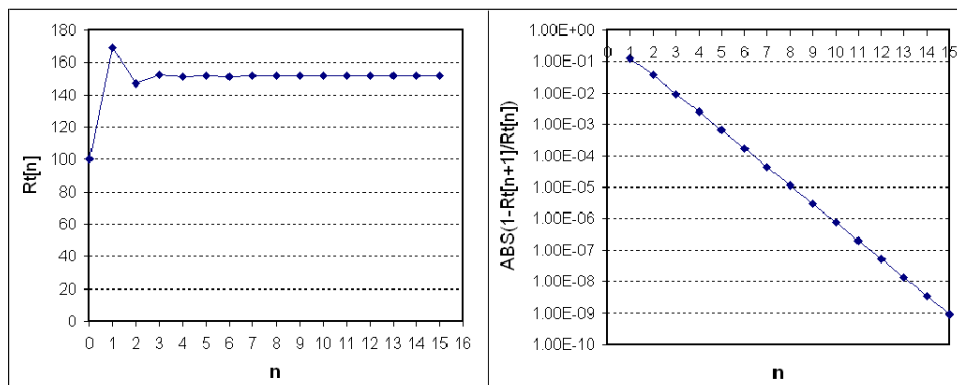


Fig 3.26. Course of the iteration process at:  $V_E=10$  V;  $R_0 = 20$  Ohm;  $R_{QT0} = 100$  Ohm;  $Z_Q = 100$  grad/W;  $\alpha = 0,01$  grad $^{-1}$

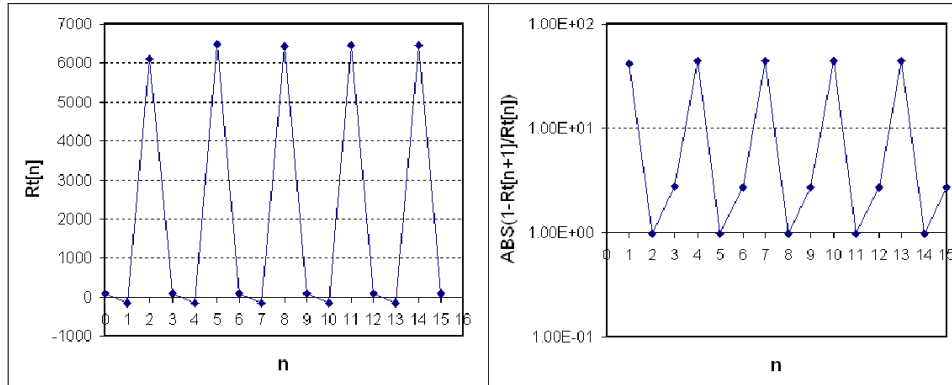


Fig 3.27. Course of the iteration process at:  $V_E = 10$  V;  $R_0 = 100$  Ohm;  $R_{QTO} = 100$  Ohm;  $Z_Q = 100$  grad/W;  $\alpha = -0,1$  grad-1

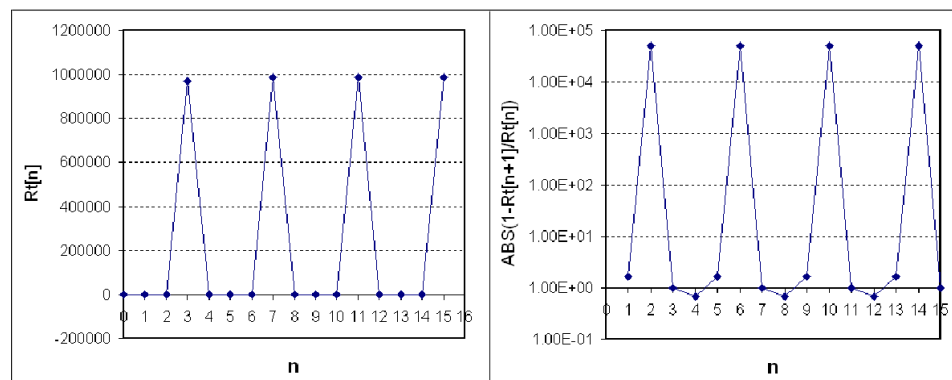


Fig 3.28. Course of the iteration process at:  $V_E = 10$  V;  $R_0 = 20$  Ohm;  $R_{QTO} = 100$  Ohm;  $Z_Q = 100$  grad/W;  $\alpha = -0,01$  grad-1

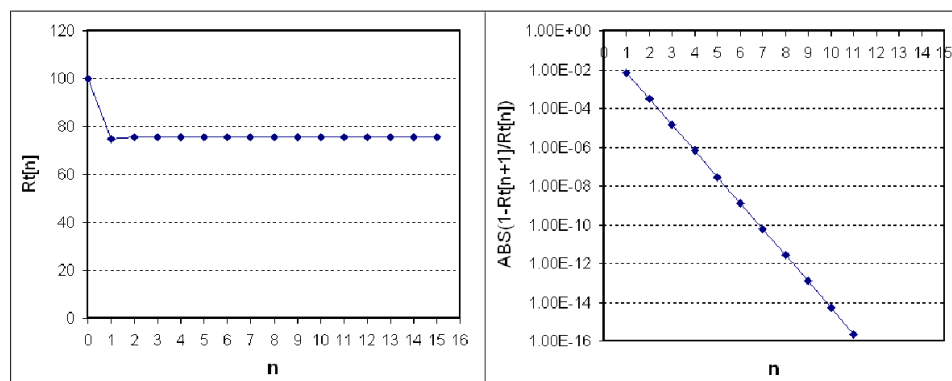


Fig 3.29. Course of the iteration process at:  $V_E = 10$  V;  $R_0 = 100$  Ohm;  $R_{TO} = 100$  Ohm;  $Z_Q = 100$  grad/W;  $\alpha = -0,01$  grad-1

The iteration process is still more rapid at:  $V_E = 10$  V;  $R_0 = 20$  Ohm;  $R_{Q70} = 100$  Ohm;  $Z_Q = 100$  grad/W;  $\alpha = 0,01$  grad $^{-1}$ , for which  $D[10] = 10^{-6}$ . However, for the next two examples with negative values of the temperature coefficient of the resistance  $R_0 = 100$  Ohm;  $R_{Q70} = 100$  Ohm;  $Z_Q = 100$  grad/W;  $\alpha = -0,1$  grad $^{-1}$  (see Fig 3.27) and  $R_0 = 20$  Ohm;  $R_{Q70} = 100$  Ohm;  $Z_Q = 100$  grad/W;  $\alpha = -0,01$  grad $^{-1}$  (see Fig 3.28) the failure of the iteration process takes place. The latter example shows that the iteration process is successful also for the negative values of the temperature coefficient of the resistance  $R_0 = 100$  Ohm;  $R_{70} = 100$  Ohm;  $Z_Q = 100$  grad/W;  $\alpha = -0,01$  grad $^{-1}$ . Thus, in each specific case prior to performing model study of the circuit of primary converter of the flow sensors in package PSpice and MicroCAP it is necessary to carry out the express-analysis of the stability of the iteration process. The examples of the successful modeling study are given in Fig 3.30 and Fig 3.31.

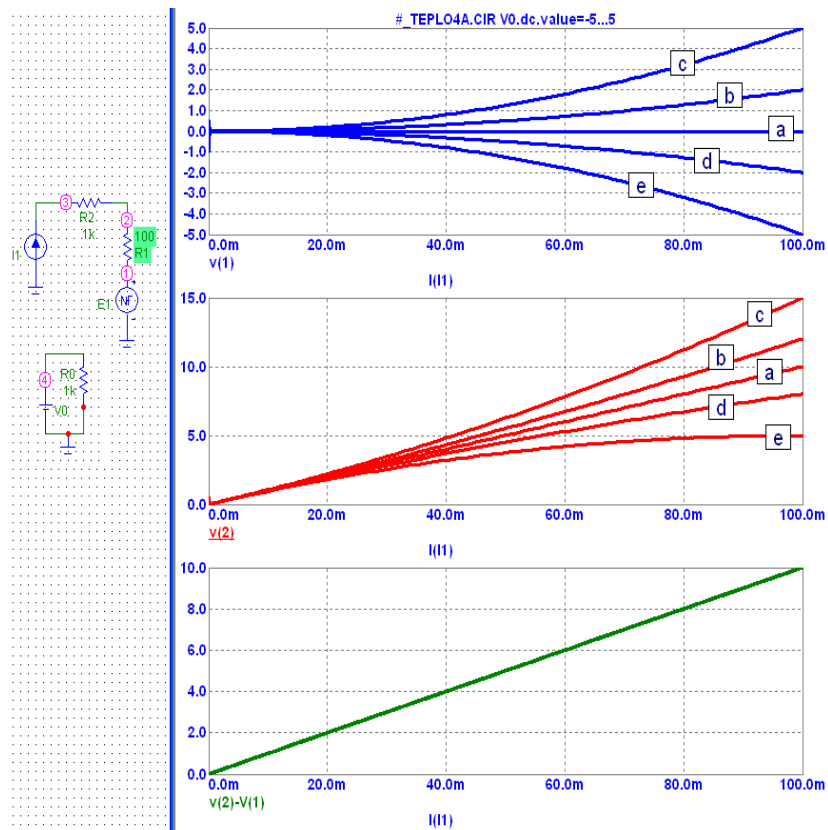


Fig 3.30. DC example of the successful analysis of VAC of thermoresistive converter with current supply source



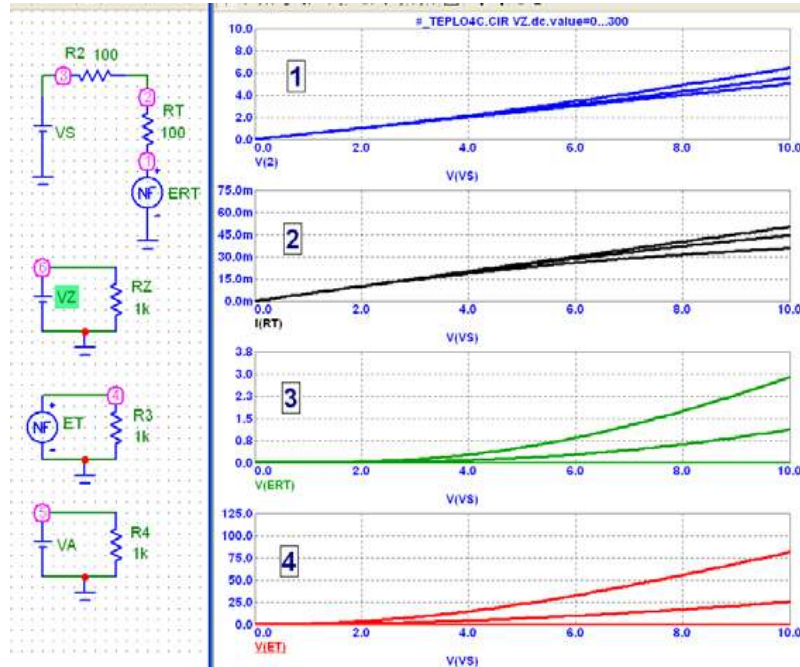


Fig 3.31. DC example of the successful analysis of VAC of thermoresistive converter with current supply source

### 3.4. Electric thermal modeling of the temperature-dependent VAC of the diode-type converters

Besides the measuring converters of the resistive type, considered above, thermal sensor devices of flow rate measurement can use the converters of the diode and transistor types. As the resistive converters diode and transistor converters are heated by their supply current, but the information value of the temperature and the flow rate in diode converters is voltage drop on the forward-biased p-n junction, and in the transistor-based converters – emitter or collector current.

We will consider the principle of construction of the diode converter model, which enables us to study the impact of the diode heating current on the temperature drift of its VAC. First we will analyze the temperature voltage coefficient of the forward - biased p-n junction  $dV_{pn}/dT$ . For silicon p-n junction at voltages, characteristic for the direct bias voltages  $V_{pn} \gg \phi_T$ , condition takes place that is adequate:

$$\exp \frac{V_{pn}}{m\phi_T} \gg 1$$

Hence, the expression of VAC can be simplified:

$$I = I_S \left( \exp \frac{V_{pn}}{m\phi_T} - 1 \right) \approx I_S \exp \frac{V_{pn}}{m\phi_T},$$

where  $I_S$  – is the saturation current of p-n-junction;  $\phi_T = kT/q$  – temperature potential;  $m$  – nonideality coefficient of p-n junction;  $k$  – is Boltzman constant;  $q$  – is the charge of the electron;  $T$  – is an absolute temperature.

Temperature characteristic of the saturation current in the first approximation is presented by the expression [100, 101]:

$$I_S = CT^3 \exp \left( -\frac{qE_{G0}}{kT} \right),$$

where  $C$  – is a constant,  $E_{G0}$  – is the energy gap band of the silicon at  $T = 0$  K ( $E_{G0} = 1.205$  V).

Further, having performed the corresponding transformation and differentiation:

$$V_{pn} = m\phi_T \ln \frac{I_{pn}}{I_S}; \quad \frac{dV_{pn}}{dT} = \frac{mk}{q} \ln \frac{I_{pn}}{I_S} - m\phi_T \frac{d(\ln I_S)}{dT} = \frac{V_{pn}}{T} - m\phi_T \frac{d(\ln I_S)}{dT};$$

$$\ln I_S = \ln C + 3 \ln T - \frac{qE_{G0}}{mkT};$$

$$\frac{d(\ln I_S)}{dT} = \frac{3}{T} + \frac{qE_{G0}}{mkT^2};$$

we obtain the function of the voltage temperature coefficient  $VTC_{pn}$ :

$$\begin{aligned} TKV_{pn} &= \frac{dV_{pn}}{dT} = \frac{V_{pn}}{T} - m\phi_T \left( \frac{3}{T} + \frac{qE_{G0}}{mkT^2} \right) = \frac{V_{pn}}{T} - 3 \left( \frac{mk}{q} + \frac{E_{G0}}{T} \right) = \\ &= - \left( \frac{E_{G0} - V_{pn}}{T} + 3 \frac{mk}{q} \right). \end{aligned}$$

For the ideal model of p-n junction  $m = 1$ . Then, having substituted  $k = 1,38 \cdot 10^{-23}$  J/K,  $q = 1,602 \cdot 10^{-19}$  K, if  $T = 300$  K we find

$$TKV_{pn} = - \left( \frac{1205(MB) - V_{pn}(MB)}{T} + 0.26 \right) \left[ \frac{MB}{K} \right].$$

In particular, at  $T = 300\text{K}$  for typical value  $V_{pn} = 650\text{ mV}$  we obtain the temperature coefficient of the voltage on the forward biased p-n junction  $\text{TKV}_{pn} \approx -2,1\text{ mV/K}$ .

The simulation modeling of the voltage drop temperature dependence at forward-biased p-n junction at different currents (1  $\mu\text{A}$ , 10  $\mu\text{A}$ , 100  $\mu\text{A}$ , 1 mA, 10 mA, 100 mA, 1 A) is shown in Fig 3.32. The research, carried out, proves the results of theoretical calculations regarding the dependence of the voltage temperature coefficient  $\text{VTC}_{pn}$  on forward biased p-n junction on the current – at the current increase  $I_{pn}$ , and voltage increase  $V_{pn}$ , absolute value of the temperature coefficient decreases from  $\text{VTC}_{pn} \approx -2,5\text{ mV/K}$  (at  $I = 1\ \mu\text{A}$ ) to  $\text{VTC}_{pn} \approx -1,5\text{ mV/K}$  (at  $I = 100\text{ mA}$ ).

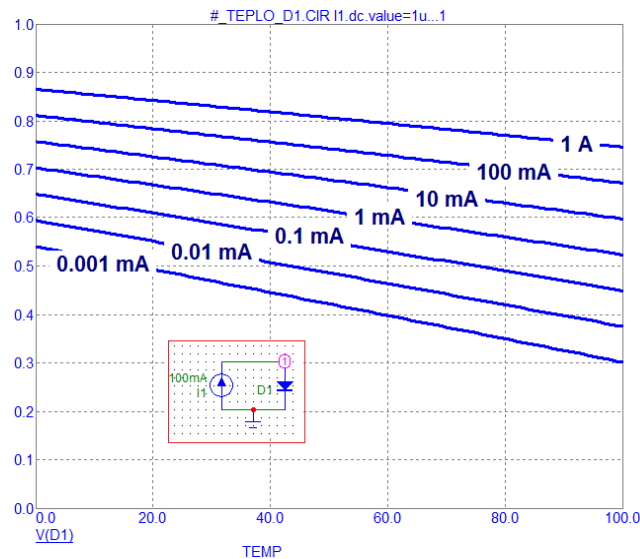


Fig 3.32. Temperature dependence of the voltage drop on forward biased p-n junction at various currents

The results of the study of the straight VAC at various temperatures (0, 20, 40, 60, 80, 100°C) are shown in Fig. 3.33. Dotted line shows VAC of the diode in the process of its self-heating. However, this characteristic is obtained as a result of the multi-stage simulation, during the first modeling, families of VAC of the diode are calculated in PSpice or MicroCAP at various temperatures, during the second modeling, at the preset thermal resistance  $Z_{\theta}$  and power  $P_{\theta}(T)$  determined at the first stage – the overheating temperature of the diode structure  $\Delta T$ . Further, temperature drift is overlapped on the family of VAC, obtained at the first stage at correspondingly selected values of the current and

voltage on p-n junction. It is obvious, that such multistage process requires several iterations, that makes the calculation of the diode VAC in the mode of its self-heating ineffective and impossible, applying the traditional packages of circuit simulation.

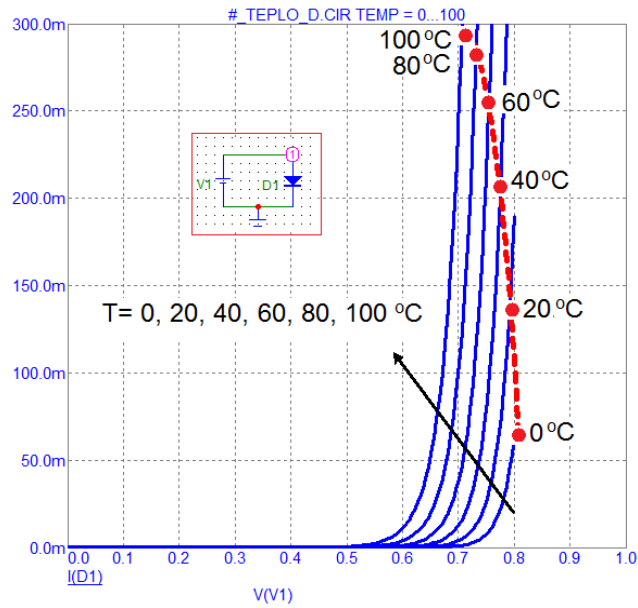


Fig 3.33 Example of DC analysis of VAC of the diode

Thus, similarly to the above-considered problem of the thermoresistive converter modeling, the problem of the electrothermal modeling of diode VAC at its self-heating is set.

For this purpose we will make use of the technique of the thermoresistive converter equivalent circuit synthesis, developed above (in particular, shown in Fig 3.31), however, instead of the resistor the diode will be used. The example of the electric thermal study of the diode model, synthesized in such a way is shown in Fig 3.34. Temperature-dependent component of the output voltage of the diode model is presented by the controlled voltage source ERT, thermal resistance of the diode structure - by the source VZ, diode temperature - by the source of ET, and the function of temperature dependence of the voltage at p-n junction - by the source VA. In the process of the DC analysis of VAC overheating temperature of the diode relatively the environment is determined by the expression  $\Delta T = T - T_0 = P_Q(T)Z_Q = V_{pn}(T)I_{pn}(T)Z_Q$ , and temperature-dependent component of the output voltage  $V_{pn}(T) = \Delta T \cdot TKV(I_{pn})$ .

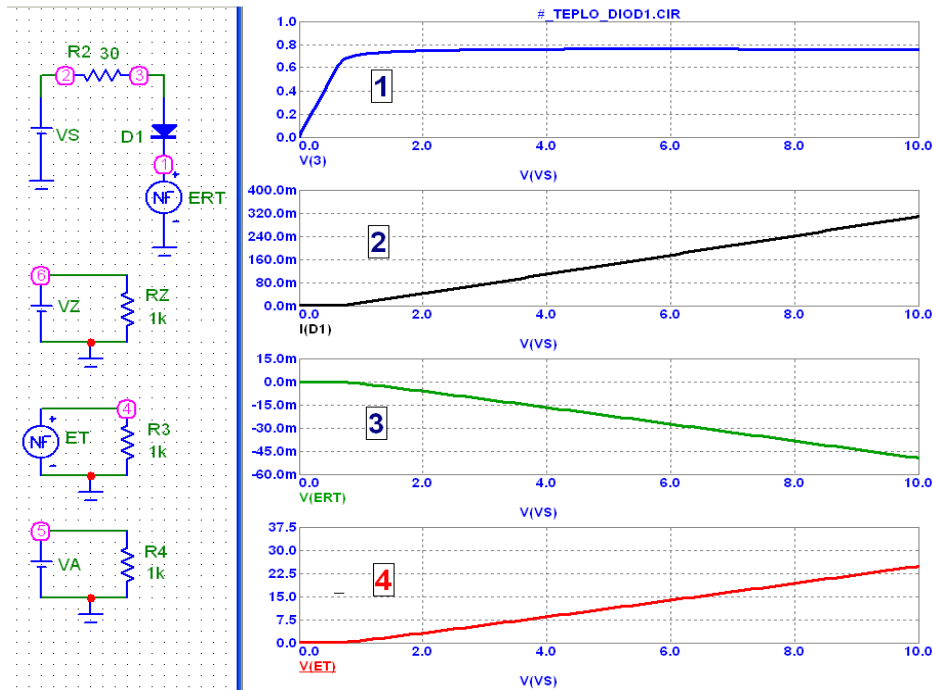


Fig 3.34. Main components of the signal of the electric thermal model of the diode: 1 – output voltage; 2 – current; 3 – temperature-dependent component of the output voltage; 4 – temperature

The results of the example of the electric thermal analysis of the VAC of the diode in self-heating mode by the supply current at: a –  $Z_{\theta} = 0$  grad/W; b –  $Z_{\theta} = 30$  grad/W; c –  $Z_{\theta} = 100$  grad/W are shown in Fig 3.35. As it is seen, VAC of the diode not only rotates on the voltage axis leftward but at considerable self-heating there appears a VAC section with negative differential resistance - with the increase of the current the overheating temperature increases, thus, voltage at the barrier of p-n junction decreases. In case of non-controlled heating there appears the well known from literature on power electronics [176], the phenomenon of "current filamentation" – the process of the overheating of the section of p-n junction with the highest temperature avalanche concentrates the current of the diode, overheating still more and, at last, destroying. It is obvious, that this phenomenon must be taken into account in the process of thermal anemometers development on self – heating diode and transistor structures.

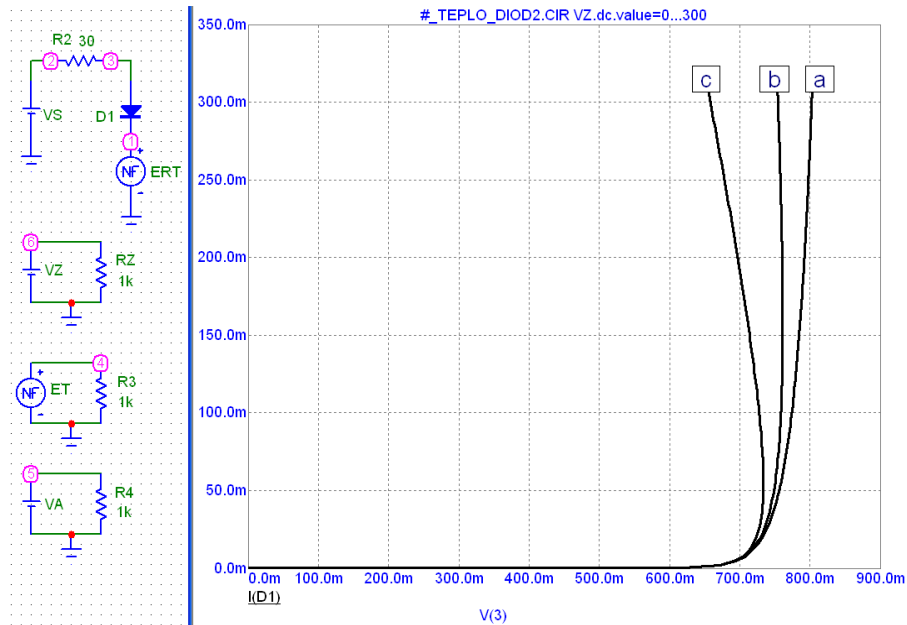


Fig 3.35. Results of electric thermal analysis of diode VAC in self-heating mode by supply current

The obtained result proves that the suggested electric thermal model adequately describes real processes, occurring in the semiconductor structure of p-n junction and, at correspondingly set parameters of the model (including the considered-above limits of the correct iteration of DC analysis of the elements with the section of negative differential resistance), provides high efficiency of the process of the development of the diode converters of thermal flow sensors.

### 3.5. Electric thermal modeling of temperature-dependent VAC of the transistor-type converters

Primary converters of thermal flow sensors can serve not only thermoresistive or diode structures but transistors, mainly bipolar n-p-n structures. Their advantage is a wide range of the supple (heating) modes and temperature measurement modes selection. Basic heating in the bipolar structures is realized by the heat release on the reverse-biased p-n junction. As it will be shown in Section 4, unlike thermoresistive converters the usage of the transistor structure enables it to form the current output that provides higher values of transducing steepness.

From the point of view of primary converters of thermal flow sensors, the advantage of the transistor structures as compared with the diode structures is

more efficient usage of the supply circuit energy - voltage drop on diode structures, as a rule, does not exceed 0.8 V (for silicon structures), it means, in particular, that at 5 V supply source practically the whole voltage ( $5 - 0.8 = 4.2$  V) drops on current forcing circuit. It is obvious that not more than 20 % of supply circuit energy will be spent on heating the diode structure. Instead, the voltage drop on the transistor structure (on reverse-biased collector p-n junction) can be randomly regulated by the resistive divider of basic circuit voltage, that provides maximum energy profit.

According to the problems, put forward in this section, we will consider the method of the synthesis of the electrothermal model of the transistor structures of thermal flow sensors. Analyzing the model of the bipolar transistor from the point of view of the impact of self-heating temperature on VAC, it is necessary to consider, at least, three mechanisms of temperature impact. It should be noted, that, as in the models presented before, we speak not only of the impact of the ambient temperature on the parameters of the transistor, but on its self-heating, i.e., direct impact of power released in the transistor structure on its electric physical parameters. It is obvious that model studies of self-heating must be conducted in a single cycle, when the temperature is not an independent value but is determined by the power of the transistor

The first mechanism of the temperature impact is analogous to the above-mentioned diode structures - increase of temperature stipulates the decrease of voltage drop on p-n junction  $V_{pn} = f_1(T)$  of the transistor structure. In case of direct connection of the transistor the temperature drift of voltage on emitter - base junction is important, and in case of inverse connection - on collector-base junction. The second mechanism is connected with the sharp increase of the reverse currents of p-n junction  $I_s = f_2(T)$  in the process of their heating - mainly, reverse-biased collector-base junction. The third mechanism of the impact - it is the temperature drift of the current increase coefficient of the transistor structure  $B_F = f_3(T)$ . These three mechanisms were taken into consideration in the process of model development (equivalent circuit) of the electric thermal analysis of the bipolar transistor VAC (Fig 3.36).

The given equivalent circuit is based on Ebers-Moll model (if necessary it may be based on the still more complex Poon-Gummel charging model) as well as on the principles of electric thermal modeling of the resistive and diode structures, considered in the previous sections.

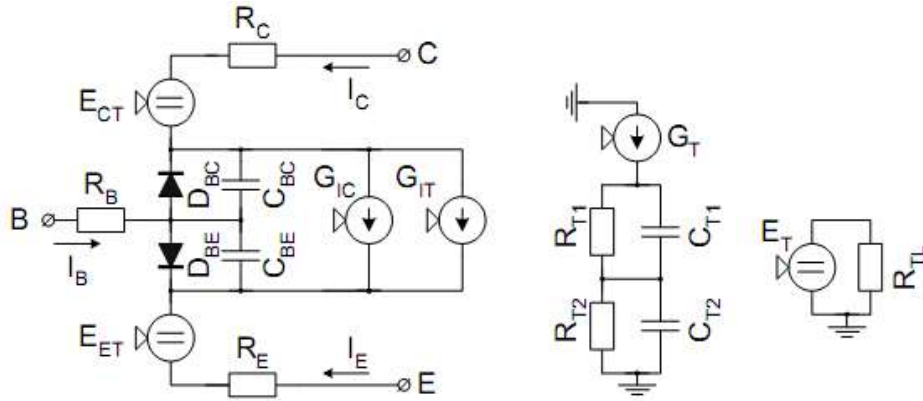


Fig 3.36. Model of electric thermal analysis of the bipolar transistor VAC

Conventional for Ebers-Moll model [66, 67] is emitter and collector p-n junction  $D_{BE}$ ,  $D_{BC}$ , stray barrier capacitance of which is presented by the capacitors  $C_{BE}$ ,  $C_{BC}$ . Resistive components of the transistor structure are presented by the resistances of base, emitter and collector sections  $R_B$ ,  $R_E$ ,  $R_C$ . Current transmission coefficient of the structure is described by the controlled current source  $G_{IC}$ . Mathematical presentation of such a traditional transistor model is described in detail in the monographs and instruction manuals, using PSpice or MicroCAP packages [66, 67], that is why, its further consideration is not performed.

The characteristic feature of the suggested model is the in the presence of two controlled voltage sources  $E_{CT}$ ,  $E_{ET}$  and controlled current source  $G_T$ . Besides, the electric thermal model contains the above-considered (in particular, in Fig 3.9) circuits of pulse thermal relaxation  $G_T$ ,  $R_{T1}$ ,  $C_{T1}$ ,  $R_{T2}$ ,  $C_{T2}$  and thermal resistance  $E_T$ ,  $R_{TL}$ . Principles of voltage sources specification  $E_{CT}$ ,  $E_{ET}$ , which form temperature-dependent component of the voltage drop on the forward-biased p-n junction  $\Delta V_{pn} = f_i(T)$ , have already been considered in the process of the electric thermal study of the diode structures.

The impact of the temperature on the current of the reverse-biased p-n junction  $I_S = f_2(T)$  similarly Ebers-Moll model can be represented in the form:

$$I_S T = I_{S0} \exp\left(\left(\frac{T}{T_0} - 1\right) \frac{E_G(T)}{\phi_T}\right) \left(\frac{T}{T_0}\right)^{X_{T1}},$$

where  $X_{T1}$  – is the exponent of the temperature dependence of the reverse current  $I_{S0}$ .

The reverse currents (typically not greater than several microamperes) as compared with the heating current (hundreds of milliamperes) can be neglected.



However, the participation of the reverse-biased collector p-n junction current in the total basic current, amplified several hundreds of times, cannot be neglected. That is why, it is expedient to combine it with the third mechanism - temperature drift of current amplification factor of the transistor structure  $B_F = f_3(T)$ :

$$B_F(T) = B_F \left( \frac{T}{T_0} \right)^{X_{TB}}$$

where  $X_{TB}$  – is the exponent of the temperature dependence of the current amplification factor  $B_F$ . This combined mechanism is presented by the controlled source  $G_{TT}$ .

For the demonstration of the efficiency of the developed electric thermal model of the transistor self heating we will consider two typical results of its output VAC modeling (Fig. 3.37-3.40).

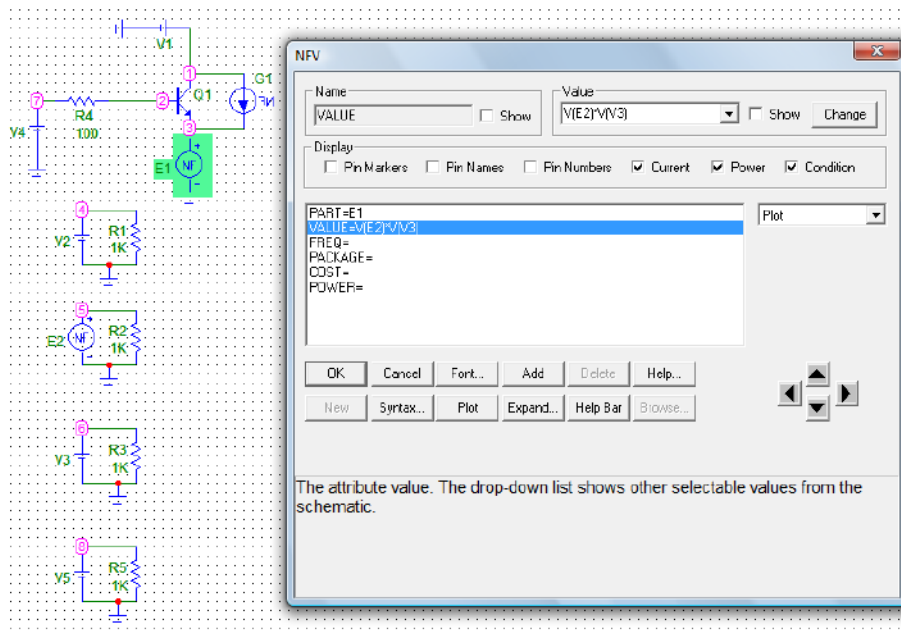


Fig 3.37. Specification of the controlled voltage source of the electric thermal model of the bipolar transistor

To simplify the results, given below, not a separate components of the transistor equivalent circuit are used but the conventional Ebers-Moll model (n-p-n transistor Q1) is used, the given model, for carrying out the electric thermal modeling is supplemented with the corresponding controlled sources: source E1 describes functional dependence  $\Delta V_{pn} = f_1(T)$ , source G1 – functional dependencies  $I_s = f_2(T)$  and  $B_F = f_3(T)$ , source V2 – thermal resistance of the

transistor structure, source E2 - overheating temperature of the structure, relatively the ambient temperature, source V3 –  $TKV_{pn}$ , coefficient, and source V5– coefficients  $X_{T1}$  and  $X_{TB}$ . The supply voltage of the collector circuit is supplied from the source V1, and base circuit - from the source V4 and resistor R4.

The first result of modeling (Fig. 3.38) is obtained only with the account of the temperature dependence of the voltage drop on the emitter p-n junction. It can be seen that if the transistor current increases (signal 1), its heating occurs and (signal 2) voltage drop decrease on the emitter p-n junction (signal 3) takes place. These effects increase if the thermal resistance (graphs a, b, c) of the transistor structure increases.

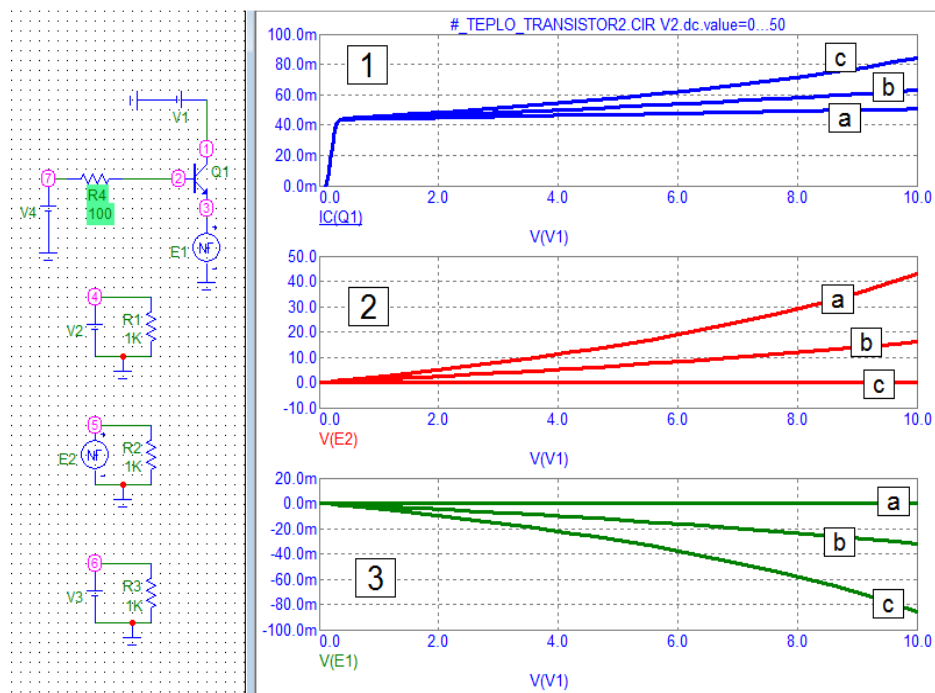


Fig 3.38. Result of DC analysis of the bipolar transistor output VAC with the account of  $V_{pn} = f_i(T)$  mechanism at several values of the thermal resistance  $Z_{\theta}$

The second result of modeling (Fig 3.40) takes into account all the above-considered mechanisms of the temperature impact. As it is seen, the modulation of the transistor VAC in the process of its self heating is greater, it is stipulated not only by the temperature drift of the voltage on the emitter p-n junction but also by the increase of the current amplification coefficient of the transistor in the process of its self-heating.

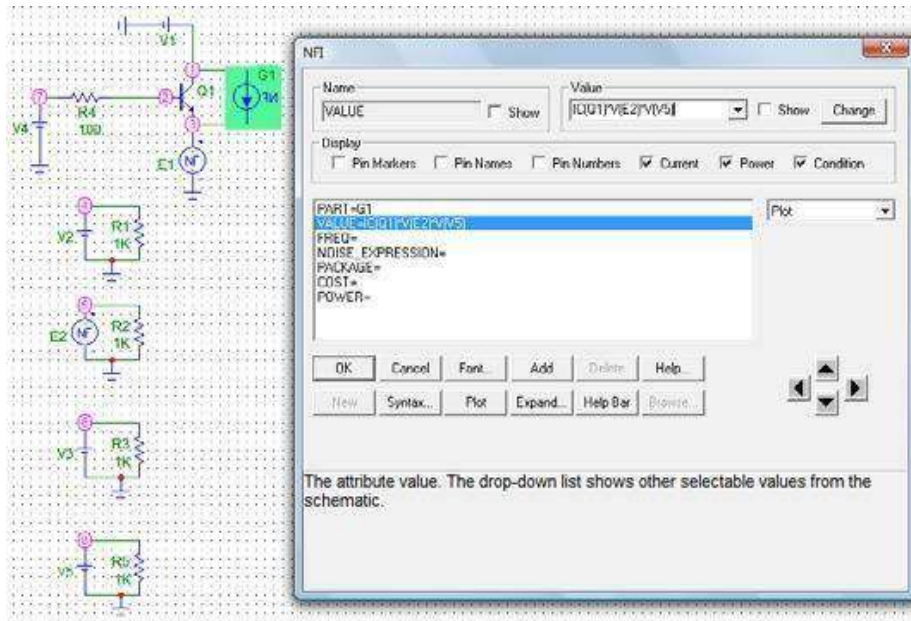


Fig 3.39. Specification of the controlled current source of the bipolar transistor electric thermal model

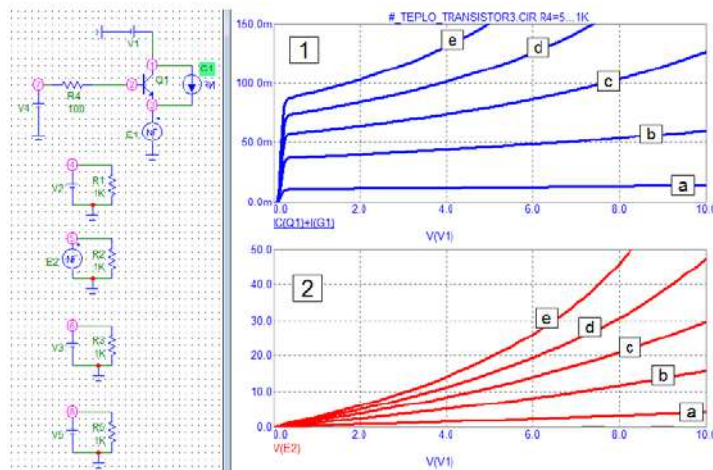


Fig 3.40. Result of DC analysis of bipolar transistor VAC with the account of the mechanisms  $V_{pn} = f_1(T)$ ,  $I_s = f_2(T)$ ,  $B_F = f_3(T)$  at several values of thermal resistance  $Z_{\theta}$

It is obvious, that from the point of view of practical usage of the transistors in the circuits of measuring converters of thermal flow sensors it is necessary to provide not only the sufficient heating of the transistor structure but also the

sufficient electric thermal stability of its operation. For this purpose it is necessary to use, in particular, emitting stabilizing resistors or differential connection of the pair of the transistors with current supply.

## 4. Mathematical models of static and dynamic characteristics of the input transistor stages of the push-pull dc amplifiers

### 4.1. Static transfer characteristics of the input stages of the push-pull dc amplifiers

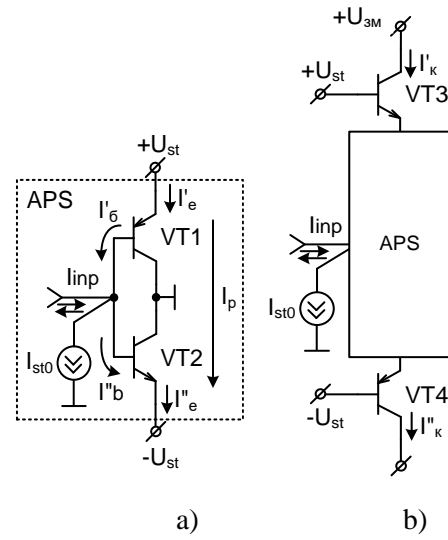
Development of microelectronic technologies and the possibility of manufacturing of the complementary bipolar transistors on one crystal promote the developers to design new push-pull symmetric structures, oriented on the principle of the currents amplification and potentially have higher operation rate [128, 177]. However, for the manufacturing of such amplifiers, besides the solution of the problem of the mode setting on IAS direct current, it is necessary to take measures regarding the symmetrization of the transfer factor of IPPS on the paraphrase outputs and IAS.

It should be noted that the characteristics of PPDCA greatly depend on the principle of IPPS construction.

IPPS contains core, stages and SVU. Structural functional organization of the core of the IPPS circuit with the compensation of zero shift is presented in Fig 4.1a. Its base is the input push-pull APS. To provide direct current mode the cascading is used (Fig. 4.1b). The bases are connected to the voltages  $+U_{st}$  and  $-U_{st}$ . These voltages are generated by SVU. To provide the direct current mode of APS the cascading with the general base is performed. For the determination of the potential characteristics of APS CCG F1 and F2 are introduced in the circuit, they enable the elimination of the impact of the amplifying and output stages of PPDCA (Fig. 4.1c) [178– 181]. Sources of current I1 and I2 are used for setting the balanced direct current mode of the above-mentioned stage. Source of current  $I_{st0}$  provides the compensation of zero shift current.

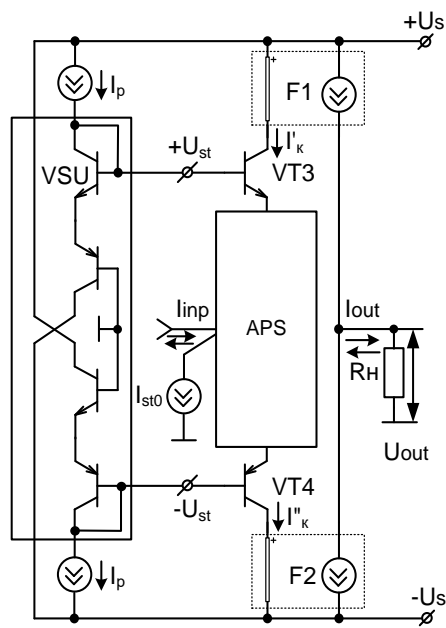
We will deduce the analytical relations for the determination of the transfer characteristic. It should be noted that the general voltage drop in the circuit of

$$\text{the stage shift } U_{\Sigma} = U_{st} + \left| -U_{st} \right| = U_{de1} + U_{de2}$$



a)

b)



c)

Fig 4.1. Input push-pull stage of PPDCA on the base of the bipolar transistors with paraphase outputs: a) amplifier-phase-splitter; b) principle of paraphase outputs cascading; c) circuit organization of single-stage PPDCA using CCG

In its turn:

$$U_{de1} = \varphi_T \ln \frac{I'_e}{I_0}, \quad U_{de2} = \varphi_T \ln \frac{I''_e}{I_0},$$

where  $\varphi_T = \frac{kT}{q} \approx 25.mB$  – is thermal potential;

$I_0 \approx 10^{-15}$  A – is thermal current.

That is why:

$$U_{\Sigma} = \varphi_T \ln \frac{I'_e}{I_0} + \varphi_T \ln \frac{I''_e}{I_0} = \varphi_T \ln \frac{I'_e I''_e}{I_0^2}. \quad (4.1)$$

Taking into account the conditions of the emitter currents balance and the equality  $I'_e I''_e = I_p^2$ , derived in [165], we obtain:  $I'_e = I''_e = I_p$ . Potentiating (4.1) and with the account of  $I_{inp}$ , we obtain the expressions, which describe the transfer characteristic of IPPS in large signal zone [178, 180, 182]:

$$I'_c = \left( \frac{1}{2} I_{inp} + \sqrt{\frac{I_{inp}^2}{4} + \frac{I_p^2}{(1+B') \cdot (1+B'')}} \right) \cdot (1+B');$$

$$I''_c = \left( \frac{1}{2} I_{inp} - \sqrt{\frac{I_{inp}^2}{4} + \frac{I_p^2}{(1+B') \cdot (1+B'')}} \right) \cdot (1+B''),$$

where  $B', B''$  – are static transfer coefficients VT1 and VT2 corresponding to the circuit of the general emitter (GE).

In their turn, the expressions, describing the collector currents  $I'_c, I''_c$  of the transistors VT3 and VT4 have the form [182]:

$$I'_c = \left( \frac{1}{2} I_{inp} + \sqrt{\frac{I_{inp}^2}{4} + \frac{I_p^2}{(1+B') \cdot (1+B'')}} \right) \cdot (1+B') \cdot A''; \quad (4.2)$$

$$I''_c = \left( \frac{1}{2} I_{inp} - \sqrt{\frac{I_{inp}^2}{4} + \frac{I_p^2}{(1+B') \cdot (1+B'')}} \right) \cdot (1+B'') \cdot A',$$

where  $A', A''$  – are static transfer coefficients of VT3 i VT4 corresponding to the circuit of GB.

To prove the adequacy of the obtained mathematical models, graphs in Mathcad 14 are constructed on their bases, the comparison with the results of the computer simulation of the electric circuit (see Fig. 4.1c) in Micro-Cap program 9.0.3.0.1 is carried out. Dependence graphs of the collector currents  $I'_c = f(I_{inp})$ ,  $I''_c = f(I_{inp})$  and general current, determined as  $I_{out} = I'_c + I''_c$ , are shown in Fig. 4.2. Convergence of the graphs proves the adequacy of the suggested mathematical models.

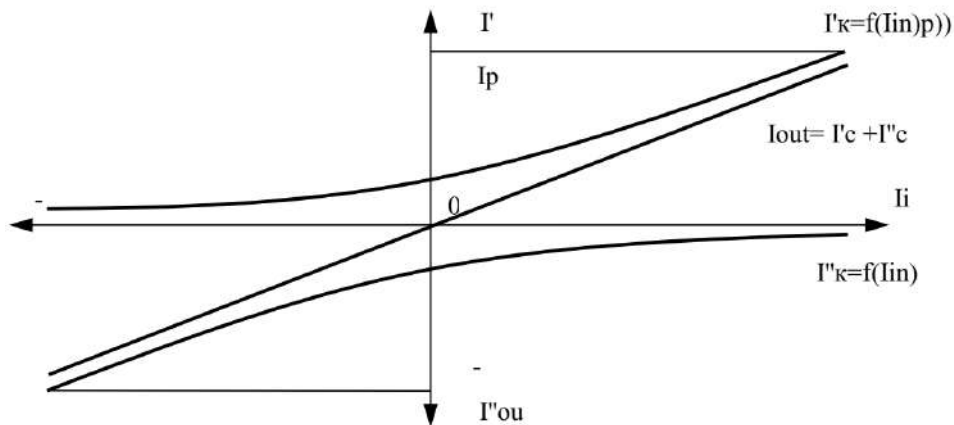


Fig 4.2. Static transfer characteristics on paraphase and general outputs of the circuit

For the determination of the transfer coefficients, we will construct the equivalent circuit, shown in Fig. 4.3.



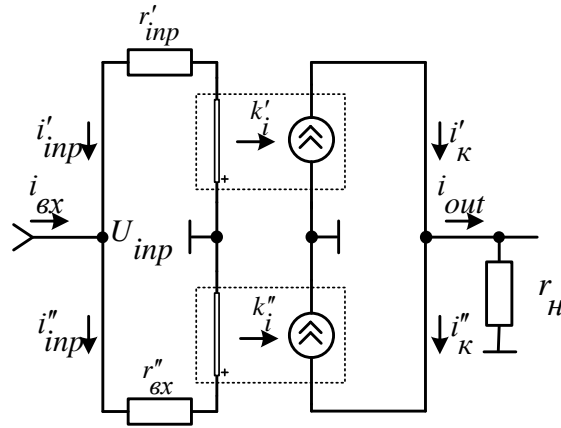


Fig 4.3. Equivalent circuit of the input stage in the small signal mode

In this case

$$c'_i = \frac{i'_c}{i'_inp}, \quad c''_i = \frac{i''_c}{i''_inp}, \quad (4.3)$$

where  $c'_i, c''_i$  – are the transfer coefficients on upper and lower channels, correspondingly.

Taking into account the equality for the determination of the transfer coefficients and the fact that the transistors VT1 and VT2 are connected by the circuit of the general collector (GC) and the transistors VT3 and VT4-- by the circuit GB, we can write down the equalities [178, 182]:

$$c'_i = \chi' \cdot (1 + \beta') \cdot \alpha'';$$

$$c''_i = \chi'' \cdot (1 + \beta'') \cdot \alpha',$$

where  $\beta', \beta''$  – are small signal transfer coefficients of the transistors VT1 and VT2, correspondingly;  $\chi', \chi''$  – are low and upper channels branching coefficients  $i_{inp}$ , correspondingly;  $\alpha', \alpha''$  – are small signal transfer coefficients of the emitter currents of the transistors VT3 and VT4, correspondingly.

Values  $\chi'$  and  $\chi''$  can be determined in the form:

$$\chi' = \frac{i'_{inp}}{i_{inp}}; \quad \chi'' = \frac{i''_{inp}}{i_{inp}}.$$

Here

$$i'_{inp} = \frac{U_{inp}}{r'_{inp}}; \quad i''_{inp} = \frac{U_{inp}}{r''_{inp}},$$

where  $U_{inp}$  – is the voltage drop in the point of connection of transistors VT1 and VT2 bases ;  $r'_{inp}$ ,  $r''_{inp}$  – are the input resistances of the upper and low channels, correspondingly.

Having taken into account that  $r'_e = r''_e = r_e$ ,  $r'_{inp}$ ,  $r''_{inp}$ , we obtain:

$$r'_{inp} = r'_b + 2r_e \cdot (1 + \beta'); \\ r''_{inp} = r''_b + 2r_e \cdot (1 + \beta'').$$

Here  $U_{inp}$  are defined as

$$U_{inp} = i_{inp} \cdot r'_{inp} \parallel r''_{inp}.$$

Taking into account the previous expressions we obtain:

$$\chi' = \frac{\beta''}{\beta' + \beta''}; \quad \chi'' = \frac{\beta'}{\beta' + \beta''}.$$

Taking into account (4.2), we obtain the expressions that describe the transfer characteristic of IPPS in the small signal zone

$$i'_k = \frac{\beta' \cdot \beta'' \cdot \alpha''}{\beta' + \beta''} \cdot i'_{inp}; \\ i''_k = \frac{\beta' \cdot \beta'' \cdot \alpha'}{\beta' + \beta''} \cdot i''_{inp}.$$

Taking into consideration that  $\alpha' \approx \alpha'' \approx 1$ ,  $\beta' \gg 1$ ,  $\beta'' \gg 1$ , and the expression (4.3), we have

$$k'_i \approx k''_i = \frac{\beta' \cdot \beta''}{\beta' + \beta''}.$$

Total amplification factor will be defined as  $k_i = k'_i + k''_i$ . Taking into account, that  $\alpha' \approx \alpha'' \approx 1$ , we obtain

$$k_i = 2 \cdot \frac{\beta' \cdot \beta''}{\beta' + \beta''}.$$

Current, flowing across the loading resistor  $R_H$ , is defined as

$$I_l = I'_K - I''_K.$$

Taking into consideration the expression (4.2) and assuming that  $B' \approx \beta'$ ,  $B'' \approx \beta''$ ,  $A' \approx \alpha'$ ,  $A'' \approx \alpha''$ , we obtain the function, which describes the transfer characteristic of IPPS of the current amplifier with the symmetric structure

$$I_l = \frac{\beta' \alpha'' + \beta'' \alpha'}{2} I_{inp} + (\beta' \alpha'' - \beta'' \alpha') \cdot \sqrt{\frac{I_{inp}^2}{4} + \frac{I_p^2}{\beta' \cdot \beta''}}. \quad (4.4)$$

One of the variants of PPDCA circuit with IPPS with the emitter outputs construction and their further looping [183] is the variant, shown in Fig. 4.4.

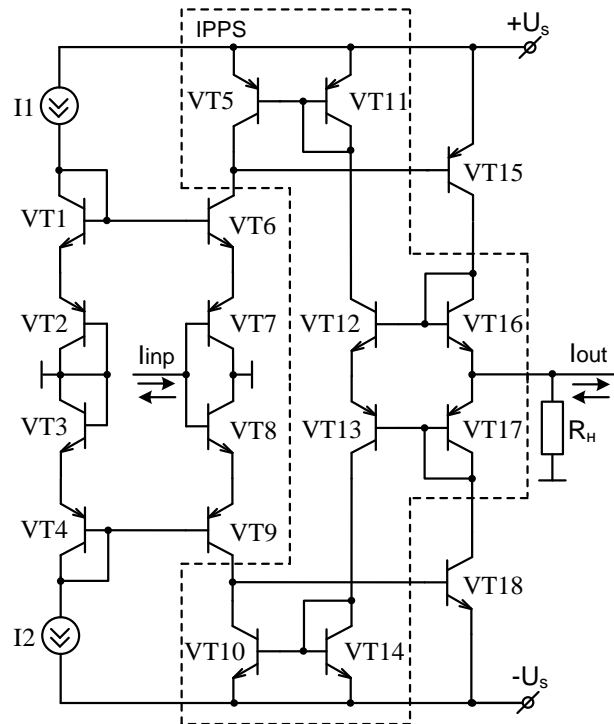


Fig 4.4. Circuit diagram of the push-pull DCA with the input push-pull stage on the bipolar transistors

The amplifier contains IPPS, built on the complementary transistors VT6–VT9. Working point of this stage is set by the voltage drop on the transistors

VT1–VT4 in diode connection, level of which is provided by the current values of the generators I1 and I2.

The circuit also has two symmetric IAS on the transistors VT15 and VT18 for the amplification of the counter phase signals. Working points of these transistors are set by introduction of BDCR in the circuit, it is built on the transistors VT12, VT13, VT16, VT17 and also CR: upper – on the transistors VT5, VT11 and low – on the transistors VT10, VT14.

The above-mentioned principle of the working point setting is provided by the self-balancing of the collector currents of the transistors VT15 and VT18, by means of acting the selected FB so that in the channel with smaller amplification  $K_i$  increases and in the channel with greater amplification – it decreases. It lasts until the amplification factors in the upper and lower channels become equal. That is, on the condition  $I_{inp} = 0$ ,

$$I_{K9} \approx I_{K9} \approx I_{K15} \approx I_{K18} \approx I_{K12} \approx I_{K13} \approx I_{K5} \approx I_{K10} \approx I_1 \approx I_2.$$

Proceeding from the last relation, it should be noted, that the working points of the transistors, both of upper and low channels are set by expressions of the currents of the generators I1 and I2.

Taking into account (4.4), we obtain the function that describes the transfer characteristic of such amplifier:

$$I_l = \frac{\beta_7 \alpha_6 \beta_{15} + \beta_8 \alpha_9 \beta_{18}}{2} I_{ex} + (\beta_7 \alpha_6 \beta_{15} - \beta_8 \alpha_9 \beta_{18}) \sqrt{\frac{I_{inp}^2}{4} + \frac{I_p^2}{\beta_7 \cdot \beta_8}}.$$

Graphic representation of AFC of the general  $K_i$  and  $K_i'$  (upper) and (low)  $K_i''$  amplification channels of the amplifier, shown in Fig. 4.4, are presented in Fig. 4.5, it proves the symmetry of the amplification factors.

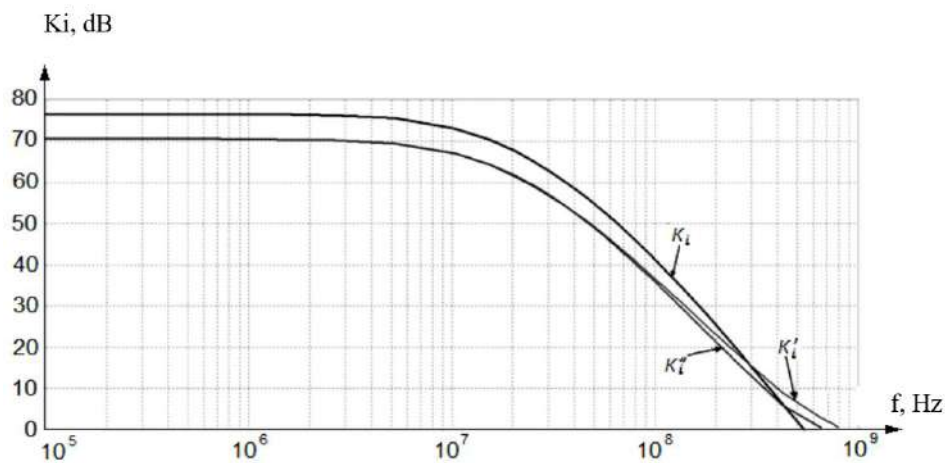


Fig. 4.5. AFC of PPDCA with the input push-pull stage

## 4.2. Determination and minimization of the static errors of the push-pull direct currents amplifiers input stages

### 4.2.1. Compensation of the zero shift

The linearity of the transfer characteristic is the component of the general accuracy of the device's operation. There exist two methods of decreasing PPDCA errors. The first method – technological, in this case element base is improved. The second – circuit engineering, when different schemes of static errors compensation are used in the structure of the amplifier.

It is known, that besides the setting of the working points of the core, it is necessary to perform balancing of VT1 and VT2 (see Fig. 4.1) [178]. To perform balancing separate generator  $I_{st0}$  is used, it provides the compensation of zero current shift. Circuit engineering realization of the current source  $I_{st0}$  is shown in Fig. 4.6 [184].

We define the required value of this current. If  $I_{inp} = 0$  and according to the Kirchhoff current law we obtain:

$$I_{st0} - I'_{inp} + I''_{inp} = 0,$$

where  $I'_{inp}, I''_{inp}$  – are the components of the input current branching by the bases of the transistors VT1 and VT2, correspondingly (see Fig. 4.1a). In this connection:

$$I'_{inp} = \frac{I'_e}{1+B'}; \quad I''_{inp} = \frac{I''_e}{1+B''}.$$

Taking into consideration the above-mentioned equalities and the condition of the balance, we obtain:

$$I_{st0} = I_p \cdot \frac{B'' - B'}{(1+B') \cdot (1+B'')} \approx I_p \cdot \frac{B'' - B'}{B'B''}.$$

We will analyze the relationship of currents in the circuit of the current  $I_{st0}$  source (see Fig. 4.6). In this device the formation of  $I_{st0}$  is carried out according to the parametric principle.

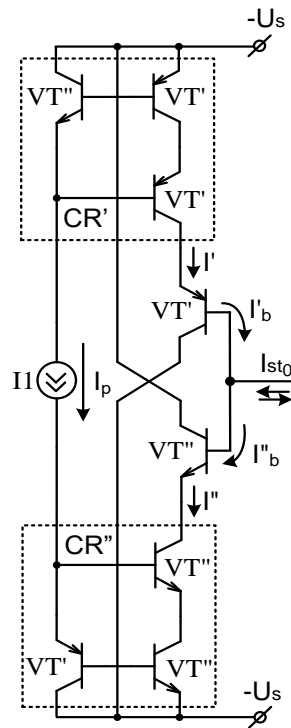


Fig. 4.6. Circuit engineering realization of the current source of zero shift compensation

We will determine the values of  $I'$ ,  $I''$  and  $I_{st0}$ , which are formed by the current reflectors BC', BC'' and transistors VT', VT'', correspondingly. In this case

$$I' = I_p \cdot B'; \quad I'' = I_p \cdot B'';$$

$$I'_B = \frac{I'}{1+B'}; \quad I''_B = \frac{I''}{1+B''}; \quad I_{st0} = I'_b - I''_b.$$

Taking into account the above-mentioned equalities, we obtain

$$I_{st0} = I_p \cdot \frac{B'' - B'}{(1+B') \cdot (1+B'')} \approx I_p \cdot \frac{B'' - B'}{B'B''}. \quad (4.5)$$

Thus, hypothetically, we have the equality of the currents. It should be noted, in practice, if the additional measures are not taken, this convergence will be on the level of 5 % [181].

#### 4.2.2. Definition and minimization of the non-linearity of the transfer characteristic

As it is known, non-linearity of IPPS greatly defines non-linearity of the transfer characteristic of PPDCA [182, 185].

Considering the circuit, shown in Fig. 4.1c as well as the expression (4.4), which describes the transfer characteristic of IPPS, we can define that non-linearity of the first stage is transferred at the output as a result of the asymmetry of the amplifiers "arms". In case of zero input current we have

$$I'_z = (\beta' \alpha'' - \beta'' \alpha') \cdot \sqrt{\frac{I_p^2}{\beta' \cdot \beta''}} \Big|_{I_{inp} = 0}.$$

The increment of the output current can be defined as

$$\Delta I_z = I_z(I_{inp}) - I'_z(I_{inp}).$$

Taking into account (4.4), we have

$$\Delta I_z = \frac{\beta' \alpha'' + \beta'' \alpha'}{2} I_{inp} + (\beta' \alpha'' - \beta'' \alpha') \left( \sqrt{\frac{I_{inp}^2}{4} + \frac{I_p^2}{\beta' \cdot \beta''}} - \sqrt{\frac{I_p^2}{\beta' \cdot \beta''}} \right). \quad (4.6)$$

Graphs of dependences  $\Delta I_z = f(I_{inp})$  obtained by means of computer simulation in Mathcad 14 and Micro-Cap 9.0.3.0.1 programs, are shown by solid

line in Fig. 4.7. Dependence graph  $I_{out} = k_i \cdot I_{inp}$  for PPDCA with the ideal transfer characteristic is shown by the dotted line.

Taking into account (4.2), it should be noted that the functions  $\Delta I'_\kappa = f(I_{inp})$  and  $\Delta I''_\kappa = f(I_{inp})$  have two zones:

- 1)  $|I_{inp}| \ll 2I_p$  – small signal zone ; 2)  $|I_{inp}| \leq 2I_p$  – large signal zone.

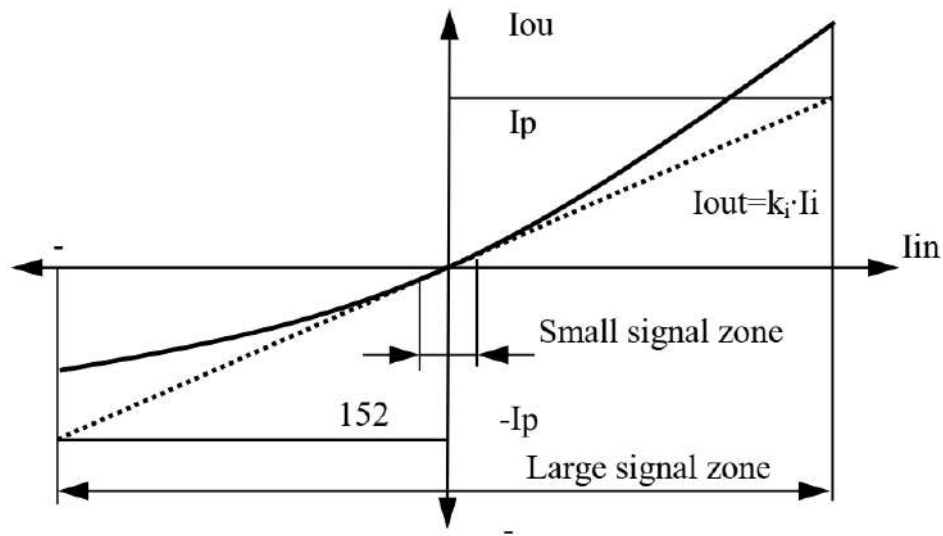


Fig. 4.7. Dependence graph

In small signal zone the increment of the current  $\Delta I'_\kappa \approx \Delta I''_\kappa \approx \frac{1}{2} I_{inp}$ . In large signal zone  $\Delta I'_\kappa \approx \Delta I''_\kappa \approx \Delta \approx I_{inp} - I_p$ .

Having taken into account (4.4) and the conditions of small signal zone and large signal zone availability, we obtain:

$$\text{if } |I_{inp}| \ll 2I_p : \Delta I_z \approx \beta'' \alpha' I_{inp} - (\beta'' \alpha' - \beta' \alpha'') \cdot I_p,$$

$$\text{and if } |I_{inp}| \leq 2I_p : \Delta I_z \approx \beta' \alpha'' I_{inp} - (\beta'' \alpha' - \beta' \alpha'') \cdot I_p.$$

For linearity error determination differential techniques can be applied. For the realization of the first differential technique and construction of the graph of static transfer characteristic it is necessary to perform the following steps:



- select the range in which the study is carried out;
- select subrange AB as it is shown in Fig. 4.8, where the static transfer characteristic approaches the linear function;
- determine the coordinates of the points (x1, y1) and (x2, y2).

After determining these points it is necessary to separate the difference, i.e., determine how the transfer function differs from the direct.

For PPDCA this function will be described by the equation

$$\Delta I_z = f(I_{inp}) + (k \cdot I_{inp} + b).$$

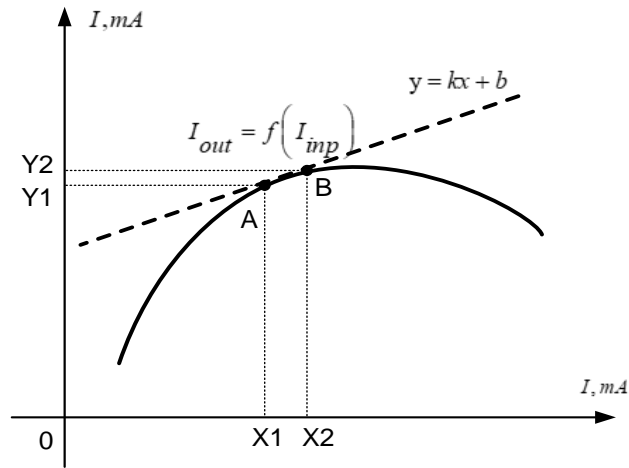


Fig. 4.8. Determination of the intersection points coordinates

To determine the coefficients  $k$  and  $b$ , it is necessary to solve the system of equations

$$\begin{cases} y_1 = k \cdot x_1 + b; \\ y_2 = k \cdot x_2 + b. \end{cases}$$

Coefficients  $k$  and  $b$  are determined in the following way:

$$\begin{cases} b = y_1 - k \cdot x_1; \\ k = \frac{y_2 - y_1}{x_2 - x_1}. \end{cases}$$

As a result we obtain the graph of linearity error, shown in Fig. 4.9.

Studying the transfer characteristic of any DCA it is expedient to use one of the switching circuits, shown in Fig. 4.10 [186].

The considered differential technique of the linearity error determination can be used in cases both with and without using the FB resistor.

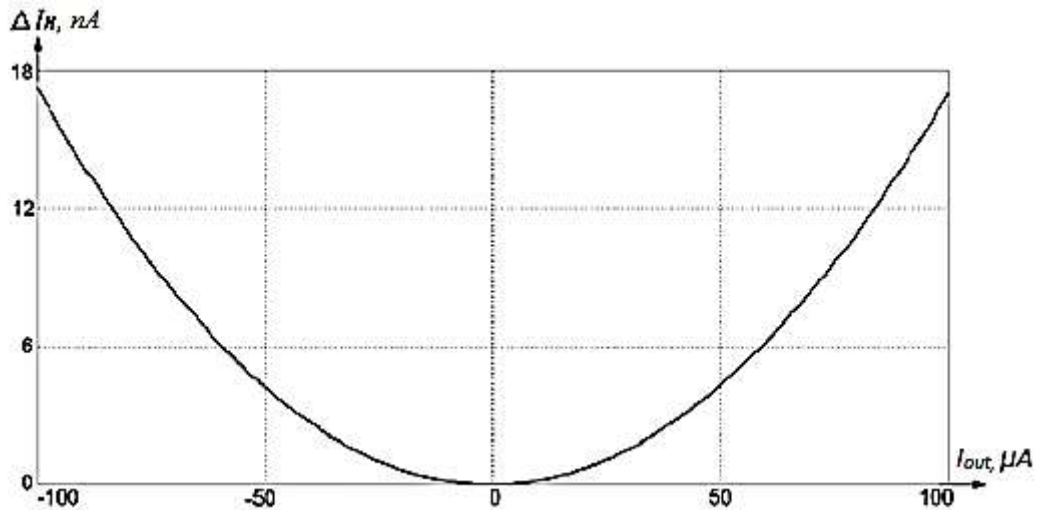


Fig. 4.9. Nonlinearity of the static transfer characteristic of PPDCA with the input push-pull stage

To realize the second differential technique it is necessary:

- 1) switch on PPDCA according to the circuit, shown in Fig. 4.10b;
- 2) by means of accurate selection of the load resistor nominal select the mode, when  $I_{inp} \approx I_N$ ;

- 3) by means of the package of application programmers', plot the characteristic  $\Delta I_N = I_N - I_{inp} \cdot R_M$ .

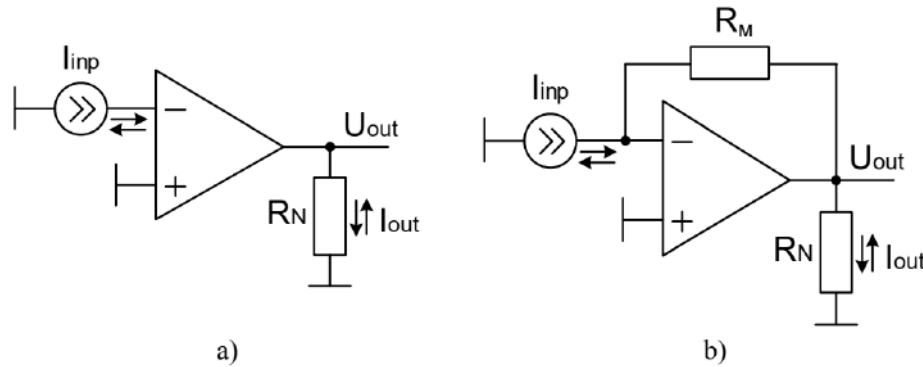


Fig. 4.10. PPDCA switching circuits: a) without the feedback; b) with the feedback

The considered techniques give the same results, but the first technique is more universal.

Table 4.1 contains the results of the computer simulation of two PPDCA from the Fig. 4.1c and Fig. 4.4, switched by the circuit in Fig. 4.10a.

Table 4.1 – PPDCA linearity error

Signal range		Linearity errors			
		Circuit I (Fig. 4.1c)		Circuit II (Fig. 4.4)	
input	output	absolute	relative	absolute	relative
$\pm 30$ nA	$\pm 10$ mA	40,4 pA	0,0002%	206 pA	0,001%
$\pm 1,2$ mA	$\pm 100$ mA	36 nA	0,018%	18 nA	0,009%

From Table 4.1 the conclusion can be drawn, that PPDCA with BDCR will operate better in the wide range of the input currents and the circuit with the ideal current generators gives good results until the basic currents of the transistors VT6 and VT7 exceed several microamperes.

### 4.3. Nonlinear distortions of the transfer characteristic of the input stages in the frequency zone

Characteristics of DCA, especially, their non-linear distortions, lead to the emergence of uncorrected errors in multiple-digit analog-to-digital systems and limit their accuracy.

For the assessment of these errors CNLD is used [122, 131]. It characterizes the level of the output signal distortion relative to the input signal in the preset frequency range and enables it to determine the dynamic component of the linearity error of the transfer characteristic of the amplifier. Considering the

expression (4.6) for the determination of the increment of the output current, flowing in the load, we denote

$$\frac{\beta' \alpha'' + \beta'' \alpha'}{2} = \beta_{aver} - \text{average amplification factor in the upper and lower channels;}$$

channels;

$$\beta' \alpha'' - \beta'' \alpha' = \Delta\beta - \text{is the absolute difference between the amplification}$$

$$\text{factors } \frac{I^2}{\beta' \cdot \beta''} = I \text{ [184].}$$

We will assess the dynamic distortions of the output signal of the IPPS. Let the input signal be the current in the form

$$\tilde{I}_{inp} = I_{inp} \cdot \sin \omega t .$$

Substituting these formulas in (4.6), we obtain [184]

$$\Delta I_N = \beta_{aver} \cdot \tilde{I}_{inp} \cdot \sin \omega t + \Delta\beta \left( \sqrt{\frac{\tilde{I}_{inp}^2}{4} \cdot \sin^2 \omega t + I^2} - I \right). \quad (4.7)$$

Decomposing the output signal (4.7) into harmonics of the Fourier series, we obtain

$$\Delta I_N = \frac{a_0}{2} + \sum_{k=1}^{\infty} (a_k \cos n\omega t + b_k \sin n\omega t) .$$

From the previous expression we determine  $a_0$

$$a_0 = \frac{\omega}{\pi} \Delta\beta \int_{-\frac{\pi}{\omega}}^{\frac{\pi}{\omega}} \left( \sqrt{\frac{\tilde{I}_{inp}^2}{4} \cdot \sin^2 \omega t + I^2} - I \right) dt ,$$

replacing  $y = \omega t$ , we will rewrite the previous formula in the following way:

$$a_0 = \frac{\Delta\beta}{\pi} \int_{-\pi}^{\pi} \left( \sqrt{\frac{\tilde{I}_{inp}^2}{4} \cdot \sin^2 y + I^2} - I \right) dy .$$

It is expedient to perform transformation of the similar expressions, using the complete elliptical beta and gamma integrals [187, 188]:

$$K(m) = \int_0^{\frac{\pi}{2}} \frac{d\varphi}{\sqrt{1-m^2 \sin^2 \varphi}}, \quad (4.8)$$

$$E(m) = \int_0^{\frac{\pi}{2}} \sqrt{1-m^2 \sin^2 \varphi} d\varphi. \quad (4.9)$$

In this connection

$$a_0 = 2 \cdot \Delta\beta \left[ \frac{1}{\pi} \sqrt{4I^2 + \tilde{I}_{inp}^2} E \left( \frac{\tilde{I}_{inp}}{\sqrt{4I^2 + \tilde{I}_{inp}^2}} \right) - I \right]. \quad (4.10)$$

For the determination of  $a_0$ , by means of expanding the expression (4.10) in Taylor series, it is necessary to take into account the availability of the two zones of the input signal:

small signal zone, when  $\tilde{I}_{inp} \leq 2I$ , in this connection

$$a_0 = \Delta\beta \frac{\tilde{I}_{inp}}{I},$$

large signal zone, when  $\tilde{I}_{inp} > 2I$ , in this connection

$$a_0 = \Delta\beta \frac{2}{\pi} \tilde{I}_{inp}.$$

The coefficient of zero is harmonic (i. e., the relation of the constant component of the output signal, emerging as a result of non-linearity to the amplitude of the input sinusoidal signal) can be assessed by means of such relation [189]:

$$\nu_k = \frac{|a_k|}{b_1}, \quad (4.11)$$

where as

$$b_1 = \beta_{aver} \cdot \tilde{I}_{inp}. \quad (4.12)$$

Taking into consideration the expressions (4.10) and (4.12), the value of the zeroth harmonic and substituting them in the expression (4.11), we obtain

$$v_0 = \frac{|a_0|}{2b_1} = 2\gamma \left[ \frac{\sqrt{4+x^2}}{\pi x} E\left(\frac{x}{\sqrt{4+x^2}}\right) - \frac{1}{x} \right],$$

where  $\gamma = \frac{\Delta\beta}{\beta_{aver}}$  – is the relative spread of the amplification factors in the

upper and lower channels;  $x = \frac{\tilde{I}_{inp}}{I}$  – is the relation of input current amplitude to the bias current of IPPS.

If  $x \leq 1$  – we have small input signal mode, in this case, expanding in Taylor series we obtain

$$v_0 = \frac{\gamma x}{8} + O(x^2) = \frac{\Delta\beta}{8 \cdot \beta_{aver}} \cdot \frac{\tilde{I}_{inp}}{I} + O(x^2).$$

If  $x \geq 1$  – we have the mode of large input signal. In this case  $v_0$  is determined in the following way:

$$v_0 = \frac{2\gamma}{\pi} + O(x^2) = \frac{2}{\pi} \frac{\Delta\beta}{\beta_{aver}} + O(x^2),$$

where  $O(x^2)$  – is Taylor remains in the form of Peano.

In the first approximation the item  $O(x^2)$  can be neglected, as it is far smaller than the first member of Taylor series.

As  $a_1 = 0$ , and if  $k \geq 1$ , all  $a_{2k-1} = 0$ ;  $b_k = 0$ , if  $(k > 1)$ . Taking into account this and (4.11) we can determine, that  $v_{2k-1} = 0$ .

Values of higher harmonics  $a_k$  we will estimate by the values of the second harmonic amplitude

$$a_2 = \frac{\Delta\beta}{\pi} \int_{-\pi}^{\pi} \left( \sqrt{\frac{\tilde{I}_{inp}^2}{4} \cdot \sin^2 y + I^2} \right) \cos 2y dy.$$

Using the complete elliptical beta and gamma integrals (4.8) and (4.9), we obtain the value of  $a_2$  on in the form of

$$a_2 = \frac{2\Delta\beta}{3\pi} \sqrt{4I^2 + \tilde{I}_{inp}^2} \left[ 8 \frac{I^2}{\tilde{I}_{inp}^2} E \left( \frac{\tilde{I}_{inp}}{\sqrt{4I^2 + \tilde{I}_{inp}^2}} \right) - \left( 8 \frac{I^2}{\tilde{I}_{inp}^2} + 1 \right) K \left( \frac{\tilde{I}_{inp}}{\sqrt{4I^2 + \tilde{I}_{inp}^2}} \right) \right].$$

Taking into account the expressions (4.11) and (4.12), we have

$$v_2 = \frac{|a_2|}{b_1} = \frac{2\gamma}{3\pi} \frac{\sqrt{4+x^2}}{x^3} \left[ (8+x^2) E \left( \frac{x}{\sqrt{4+x^2}} \right) - 8K \left( \frac{x}{\sqrt{4+x^2}} \right) \right].$$

If  $x \leq 1$ :

$$v_2 = \frac{\gamma x}{16} + O(x^3), \quad (4.13)$$

$$v_2 = \frac{\Delta\beta}{16 \cdot \beta_{aver}} \cdot \frac{\tilde{I}_{inp}}{I} + O(x^3). \quad (4.14)$$

$$\text{If } x \geq 1: \quad v_2 = \frac{2\gamma}{3\pi} + O(x^3) = \frac{2}{3\pi} \frac{\Delta\beta}{\beta_{aver}} + O(x^3).$$

For the assessment of the accuracy of the expression (4.14) for the harmonics coefficient and impact of the input signal, we take into consideration Taylor remainder:

$$\begin{aligned} & \sqrt{\frac{\tilde{I}_{inp}^2}{4} \sin^2 y + I^2} = I \cdot \left( 1 + \frac{\tilde{I}_{inp}^2}{8I^2} \sin^2 y - \frac{1}{128} \cdot \frac{\tilde{I}_{inp}^4}{I^4} \sin^4 y + \dots \right) = \\ & = I \cdot \left[ 1 + \frac{1}{16} \cdot \frac{\tilde{I}_{inp}^2}{I^2} - \frac{3}{1024} \cdot \frac{\tilde{I}_{inp}^4}{I^4} - \left( \frac{1}{16} \frac{\tilde{I}_{inp}^2}{I^2} - \frac{1}{16^2} \cdot \frac{\tilde{I}_{inp}^4}{I^4} \right) \cos 2y - \frac{1}{2^{10}} \cdot \frac{\tilde{I}_{inp}^4}{I^4} \cos 4y + \dots \right]. \end{aligned} \quad (4.15)$$

As it is seen, in the expression, besides the second harmonic, the fourth harmonic is present.

For the determination of CND such an expression is accepted [131]:

$$CND = \frac{\sqrt{\sum_{k=2}^{\infty} A_k^2}}{\sqrt{\sum_{k=1}^{\infty} A_k^2}},$$

where  $A_k = \sqrt{a_k^2 + b_k^2}$  – is the coefficient of the n-th harmonic;  $a_k, b_k$  – are k-th coefficients of the Fourier series.

As the input signal of the sinusoidal form contains only one harmonic  $A_1 = \sqrt{a_1^2 + b_1^2} = b_1$ , then, it is expedient to use the expression for the determination of the harmonics coefficient [131, 189]

$$K_H = \frac{\sqrt{\sum_{n=2}^{\infty} A_n^2}}{A_1}.$$

Taking into account the expression (8), we obtain

$$K_H = \frac{\sqrt{a_2^2 + a_4^2 + a_6^2 + \dots + a_n^2 + \dots}}{b_1}. \quad (4.16)$$

Taking into consideration (4.16), we will rewrite the expression for the assessment of the harmonics coefficient in analytically simpler form:

$$\bar{K}_H = \frac{|a_2| + |a_4|}{|b_1|}. \quad (4.17)$$

It is easy to notice that always  $\bar{K}_H \geq K_H$ . In this case, the expression (4.17) determines the harmonics coefficient with conservative value relative to the expression (4.18).

According to (4.17) and taking into account that  $\frac{\tilde{I}_{inp}}{I} = x$ , we obtain

$$\begin{aligned} \bar{K}_H &= \gamma \left[ \frac{x}{16} - \frac{x^3}{16^2} + \frac{x^3}{4 \cdot 16^2} \right] = \gamma \left[ \frac{x}{16} - \frac{3}{2 \cdot 10} x^3 \right] = \frac{x\gamma}{16} \left[ 1 - \frac{3}{64} x^2 \right], \\ \gamma &= \frac{\Delta\beta}{\beta_{aver}}, \\ \bar{K}_H &= \frac{\Delta\beta}{16 \cdot \beta_{aver}} \cdot \frac{\tilde{I}_{inp}}{I} \left( 1 - \frac{3}{64} \cdot \frac{\tilde{I}_{inp}^2}{I^2} \right). \end{aligned} \quad (4.18)$$



Term

$$\frac{3}{64}x^2 = 0,047 \left( \frac{\tilde{I}_{inp}}{I} \right)^2$$

gives relative error of the expression (4.14) for the harmonics coefficient. At the same time, this term may serve for the assessment of the linearity error. However, the emergence of the sign «minus» is connected with the limitation of the convergence series radius by the degrees  $x$  for  $\bar{K}_H$ . That is why, by means of the introduction of  $\langle 0 \delta \langle \delta 1 \rangle$  parameter, we have another expansion:

$$\alpha^2 = \frac{x^2}{x^2 + 8},$$

$$\sqrt{\frac{\tilde{I}_{inp}}{4} \sin^2 y + I^2} = \sqrt{I^2 + \frac{\tilde{I}_{inp}^2}{8}} \cdot \sqrt{1 - \frac{\tilde{I}_{inp}^2}{\tilde{I}_{inp}^2 + 8I^2} \cos 2y} = I \cdot \sqrt{1 + \frac{x^2}{8}} \sqrt{1 - \alpha^2 \cos 2y}$$

We will expand the expression in a Taylor series:

$$\begin{aligned} \sqrt{1 - \alpha^2 \cos 2y} &= 1 - \frac{1}{2} \alpha^2 \cos 2y - \frac{1}{8} \alpha^4 \cos^4 2y - \frac{1}{16} \alpha^6 \cos^6 2y \dots = \\ &= 1 - \frac{1}{16} \alpha^4 - \frac{1}{2} \alpha^2 \cos 2y - \frac{\alpha^4}{16} \cos 4y - \dots \end{aligned}$$

In the process of this expansion we will retain the expanded terms not higher than 4-th degree by. Then we obtain

$$\begin{cases} a_2 = -I \cdot \sqrt{1 + \frac{x^2}{8}} \cdot \frac{1}{2} x^2 \cdot \Delta\beta; \\ a_3 = 0; \\ a_4 = -\Delta\beta \cdot I \cdot \sqrt{1 + \frac{x^2}{8}} \cdot \frac{\alpha^4}{16}; \\ a_5 = 0. \end{cases}$$

According to (4.16) the coefficient of the higher harmonics

$$\bar{K}_H = \gamma \frac{\alpha}{4\sqrt{2}} \left( 1 + \frac{\alpha^2}{8} \right). \quad (4.19)$$

In this case, has the sign «plus», that indicates the stable character of the decomposition by degrees.

If  $x \leq 1$ :

$$\alpha \approx \frac{x}{2\sqrt{2}},$$

That is why, in the first approximation, as previously in (4.13),  $\bar{K}_H = \frac{\gamma x}{16}$  and the relative error is

$$\frac{\alpha^2}{8} \approx \frac{3}{64} x^2.$$

However, if the expression (15) is expanded in powers, we again obtain (4.18). Simultaneously, in accordance with the described above, (4.19) should be assumed as the final expression. Fig. 4.11 shows, how the input current influences the values of the harmonics  $a_2$  and  $a_4$ .

Analysis of the graph shows that the amplitude of the fourth harmonics  $a_4$  is considerably (by 5–6 orders) less than the value of the second harmonic  $a_2$ . This also concerns the sixth harmonic  $a_6$ , which will be far smaller, as compared with  $a_4$ . That is why; it and the harmonics of the higher orders may be neglected.

Table 4.2 contains the results of computer simulation of two PPDCA from Fig. 4.1c and Fig. 4.4 in the program Micro-Cap 9.0.3.0.1.

Simulation was carried out in small signal zone at the value of the input current 1 nA ( $I_p = 1 \text{ mA}$ ,  $K_i = 65,2 \text{ dB}$ ). To evaluate errors, introduced by IPPS into the amplification circuit on the condition of balancing, FB is introduced in the circuit of the device.

Table 4.2 – Value of CND depending on the frequency of the input signal

Frequency f, kHz	0,1	1	10	20	100	1000
PPDCA, using CND (Fig. 4.1c)						
CND, %	$3,1 \cdot 10^{-4}$	$3,12 \cdot 10^{-4}$	$3,13 \cdot 10^{-4}$	$3,14 \cdot 10^{-4}$	$6,25 \cdot 10^{-4}$	$2,63 \cdot 10^{-3}$
With the feedback (Fig. 4.4)						
CND, %	$7,76 \cdot 10^{-4}$	$7,82 \cdot 10^{-4}$	$9,83 \cdot 10^{-4}$	$1,14 \cdot 10^{-3}$	$1,57 \cdot 10^{-3}$	$6,7 \cdot 10^{-3}$
Without the feedback (Fig. 4.4)						
CND, %	$2,24 \cdot 10^{-3}$	$2,25 \cdot 10^{-3}$	$2,27 \cdot 10^{-3}$	$2,34 \cdot 10^{-3}$	0,012	1,24

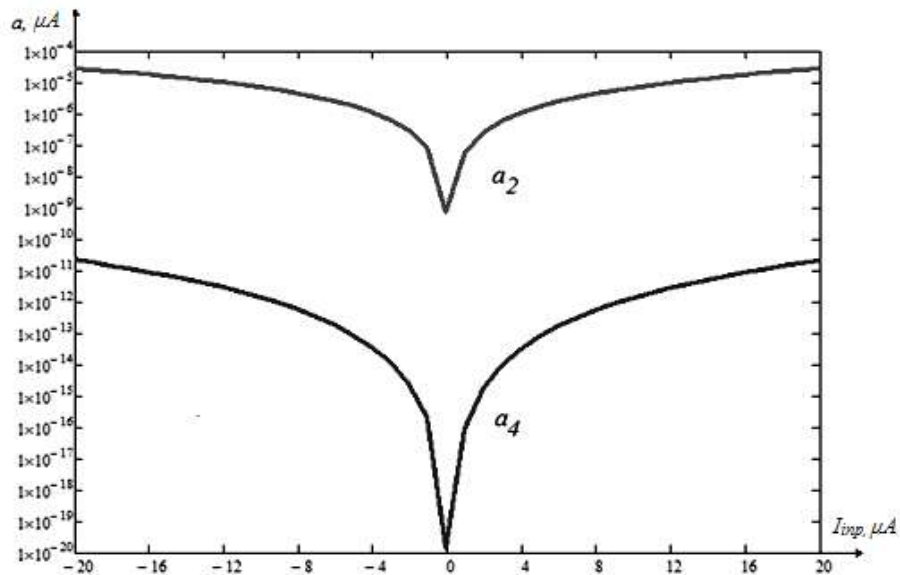


Fig. 4.11. Graph of the functional dependences of the amplitudes of the second and fourth harmonic on the input signal

It is seen, from the suggested results, that CND of PPDCA depends on the frequency and the amplitude of the input signal and it is minimal in rather wide range. The increase of the values of these parameters will lead to the increase of the CND of the amplifiers.

#### 4.4. Models of AFC and PFC of the input stages

Modern design of the analog circuits is based on the computer simulation, using the package of circuit engineering analysis, in particular MicroCap, OrCAD and others [181]. They use the detailed libraries of the components in SPICE format. The models of the integrated transistors on the base of the equivalent circuits with the controlled current generators were suggested [179]. Such an approach allows the general analysis of the analog circuits, irrespective of the specific element base, taking into account only fundamental relations of the characteristics in the transistor stages.

For composing of the mathematical models of AFC and PFC it is necessary to consider circuit engineering organization of IPPS circuits of the symmetric direct current amplifiers with common collector with staging both by emitters (see Fig. 4.1c) and by emitters and collectors [190]. Equivalent small signal

circuit is built on the base of general T-like equivalent circuits of the transistors [171, 179].

Having considered IPPS of PPDCA, it is determined that the transistors VT1 and VT2 are connected with the GC, transistors VT3 and VT4 – with GB. Using common T-like equivalent circuits of the transistors GB and GC [179] it is possible to construct small signal equivalent circuit, shown in Fig. 4.12a.

It is necessary to determine the transfer coefficients  $K_i(f)$ ,  $K'_i(f)$ ,  $K''_i(f)$ , and phase characteristics  $\varphi(f)$ ,  $\varphi'(f)$ ,  $\varphi''(f)$  of the small signal equivalent circuit of IPPS of PPDCA with common collector and the emitters looping.

Total amplification factor is determined as the sum of the transfer coefficients in upper and lower channels:

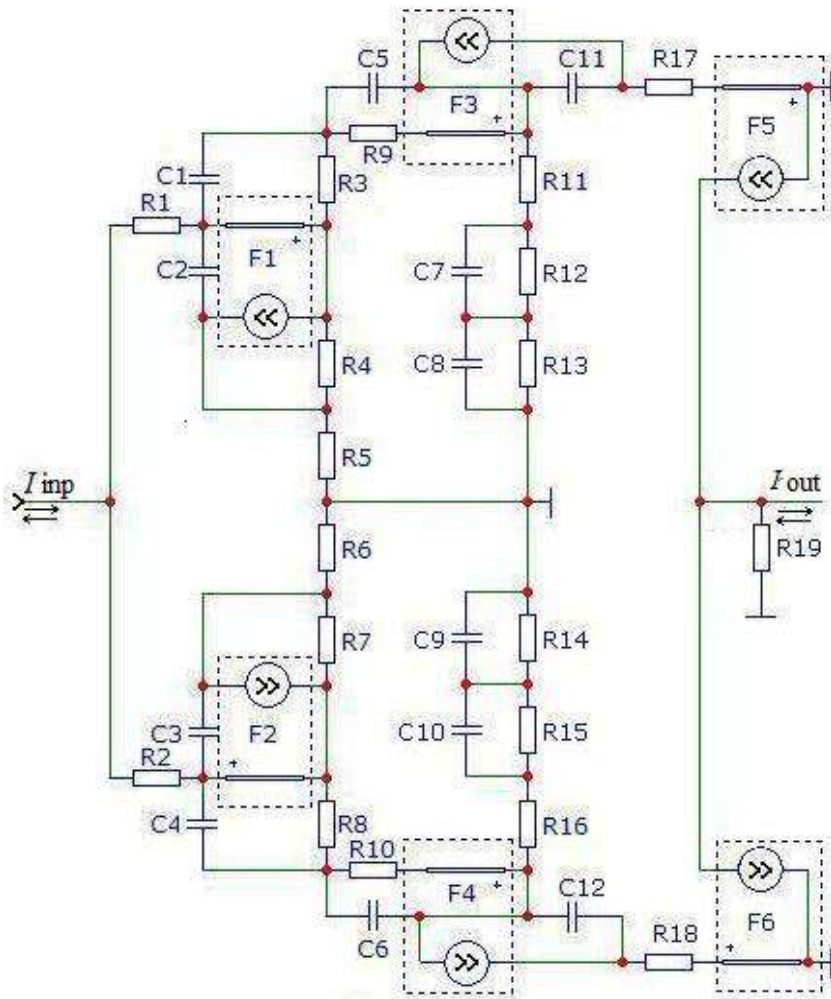
$$K_i(f) = K'_i(f) + K''_i(f), \quad (4.20)$$

where  $K'_i(f)$ ,  $K''_i(f)$  – are amplification factors in the upper and lower channels, correspondingly, which can be determined in the following way:

$$K'_i(f) = \frac{I'_{out}(f)}{I_{inp}}; \quad (4.21)$$

$$K''_i(f) = \frac{I''_{out}(f)}{I_{inp}},$$

where  $I'_{out}$ ,  $I''_{out}$  are output currents of the upper and lower channels, correspondingly.



a)

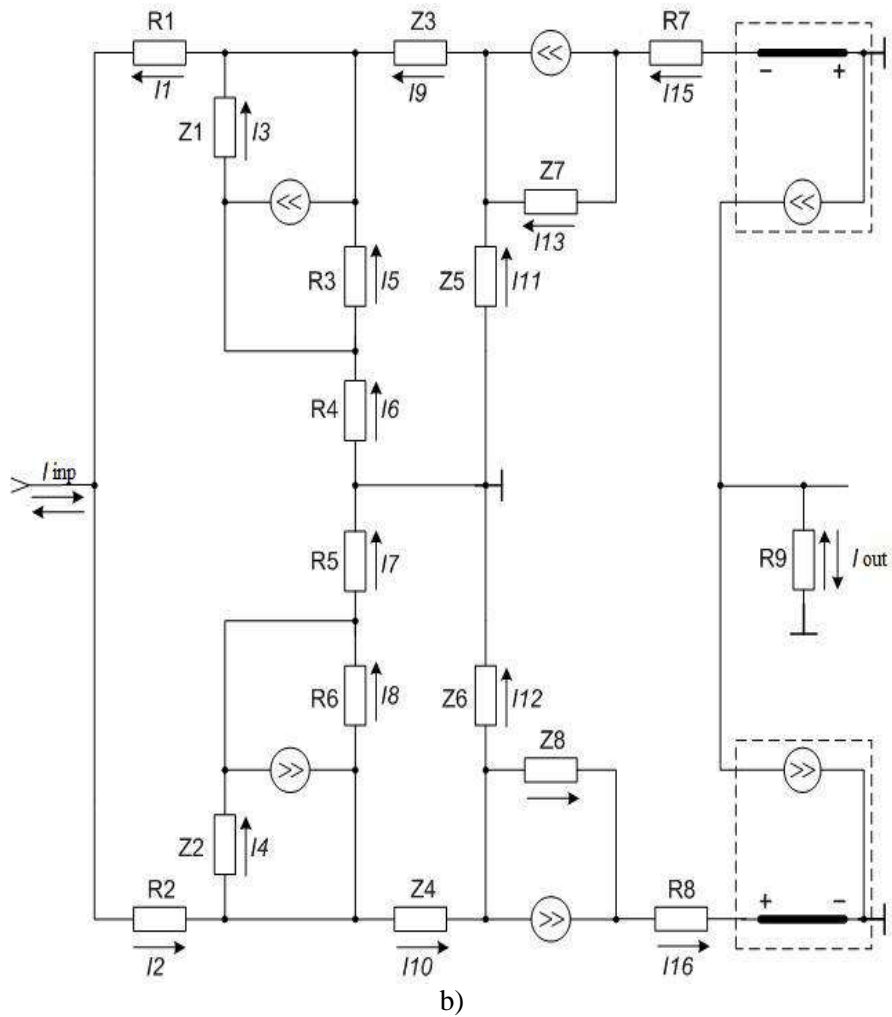


Fig. 4.12. Small signal equivalent circuits of the input push-pull stages: a) in SPICE format; b) with the presentation of the elements parameters in the complex form

For the phase characteristics

$$\begin{cases} \varphi(f) = \varphi(I_{out}(f)); \\ \varphi'(f) = \varphi(I'_{out}(f)); \\ \varphi''(f) = \varphi(I''_{out}(f)). \end{cases} \quad (4.22)$$

To determine  $I'_{out}, I''_{out}$  we will use the common Kirchoff method [191, 192], namely – its first and second laws. Also it is necessary to perform transformations, which will help to simplify the equivalent circuit, shown in Fig. 4.12a, by writing down the characteristics of the elements in the complex form. Equivalent circuit after the transformation is presented in Fig. 4.12b.

We have the following equations [190]:

$$\begin{cases}
 I_1(f) - I_2(f) = -1; \\
 -(1 - \beta') \cdot I_1(f) + I_3(f) + I_5(f) + I_9(f) = 0; \\
 (1 + \beta'') \cdot I_2(f) - I_4(f) - I_8(f) - I_{10}(f) = 0; \\
 \beta' \cdot I_1(f) - I_3(f) - I_5(f) + I_6(f) = 0; \\
 -\beta'' \cdot I_2(f) + I_4(f) - I_7(f) + I_8(f) = 0; \\
 -(1 - \alpha'') \cdot I_9(f) + I_{11}(f) + I_{13}(f) = 0; \\
 (1 - \alpha') \cdot I_{10}(f) - I_{12}(f) - I_{14}(f) = 0; \\
 -\alpha'' \cdot I_9(f) - I_{13}(f) + I_{15}(f) = 0; \\
 \alpha' \cdot I_{10}(f) + I_{14}(f) - I_{16}(f) = 0; \\
 R_3 \cdot I_5(f) + R_4 \cdot I_6(f) - Z_3(f) \cdot I_9(f) - Z_5(f) \cdot I_{11}(f) = 0; \\
 R_5 \cdot I_7(f) + R_6 \cdot I_8(f) - Z_4(f) \cdot I_{10}(f) - Z_6(f) \cdot I_{12}(f) = 0; \\
 Z_5(f) \cdot I_{11}(f) + Z_7(f) \cdot I_{13}(f) - R_7 \cdot I_{15}(f) = 0; \\
 Z_6(f) \cdot I_{12}(f) - Z_8(f) \cdot I_{14}(f) - R_8 \cdot I_{16}(f) = 0; \\
 Z_1(f) \cdot I_3(f) + R_4 \cdot I_6(f) - Z_3(f) \cdot I_9(f) - Z_7(f) \cdot I_{13}(f) - R_7 \cdot I_{15}(f) = 0; \\
 Z_2(f) \cdot I_4(f) + R_5 \cdot I_7(f) - Z_4(f) \cdot I_{10}(f) - Z_8(f) \cdot I_{14}(f) - R_8 \cdot I_{16}(f) = 0; \\
 R_1 \cdot I_1(f) + R_2 \cdot I_2(f) + Z_1(f) \cdot I_3(f) + Z_2(f) \cdot I_4(f) + R_4 \cdot I_6(f) + R_5 \cdot I_7(f) = 0.
 \end{cases} \quad (2.23)$$

Correspondingly  $R_1 = r'_b$ ;  $R_2 = r''_b$ ;  $R_3 = r'_c^*$ ;  $R_4 = R_8 = r'_{cc}$ ;  $R_5 = R_7 = r''_{cc}$ ;

$$R_6 = r''_c^*;$$

$$\begin{aligned}
Z_1(f) &= \frac{1}{j \cdot 2 \cdot \pi \cdot f \cdot C'_{bc}} \\
Z_3(f) &= \frac{r_e \cdot \frac{1}{j \cdot 2 \cdot \pi \cdot f \cdot C'_{be}}}{r_e + \frac{1}{j \cdot 2 \cdot \pi \cdot f \cdot C'_{be}}} + \frac{r_e \cdot \frac{1}{j \cdot 2 \cdot \pi \cdot f \cdot C''_{be}}}{r_e + \frac{1}{j \cdot 2 \cdot \pi \cdot f \cdot C''_{be}}} \\
Z_2(f) &= \frac{1}{j \cdot 2 \cdot \pi \cdot f \cdot C''_{bc}} \\
Z_4(f) &= \frac{r_e \cdot \frac{1}{j \cdot 2 \cdot \pi \cdot f \cdot C'_{be}}}{r_e + \frac{1}{j \cdot 2 \cdot \pi \cdot f \cdot C'_{be}}} + \frac{r_e \cdot \frac{1}{j \cdot 2 \cdot \pi \cdot f \cdot C''_{be}}}{r_e + \frac{1}{j \cdot 2 \cdot \pi \cdot f \cdot C''_{be}}} \\
Z_5(f) &= \frac{1}{j \cdot 2 \cdot \pi \cdot f \cdot C''_{bc}}; \quad Z_6(f) = \frac{1}{j \cdot 2 \cdot \pi \cdot f \cdot C'_{bc}}
\end{aligned}$$

where  $r'_b, r''_b, r'_c, r''_c, r'_{cc}, r''_{cc}$  – are resistances of the bases, collectors (according to the connection scheme GC and GE), volume resistances of p-n-p and n-p-n collectors of the transistors, correspondingly;  $C'_{bc}, C''_{bc}, C'_{be}, C''_{be}$  – p-n-p and n-p-n of base-collector, base-emitter junctions capacitance, correspondingly;  $r_e = r'_e = r''_e$  – resistance of the emitter of p-n-p and n-p-n transistors, correspondingly.

For the solution of the equations system Cramer method was used [192–194], for this purpose the system of equations (4.23) will be written in the form of A matrix:



$$A = \begin{bmatrix} 1 & -1 & 0 & 0 & 0 & \dots & 0 & 0 & 0 & 0 & 0 \\ \beta' - 1 & 0 & 1 & 0 & 1 & \dots & 0 & 0 & 0 & 0 & 0 \\ 0 & \beta'' + 1 & 0 & -1 & 0 & \dots & 0 & 0 & 0 & 0 & 0 \\ \beta' & 0 & -1 & 0 & -1 & \dots & 0 & 0 & 0 & 0 & 0 \\ 0 & -\beta'' & 0 & 1 & 0 & \dots & 0 & 0 & 0 & 0 & 0 \\ \vdots & \vdots & \vdots & \vdots & \vdots & \vdots & \vdots & \vdots & \vdots & \vdots & \vdots \\ 0 & 0 & 0 & 0 & 0 & \dots & 0 & Z_7(f) & 0 & -R_7 & 0 \\ 0 & 0 & 0 & 0 & 0 & \dots & Z_6(f) & 0 & -Z_8(f) & 0 & -R_8 \\ 0 & 0 & Z_1(f) & 0 & 0 & \dots & 0 & -Z_7(f) & 0 & -R_7 & 0 \\ 0 & 0 & 0 & Z_2(f) & 0 & \dots & 0 & 0 & -Z_8(f) & 0 & -R_8 \\ R_1 & R_2 & Z_1(f) & Z_2(f) & 0 & \dots & 0 & 0 & 0 & 0 & 0 \end{bmatrix}$$

$I'_{out}(f), I''_{out}(f)$  are determined as:

$$\begin{aligned} I'_{out}(f) &= I_{15}(f) = \frac{\Delta B}{\Delta A}; \\ I''_{out}(f) &= I_{16}(f) = \frac{\Delta C}{\Delta A}, \end{aligned} \quad (4.24)$$

where  $\Delta A, \Delta B, \Delta C$  – are the determinants of the matrix  $A, B, C$  correspondingly.

In their turn matrices  $B$  and  $C$  are determined by means of replacing the corresponding column of the matrix  $A$  by the matrix of free terms of the equations system (4.23) [192, 194].

Taking into account (4.21–4.24) and taking  $I_{inp} = 1$ , for obtaining AFC it is necessary to take the absolute value and for PFC – argument [179, 191, 192].

Analyzing the system of equations (4.24) and further mathematical calculations the conclusion can be reached, that this requires large volume of complex computations that is why, to carry out the analysis of the mathematical model of AFC and PFC we will make use of the simplified formulas of the transfer coefficients of the transistor stages [131]:

for AFC and PFC correspondingly

$$k_i(f) = \frac{\alpha}{\sqrt{1 + \left(\frac{f}{f_p}\right)^2}}, \quad (4.25)$$

$$\varphi(f) = \arctg\left(\frac{f}{f_p}\right) + \varphi_c,$$

where  $f_p$  – is the frequency of the pole on the level of «-3 dB»,

$\varphi_c = \arctg\left(\frac{f}{f_{\max}}\right)$  – is additional phase shift;  $f_{\max} = \sqrt{\frac{f_t}{8\pi \cdot C_{bc} \cdot r_b}}$  – is

maximal generation frequency [177] of the transistor;  $f_{\max}$  – is limiting the frequency of the transistor to the level of 0 dB for the GE stage.

Taking into account the switching circuits of the transistors in IPPS of PPDCA with common collector, looping by the emitters and taking into account (4.25) for GC circuit we will write:

$$K_{i_{T1}}(f) = K'_{i_{GC}} = \frac{\beta_{p-n-p}}{\sqrt{1 + \left(\frac{f}{f_{p_{T1}}}\right)^2}}; \quad (4.26)$$

$$K_{i_{T2}}(f) = K''_{i_{GC}} = \frac{\beta_{n-p-n}}{\sqrt{1 + \left(\frac{f}{f_{p_{T2}}}\right)^2}},$$

where  $f_{p_{T1}}$  and  $f_{p_{T2}}$  – are poles of the transistors VT1 and VT2.

For GB we will write:

$$K_{i_{T3}}(f) = K'_{i_{GB}} = \frac{\alpha_{n-p-n}}{\sqrt{1 + \left(\frac{f}{f_{p_{T3}}}\right)^2}}; \quad (4.27)$$

$$K_{i_{T4}}(f) = K''_{i_{GB}} = \frac{\alpha_{p-n-p}}{\sqrt{1 + \left(\frac{f}{f_{p_{T4}}}\right)^2}},$$

where  $f_{p_{T3}}$  and  $f_{p_{T4}}$  – are the poles of the transistors VT3 and VT4.

In their turn  $K'_i(f), K''_i(f)$  are determined as [178, 180]:

$$K'_i(f) = \chi' \cdot Ki_{T1}(f) \cdot Ki_{T3}(f); \quad (4.28)$$

$$K''_i(f) = \chi'' \cdot Ki_{T2}(f) \cdot Ki_{T4}(f),$$

where  $\chi', \chi''$  – are the coefficients of the input current splitting in the upper and lower channels, correspondingly.

In their turn  $\chi', \chi''$  are determined in the following way [178, 180]:

$$\chi' = \frac{\beta''}{\beta' + \beta''} = \frac{\beta_{n-p-n}}{\beta_{p-n-p} + \beta_{n-p-n}}; \quad (4.29)$$

$$\chi'' = \frac{\beta'}{\beta' + \beta''} = \frac{\beta_{p-n-p}}{\beta_{p-n-p} + \beta_{n-p-n}},$$

where  $\beta', \beta''$  – are the coefficients of the base current amplification of the transistors VT1 and VT2 correspondingly.

Taking into account (4.26), (4.27), (4.28), (4.29), we obtain  $K'_i(f)$  and  $K''_i(f)$ .

On the base of (4.20) common amplification factor can be considered as the vector  $\vec{K}_i(f)$ , that is determined as the sum of vectors  $\vec{K}'_i(f), \vec{K}''_i(f)$  [194].

For the determination of the total  $\vec{K}_i(f)$  we use the cosine law (Fig. 4.13a):

$$K'_i(f) = \frac{\beta_{n-p-n}}{\beta_{p-n-p} + \beta_{n-p-n}} \cdot \frac{\beta_{p-n-p}}{\sqrt{1 + \left(\frac{f}{f_{pT1}}\right)^2}} \cdot \frac{\alpha_{n-p-n}}{\sqrt{1 + \left(\frac{f}{f_{pT2}}\right)^2}}; \quad (4.30)$$

$$K''_i(f) = \frac{\beta_{p-n-p}}{\beta_{p-n-p} + \beta_{n-p-n}} \cdot \frac{\beta_{n-p-n}}{\sqrt{1 + \left(\frac{f}{f_{pT2}}\right)^2}} \cdot \frac{\alpha_{p-n-p}}{\sqrt{1 + \left(\frac{f}{f_{pT4}}\right)^2}},$$

$$K_i(f) = \sqrt{K_i'^2(f) + K_i''^2(f) - 2 \cdot K_i'(f) \cdot K_i''(f) \cdot \cos \left[ [180 - \Delta\varphi] \cdot \frac{\pi}{180} \right]} \quad (4.31)$$

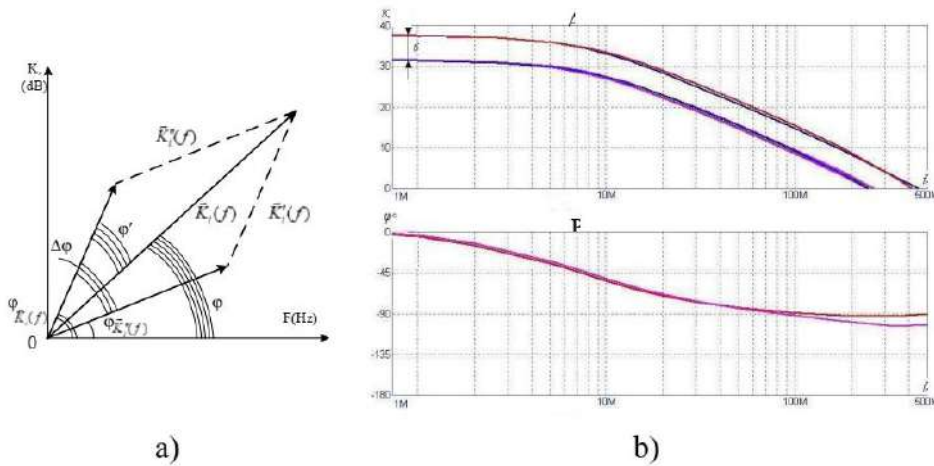


Fig. 4.13. Graphic interpretation of the transfer coefficients for the input push-pull stage with common collector and looping by the emitters: a) vector diagram; b) AFC and PFC.

To determine the angle  $\varphi'(f)$  it is necessary to apply the law of sines where

$$\varphi'(f) = \frac{180}{\pi} \cdot \frac{K_{i_1} \cdot \sin \left[ \Delta\varphi(f) \cdot \frac{180}{\pi} \right]}{\sqrt{K_{i_1}^2(f) + K_{i_2}^2(f) - 2 \cdot K_{i_1}(f) \cdot K_{i_2}(f) \cos \left[ (180 - \Delta\varphi(f)) \cdot \frac{\pi}{180} \right]}}. \quad (4.32)$$

By means of the expressions (4.30), (4.31) and (4.32) the transfer coefficients in the upper and lower amplification channels, as well as the values of the common amplification factor and its phase characteristic can be determined. For the verification of the adequacy of the suggested models of AFC and PFC simulation in the program environment MicroCap and MathCAD was used. For this purpose we use the obtained analytical relations and small signal and electric circuits, shown in Fig. 4.1c and Fig. 4.12a. Simulating the circuits by means of the MicroCap program, we obtain the convergence of the results of the analysis of the analytical equations of AFC and PFC, small signal equivalent circuit as well as electric circuit. Graphs AFC and PFC are presented in Fig. 4.13b.

## 5. Methods of circuit-functional organization of the highlinear analog devices on the base of the push-pull structures

### 5.1. Methods of circuit organization of the highlinear buffer devices on the base of the push-pull structures

#### 5.1.1. Circuit organization and models of the transfer characteristics of the cores of the push-pull buffer devices

Buffer devices are power amplifiers and are intended for the coordination of the signal generator resistance with the load resistance [170]. Voltage buffer (VB) performs the role of the resistances transformer with high input and low output resistances. Transfer coefficient of VB voltage equals unit. Current, supplied by VB in the load, may be far greater than the input current. Such buffer devices are called voltage repeaters [177].

Several approaches to the construction of the VB on the base of the push-pull symmetric structures can be suggested [170, 195]. Irrespective of the specific circuit engineering realization, generalized structural functional scheme of the buffer device has the form, shown in Fig.5.1

Static transfer characteristic of such type of the devices has the common error

$$\Delta U_{out} = U_{out} - U_{inp}. \quad (5.1)$$

In its turn it can be decomposed into several components, namely:

zero shift error  $\Delta U_{sh0}$ , and  $\Delta U_{sh0} = \Delta U_{out}$ , if  $U_{inp} = 0$ ;

scale error  $\Delta U_{sc}$ , and  $\Delta U_{sc} = U_{out} - U_{inp} - \Delta U_{sh0}$ ;

linearity error  $\Delta U_l$ , and  $\Delta U_l = \Delta U_{sc} - K \cdot U_{inp}$ , and  $K = \frac{y_2 - y_1}{x_2 - x_1}$ ,

where  $x_1, x_2, y_1, y_2$  – are the coordinates of the straight line points that passes across the linear section of the transfer characteristic [182].

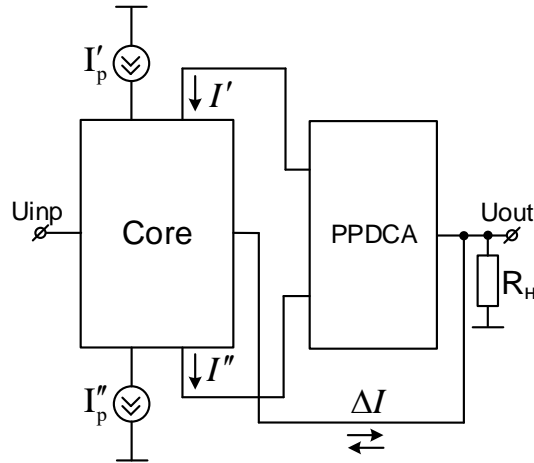


Fig. 5.1. Generalized structural-functional scheme of the push-pull buffer device

At the same time, it can be written that in the ideal case  $\Delta I = 0$ . Taking into account the equalities  $I'_p = I''_p = I_p$ ;  $I' \cdot I'' = I_p^2$ , which are introduced into [165] and that  $\Delta I = |I' - I''|$ , it is easy to notice that the condition of the balance is the equality  $I = I$ . It should be noted that the core determines the potential characteristics of the whole circuit, whereas PPDCA provides the increase of the loading capacity and keeps up the level of the linearity error [195]. At the same time, levels of the separate components may greatly depend on the specific circuit engineering realization of the core of the device.

The known circuit [170], presented in Fig. 1.24 has considerable zero shift error. It is stipulated by the non-balance of voltages of base-emitter junctions of n-p-n and p-n-p of VT6 and VT7 transistors correspondingly.

For the stabilization of the voltages of the collector junctions of the transistors of the output stages of the core the cascades on the transistors VT1, VT5 and VT4, VT8 are introduced, correspondingly. It efficiently stabilizes the characteristics of the working points of the transistors VT6 and VT7, in particular, collector currents and voltages of base-emitter junctions and decreases the level of the scale errors and linearity. At the same time, the imperfection of the transistors VT5 and VT8 of the cascades, namely the dependence  $\beta\beta$  on the voltage of base-emitter junctions leads to the change of their basic currents and does not allow further minimization of these components. This, in turn, leads to the change of the emitter currents of the transistors VT2, VT3 and simultaneously to the change of base-emitter voltages of these transistors that automatically is transferred to the output of the circuit and causes the emergent of the zero shift error.

Output voltage of such circuit is determined in the form [195]:

$$U_{out} \approx U_{inp} + (U_{be})_{VT2} - (U_{be})_{VT6},$$

$$U_{out} \approx U_{inp} - (U_{be})_{VT3} + (U_{be})_{VT7},$$

where  $U_{inp}$  – is the input voltage;  $(U_{be})_{VT2}, (U_{be})_{VT3}$  – are base-emitter voltages of the transistors VT2, VT3;  $(U_{be})_{VT6}, (U_{be})_{VT7}$  – are base-emitter voltages of the transistors VT6, VT7, and  $(U_{be})_{VT2} \approx (U_{be})_{VT6}$ ,  $(U_{be})_{VT3} \approx (U_{be})_{VT7}$ .

For the integral transistors the level of zero shift error reaches the values of 10-50 mV.

Scale and linearity errors greatly depend on the impact of voltages change of the collector-emitter junctions of the core transistors in the range of the output signal.

It should be noted that the factors, exercising negative impact of the circuits characteristics, are [195]:

- 1) dependence of the voltage of base-emitter junction  $U_{be}$  of the transistor on the voltage of collector-emitter  $U_{ce}$  junction;
- 2) dependence of the collector current  $I_c$  of the transistor on the voltage of the collector-emitter junction, it is stipulated by the limiting values of the collector junction resistance  $r_c^*$ ;
- 3) dependence of transistor  $\beta$  on the voltage on the voltage of the collector-emitter junction  $U_{ce}$ .

To decrease zero shift error, it is suggested to construct the circuit, as it is shown in Fig. 5.2a, i.e. by means of introducing the chains of n-p-n and p-n-p transistors, which would perform the self-balancing of the voltages of p-n junctions [195].



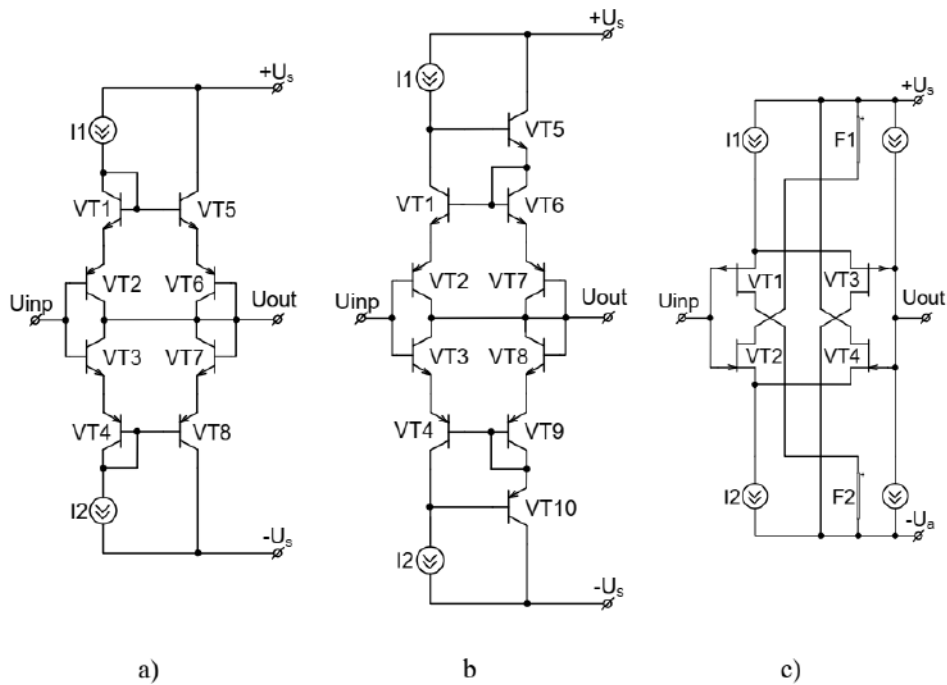


Fig 5.2. Circuit –engineering organization of the buffer device core: a) with the voltages balancing of base-emitter junctions ; b) with the cascading of the current outputs on the base of Wilson circuits; c) with the differential stages on field effect transistors with input-output self balancing

In this case, the output voltage of such circuit is determined :

$$U_{out} \approx U_{inp} + (U_{be})_{VT2} + (U_{be})_{VT1} - (U_{be})_{VT5} - (U_{be})_{VT6};$$

$$U_{out} \approx U_{inp} - (U_{be})_{VT3} - (U_{be})_{VT4} + (U_{be})_{VT7} + (U_{be})_{VT8},$$

where  $(U_{be})_{VT1} - (U_{be})_{VT8}$  – base-emitter voltage of the transistors VT1–VT8, and  $(U_{be})_{VT1} \approx (U_{be})_{VT5}; (U_{be})_{VT2} \approx (U_{be})_{VT6}; (U_{be})_{VT3} \approx (U_{be})_{VT7}; (U_{be})_{VT4} \approx (U_{be})_{VT8}$ .

Such system has low error of zero shift, it reaches the level of 200–500  $\mu V$ , but has greater linearity error than the circuit in Fig. 1.24. At the sametime it should be noted that the problem of the voltage dependence of base-emitter junction of VT5 and VT8 transistors on the voltage of collector- emitter.

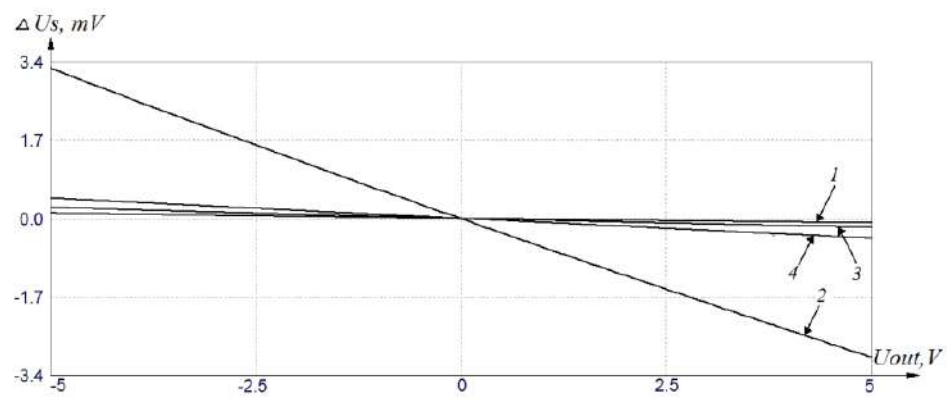
To eliminate these errors, the simple cascade circuit on the transistors VT1, VT5 and VT4, VT8 can be replaced by the cascades, built on the base of Wilson circuits. The circuit of the buffer device [196], shown in Fig. 5.2b is suggested. Such a circuit has low linearity error, which is equal to the error of the linear circuit in Fig. 1.24 and low error of the zero shift, on the level of 100-200  $\mu\text{V}$ . Such circuit engineering organization of the core decreases the impact of the voltages of base-emitter junctions of the transistors VT6 and VT9 but the problem of the base current impact of the transistors VT5 and VT10 still remains.

Specific feature of the buffer devices, based on the bipolar transistors, is the availability of the input base current. That is why; the cardinal solution of this problem is the usage of the field-effect transistors with the controlled p-n junctions (Fig 5.2c). Such circuit provides low linearity error and zero shift error, that depends on drain-to-source voltage balancing and cut-off-source voltages spread of the transistor pairs VT1, VT3 and VT2, VT4.

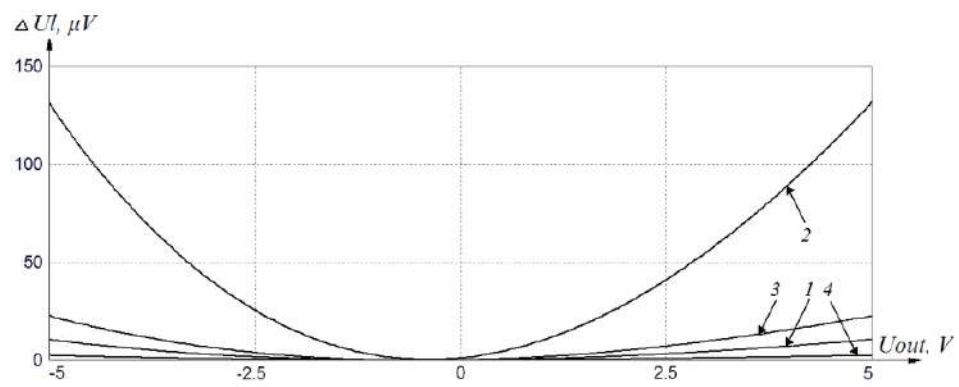
At the same time, it should be noted that any of the considered circuits does not provide minimization of the linearity error in the range of the output signal. It is proved by the simulation of the scale errors and linearity of the transfer characteristic of the buffer device, shown in Fig. 5.3. In the graphs the curves 1-4 are referred to the circuits of the buffer device cores in Fig. 1.24 and Fig. 5.2a-c correspondingly.

For the determination of the components, influencing the emergence of  $\Delta U_{out}$  it is expedient to consider the equivalent circuit of the buffer devices core output, shown in Fig. 5.4a. It contains:  $r_b', r_b''$ ,  $r_c^*, r_c^{**}$  – are the resistances of the bases and collectors of the transistors VT5 and VT8, correspondingly;  $r_e', r_e''$  – are the resistances of emitters of the transistors VT 5 and VT8 correspondingly, and  $r_e' = r_e'' = r_e$ ;  $r_d', r_d''$  – are the resistances of p – n junctions of the transistors VT6 and VT7 in diode connection of the transistor, and  $r_d' = r_d'' = r_d = r_e$ ;  $U', U''$  – are voltages of the buses of the positive and negative supply, correspondingly.

It is expedient to convert the circuit in the form, shown in Fig. 5.4b.



a)



b)

Fig. 5.3. Errors of the transfer characteristics of the buffer device cores: a) scale; b) linearity

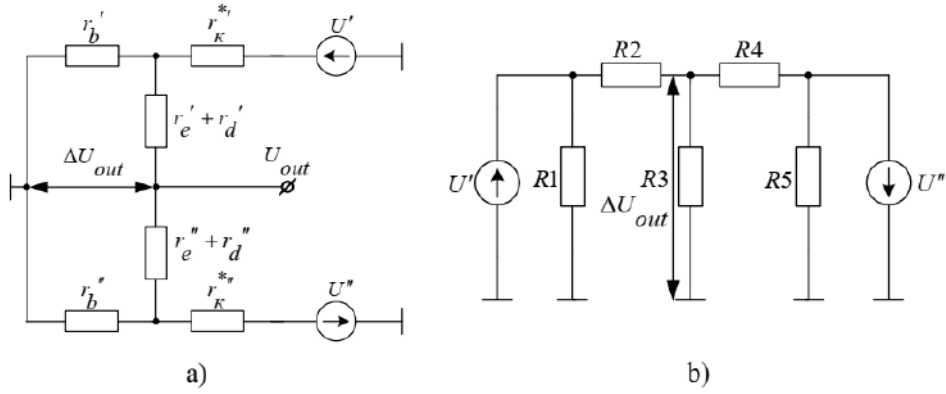


Fig 5.4. Equivalent small signal circuits of the buffer device core: a) output; b) after the conversion

$$R1 = r_c^{*i} + r_b^{*i} + \frac{r_c^{*i} \cdot r_b^{*i}}{2 \cdot r_e}; \quad R2 = 2 \cdot r_e + r_c^{*i} + \frac{2 \cdot r_e \cdot r_c^{*i}}{r_b^{*i}}; \quad R3 = \frac{R3' \cdot R3''}{R3' + R3''},$$

$$\text{where } R3' = 2 \cdot r_e + r_b^{*i} + \frac{2 \cdot r_e \cdot r_b^{*i}}{r_c^{*i}};$$

$$R3'' = 2 \cdot r_e + r_b^{*n} + \frac{2 \cdot r_e \cdot r_b^{*n}}{r_c^{*n}}; \quad (5.2)$$

$$R4 = 2 \cdot r_e + r_c^{*n} + \frac{2 \cdot r_e \cdot r_c^{*n}}{r_b^{*n}}; \quad R5 = r_c^{*n} + r_b^{*n} + \frac{r_c^{*n} \cdot r_b^{*n}}{2 \cdot r_e}.$$

Applying the method of the superposition [192] we can rewrite the equation (5.1) in the form:

$$\Delta U_{out} = \Delta U'_{out} + \Delta U''_{out}, \quad (5.3)$$

where  $\Delta U'_{out} = f(U')$ ,  $\Delta U''_{out} = f(U'')$  – are the voltage increments in the upper and bottom channels, which, in their turn, are determined as

$$\begin{aligned}\Delta U'_{out} &= U' \cdot \frac{R3}{R2 + R3}; \\ \Delta U''_{out} &= U'' \cdot \frac{R3}{R4 + R3}.\end{aligned}\tag{5.4}$$

Taking into account the above-mentioned dependences and equations (5.3), we obtain

$$\Delta U_{out} = \frac{[U' \cdot (R4 + R3) + U'' \cdot (R2 + R3)] \cdot R3}{(R2 + R3) \cdot (R4 + R3)}.\tag{5.5}$$

By means of the substitution in the equation (5.5) of the values from (5.2) we obtain the absolute error.

Relative error [192] is determined in the form:

$$\delta = \frac{\Delta U_{out}}{U_{out}} \cdot 100\%.$$

Having substituted in (5.4) the values from (5.2) and taking into account that in the real circuits  $r'_b \ll r_c^{*i}$ ,  $r''_b \ll r_c^{*n}$  and  $r'_b \approx r''_b$  we obtain

$$\Delta U'_{out} \approx U' \cdot \frac{2 \cdot r_e}{r_c^{*i}}, \quad \Delta U''_{out} \approx U'' \cdot \frac{2 \cdot r_e}{r_c^{*n}}.$$

It is easy to notice that the linearity error greatly depends on the value of  $r_c^{*i}$  and  $r_c^{*n}$ , as well as  $r_e$ , the value of which is 2-3 orders less than the values of  $r_c^{*i}$  and  $r_c^{*n}$ .

### 5.1.2. Methods of linearity error decrease, zero shift and loading capacity increase of the buffer devices

To provide high linearity of the transfer characteristic of the core, several variants of their circuit-functional organization are suggested:

- introduction in the core the cascades, built on the field-effect transistors in the core;
- construction of the core cascades on the composed Schottky transistors;
- usage of parametric stabilization of the transistors stages supply voltages.

The first method allows increasing the resistance of the current outputs [131] (Fig. 5.5a). As a result, the stabilization of the collector-emitter junction voltages of the transistors VT6 and VT9 is provided, and base currents of these transistors can be neglected. Taking into account the dependences (5.4) the voltage increments in upper and lower channels can be written as

$$\Delta U'_{out} \approx U' \cdot \frac{2 \cdot r_e}{r'_{cl}(1 + S' \cdot R'_{cl})}; \quad \Delta U''_{out} \approx U'' \cdot \frac{2 \cdot r_e}{r''_{cl}(1 + S'' \cdot R''_{cl})},$$

where  $r'_{cl}, r''_{cl}$  – are differential output resistances;  $S', S''$  – slopes of the transfer characteristics;  $R'_e, R''_e$  – are volume resistances of the sources of n-channel and p-channel field-effect transistors, correspondingly [131]. Usage of the cascades on the field-effect transistors enables an increase by 1-2 orders of linearity, as compared with the circuit in Fig. 1.24.

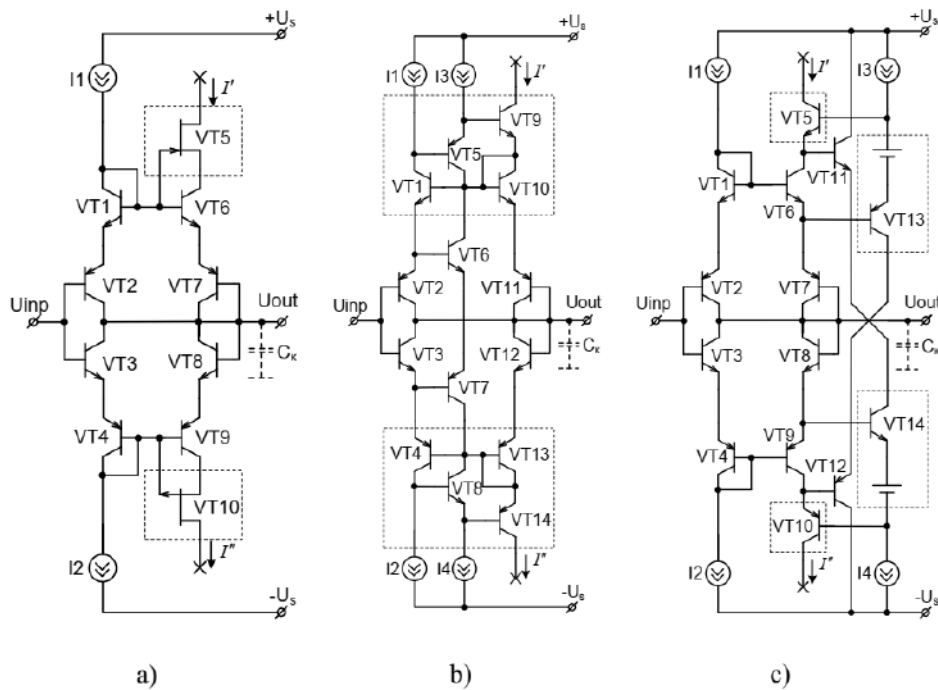


Fig. 5.5. Circuit-functional organization of the input circuits of high linear buffer devices: a) with cascodes on the field-effect transistors; b) with cascode current reflectors on the composed Shottky transistors; c) with parametric stabilization of voltages of the collector-emitter output stages

The second method enables to decrease the impact of base currents of the transistors VT9 and VT14 in  $\beta_{n-p-n}$  and  $\beta_{p-n-p}$  correspondingly

(Fig. 5.5b). In this case, the linearity error decreases  $\frac{\beta_{\min}}{2}$  times, where  $\beta_{\min}$  – is the smallest value of  $\beta$  of the pair of the transistors VT9 and VT14. Taking into account the dependences (5.4) the increments of upper and low channels voltage can be written as

$$\Delta U'_{out} \approx U' \cdot \frac{4 \cdot r_e}{r'_{out} \cdot \beta_{n-p-n}}; \quad \Delta U''_{out} \approx U'' \cdot \frac{4 \cdot r_e}{r''_{out} \cdot \beta_{p-n-p}}. \quad (5.6)$$

However, it is necessary to take measures regarding the correction of the transient characteristic, as the usage of the compound transistors leads to the appearance of the additional pole at high frequencies.

The third method enables to increase the linearity and maintain the level of fast acting, as compared with the circuit shown in Fig. (1.24.(Fig 5.5c). The value of the linearity area is smaller than in the circuit that uses the compound Shottky transistors. The voltage increments for such circuits are described by the relations [5.6].

Graphs of scale and linearity errors of the transfer characteristics as well as transient characteristics of high linear buffer devices are shown in Fig. 5.6 and Fig. 5.7, correspondingly. In graphs the curves 1-3 correspond to the circuits in Fig. 5.5a-c.

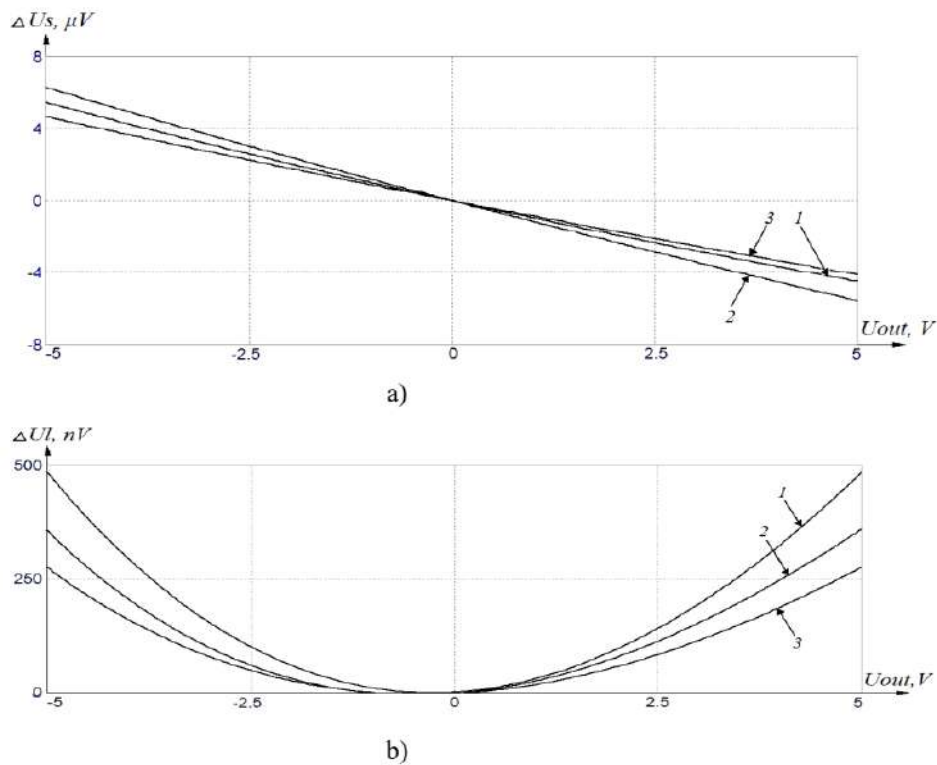


Fig. 5.6. Errors of the transfer characteristics of the buffer device cores in the range of  $U_{out}$ : a) scale; b) linearity

The characteristic feature of the buffer devices on the bipolar transistors is the availability of non-zero input current, that leads to the emergence of zero shift  $\Delta U_{sh0}$  error. For this purpose the separate generator  $I_{sh0}$  is used, it provides the compensation of zero shift current. Main requirements to such device are:

- stability of  $I_{sh0}$  in the range of the input signal;
- high output resistance.

To decrease zero shift error of the buffer device core the circuit engineering organization of current  $I_{sh0}$  source is suggested, it is shown in Fig. 5.8.



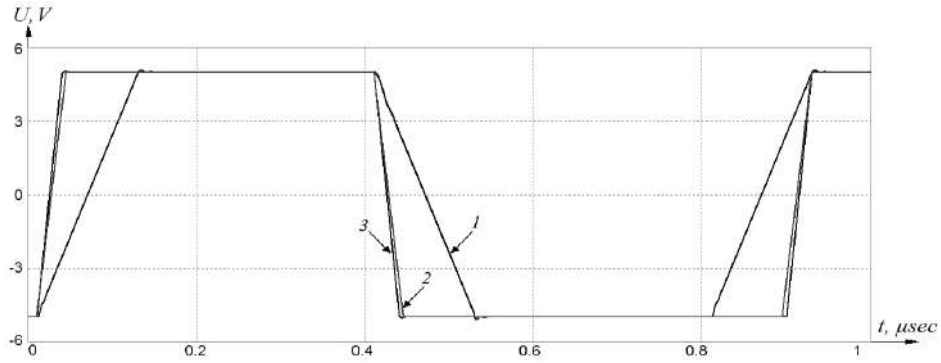


Fig. 5.7. Transient characteristics of the buffer device cores

The value of the current is defined by the expression (4.5). Characteristic feature of this circuit as compared with the circuit shown in Fig. 4.6 is that due to the usage of Shiklai transistors in BC', BC'' the output resistance is increased and the accuracy of  $I_{sh0}$  setting is provided. The linearity error of zero shift

source increases  $\frac{\beta_{\min}}{2}$  times, where  $\beta_{\min}$  – is the smallest value  $\beta$  of the pair of transistors VT' and VT''.

The drawback of the considered circuits is low loading capacity, which is greatly determined by the output resistance of the circuit  $r_{out}$ . And

$$r_{out} = r_e.$$

Nonzero value of the output resistance leads to the change of the scale and worsening of the linearity of the transfer characteristics.

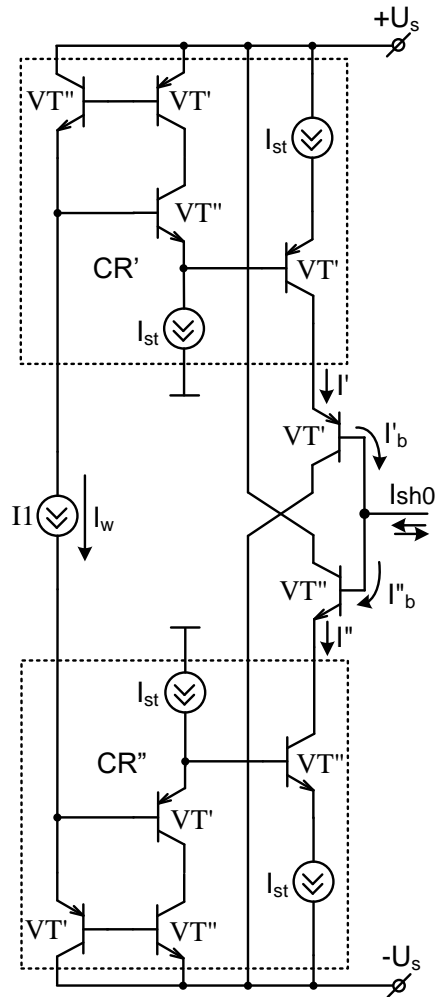


Fig. 5.8. Circuit engineering realization of current source compensation of zero shift of buffer device core

To improve the loading capacity and maintain the preset linearity, it is expedient to introduce PPDCA in the circuit. The generalized structure of such a buffer device is shown in Fig. 5.9.

It consists of the amplifying stages  $K'_i$  and  $K''_i$ , circuit of working points auto balancing (CWPAB) and current reflectors CR1 and CR2. CWPAB enables to obtain the proportional dependence between final transfer coefficient and balancing their value and signal range.

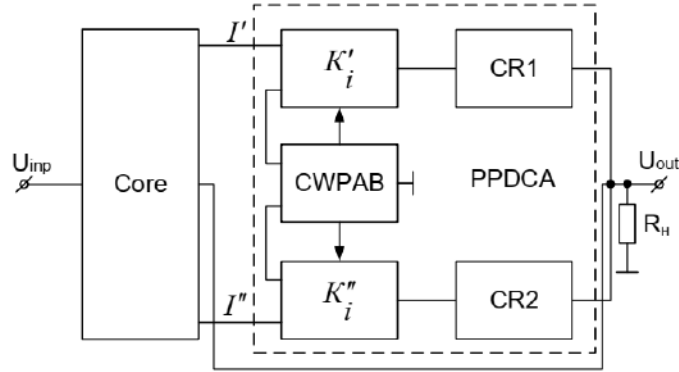


Fig. 5.9. Structural-functional organization of high linear buffer device, based on push-pull symmetric structure

The condition of the self balancing is the execution of the equality  $\frac{I'}{I_p} = \frac{I_p}{I''}$ , where  $I_p$  – is the current of the working point;  $I', I''$  – are control currents of the level. In this case  $K'_i = K''_i$ .

Introduction of PPDCA in FBC of the circuit, namely between the core and loading, enables to decrease the output resistance to the level

$$r_{out} = \frac{r}{K_i},$$

where  $K_i$  – is the general amplification factor of PPDCA.

## 5.2. Methods of circuit organization of current-voltage and voltage voltage-current converters, based on push-pull current amplifiers

Current-voltage (CVC) and voltage-voltage (VVC) converters are analog units, which can be constructed on the base of the operation amplifiers (OA) with large transfer coefficients ( $10^6$ – $10^8$ ). However, the application of the conventional OA has its drawbacks, namely: non-linearity decreases at the expense of increasing amplification factor with the increasing the depth of the feedback, in its turn, this leads to the worsening of AFC and PFC. It requires their correction and decreases fast acting [127]. Better indices have PPDCA, manufactured by the leading companies. However, they also have some drawbacks: low amplification on the stage and, as a result, to achieve large

amplification factors ( $10^6$ – $10^8$ ), it is necessary to increase the number of the amplifying stages [133]. At the same time, it is worth mentioning that some metrological characteristics of CVC and VVC, such as linearity of the transfer characteristic, are difficult to correct.

The generalized structural diagram of CVC and VVC on the base of PPDCA, is shown in Fig. 5.10.

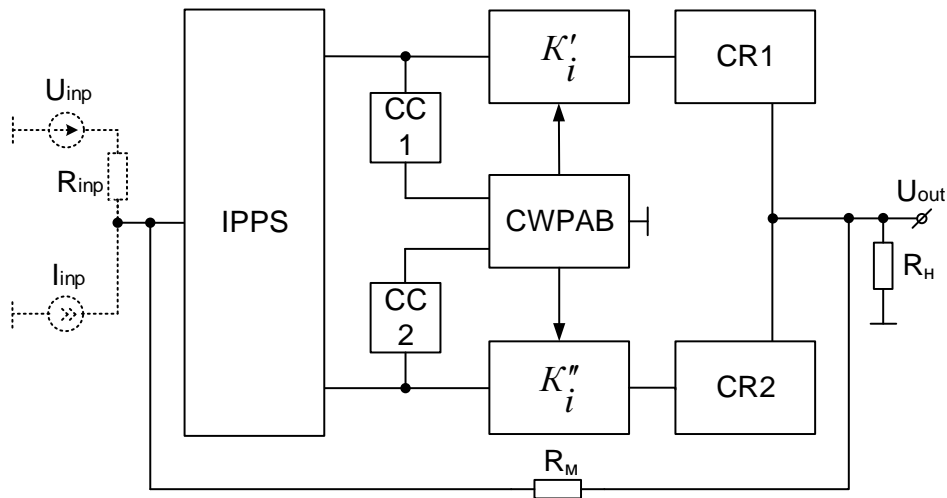


Fig. 5.10. Generalized structural diagram of CVC and VVC on the base of PPDCA

Depending on the type of the converter the input signal can be both in the form of current  $I_{inp}$  and in the form of the voltage  $U_{inp}$ . Output signal is voltage  $U_{out}$ .

The converter contains IPPS, two symmetrical IAS  $K'_i$  and  $K''_i$  for the amplification of the counterphase signals. Working points of these stages are set by the SWPAB by means of current compensators KC1 and KC2. The given principle of the working point setting is provided by means of the selective feedback so that in the channel with smaller amplification  $K_i$  increases and in the channel with greater amplification – it decreases. It lasts until the amplification factors in the upper and lower channels equalize.

It is worth mentioning that the PPDCA characteristics depend on the principle of IPPS construction. We will consider the method of structural functional organization of the input stages of PPDCA, which could serve as the basis of CVC and VVC construction [197]. Structures of PPDCA, shown in Fig. 5.11 will be considered.

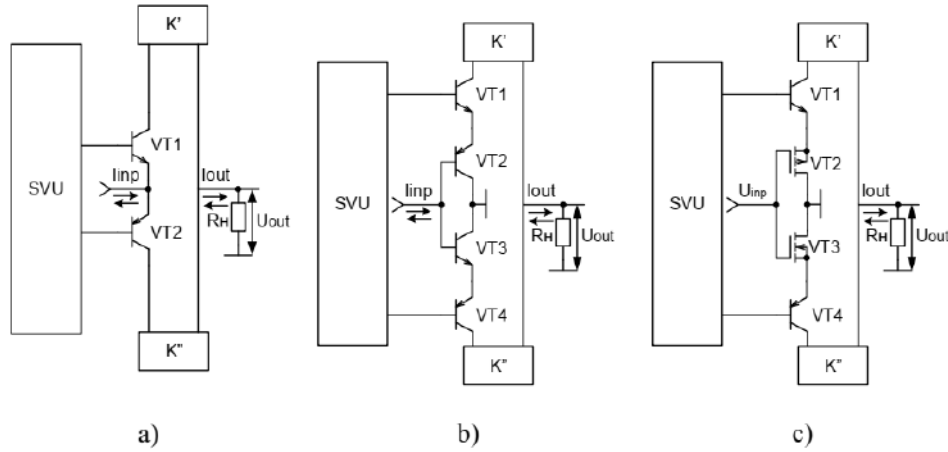


Fig. 5.11. Structural functional organization of the input stages of PPDCA with: a) low; b) average; c) high input resistances

Their basics are the input stages, built in the form of the self complementary circuit with a common base (see Fig. 5.11a), push-pull APS of the input current on the bipolar transistors (see Fig. 5.11b), push-pull APS of the input voltage on the complementary field-effect transistors (see Fig. 5.11c) [178, 180, 197]. VSU provides direct current mode.

Depending on the value of the input current  $r_{inp}$ , the input stages conventionally can be divided into [197]:

with low input resistance –  $r_{inp} < 10 \cdot r_e$  ;

with average input resistance –  $10 \cdot r_e \leq r_{inp} < 10^4 \cdot r_e$  ;

with high input resistance –  $r_{inp} \geq 10^4 \cdot r_e$  .

The specific value of the input current  $r_{inp}$  depends on the value of the working point current.

To obtain the detailed transfer characteristics of CVC and VVC on the base of PPDCA it is necessary to consider their equivalent circuits, shown in Fig. 5.12.

To organize the operation mode the amplifier is surrounded by the circuit of the deep feedback. FBC is organized by means of connecting  $R_M$  between the output and inverse input of the circuit.

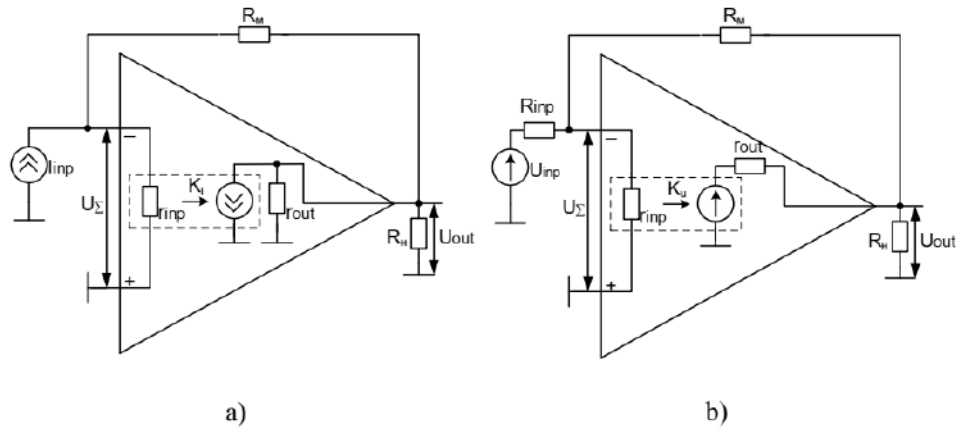


Fig 5.12. Equivalent circuit of the converters: a) current-voltage; b) voltage-voltage

In the literature sources [167, 198], where CVC and VVC are described, their transfer characteristics are given, they have the following form:

$$\text{CVC: } U_{out} \approx I_{inp} \cdot R_M, \quad \text{VVC: } U_{out} \approx -U_{inp} \cdot \frac{R_M}{R_{inp}}. \quad (5.7)$$

These expressions take into consideration only the parameters of the external circuits for the ideal amplifiers. However, these formulas do not take into consideration the characteristics of the amplifier itself, namely: input  $r_{inp}$  and output  $r_{out}$  resistances, which lead to the emergence of the linearity errors of CVC and VVC. It should also take into account the impact of the load resistance  $R_l$ . As the base of the converters is the amplifier it is expedient to take into consideration its internal current transfer coefficient  $-K_i$  and voltage transfer coefficient  $-K_u$ , determined at the broken feedback path and are described by the relations:

$$K_i = \frac{i_{out.in}}{i_{inp}}; \quad K_u = \frac{U_{out.in}}{U_\Sigma}, \quad (5.8)$$

where  $i_{out.in}$  – current at the output of the amplifier in case of the broken feedback path ( $r_{out} \rightarrow \infty, R_M \rightarrow \infty$ );  $U_{out.in}$  – voltage at the output of the

amplifier in case of the broken feedback path ( $r_{out} = 0, R_M \rightarrow \infty$ );  $U_\Sigma$  – total voltage drop at the input of the amplifier, caused by available input resistance  $r_{inp}$  (quasi zero voltage);  $i_{inp}$  – input current,  $i_{inp} = \frac{U_\Sigma}{r_{inp}}$ .

We will introduce the transfer characteristics of CVC and VVC, taking into consideration such parameters as:  $r_{inp}, r_{out}, R_{inp}, R_H, R_M, K_i, K_u$ .

Analyzing these equivalent circuits and applying Kirchhoff first and second laws for CVC, we obtain such system of equations:

$$\begin{cases} I_{inp} - i_{inp} - I_M = 0; \\ I_M + i_{out} + I_H - i_{out.in} = 0; \\ U_\Sigma + U_M - U_{out} = 0; \\ U_{out} - U_H = 0, \end{cases} \quad (5.9)$$

where  $I_M$  – current, flowing across the resistor  $R_M$ ;  $i_{out}$  – current at the output of the amplifier,  $U_M$ ;  $U_H$  – voltage drop at the resistors  $R_M, R_H$ . The most critical, when the errors of the transfer characteristic emerge, is the available  $U_\Sigma$ , caused by  $r_{inp}$  [131,167,197]. We will introduce the transfer characteristic of CVC, taking into account  $r_{inp}$ .

Taking into consideration the first and the second equations from the system (5.9), we obtain

$$U_{out} = i_{inp} (r_{inp} - R_M) + I_{inp} \cdot R_M. \quad (5.10)$$

It follows from the expression (5.8) that  $I_M = i_{inp} \cdot K_i$ . Having substituted in the first equation of the system (5.9), we obtain

$$i_{inp} = \frac{I_{inp}}{1 + K_i}.$$

Taking into account this expression and (5.10), we obtain the transfer characteristic of CVC

$$U_{out} = I_{inp} \cdot \frac{r_{inp} + R_M \cdot K_i}{1 + K_i}. \quad (5.11)$$

Taking into consideration the value of  $R_H$ , and the second equation

from the system (5.9) and the fact that  $I_H = \frac{U_{out}}{R_H}$ , we obtain

$$i_{inp} = \frac{I_{inp} + \frac{U_{out}}{R_H}}{1 + K_i}.$$

Substituting the obtained expression into the equality (5.10), we will write the transfer characteristic of CVC

$$U_{out} = I_{inp} \cdot \frac{r_{inp} + R_M \cdot K_i}{1 + K_i + \frac{R_M - r_{inp}}{R_H}}. \quad (5.12)$$

But the amplifier has the output resistance  $r_{out}$ , taking into account this resistance, we obtain

$$i_{inp} = \frac{I_{inp} + U_{out} \cdot \frac{r_{out} + R_H}{r_{out} \cdot R_H}}{1 + K_i}.$$

Let  $\frac{r_{out} + R_H}{r_{out} \cdot R_H} = \frac{1}{R_{av}}$ , then, taking into account the equality (5.10) we will

write the transfer characteristic of CVC in the form

$$U_{out} = I_{inp} \cdot \frac{r_{inp} + R_M \cdot K_i}{\left(1 + \frac{R_M}{R_{av}}\right) \cdot (1 + K_i) - \frac{r_{inp} + R_M \cdot K_i}{R_{av}}}. \quad (5.13)$$

Taking into consideration the analytical expressions (5.11), (5.12), (5.13), which describe the transfer characteristic of CVC with the account of the



amplifier parameters (  $r_{inp} \ll R_M, r_{out} \ll R_H, K_i \gg 1$  ), by means of mathematical simplifications, we obtain the approximated expression (5.7) for CVC.

Applying Kirchhoff first and second laws for VVC we obtain such system of equations:

$$\begin{cases} I_{inp} - i_{inp} + I_M = 0; \\ i_{out} - I_M - I_H = 0; \\ U_{in} - U_{R_{inp}} - U_{\Sigma} = 0; \\ U_{out.in} - U_{r_{out}} - U_{\Sigma} - U_M = 0; \\ U_H - U_M - U_{\Sigma} = 0, \end{cases} \quad (5.14)$$

where  $U_{R_{inp}}, U_{r_{out}}$  – voltages drop at the resistances  $R_{inp}, r_{out}$ , correspondingly.

We will derive the transfer characteristic of CVC with the account of  $R_{inp}$  and  $r_{inp}$ . Taking into consideration the first equation of the system (5.14) and Ohm's law we obtain

$$\frac{U_{R_{inp}}}{R_{inp}} - \frac{U_{\Sigma}}{r_{inp}} + \frac{U_M}{R_M} = 0. \quad (5.15)$$

As in the given case  $r_{out} = 0$ , then  $U_{out} = U_{out.in}$ . It follows from the expression (5.7):  $U_{\Sigma} = \frac{U_{out}}{K_u}$ . Thus  $U_M = (K_u - 1) \cdot U_{\Sigma}$ . Considering these expressions and the third expression of the system (5.14) and (5.15), the transfer characteristic of VVC is obtained.

$$U_{out} = U_{inp} \cdot \frac{r_{inp} \cdot R_M \cdot K_u}{R_M \cdot (r_{inp} + R_{inp}) - (K_u - 1) \cdot r_{inp} \cdot R_{inp}}. \quad (5.16)$$

Taking into account the value of  $R_n$ , if  $r_{out} = 0$ , the convergence of the transfer characteristic with the expression (5.16) is obtained, as  $U_{out} = U_{out.in}$  and the signal is completely transferred into loading. But in practice the amplifier has  $r_{out} \neq 0$ , taking it into consideration, we obtain the transfer characteristic of VVC.

$$U_{out} = U_{inp} \cdot \frac{r_{inp} \cdot R_M \cdot R_H \cdot (K_u \cdot R_M + r_{out})}{\left[ r_{out} \cdot R_H + R_M \cdot (r_{out} + R_H) \right] \cdot \left[ r_{inp} \cdot R_{inp} + R_M \cdot (r_{inp} + R_{inp}) \right]} - \quad (5.17)$$

$$\frac{-r_{inp} \cdot R_{inp} \cdot R_H \cdot (K_u \cdot R_M + r_{out})}{\left[ r_{out} \cdot R_H + R_M \cdot (r_{out} + R_H) \right] \cdot \left[ r_{inp} \cdot R_{inp} + R_M \cdot (r_{inp} + R_{inp}) \right]}$$

Taking into consideration the analytical expressions (5.16), (5.17) which describe the transfer characteristic of VVC with the account of the amplifier parameters ( $r_{inp} \gg R_M$ ;  $r_{inp} \gg R_{inp}$ ;  $R_M \approx R_{inp}$ ;  $r_{out} \gg R_H$ ;  $K_u \gg 1$ ), by means of mathematical simplifications, we obtain the approximated expression (5.7) for VVC.

The presence of  $r_{inp}$  leads to the emergence of  $U_\Sigma$ , that, in its turn, results in the appearance of linearity error. To evaluate the impact of the input resistance of PPDCA on the linearity error of CVC and VVC, we will consider the example on the base of the real values:

For CVC:  $I_{inp} = \pm 1 \text{ mA}$ ,  $U_{out} = \pm 10 \text{ B}$ ,  $R_M = \pm 10 \text{ kOhm}$ ,  $K_i = 100$ ,  $r_{inp} = 25 \Omega$ .

Absolute error [192] is determined as

$$\Delta U_{out} = U_{out} - U'_{out}, \quad (5.18)$$

where  $U'_{out} = I_{inp} \cdot \frac{R_M \cdot K_i}{1 + K_i}$  – voltage at the output of CVC, if  $r_{inp} = 0$ .

Taking into account the above-mentioned expressions and expression (5.11) we obtain

$$\Delta U_{out} = I_{inp} \cdot \frac{r_{inp}}{1 + K_i}. \quad (5.19)$$

The relative error [192] is determined as

$$\delta = \frac{\Delta U_{out}}{U_{out}} \cdot 100 \% . \quad (5.20)$$

Taking into account the above-mentioned expressions, we obtain the expression for the description of the relative error of CVC

$$\delta = \frac{r_{inp}}{R_M \cdot (1 + K_i)} \cdot 100 \% . \quad (5.21)$$

Taking into account the expressions (5.19) and (5.21) and real parameters of CVC we determine that the absolute error  $\Delta U_{out} = 248 \mu V$ , and the relative error  $\delta = 0,0025 \%$ .

For VVC  $U_{inp} = \pm 10 V$ ;  $U_{out} = \pm 10 V$ ;  $R_M = \pm 10 k\Omega$ ;  $K_u = 100$ ;  $R_{inp} = 10 k\Omega$ ;  $r_{inp} = 1 M\Omega$ ;  $r_{inp} \gg R_M, R_{inp}$ .

Taking into consideration the expressions (5.7) and (5.18) we obtain

$$\Delta U_{out} = U_{inp} \cdot \frac{-R_M \cdot [r_{inp} \cdot R_{inp} + R_M \cdot (r_{inp} + R_{inp})]}{R_{inp} \cdot [R_M \cdot (r_{inp} + R_{inp}) - (K_u - 1) \cdot r_{inp} \cdot R_{inp}]} . \quad (5.22)$$

Taking into account the expression (5.20), the relative error of VVC will have the form

$$\delta = - \frac{r_{inp} \cdot R_{inp} + R_M \cdot (r_{inp} + R_{inp})}{R_M \cdot (r_{inp} + R_{inp}) - (K_u - 1) \cdot r_{inp} \cdot R_{inp}} \cdot 100 \% . \quad (5.23)$$

Taking into consideration the expressions (5.22), (5.23) and real parameters of VVC we determine that the absolute error  $\Delta U_{out} = 100 \mu V$ , and the relative error  $\delta = 0,001 \%$ .

### 5.3. Minimization of the linearity errors and zero shift of current-voltage and voltage-voltage converters

Having considered structural functional organization of the high linear CVC and VVC on the base of PPDCA, it is expedient to evaluate the advantages and disadvantages of PPDCA application with low, average and high input resistances as well as analyze the linearity errors, taking into account the parameters of the elements of the external and internal circuits of the amplifier and load resistance.

At the same time, considering the equivalent circuits of CVC and VVC, shown in Fig. 5.12, it is easy to notice that in the formulas (5.7), the key characteristics of the amplifier are not taken into account, namely: input  $r_{inp}$  and output  $r_{out}$  resistances, load resistance  $R_l$ , which influence the level of CVC and VVC linearity errors. In [197] the assessment of the impact of the input resistance of PPDCA on CVC and VVC linearity error is performed.

Depending on the factors, influencing the transfer characteristic, such detailization levels can be distinguished [199]:

$$R_M, r_{inp}, K_i \text{ (or } K_u \text{)};$$

$$R_M, R_H, r_{inp}, K_i \text{ (or } K_u \text{)};$$

$$R_M, R_H, r_{inp}, r_{out}, K_i \text{ (or } K_u \text{)}.$$

At the first level of the detailization, the transfer characteristic equation of CVC has the form (5.11), absolute and relative errors are determined by the equalities (5.19) and (5.21), correspondingly.

At the second level of the detailization, the transfer characteristic of CVC has the form (5.12). Taking into consideration the equalities (5.18), (5.20) we obtain the relation for the description of the absolute and relative errors of CVC:

$$\Delta U_{out} = I_{inp} \cdot \frac{r_{inp} \cdot R_H \cdot (1 + K_i) - R_M \cdot K_i \cdot (R_M - r_{inp})}{(1 + K_i) \cdot [R_M - r_{inp} + R_H \cdot (1 + K_i)]}; \quad (5.24)$$

$$\delta = \frac{r_{inp} \cdot R_H \cdot (1 + K_i) - R_M \cdot K_i \cdot (R_M - r_{inp})}{R_M \cdot (1 + K_i) \cdot [R_M - r_{inp} + R_H \cdot (1 + K_i)]} \cdot 100\%. \quad (5.25)$$

At the third level of the detailization, the transfer characteristic of CVC has the form (5.13). With the account of the equalities (5.18), (5.20), we obtain the relation for the description of the absolute and relative errors of CVC:

$$\Delta U_{out} = I_{inp} \cdot \frac{r_{inp} \cdot R_{av} \cdot (1 + K_i) - R_M \cdot K_i \cdot (R_M \cdot (1 + 2 \cdot K_i) - r_{inp})}{(1 + K_i) \cdot [R_M \cdot (1 + 2 \cdot K_i) - r_{inp} + R_{av} \cdot (1 + K_i)]}; \quad (5.26)$$

$$\delta = \frac{r_{inp} \cdot R_{av} \cdot (1 + K_i) - R_M \cdot K_i \cdot (R_M \cdot (1 + 2 \cdot K_i) - r_{inp})}{R_M \cdot (1 + K_i) \cdot [R_M \cdot (1 + 2 \cdot K_i) - r_{inp} + R_{av} \cdot (1 + K_i)]} \cdot 100\%. \quad (5.27)$$

Taking into consideration the analytical expressions (5.24 – 5.27) which describe the absolute and relative errors of CVC with higher levels of the digitization and taking into account the parameters of the amplifier  $\left( r_{inp} \ll R_M, r_{out} \ll R_H, K_i \gg 1 \right)$ , by means of mathematical simplifications we obtain the expressions (5.19), (5.21) with lower level of digitization for CVC. The expressions (5.19) and (5.21) account for the most critical parameters of CVC [131, 167, 197, 199].

The transfer characteristic of CVC at the first level of digitization has the form (5.16). With the account of the equalities (5.18) and (5.20) we obtain the relation for the description of the absolute and relative errors of CVC, which will have the form (5.22) and (5.23), correspondingly.

At the second level of digitization we obtain the convergence of the transfer characteristic of VVC, absolute and relative errors the expressions (5.16), (5.22) and (5.23) correspondingly, as  $U_{out} = U_{out.in}$  and the signal is completely sent into the loading. However in practice the amplifier has  $r_{out} \neq 0$  taking this into account, we obtain the transfer characteristic of VVC for the third level of detailization, which will have the form (5.17). With the account of the equalities (5.18) and (5.20) we obtain the relation for the description of the absolute and relative errors of VVC:

$$\Delta U_{out} = U_{inp} \cdot \frac{R_M \cdot \left[ r_{inp} \cdot R_{inp} \cdot R_H \cdot (K_u \cdot R_M + r_{out}) + \left[ r_{out} \cdot R_H + R_M \cdot (r_{out} + R_H) \right] \right] \times}{R_{inp} \cdot \left[ \left[ r_{inp} \cdot R_H + R_M \cdot (r_{out} + R_H) \right] \cdot \left[ r_{inp} \cdot R_{inp} + R_M \cdot (r_{inp} + R_{inp}) \right] - \right.} \quad (5.28)$$

$$\left. \times \left[ r_{inp} \cdot R_{inp} + R_M \cdot (r_{inp} + R_{inp}) \right] - r_{inp} \cdot R_{inp} \cdot R_H \cdot (K_u \cdot R_M + r_{out}) \right] \cdot \left[ r_{inp} \cdot R_{inp} + R_M \cdot (r_{inp} + R_{inp}) \right] - \left[ r_{out} \cdot R_H + R_M \cdot (r_{out} + R_H) \right] \cdot \left[ r_{inp} \cdot R_{inp} + R_M \cdot (r_{inp} + R_{inp}) \right] - r_{inp} \cdot R_{inp} \cdot R_H \cdot (K_u \cdot R_M + r_{out}) \right] \cdot 100\%.$$

$$\delta = - \frac{r_{inp} \cdot R_{inp} \cdot R_H \cdot (K_u \cdot R_M + r_{out}) + \left[ r_{out} \cdot R_H + R_M \cdot (r_{out} + R_H) \right] \times}{\left[ r_{out} \cdot R_H + R_M \cdot (r_{out} + R_H) \right] \cdot \left[ r_{inp} \cdot R_{inp} + R_M \cdot (r_{inp} + R_{inp}) \right] - \left[ r_{inp} \cdot R_{inp} + R_M \cdot (r_{inp} + R_{inp}) \right] - r_{inp} \cdot R_{inp} \cdot R_H \cdot (K_u \cdot R_M + r_{out})} \cdot 100\%.$$

Taking into account the fact that in practice the parameters of the amplifier are related as  $r_{inp} \gg R_M$ ,  $r_{inp} \gg R_{inp}$ ,  $R_M \approx R_{inp}$ ,  $r_{out} \ll R_H$ ,  $K_u \gg 1$  and taking into consideration the analytical expressions (5.28) and (5.29), by means of mathematical simplifications we obtain the expressions (5.22) and (5.23) with the lower level of digitization for VVC. The expressions (5.22) and (5.23) take into account the most critical parameters of VVC [131, 167, 197, 199].

As it is known, the considerable impact on the emergence of the transfer characteristic error is made by  $U_\Sigma$  [197, 199]. That is why, for the construction of the high linear CVC it is expedient to use PPDCA with low input resistance  $r_{inp}$  (Fig.5.11a). Conventionally, for the reduction of  $U_\Sigma$  the amplifiers with high current gain  $K_i$  are used. Modern amplifiers, manufactured by the leading companies of the world, provide the gains at the level of 120...140 dB [200]. Increase of the current gain  $K_i$  of PPDCA is possible, by means of introduction of one, two, three stage IAS and PPIS with the average input resistance and amplification (Fig. 11b) [166, 197]. The linearity error is inversely proportional to the current gain  $K_i$ . At the same time, the application of such an approach enables to solve the problem of stage amplification [178, 180 197]. It is possible to decrease the linearity error increasing additionally the depth of FB  $R_M$ . However, such an approach will result in the decrease of the operation speed [167]. For the construction of VVC it is expedient to use

PPDCA, based on the complementary field-effect transistors (Fig. 5.11c). Such PPDCA, although have high input resistance, can be used for the operation with the input signals in the form of voltage and sources of the capacitive signals, also they provide amplification, enabling to solve the problem of stage amplification.

## **6. Circuit engineering realization of signal converters of the thermal sensors and high-linear analog devices of biomedical designation**

Proceeding from the results of modeling analysis and optimization of the circuits of primary converters of microelectronic thermal flow sensors, considered in the previous sections, we will examine main approaches to circuit realization of the signal converters of the above-mentioned sensor devices. The actuality of the problem of circuit engineering of sensor flow devices, including thermal flow sensors of biomedical designation, is stipulated by several factors.

First, circuit solutions, applied in the conventional signal converters, in particular, for measuring circuits of thermoresistive type, do not meet the requirements regarding the minimization of the energy expenses of microelectronic thermal flow sensors. Secondly, due to the transition to low voltage supply sources, minimization of the parasitic impact on the result of the measurement of the resistances of signal transmission lines becomes very important. Third, in the process of the development of sensor devices of flow speed measurement, all the requirements, regarding their correspondence to modern trends of microelectronic sensors development, in particular, interface compatibility, possibility of program control of the measuring process, expanded functional possibilities, correspondence to the intelligent sensors IEEE1451.2 standard, correspondence to the requirements to the equipment of biomedical designation.

Besides, it is necessary to take into account the trends of the development of modern microelectronics element base, renovation of which occurs every several years. Only the correspondence to the level of the last generation of element base makes electronic devices compatible. That is why, the realization of the approaches, obtained in the given research on modern element base, in particular, high linear analog devices is very important.

### **6.1. Recommendations regarding the construction of temperature mode controllers**

The most important parameter of the thermoanemometric sensors is the temperature of the heater. As a rule, the warming up of the heater is performed by the fixed power, connecting it to the stable supply voltage. The power is selected so that the heating temperature was several tens of degrees. Such approach provides simple circuit engineering realization and calibration of the flow sensors. Flow temperature has a minor impact on the calibration



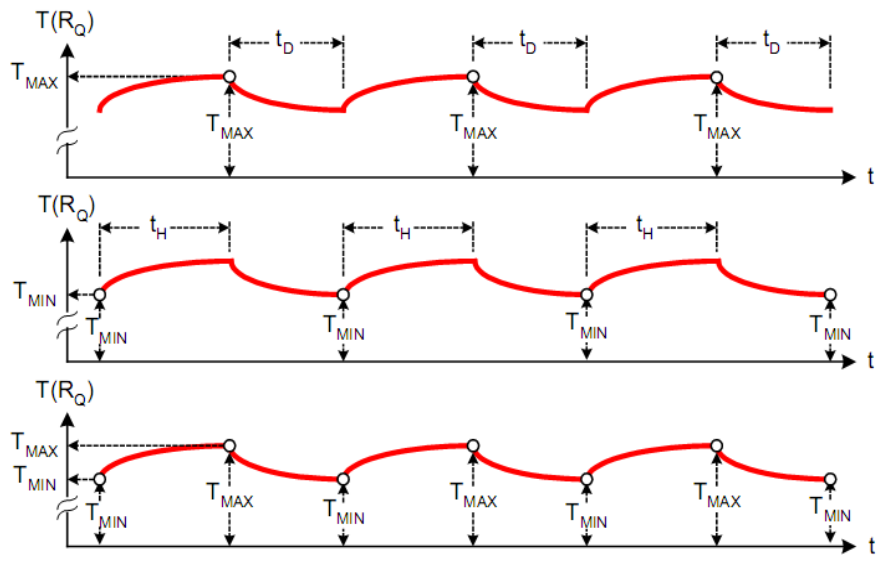
characteristic – at stable thermal resistance of the sensors structure with the change of the flow temperature the temperature of the heater will also change thus the temperature difference in the direction of the flow motion, in the first approximation will be only the function of the flow speed.

However when the flow speed increases above a certain value the loss of sensor sensitivity is observed, i.e., the decrease of temperatures  $TS_2$ – $TS_1$  difference, it is stipulated by the corresponding decrease of the heater temperature (HT) as a result of its intensive cooling by the flow. It is obvious that such a solution is not expedient from the point of view of efficient energy consumption. Besides, in the flow sensors of medical designation, in particular, for measuring of the speed or voluminous losses of biological fluids in the devices for biochemical analysis, it is inadmissible the expedience of the heater temperature above a certain critical value at which thermal degradation of the substance occurs.

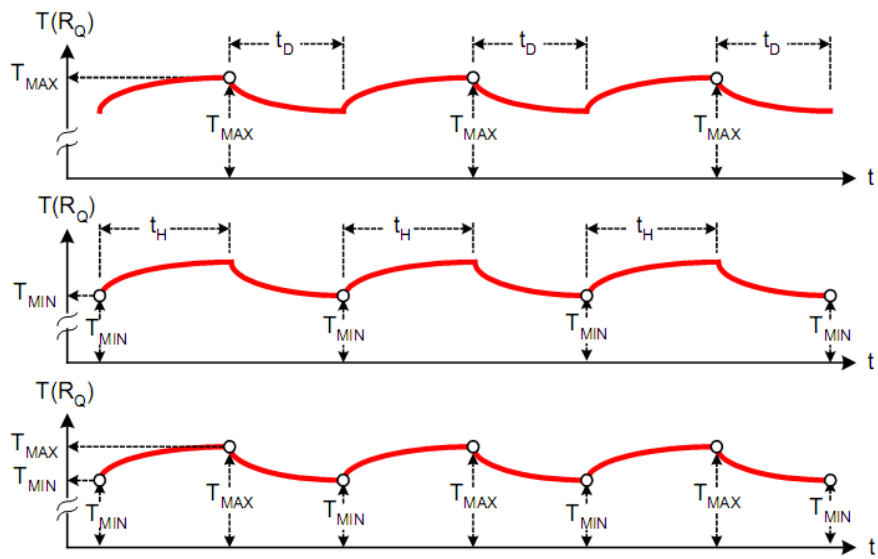
Proceeding from the above-mentioned, the problem of the development of the controllers of thermoanemometers flow sensors temperature mode is put forward, these devices enable to expand the range of flow speed measurement, minimize the energy consumption of the device and limit the heating of the flow substance. This task provides the solution of two problems. The first problem is the necessity to measure the temperature of the heater without using the additional temperature sensor. The information value of the heater temperature must be the dependence of its resistance on the temperature. The second problem is the necessity of using band-pulse key circuits of warming up power control, unlike the circuits of linear control; it provides high energy efficiency of the controller.

The principle of temperature stabilization of the heater of thermoanemometric flow sensor, when thermoresistive structure of the heater is used both as the source of heat and a sensor of its temperature, provide the formation of the pulse mode of the periodic switching between heating and cooling of the structure [101]. The necessary condition of such mode realization is the available temperature difference of the resistance (TCR) of the heater. As a rule, the realization of such condition is not problematic – greater part of the heaters materials are of thermoresistive type, for instance, cooper, silicon or polysilicon, the values of TCR is within the range of (0,1–0,5) %/°C. Thus, the task is reduced to periodic measurement of the resistance of the thermoresistive heater and fixation of this resistance at certain level by means of switching from heating to cooling.

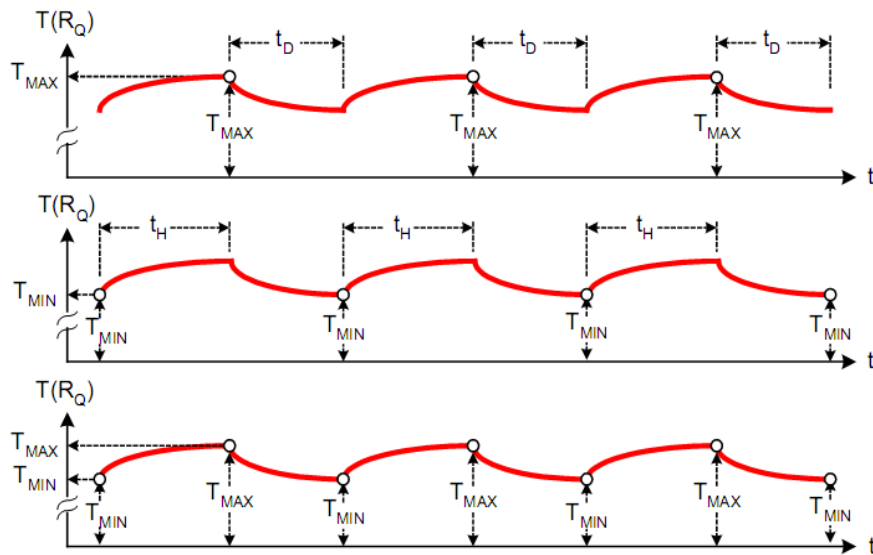
The periodic switching mode can be realized by the following criterion: fixation of cooling phase duration (Fig 6.1a), fixation of heating phase duration (Fig 6.1b), and the preset temperature hysteresis between the periods of heating and cooling (Fig 6.1c).



a)



b)



c)

Fig 6.1. Time diagram of thermostability: a) with fixed duration of cooling phases; b) heating; c) preset hysteresis of heating-cooling

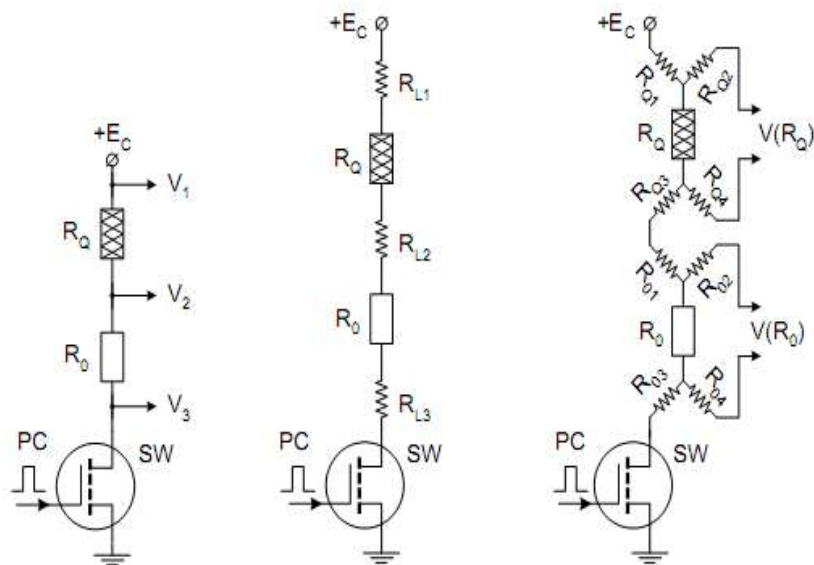
In the first of them, measurement of the heater temperature is performed in the process of its heating, which lasts till the moment of reaching the preset temperature value ( $T_{MAX}$ ). After that the phase of cooling starts. In order to minimize the switching losses the cooling stage has a certain fixed duration ( $t_D$ ), in the process of which thermal relaxation occurs. For typical thermal anemometers the value of thermal relaxation can be approximately 1% of the difference of temperature between the heater and the flow. Taking into account the heat capacity of the structure of sensors, the duration of cooling can be 1-100ms. The second criterion – fixed duration of heating ( $t_H$ ) provides measurement of heater temperature in the process of its cooling to the value  $T_{MIN}$  after that the heating phase of the fixed duration. The third criterion provides the preset hysteresis of the temperature  $T_{MAX} - T_{MIN}$  and provides measurement of the latter in both phase, duration of these phases is not fixed.

The example of the realization of the controller of the heater temperature mode by the criterion of the fixation of the cooling phase duration, i.e., while temperature measurement in the process of heating, is presented below. As we established in the process of structural-algorithmic analysis, such mode is characterized by the optimal ratio between the accuracy of stabilization and structural expenditures for its realization.

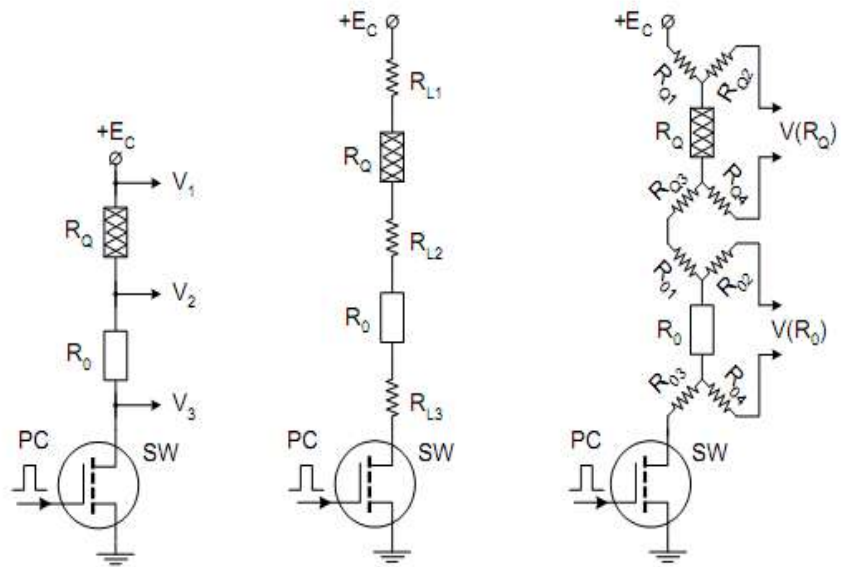
It is important to note that unlike the conventional thermoresistive circuits of temperature measurement, the application of the measuring circuits of bridge type in the given task is impossible. This is stipulated by the impact of parasitic resistance of the signal line of the thermoresistive heater.

We will analyze the given problem, for this purpose we will consider the half bridge circuit of the converter with the controlled heating power (Fig 6.2a). The circuit contains powerful switching transistor (SW), thermoresistive heater  $R_Q$ , its temperature is determined by means of measuring the voltage difference  $V_1-V_2$  and reference resistor  $R_0$ , voltage drop  $V_2-V_3$  at which is used for the measurement of current across the heater and in a number of circuits can serve as a reference value for the analog-to-digital converter. Control of the heater temperature is carried out by means of a corresponding ratio between the duration of the heating pulses and pauses between these pulses. These pulses are supplied across the interface bus from the PC or microcontroller.

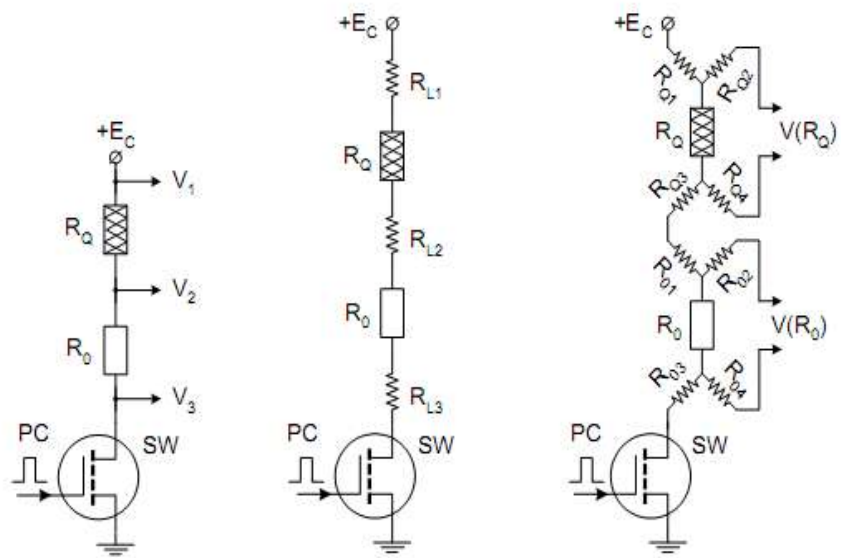
However, such simplification of the problem of voltages measurement in the circuit of the switch stage does not provide the necessary accuracy of the thermostabilization. The reason is the presence of the parasitic resistances  $R_{L1}$ ,  $R_{L2}$ ,  $R_{L3}$  of the circuit (Fig 6.2b). It is typical for the low voltage supply circuits, that are a typical requirement to modern information-measuring equipment.



a)



b)



c)

Fig. 6.2. Switching stage: a) of the temperature mode controller; b) its parasitic resistances; c) circuit of the minimization of the impact of these resistances

If  $E_C = 5V$  and heating power 1W the resistance of the thermoresistive heater is  $R_Q = 25 \text{ Ohm}$ . To minimize the losses of the thermal power at the reference resistor it is expedient to take  $R_0 = 1 \text{ Ohm}$ . Taking into account that the parasitic resistances of the circuit are also within the limits of Ohm units, measurement of the temperature by means of the direct measurement of the resistance of the thermoresistive heater or bridge circuit is impossible – parasitic resistance of the circuit introduce inadmissibly large error. To solve this problem as a rule the four-point connecting circuit is used (Fig 6.2c).

When high-ohmic input circuits [43,56] of voltage amplifiers  $V(R_Q)$ ,  $V(R_0)$  are used, the voltage drop tends to zero. However, measuring circuits of these voltages lose the common point, this makes circuit engineering of such a signal converter rather complicated and requires high precision two-channel, in particular 24 bits analog-to-digital converters with the differential input. The problem is that such analog-to-digital converters are characterized, firstly, by considerable energy consumption, and, secondly, by rather high manufacturing cost. This limits, to a great extent, the usage of such types of converters in the portable measuring devices.

Taking into account the above-mentioned, the task was put forward to develop the controller of the temperature mode of the thermoanemometric flow sensors that would combine high operation accuracy, small energy consumption and low manufacturing cost. The analysis, carried out, showed that the circuits, based on the analog integrators, would be the optimal solution of the problem. Circuits of such integrators are usually applied in the analog-to-digital converters of the double integration and sensor devices of the capacity type [95, 96]. These signal converters are most precise and at least by order exceed the parameters of the circuits with the direct digital conversion. As we will show below, push pull circuits of the analog integration are able to carry out the function of signal transform from one potential level on the other, which is very important when using four-point measuring circuits.

Basic elements of the integrators (Fig 6.3) are the operation amplifier (OA) and RC feedback circuit.

Input voltage  $V_{IN}$  is converted into the current  $I_{IN} = (V_{IN} - V_{REF}) / R$ , where  $V_{REF}$  – is a reference voltage and the current  $I_{IN}$ , accumulating the charge of the capacitor  $C$ , forms the voltage on it  $V_C$ , which in the first approximation is directly proportional to the current  $I_{IN}$  and the time of the integration  $t$  and is inverse proportional to the electric capacity of the capacitor  $C$ . Output voltage of the integrator is  $V_{OUT} = V_C + V_{REF}$ .

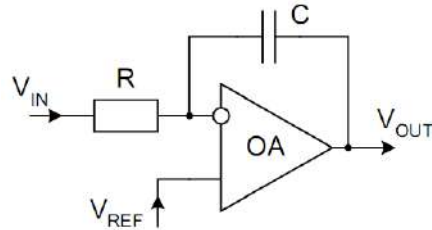


Fig. 6.3. Functional (simplified) diagram of the integrator

However, as it was mentioned above, measuring voltages  $V(R_O)$ ,  $V(R_0)$  (see Fig 6.2c) do not have a common reference point and this requires more detailed study of the processors of signal conversion. We will consider main approaches to circuit modeling of the integrator's signals. Actually, the analog integrator is not completely analog circuit; it requires switching circuits, in particular, for the determination of time intervals of the integration or setting to zero the capacitor. That is why; it refers to the approaches to mixed modeling, where both analog and digital (discrete) components are used.

To realize the mixed modeling the monitoring keys are used, as it is shown in Fig 6.4.

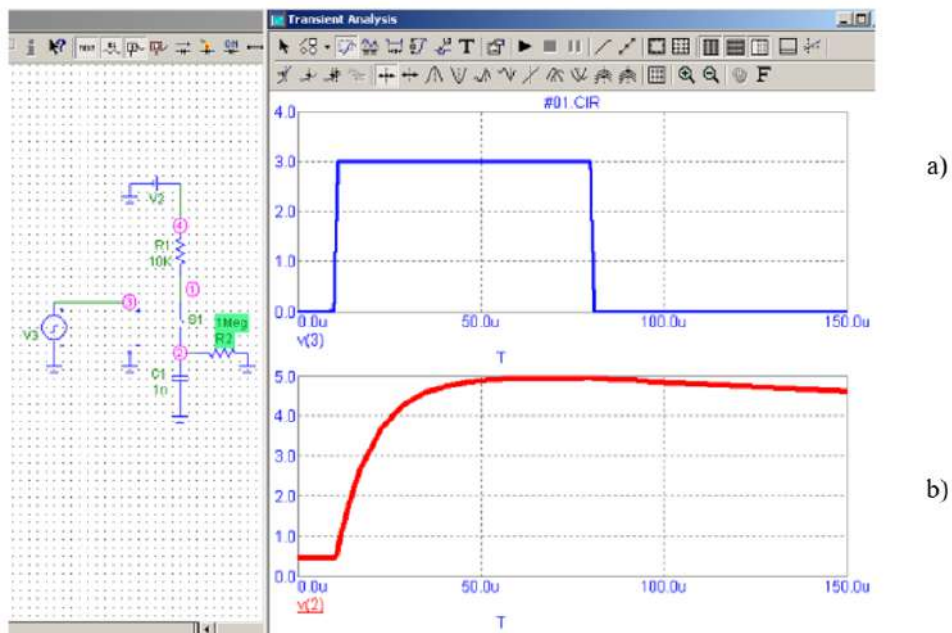


Fig. 6.4. Example of the mixed circuit modeling: a) control pulse; b) voltage at R2C1 element

Such a circuit contains the RC [43,56] section, presented by  $C1$  and  $R2$  elements, which is charged by the current across the switching key  $S1$ , the value of the current is determined by the resistor  $R1$ . Control pulse is formed by the source  $V3$ . As it can be seen from the time diagram the time constant of the circuit is determined by two parameters – resistor  $R1$  resistance in the process of charging and resistor  $R2$  resistance in the process of discharging the capacitor  $C1$ .

For modeling study of the integrator circuit it is necessary to use two sources of the pulsing voltage, the example of these sources specification is shown in Fig 6.5. The first source ( $V3$ , model PULSE1) forms time intervals of the integrated voltage pulse, and the second source ( $V6$ , model PULSE2) – period of the integrator reset (capacitor discharge).

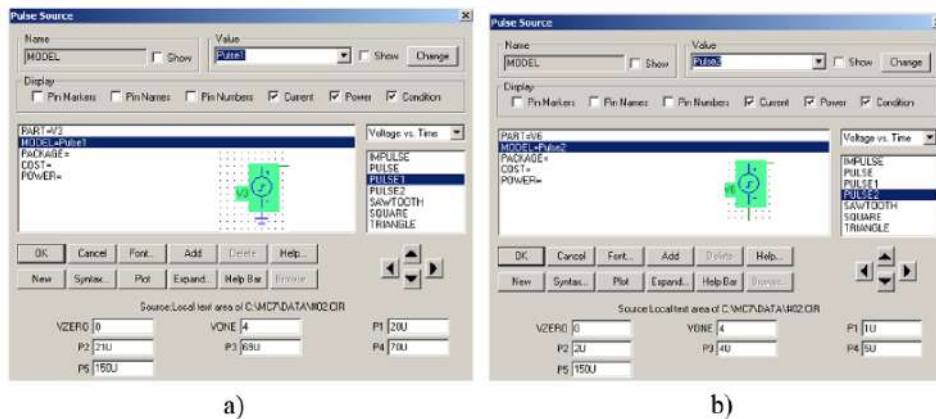


Fig. 6.5. Specification of the control sources of the pulsing voltage: a) model PULSE1; b) PULSE2

The example of the model circuit of the integrator and the result of its study is shown in Fig 6.6.

The pulses of the input voltage, the amplitude of which is determined by the source of voltage  $V2$ , are formed by the monitoring key  $S1$ . The transformation of the input voltage in the current occurs at the resistor  $R1$ , one of the outputs in the time interval of integration is connected across the monitoring key to the source of the input voltage, and the second output – to the inverse input of the operational amplifier  $X1$ . The latter is supplied by two voltage sources  $V4$  ( $-3$  V) and  $V6$  ( $+3$  V). The reset of the integrator is performed by the key  $S2$ , controlled by the pulse voltage source  $V6$ .



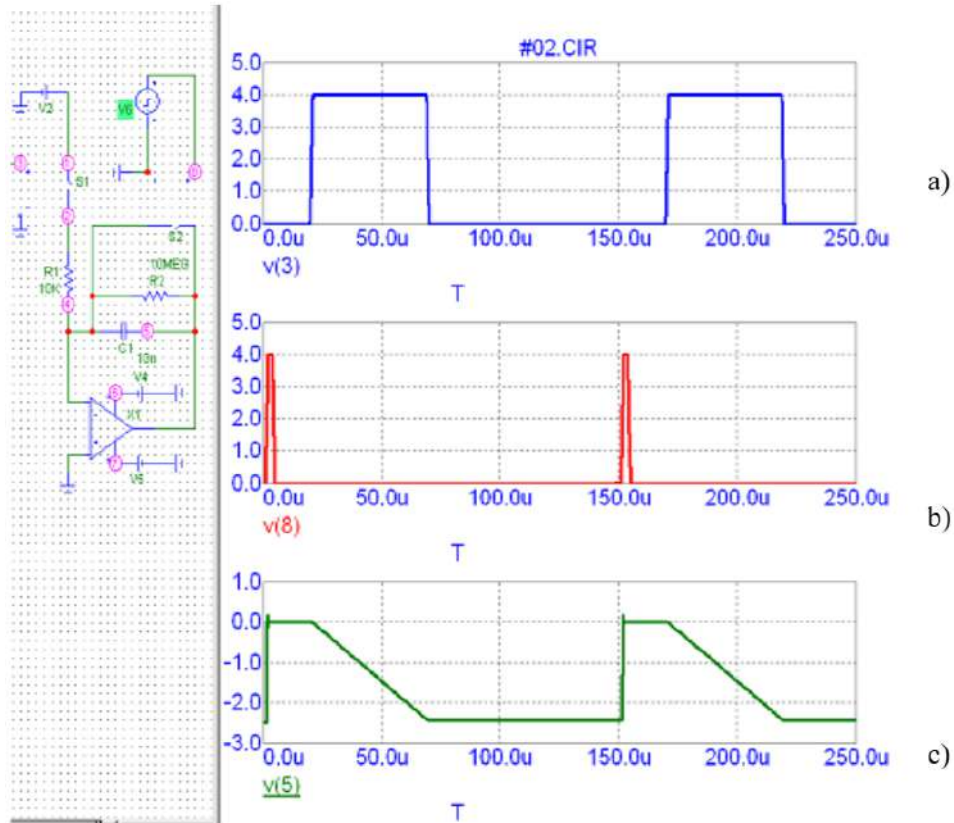


Fig. 6.6. Result of the modeling study of the integrator: a) input voltage pulses; b) reset pulses; c) output voltage pulses

The capacitor of the integrator C1 is shunted by the resistor R2 (10 mΩ), which simulates the parasitic leakage current of the capacitor and key S2. The presence of this parasitic current limits the accuracy and time characteristic, namely – time of signal storage after the integration period. As it is seen from the result of the research, three time intervals of the integrator output voltage formation are observed. In the first interval (up to 20 μsec) the output voltage is zero. Resetting is performed by the short (approximately 1 μsec) pulses. It is important to maintain zero level of the output voltage from the termination of the resetting pulse to the start of the integration of the input voltage.

In the next time interval (from 20 μsec to 70 μsec), where the source of the input voltage is connected to the integrator, the linear increase or decrease of the output voltage occurs. In case of the additive polarity of the input voltage the output voltage decreases (as it is shown in the above-mentioned example) and in case of negative polarity of the input voltage – the output voltage increases.

In the third interval (from 70  $\mu\text{sec}$  to 150  $\mu\text{sec}$ ), where the input voltage is disconnected from the integrator, the latter maintains the output voltage at the constant level (approximately – 2,5V for this example). In this interval the output voltage of the integrator is converted into a digital code, is compared with a certain reference value of the voltage or is stored till the beginning of the next cycle of the push-pull integration. After the third interval (150  $\mu\text{sec}$ ) the reset pulse is sent and the cycle of the integration operation is repeated.

Further in the work the application of the considered integrator in the circuit of push-pull integration will be shown – in the first stage the measurement of the current across thermoresistive heater was carried out, and in the second, counter phase stage – the measurement of the voltage on the heater was carried out. The result of such integration is the voltage that acts as the informative value of the temperature of the heater of thermoanemometric flow sensor and is used for temperature stabilization of its operation.

For quantitative study of the integrator parameters it is necessary to introduce the additional variable value. Besides the time, which is an argument, variable value with the discrete iteration will be the resistance of the resistor R2, which, as it was noted above, presents the leakage current and determines the accuracy of the integration. The example of the study of the leakage current impact on the stability of the output voltage is shown in Fig 6.7. It can be seen that the increase of the leakage current (decrease of the resistance of the resistor R2) leads to an undesirable drop of the output voltage of the integrator in the second time interval.

From the point of view of using the integrator as the base of the controller of the temperature mode of the thermoresistive heater of the flow sensors, such time instability of the output voltage will be the cause of the error of the voltage drop measurement and, finally, this will lead to the instability of its temperature. For example, we will assume that the admissible value of the heater temperature instability must not exceed 0,3 $^{\circ}\text{C}$  and the temperature coefficient of the thermoresistive element is 0,3%/ $^{\circ}\text{C}$ . Then the error of the voltage drop measurement must not exceed 0,1% of its absolute value. Such value of the instability of the integrator output voltage will be taken as an initial point for the optimization of the circuit operation modes and selection of its element base. Thus, in the process of the integrator circuit development, it is important to take into account the presence of leakage currents and, selecting the corresponding element base, minimization of these parasitic currents. As it will be shown further, the optimal choice of the element base is CMOS Rail-to-Rail operation amplifiers, in particular, AD8541/2/3/4 and CMOS monitoring keys, in particular, ADG774 (Analog Devices).

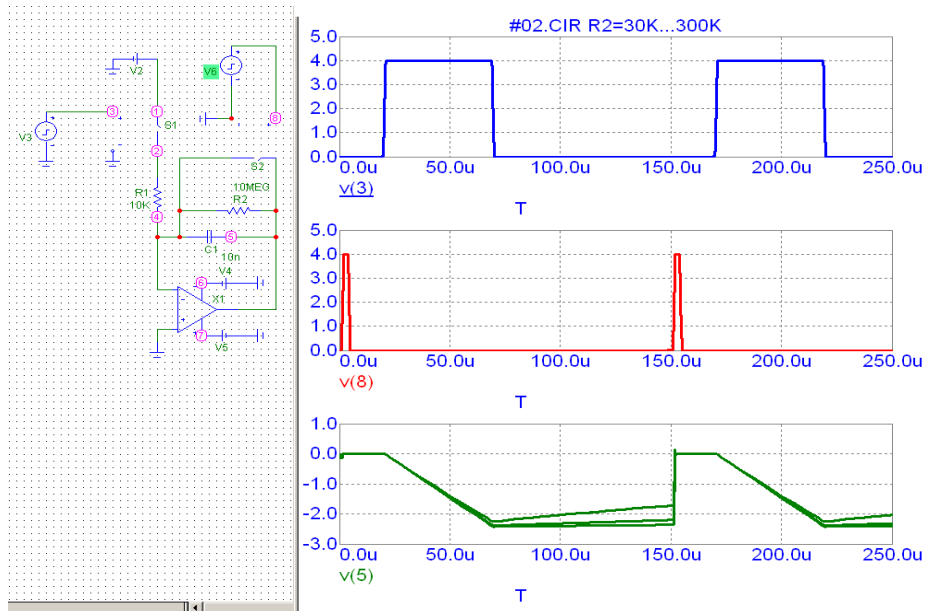


Fig. 6.7. Result of the modeling study of the integrator at R2 iteration R2 [30 KOhm, 100 KOhm, 300 KOhm] (pulses similar to Fig 6.6.)

For the realization of the task of the development of the controller of the temperature mode of the heater of thermoanemometric flow sensor the possibility of using the mode of the reference voltage potential transfer in the process of push pull integration is shown. As it will be shown further, such mode of the potential transfer is necessary from the point of view of the compensation of the voltage drop on the parasitic resistances of signal transmission line.

The diagram of the integrator with the potential transfer and the results of their model study are shown in Fig 6.8. Unlike the basic diagram of the integrator, this diagram contains one more monitoring switch S3, which in certain time intervals connects to the noninverting input of the operational amplifier the reference voltage (in the diagram – it is the voltage of the source V8). Besides the above-considered three time intervals of the basic diagram of the integrator – resetting, integration of the input voltage and storing of the result of the integration (output voltage) – this diagram is characterized by the fourth time interval – the transfer of the integration result at certain potential (100  $\mu$ sec and further).

As it can be seen, the first cycle of the input voltage integration occurs at zero voltage at the noninverting input of the operational amplifier (switch S3 is open,

zero potential is supplied across the resistor R3). By the circuit of the negative feedback of the operation amplifier this zero potential of the non inverting input is sent to the inverting input, forming the mode of “the virtual earth”.

After the termination of the first cycle of the integration, where the output voltage reaches the value of approximately  $-2,5V$  and certain time interval, where the conservation of this voltage occurs at the output of the integrator, the reference voltage, set by the source V7 (in the given example this voltage is 2V) is sent to noninverting input of the operational amplifier. This process is controlled by the pulse source V8 by closing the switch S3.

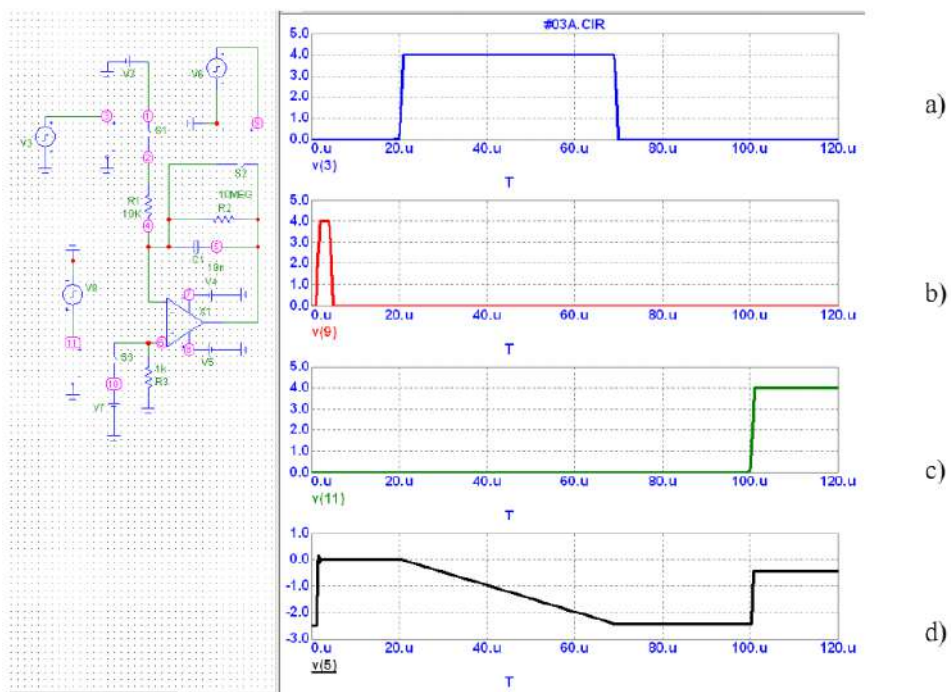


Fig. 6.8. Diagram of the inverter with the transfer of the potential and results of its modeling study: a) pulse of the input voltage control; b) resetting pulse; c) pulse of the transfer of the reference level of the voltage ; d) output signal

The circuit of the negative feedback of the operation amplifier monitors the change of the reference voltage, namely – instant transfer of the potentials at the inverting input and the output of the operation amplifier on the value, numerically equal to the voltage change on the noninverting input of the operation amplifier occurs.

For studying the accuracy of the integrator operation with the potential transfer, we suggest the technique, according to which after the intervals of transfer and storage, the voltage at noninverting input of the operational amplifier returns to the previous state (in the given case – to zero value), this enables to compare numerically the values of the output voltage prior and after the transfer time interval.

The example of the application of such a technique is shown in Fig 6.9. After the termination of the transfer time interval ( from 100  $\mu$ sec to 130  $\mu$ sec) the output voltage returns to the previous level (approximately – 2,5V). More vividly such a comparison is shown in Fig 6.10a, where it can be seen that the value of the output voltage after the termination of the transfer interval differs from its initial value – prior to the transform the output voltage was 2.43V and after – 2.41V. This stipulates the absolute value of the measurement error of 20 mV, that corresponds to 1% of the output voltage value.

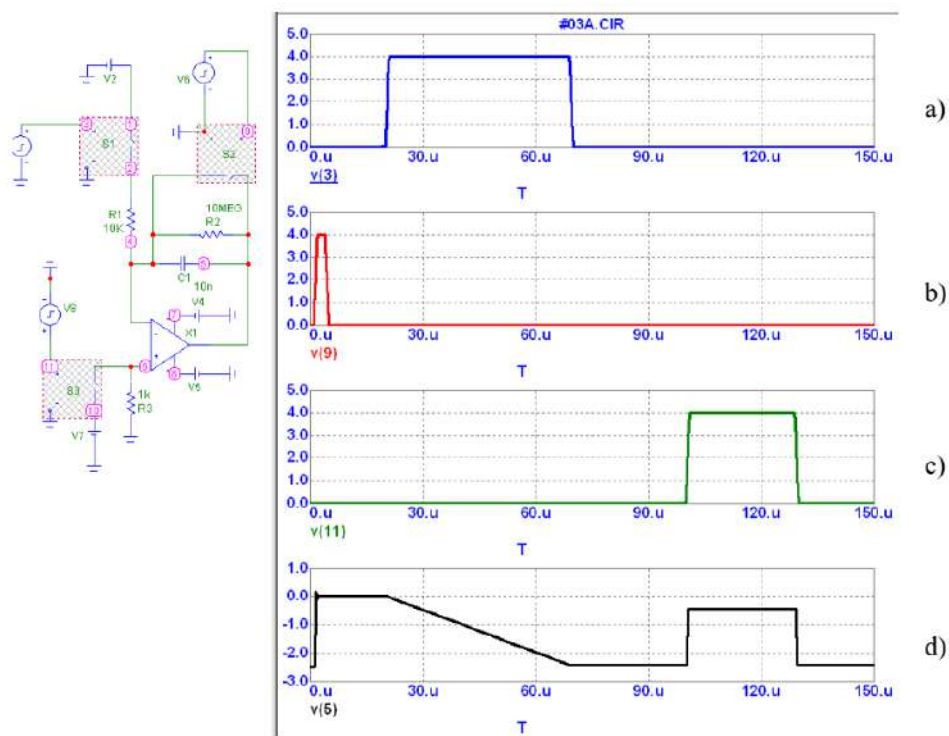


Fig. 6.9. Demonstration of the technique of the study of the integrator operation accuracy of the integrator with the potential transfer(pulses are similar to Fig 6.8)

Studies of the circuit stability are carried out by means of the discrete iteration of the leakage current of the feedback circuit of the integrator

(Fig 6.10b). As it was shown above, such leakage current is presented by the parasitic resistance (in the diagram –R2). It can be seen that if R2= 500 kΩ the difference of the output voltage prior and after the time transfer interval is approximately 4 mV, if R2 = 1 MΩ – approximately 8 mV, and if R3 = 2 MΩ – approximately 10 mV.

As it is seen, the non-stability of the output voltage of the integrator for the parameters of the element base of the circuit, integrated in the model (in particular, the input currents of the operation amplifier and the resistance of the resistor, shutting the capacitor of the integrator) do not meet the above-mentioned requirements, concerning the accuracy (typically, the error must not exceed 0,1% ). We give this example of the model study only to draw the attention to the problem of the element base selection and the results of the correct selection and real parameters of the pilot specimen of the temperature mode controller, created on the base of the integrator with the transfer of the potential will be given further in the given research.

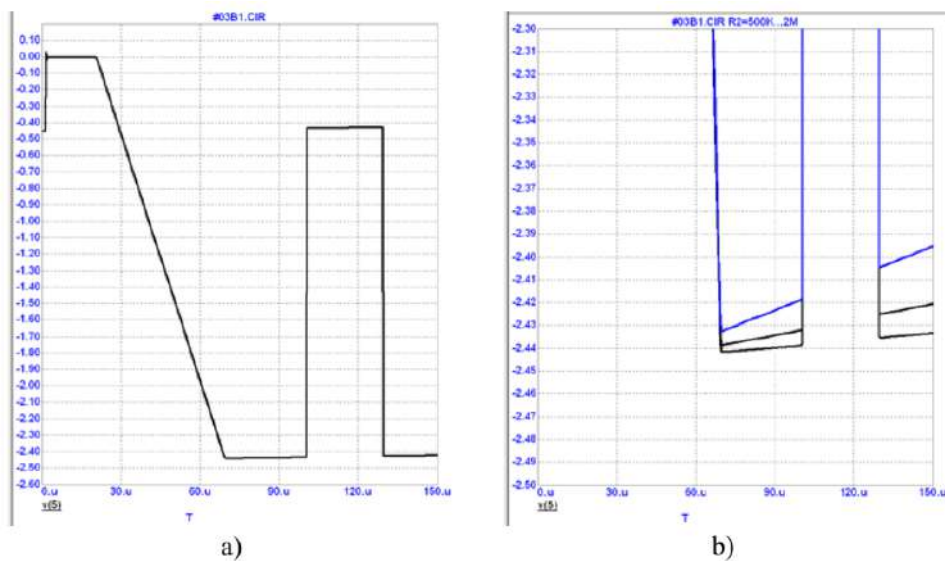


Fig. 6.10. Analysis of the instability of the integrator output voltage : a) simplified analysis; b) analysis with the iteration of R2 resistance [500 kOhm, 1 Mohm, 2 Mohm]

Proceeding from the above-considered circuit solutions and operation modes of the integrator with the potential transfer, we developed the controller of the temperature mode of the thermoresistive heater of the flow sensor. The controller contains a two-channel push-pull integrator (operation amplifier (OA) with the integration circuits  $R_1C$ ,  $R_2C$ ), comparator (CM) and paired signal switches  $SW_{1A}$ ,  $SW_{1B}$ ,  $SW_{2A}$ ,  $SW_{2B}$  (Fig 6.11). The first channel of the controller

is connected to the reference resistor  $R_0$ , the voltage drop at this resistor is the informative value of the current flowing in the circuit of the heater. The second channel is connected to the thermoresistive heater  $R_Q$ , the voltage drop at this heater is the informative value of its temperature.

Measurement and stabilization of the thermoresistive heater temperature takes place in two stages, controlled by the pulses of  $PC_1$ ,  $PC_2$ ,  $PC_3$  from the microcontroller (it is not shown in the Fig). As it was determined in the process of the problem setting, it is important to note that to realize the proposed circuit of the temperature mode controller high precision analog-digital converters are not needed.

Instead, any inexpensive microcontroller could be used, making the suggested circuit economically efficient.

For the minimization of the impact of the parasitic resistances of the signal lines, four-point connecting circuits of the reference resistor and thermoresistive heater are used. Current circuit of the scheme are  $R_{Q1}$ ,  $R_Q$ ,  $R_{Q3}$ ,  $R_{01}$ ,  $R_0$ ,  $R_{03}$ , and the voltage drops are measured in the circuit  $R_{Q2}$ ,  $R_Q$ ,  $R_{Q4}$  (for the heater) and in the circuit  $R_{02}$ ,  $R_0$ ,  $R_{04}$  (for the reference resistor).

Taking into account the fact, that the values of the currents across the parasitic resistances  $R_{Q2}$ ,  $R_{Q4}$ ,  $R_{02}$ ,  $R_{04}$  of the signal circuits of the voltage measurement is not great (determined by the input currents of the integrator, which, as a rule, do not exceed 0.1 mA), voltage drops at these parasitic resistances can be neglected.

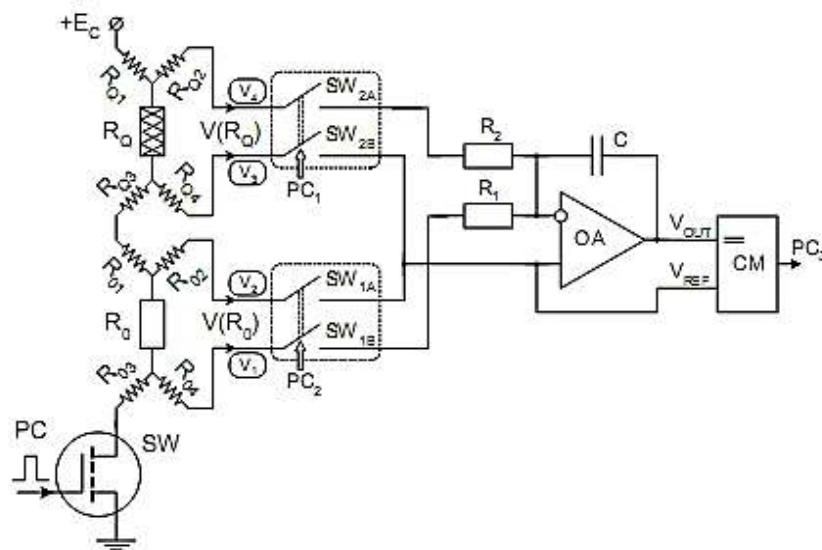


Fig. 6.11. Circuit of the temperature mode controller

The picture of voltage drops at the parasitic resistances of the current circuit  $R_{Q1}$ ,  $R_{Q3}$ ,  $R_{01}$ ,  $R_{03}$  is basically opposite. As a rule, current across them is 100 mA and more, which stipulates considerable voltage drop at the parasitic resistances of the current circuit and, as a result, it is impossible to use the line of the current circuit for the measurement of the information signal of the heater temperature.

As it will be shown further, the voltage drop at the parasitic resistances of the current circuit leads to the effect of the integrator reference voltage offset. The value of voltage  $V_2$  (output circuit  $R_{02}$ ) differs from the voltage  $V_3$  (output circuit  $R_{04}$ ) at the value of voltage drop in the line of the current circuit, presented by the resistances  $R_{01}$  and  $R_{03}$ .

We will consider the principle of the controller operation. Principal time diagrams of the temperature mode controller are shown in Fig 6.12. At the first stage switches  $SW_{1A}$ ,  $SW_{1B}$  ( $PC_1 = 1$ ,  $PC_2 = 0$ ) are closed, during the determined time  $t_1$ , for instance, during the time of microcontroller counter overflow, the capacitor  $C$  is charged.

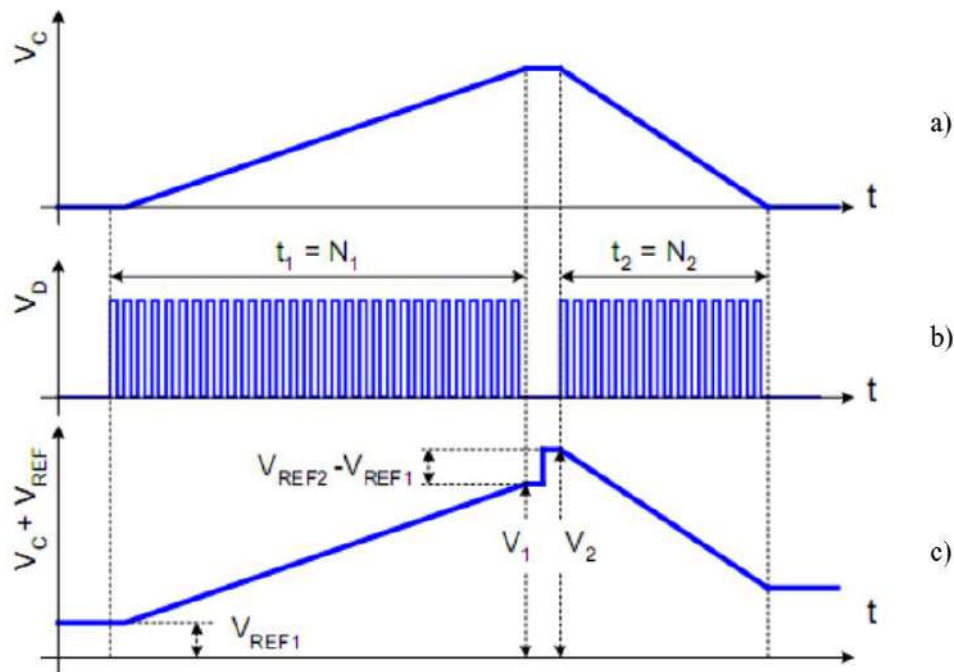


Fig. 6.12. Time diagrams, which explain the operation of the controller: a) voltage at the capacitor; b) pulses, to be counted; c) output voltage

In the process of charging the voltage difference is formed :



$$V_{OUT} - V_{REF} = \int_0^{t_1} \frac{V(R_0)}{R_1 C} dt = \frac{V(R_0) \Delta t N_1}{R_1 C},$$

where  $V_{OUT}$ ,  $V_{REF}$  – output and reference voltages of the integrator, correspondingly;  $V(R_0)$  – voltage drop at the reference resistor  $R_0$ ;  $\Delta t$ ,  $N_1$  – duration of one period of the microcontroller counter and a number of periods, determining the duration of the first stage. When the first stage is completed, the switches  $SW_{1A}$ ,  $SW_{1B}$  are open, and the counter is reset to zero.

At the second stage switches  $SW_{2A}$ ,  $SW_{2B}$  ( $PC_1 = 0$ ,  $PC_2 = 1$ ) are closed, while the capacitor  $C$  discharges during time  $t_2$ , the number of pulses of the counter  $N_2$  are calculated until reaching the condition of zero voltage at the capacitor.

$$V_{OUT} - V_{REF} = \int_0^{t_1} \frac{V(R_0)}{R_1 C} dt - \int_0^{t_2} \frac{V(R_Q)}{R_2 C} dt = \left( \frac{V(R_0) \Delta t N_1}{R_1 C} - \frac{V(R_Q) \Delta t N_2}{R_2 C} \right) \frac{\Delta t}{C} = 0.$$

This condition is controlled by means of the formation by CM comparator the corresponding logic pulse  $PC_3$ , which stops the count of the meter pulses. Number of pulses  $N_2$  is the information value of the heater  $R_Q$  temperature. The considered cycle of the push pull measurement continues until it reaches the preset temperature by the heater  $R_Q$ , immediately after that the microcontroller puts the circuit in the cooling phase.

For the study and optimization of the parameters of the thermal mode controller the model circuit, shown in Fig 6.13, was synthesized.

Designation of the greater part of elements of this model is clear from the previously shown diagrams. In particular, the source of the pulse voltage  $VP$  is intended for the control of the power switch  $SP$ , which closes and opens the heating current and the source  $VZ$  – is intended for setting the integrator to zero. The process of integration is controlled by the sources of the pulse voltage  $V1$ ,  $V2$ ,  $V3$  and  $V4$ .

Time diagrams of these sources are shown in Fig 6.14.

With the start of the heating current control pulse (see Fig 6.14a) a short pulse of the integrator setting to zero is sent (see Fig 6.14b). Further, the first stage of the integration takes place, forming the control pulses  $V2$  (see Fig 6.14c) and  $V4$  (see Fig 6.14d), which close the switches  $S2$ ,  $S4$ , at the input of the integrator the voltage drop at the reference resistor  $R_0$  is sent. As it is seen from Fig 6.15a, the voltage at non-inverting input of the operational amplifier is approximately  $V5 \approx 0,6$  V. This value is determined by the voltage drop at switch  $SP$  and stray resistance of the circuit  $RL03$  (from now on for the sake of illustration the parameters of the switch and stray resistances are selected in such a way that voltage drop on them was great and influenced the potential of the non-inverting input).

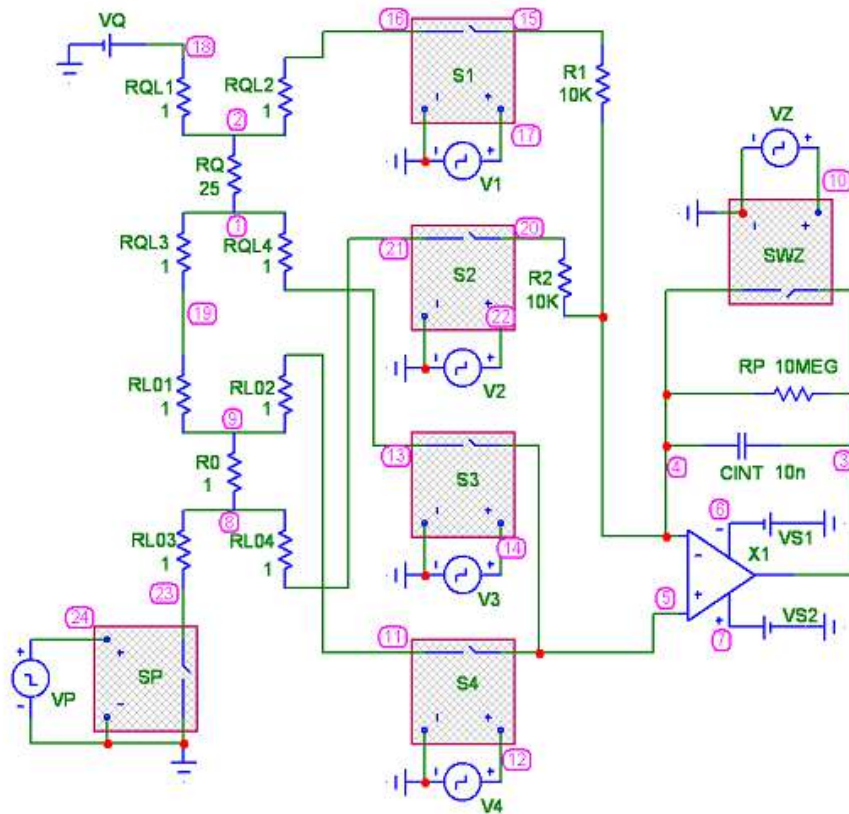


Fig. 6.13. Model circuit of the temperature mode controller

At the second stage of integration, forming the control pulses  $V1$  (see Fig 6.14c) and  $V3$  (see Fig 6.14d) which close the switches  $S1$ ,  $S3$  the voltage drop on the thermoresistor  $RQ$  is sent at the input of the integrator. At the transition from the first stage of the integration to the second stage the voltage at the non-inverting input of the operation amplifier unevenly grows at the value of the voltage drop on the stray resistance of  $RQL3$  circuit, that leads to the corresponding change at the integrator output (Fig 6.15b).

However, the voltage difference at the capacitor  $V(3)-V(5)$  (see Fig 6.15c) remains unchanged. This very difference of the voltages is of great importance as the reference voltage  $V_{REF}$  of the comparator CM always corresponds to the reference potential of the integrator capacitor (corresponds to the potential of the capacitor output, connected to the inverting input of the operational amplifier). As a result of such signal conversion the stability of the useful signal of the integrator is provided at the change of the reference voltage at non-inverting input of the operational amplifier. Thus, the research, carried out, shows the

efficiency of the push-pull integrator operation with the potential transfer in the circuit of temperature stabilization of the heater of thermoanemometric flow sensor if the considerable stray resistances of the signal circuit are available.

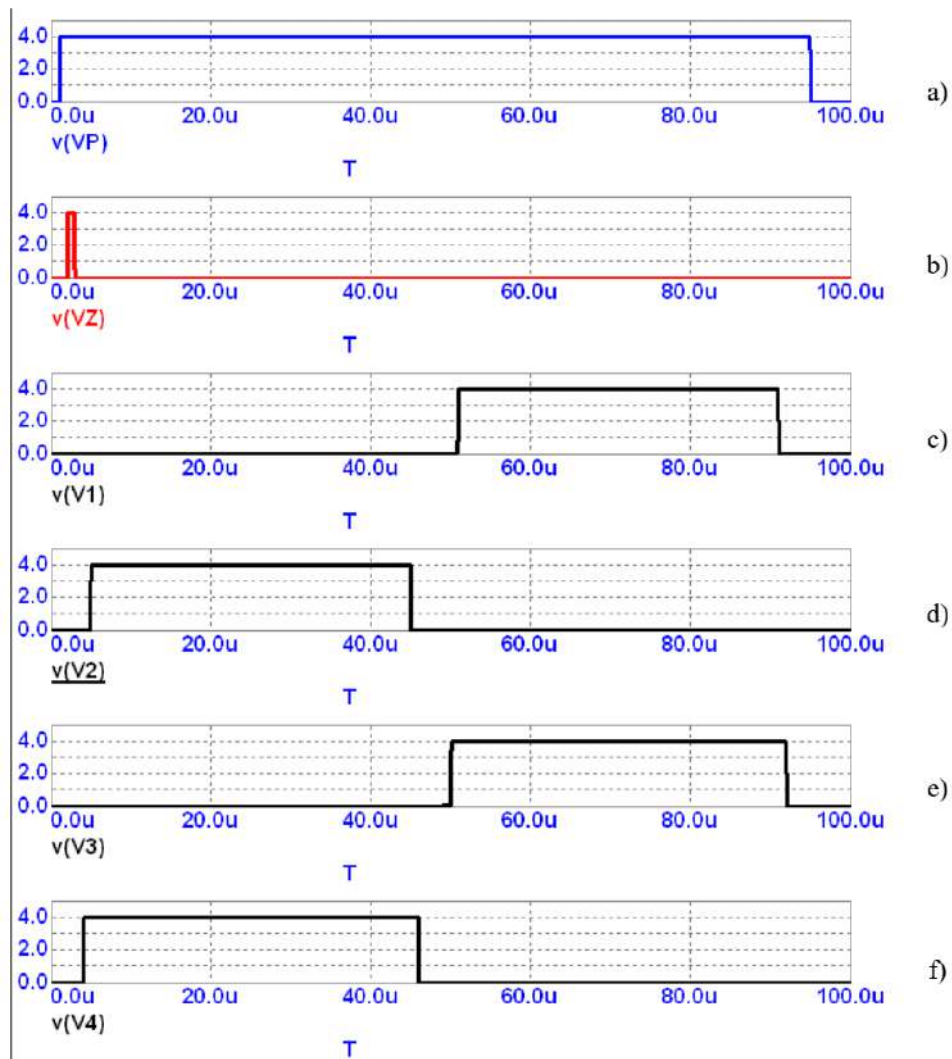


Fig. 6.14. Control pulses: a) VP; b) VZ; (b), c) V1; d) V2; e) V3; f) V4

In order to demonstrate the possibility of the integration function slope change that occurs in the process of the controller adjustment, for instance, for the determination of the preset values of the stabilization temperature, time diagrams of the controller voltages at the discrete iteration of the resistor R2

resistance are shown in Fig 6.14. This resistor determines the function of the first stage of integration. If it is necessary to control the function of the second stage of integration, the resistance of the resistor R1 is changed.

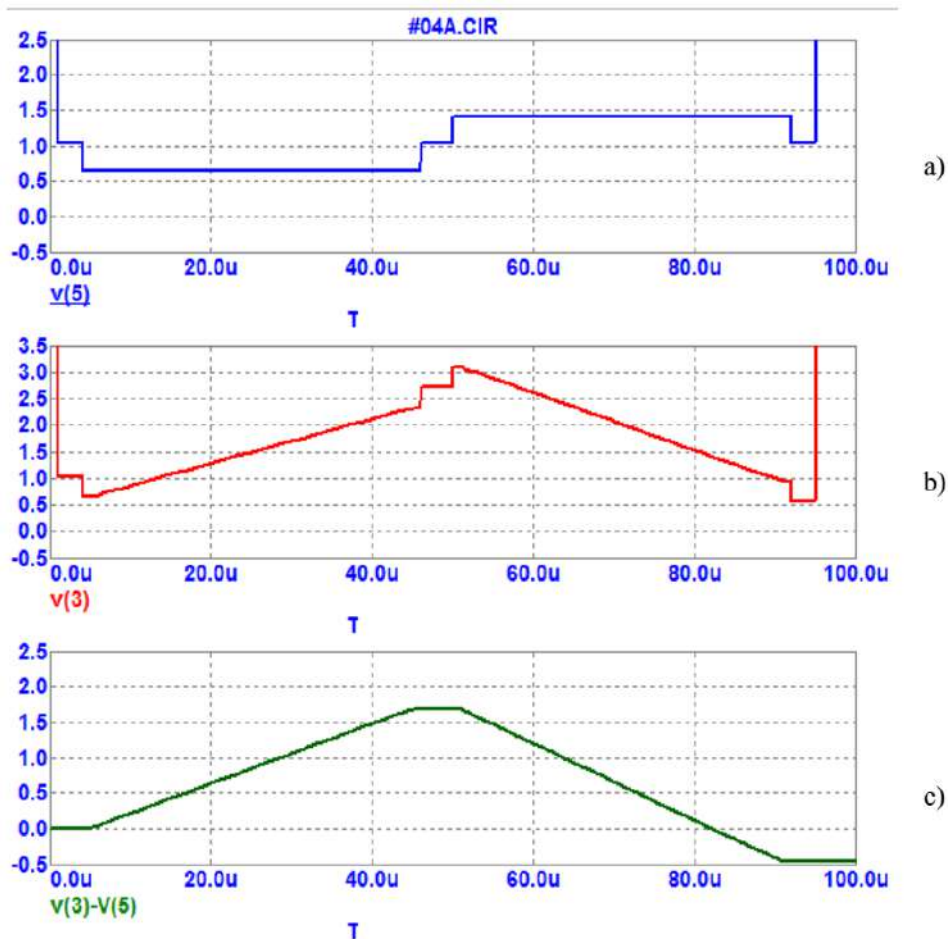


Fig. 6.15. Time voltage diagrams: a)  $V(5)$ ; b)  $V(3)$ ; b)  $V(3)-V(5)$

Timing diagrams, shown in Fig 6.17 demonstrate the impact of the circuit on the signals, this is stipulated by the change of the heater RQ resistance, in particular, if its temperature changes. Characteristic feature is the impact of this resistance on the reference potential  $V(5)$  of the non-inverting input (Fig 6.17a). Such impact is stipulated by the change of the circuit current and, as a result – change of the voltage drop at the resistor R0 and stray resistances of the signal lines of this circuit.

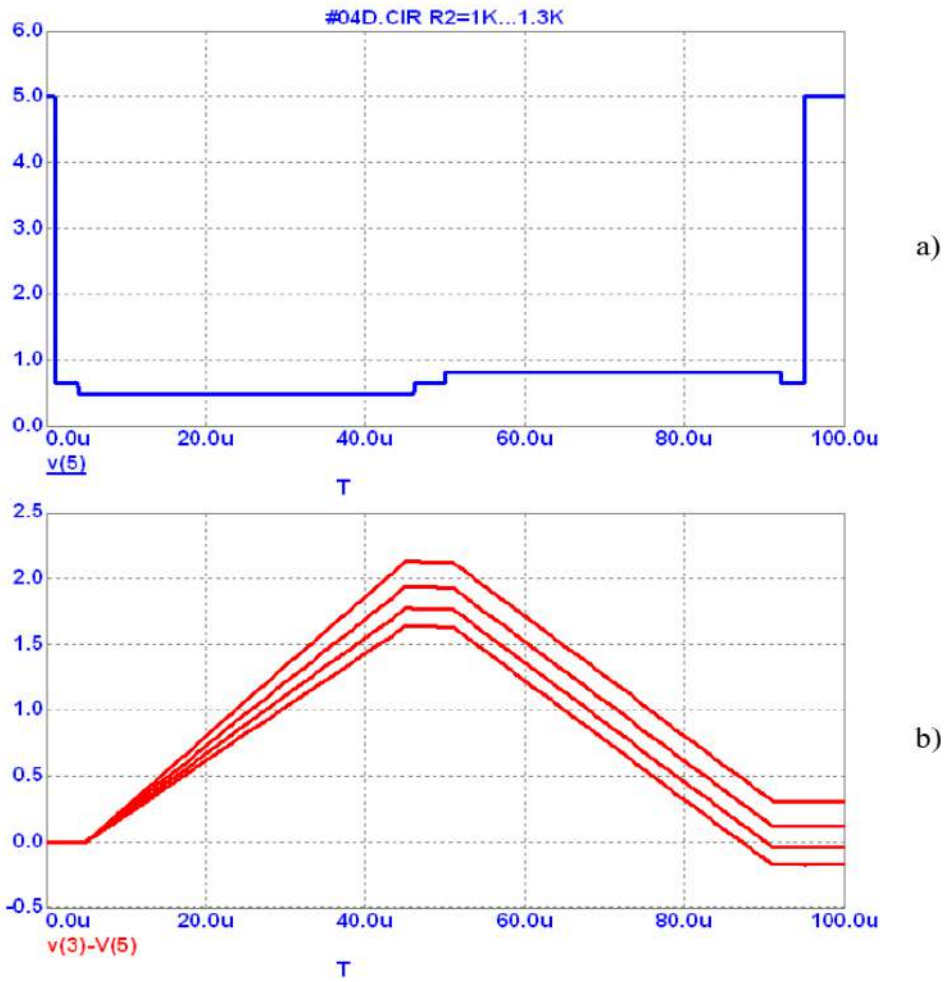


Fig. 6.16. Timing voltage diagram at the discrete iteration of R2 resistor [1,0...1,3 KOhm ]: a) V(5); b) V(3)–V(5)

As it was shown above the selection of the element base is of great importance in the process of the integrator development. First, it is necessary to minimize the input current of the operation amplifier. Taking into consideration the trends of modern electronics development (minimal energy consumption, low voltage one-pole supply, mainframe realization with the surface mounting) low voltage micropower CMOS Rail-to-Rail operation amplifiers of AD8541/2/4 were selected (see Fig 6.18) [117]. The advantages of such operation amplifiers are low values of the input current ( $I_{INP} < 4 \text{ pA}$ ), it is important from the point of view of provision of the high accuracy of the

integrator operation, wide range of the input and output voltages (practically from the minus level to the plus of the supply source), low voltage one-pole supply (from 2.7 V) and low power consumption (50  $\mu\text{A}$  per one operation amplifier).

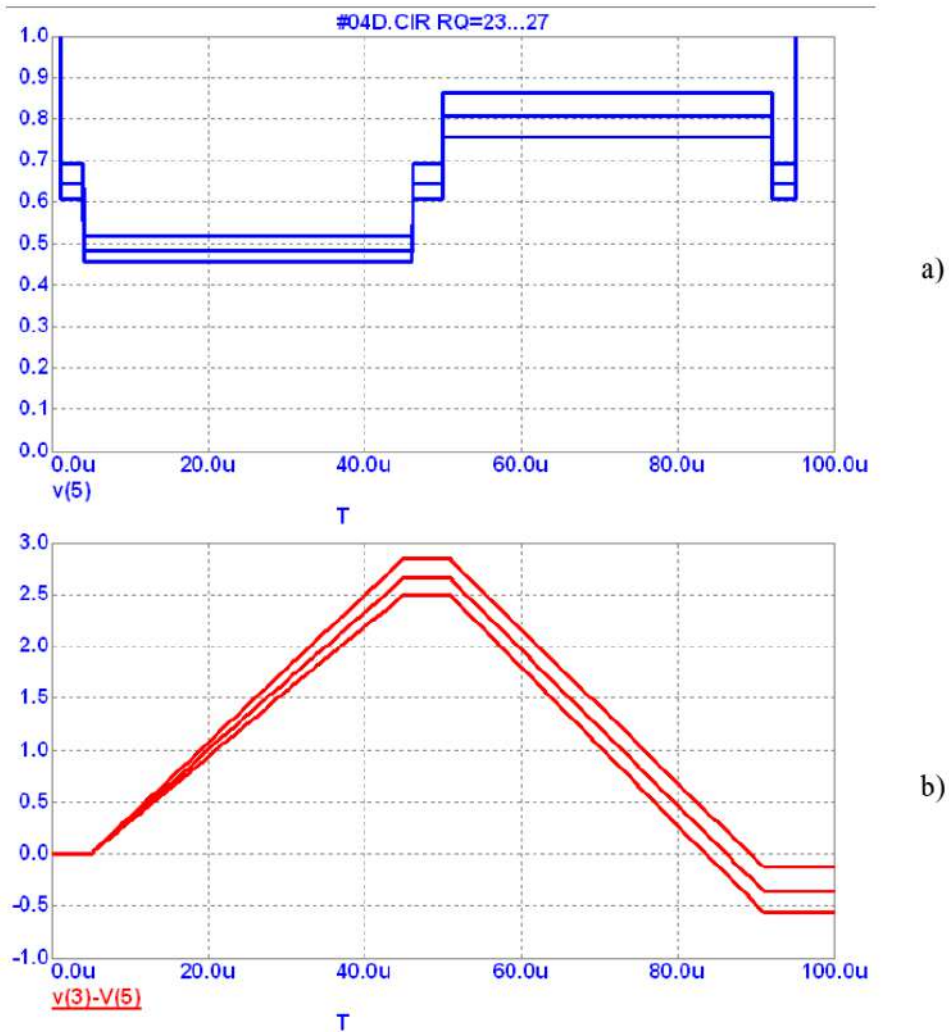



Fig. 6.17. Timing diagrams at the discrete iteration of  $RQ = 23, 25, 27$  Ohm: a) reference voltage  $V_{REF}$  of the integrator; b) voltage difference  $V_{OUT} - V_{REF}$

As the control switches (two-channel analog multiplexer), which switch the analog signals of the input circuits of the integrator, CMOS integrated circuits ADG744 are used (Fig 6.19) [201]. These switches are characterized by the

possibility of high precision switching of the bipolar signals and minimal resistance in the open state (not higher than 4  $\Omega$ ). Unique functional characteristic of such switches, having principal significance for the development of the low voltage electronic equipment is the possibility of the signals switching in the full range of the circuit supply voltage (Rail-to-Rail operation), normal switching mode takes place already at the supply voltage of 3V.



**ANALOG  
DEVICES**

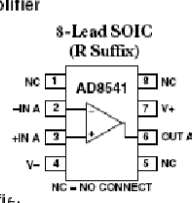
**General-Purpose CMOS  
Rail-to-Rail Amplifiers**

**AD8541/AD8542/AD8544**

**FEATURES**  
 Single Supply Operation: 2.7 V to 5.5 V  
 Low Supply Current: 45  $\mu$ A/Amplifier  
 Wide Bandwidth: 1 MHz  
 No Phase Reversal  
 Low Input Currents: 4 pA  
 Unity Gain Stable  
 Rail-to-Rail Input and Output

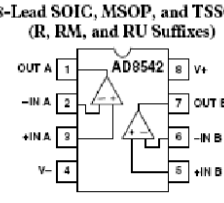
**APPLICATIONS**  
 ASIC Input or Output Amplifier  
 Sensor Interface  
 Piezo Electric Transducer Amplifier  
 Medical Instrumentation  
 Mobile Communication  
 Audio Output  
 Portable Systems

**8-Lead SOIC  
(R Suffix)**



NC = NO CONNECT

**8-Lead SOIC, MSOP, and TSSOP  
(R, RM, and RU Suffixes)**



**14-Lead SOIC and TSSOP  
(R and RU Suffixes)**

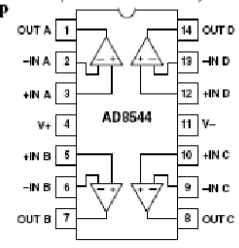


Fig. 6.18. Brief information about AD8541/2/4

Important is the selection of the power switch, which controls the supply circuit of the heater. Its determining parameter is the minimal resistance in the open state. We have selected the MOSFET transistor IRLML2803 [202], manufactured by HEXFET® technology, it is characterized by the resistance in the open state of 0,25  $\Omega$  (Fig 6.20). Such unique parameters are obtained due to the original construction of the transistor and high degree of the structure integration (actually this transistor integrates several tens of thousands of field-effect-transistors and many other elements, in particular, guard diodes and guard-rings).


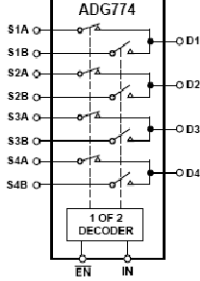
 <b>ANALOG DEVICES</b>	<b>CMOS</b> <b>3 V/5 V, Wide Bandwidth Quad 2:1 Mux</b>	<b>ADG774</b>
<p><b>FEATURES</b></p> <ul style="list-style-type: none"> <li>Low Insertion Loss and On Resistance: 4 <math>\Omega</math> Typical</li> <li>On-Resistance Flatness &lt;2 <math>\Omega</math></li> <li>Bandwidth &gt;200 MHz</li> <li>Single 3 V/5 V Supply Operation</li> <li>Rail-to-Rail Operation</li> <li>Very Low Distortion: &lt;1%</li> <li>Low Quiescent Supply Current (100 nA Typical)</li> <li>Fast Switching Times</li> <li style="padding-left: 20px;"><math>t_{ON}</math> 10 ns</li> <li style="padding-left: 20px;"><math>t_{OFF}</math> 4 ns</li> <li>TTL/CMOS Compatible</li> </ul> <p><b>APPLICATIONS</b></p> <ul style="list-style-type: none"> <li>10/100 Base-TX/T4</li> <li>100VG-AnyLAN</li> <li>Token Ring 4 Mbps/16 Mbps</li> <li>ATM25/155</li> <li>NIC Adapter and Hubs</li> <li>Audio and Video Switching</li> <li>Relay Replacement</li> </ul>	<p><b>FUNCTIONAL BLOCK DIAGRAM</b></p> 	

Fig. 6.19. Brief information about ADG774

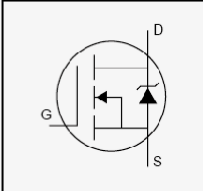
<p>International <b>IR Rectifier</b></p> <ul style="list-style-type: none"> <li>• Generation V Technology</li> <li>• Ultra Low On-Resistance</li> <li>• N-Channel MOSFET</li> <li>• SOT-23 Footprint</li> <li>• Low Profile (&lt;1.1mm)</li> <li>• Available in Tape and Reel</li> <li>• Fast Switching</li> </ul> <p><b>Description</b></p>	<p>PD - 91258D</p> <p><b>IRLML2803</b></p> <p>HEXFET<sup>®</sup> Power MOSFET</p> 	<p><math>V_{DSS} = 30V</math></p> <p><math>R_{DS(on)} = 0.25\Omega</math></p>
--	--	---

Fig. 6.20. Brief information about IRLML2803

The transistor is used only in switch mode – either completely closed or completely open. In the process of heater supply circuit switching (by the current of not higher than 1A) such operation mode and minimal resistance of the transistor in the open state provide minimal power losses and the transistor is not practically warmed up.



The external view of the studied prototypes of the controller of the temperature mode heater and the interface unit of the signal convertor of the flow sensor is shown in Fig 6.21.

In the process of the adjustment and study of the controller parameters, first of all the accuracy of the integrator operation, in particular, the instability of the output voltage in the process of the potential transfer was determined. It was shown experimentally, that due to the application of the above-mentioned Rail-to-Rail CMOS operational amplifiers and controlled switches of the analog signal the voltage instability in the process of the push-pull integrator potential transfer does not exceed 0,03%.

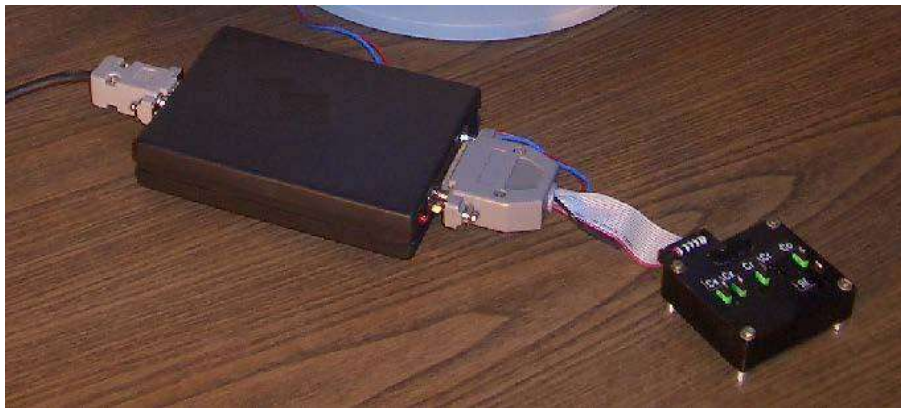


Fig. 6.21. External view of the controller prototypes (on the right) and the interface unit of the signal convertor of the flow sensor (on the left)

Main parameters of the controller of the heater temperature mode are:

- heating current – from 1mA to 1A;
- supply voltage (EV):  $+5V \pm 10\%$ ;
- type of measuring conversion: two stage integration;
- voltage measurement range: from 0.01 V to (EV-0,01) V;
- duration of one stage : from 0.01 ms to 10 ms;
- temperature stabilization error: not greater than 0,1°C.

## 6.2. Circuit engineering realization of the differential thermometer

As it was mentioned above (see Fig 2.1a, Fig.3.a) greater part of the thermal flow sensor devices are based on the measurement of the temperature difference,

emerging as a result of the modulation of the liquid or gas flow of the space distribution of the heater thermal field. For this purpose differential thermometers are used. In biomedical engineering the field of application of the differential thermometers is wider, in particular, they are used for the study of the biochemical composition of the substances, based on the amount of the released or absorbed heat in the process of exothermic or endothermic reactions, correspondingly.

However, the analysis of the literature sources and the parameters of the commercially available differential thermometers show that the separation power of these thermometers not to the fullest extent corresponds to the requirements of modern high precision measuring equipment, in particular, for the problems of biochemical analysis. Separation power of the greater part of the commercially available differential thermometers, namely, HD200, Testo922 is 0,1°C [203]. The most precise of the differential thermometers, determined by us - SBIR Model 104 High Resolution Differential Thermometer – is characterized by the separation power of 0,01°C [204].

Proceeding from the above-mentioned, the problems of further improvement of the separation power of the differential thermometers (to the values of the order 0,001°C) are allocated in a separate problem.

The analysis of the measuring circuit of the differential temperature sensor was carried out on the base of the differential transistor stage. In particular, it was shown that, unlike the thermoresistive or thermocouple measuring converters, the application of the bipolar transistor structures enables the creation of a supersensitive sensor of the temperature difference. Measuring circuits of the temperature difference on the transistor stages unlike thermoresistive primary converters provide far less self-warming by the supply current and unlike thermocouple converters – far higher slope of the conversion function.

In the process of the research, carried out, it was established that the, determining parameter of the difference temperature sensor at the differential transistor stage is not only the current of the stage (the value of the current is critical from the point of view of the self-warming of the transistor structures of the temperature sensor) but also the reference voltage of the basic circuit of the differential stage. As we showed, the optimal value of the reference voltage of the basic circuit is  $V_{REF} = 1,2-1,25$  V.

In this case, minimal dependence of the transfer function slope of the temperature difference on the value of the absolute temperature is the optimality criterion: From the practical point of view this optimality criterion is of great importance- the dependence of the transformation slope of the temperature difference on its absolute value requires the calibration of the differential thermometer for various values of the absolute temperature. Such calibration is a

rather labor-consuming process. Instead, the optimal value of the reference voltage, determined by us, allows us to develop the differential thermometer, calibration of which remains stable in a wide range of the absolute temperatures.

Below the basic circuit engineering features and operation parameters of the developed experimental prototype of the differential thermometer are considered. From the point of the view of provision high values of separation power and stability of differential thermometer on the base of the transistor differential stage important problems are not only the stability of the useful signal amplification factor but also the lack of shunting of the output circuit or the differential stage by the secondary signal converter and high separation power of further analog-to-digital conversion.

It should be noted that the typical engineering approach to the solution of the problem of the signal processing of the differential thermometer signal does not provide necessary parameters of accuracy. The problem is high output resistance of the differential stage that serves as the primary converter of the temperature difference. As it was already noted in section 3.3 to prevent self-warming of the transistors at the differential stage their working currents must be minimized. In particular, thermal resistance of the chip, small power transistor without the heatsink as a rule is  $ZQ = 500^{\circ}\text{C} / \text{Bt}$ , it is equivalent to the condition of the power of thermal loading  $POPT = 20 \text{ mW}$  per  $0,01^{\circ}\text{C}$  of the overheating of the p-n junctions of the transistor. This determines operation models of the transistors: collector current (or emitter)  $I_C = 10 \text{ mA}$  and voltage drop between the collector and emitter  $V_{CE} = 2 \text{ V}$ .

In order to prevent the shunting impact on the signal of the differential stage by the circuit of the secondary converter, located behind the differential stage, the input current of the secondary converter must not exceed 0,1% of the output current of the differential stage transistors. Value of the order 10 nA corresponds to this case. It should be noted that it is referred to the differential signal that requires the correspondingly differential input or the secondary converter, in particular, analog-to-digital converter with the differential input.

Analysis of the technical characteristics of modern precision analog-to-digital converter with the differential output shows that the sel problem can be realized on the base on 24-digital sigma-delta converter with the single crystal microconverter of ADuC826 type. Brief information about this microconverter is presented in Fig. 6.22. However, studies, performed by us, show that the quality of the voltage conversion of the differential stage with microcurrent output by means of ADuC824 is not sufficient- in the process of the signal sampling the shunting, by the input circuits or ADuC824 the output circuits of the differential stage takes place [205].

The possible solution of this problem is the application of the instrumental amplifiers, in particular, basic model AD620 or its further successors, which

provide high accuracy of the amplification of the differential signals. But such a solution is not optimal. The given instrumental amplifier has differential input, compatible with the differential signal of the circuit for temperature difference measurement. However, the output of this amplifier is not differential that does not allow it to obtain high values of signal conversion, in particular, in-phase rejection, while connecting the amplifier output with the input of analog-to-digital converter.

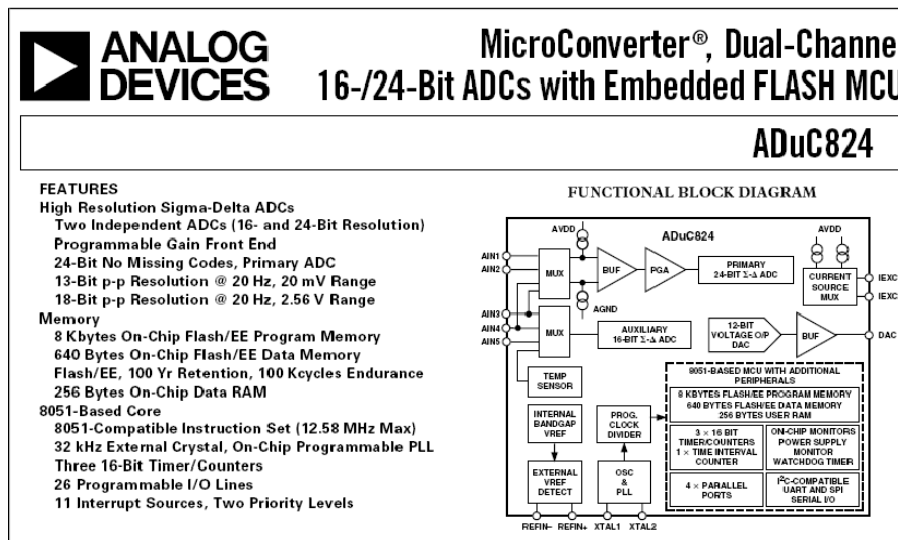


Fig.6.22. Brief information about ADuC824

Thus, the task to develop a buffer signal amplifier with the differential input and differential output, characterized by the minimal values of the input currents and minimal instability of the shift voltage, was put forward. Unlike the traditional differential amplifiers, the buffer amplifier must not connect the output voltage to the common (earth) bus; the differential component of the input voltage signal must be amplified and the in-phase component – must be transmitted without changes.

For the realization of the given task, special kind of amplifier of AD8551/2/4 type (Fig. 6.23), that operates according to the principle of signal modulation-demodulation, providing the minimal values of the offset voltage (Low Offset Voltage: 1 $\mu$ V) and its instability (Input Offset Drift: 0,005  $\mu$ V/°C) is used [117]. Integrated circuit of the amplifier is manufactured using CMOS-technology, it provides minimum values of the input currents (Ultralow Input Bias Current: 20 pA) and the possibility to operate in wide range of the input and output voltages (Rail-to-Rail Input and Output Swing) at +5/+2,7 V Single-Supply Operation. Useful current of each operational amplifier does not exceed 0,7 mA.

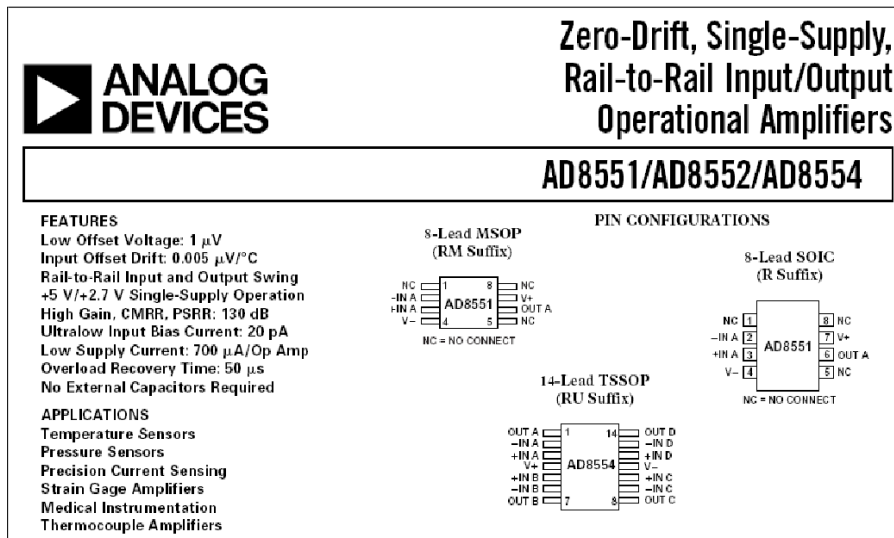


Fig. 6.23. Brief information about AD8551/2/3/4

Functional block-diagram of the differential thermometer developed by us is shown in Fig. 6.24, a), main blocks of the device are the primary converter of the temperature difference (T1, T2, R1, R2, R3), buffer signal amplifier (OA1, OA2, R4, R5, R6) and 24-bit sigma-delta analog-to-digital converter on the base of microconverter ADuC834 (basic model – 24-Bit MicroConverter ADuC824). The output of the information and control of the device is performed by PC by means of USB interface. Buffer signal amplifier as it was already mentioned, is realized on the base of high precision operational amplifier AD8552 (two operational amplifiers in one micropackage of SOIC type).

Supply of the differential thermometer may be performed directly from the bus +5 V of the USB port or from the corresponding independent voltage source. For the stabilization of the supply voltage integrated circuit of the stabilizer with low voltage drop on the control element, in particular, ADP3367AR, is used.

In the differential stage of the primary converter n-p-n transistors in micropackage construction SOT23 is used. The transistors are mounted on the probes, their external view and the circuit of the signal converter is shown in Fig.6.24, b). For the realization of the differential thermometer of the flow sensor of the thermal type with the minimal value of the thermal relaxation chip transistors in the «suspended» design execution or with MEMs construction-technological basis, in particular, membrane construction of the primary converter structure can be used.

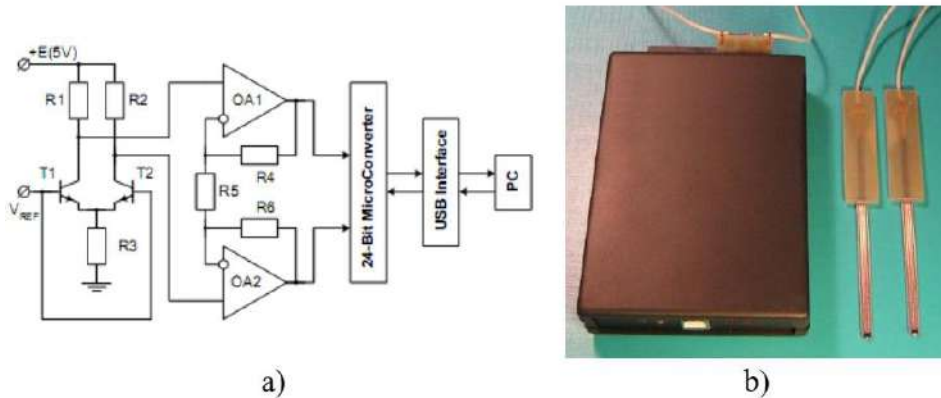


Fig. 6.24. Differential thermometer: a) function block- diagram; b) external view

The example of the result of the differential thermometer output voltage measurement is shown in Fig. 6.25. Measurements were carried out in the range of  $\pm 2500$  mV (the range is determined by the corresponding control registers of the microconverter ADuC834, as it is shown in Fig. 6.26). The slope of measuring conversion of the temperature difference (sensitivity) is  $200 \text{ mV}/^\circ\text{C}$ .

In the process of the given measurement example one of the probes was cooled at approximately  $6^\circ\text{C}$ . In the Figure the process of cooling and restoration of the previous temperature is shown.

Besides, the section of the measurement of the initial value of the temperature, where the temperatures of the probes are almost identical, are shown in the insertion.

It is seen that non-reproducibility of the measurement does not exceed  $0,02$  mV. This value corresponds to the temperature of  $10^{-4}^\circ\text{C}$ , this, at least by an order, exceeds the requirements to the differential thermometers of the sensor flow devices. We may consider that the separation power of the developed differential thermometer is limited only by the self-warming process of the primary converters and, thus, if the current of the differential stage is decreased, still higher accuracy of the temperature difference measurement can be achieved.

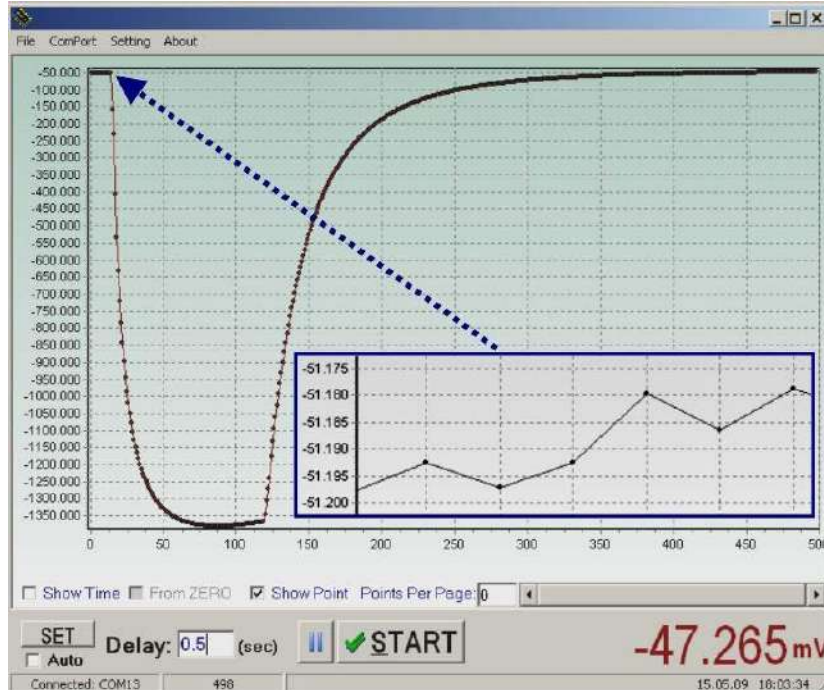


Fig.6.25. Example of the signal (voltage) measurement result of the differential thermometer (measurement range 2500 mV)

Basic operation characteristics of the differential thermometer are:

- separation power of the temperature difference measurement: not less than  $0,001^{\circ}\text{C}$ ;
- operation range: from  $-40^{\circ}\text{C}$  to  $+100^{\circ}\text{C}$ ;
- supply voltage:  $+5\text{ V} \pm 10\%$
- consumption current: not greater than  $10\text{ mA}$
- interface: USB.

As it was mentioned above, besides thermal flow sensor the developed differential thermometer with the separation power of  $0,001^{\circ}\text{C}$ , that by one order exceeds the same parameter of the known analogues [203, 204], can find application in sensor devices for the determination of biochemical composition of the substances, based on the thermal release or thermal absorption of the studied substances in the process of the corresponding biochemical reactions.

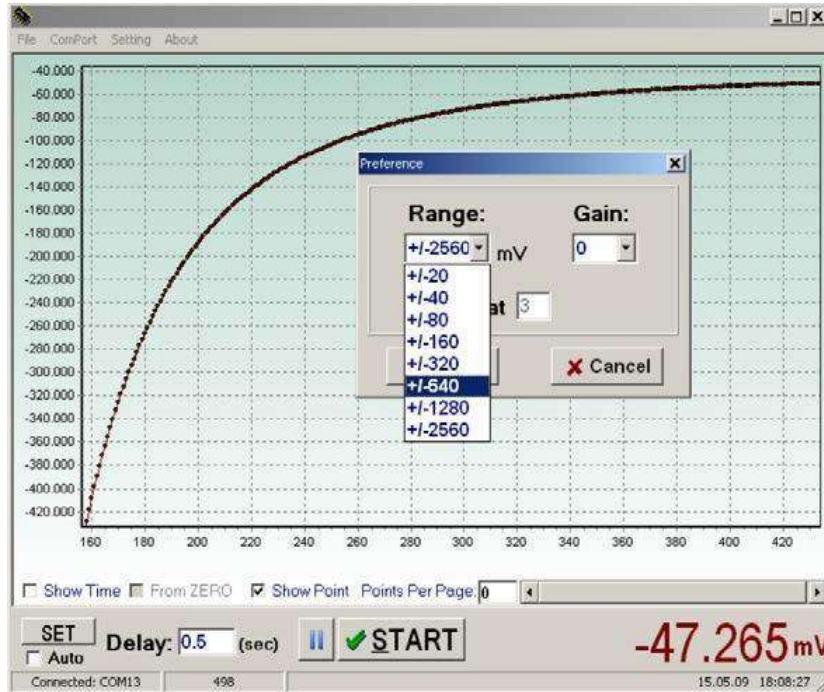


Fig.6.26. Example of the output voltage measurement range control of the differential thermometer

### 6.3. Practical realization of the signal converters of the thermal flow sensors of the biomedical design

One of the most important requirements for a new generation of microelectronic sensor devices is the reduction of the energy consumption and the transition to low voltage single pole supply sources. The possibility of the development of the sensor devices, which would meet this requirement, appeared quite recently. The reason for such slow transition to low voltage supply sources was the lack of high precision analog integrated circuits that provide the possibility of the operation at full range of voltage.

Typical integrated circuits of the analog path, in particular, operation amplifiers, are characterized by the so-called «dead» ranges of the input and output voltages, which are typically above 1 V from the potentials of the negative and positive supply sources. This means that in case of single pole 5 V supply, the voltages below 1 V and higher than 4 V cannot be used as the analog information signals. If the transition to 3 V supply is made, typical integrated circuits of the analog section practically come out of operation.

Drastic change occurred with the advent of new generation of so-called



Rail-to-Rail integrated circuits; their characteristic feature is the possibility to convert signals practically in the whole range of the supply voltage [117, 205].

In this section the approaches to the construction of the signal converters of microelectronic thermal flow sensors which meet the requirements of the low voltage energy efficient electronics. However, the application of modern Rail-to-Rail integrated circuits to reach the set goal is not sufficient. As it was already noted, the problem is that with the transition on low-voltage supply sources the resistances of the primary converters of the thermal flow sensors decrease. If the circuits, constructed on functionally integrated elements, are used which perform the controlled heating of the flow and by means of which temperature gradient in the flow is determined, then the problem of the impact of the stray resistances of the signal lines impact arises. In the first section basic circuits engineering solutions were analyzed, which partially helped to solve this problem. However, such problems as the impact of the signal lines, located between functionally integrated elements of the thermal flow sensors and energy expenses (including the stray warming up) of the output circuits of the control operation amplifiers, still are not solved. These problems, as well as the problems of practical realization of the current supply mode of the functionally integrated elements, that provides high efficiency of the signal conversion are the subject of circuit engineering studies, mentioned below.

First, we will consider the problem of the stray resistance compensation of the signal lines of the measuring circuit on the base of the differential pair of the integrated thermoresistive converters. The latter are switched on in series and connected to the supply source without the control elements. Integrated thermoresistive converters  $R_{QT1}$ ,  $R_{QT2}$  (Fig. 6.27) are heated by the supply current, and the difference of the voltage drop at these converters serves as the information value regarding the temperature gradient, stipulated by the measured flow of the fluid or gas. In order to compensate the impact of the stray resistances of the signal lines, each converter has two current ( $R_{Q1L1}$ ,  $R_{Q1L3}$  and  $R_{Q2L1}$ ,  $R_{Q2L3}$ , correspondingly) and two potential ( $R_{Q1L1}$ ,  $R_{Q1L3}$  and  $R_{Q2L1}$ ,  $R_{Q2L3}$ , correspondingly) outputs. On the condition of the minor current across the potential outputs voltage drops on them can be neglected, this provides the minimization of the stray resistance's impact of these outputs (signal lines) on the output signal.

Signal converter of the differential pair of the integrated converters must form the voltage difference  $(V_{1RQ1}-V_{2RQ1}) - (V_{1RQ2}-V_{2RQ2})$ . The problem is that the voltage  $V_{1RQ1}$  is close to the positive voltage, and voltage  $V_{2RQ2}$ —to the positive voltage of the supply source. This provides the usage of Rail-to-Rail differential amplifiers, whose function in the given problem is reduced to the precise transfer of the signal voltages difference from one potential, the value of which is non-stable value, to the other, stable potential. There arises the problem

of the selection and formation of the common potential, the output voltage of the differential amplifier will be formed relative to this potential. In case of the two-pole supply sources such common potential is the common point between the source of the positive and negative supply voltages. In case of the single-pole supply source such common potential is the middle of the supply voltage. However, in the process of the analysis, we showed that in case of single pole low voltage supply the solution when the common point is connected directly to the zero output of the supply source (Fig. 6.27) is more optimal.

As it follows from the suggested circuit at mutual equality of the resistors of the differential amplifiers  $OA_1 - R_1 = R_2 = R_3 = R_4$ ,  $OA_2 - R_5 = R_6 = R_7 = R_8$  and corresponding equations, meeting this requirement:

$$V_{-OA1} = V_{+OA1} = \frac{V_{1RQ1}}{2}; V_1 = V_{-OA1} + (V_{-OA1} - V_{2RQ1}) = V_{1RQ1} - V_{2RQ1} = V(R_{QT1});$$

$$V_{-OA2} = V_{+OA2} = \frac{V_{1RQ2}}{2}; V_2 = V_{-OA2} + (V_{-OA2} - V_{2RQ2}) = V_{1RQ2} - V_{2RQ2} = V(R_{QT2}),$$

output voltages of the differential amplifiers repeat the voltage drop at the primary converters:  $V_1 = V(R_{QT1})$ ,  $V_2 = V(R_{QT2})$ .

Important fact is that, first, these voltages are formed with relatively zero potential of the single-pole supply source and, secondly, the value of these voltages approximately equals half of the supply voltage.

This principle advantage of the suggested circuit engineering solution enables to optimize further realization of the signal converter, forming the output stage at the output pseudo-differential amplifier (at  $OA_3$ ,  $OA_4$ ) with the differential output, its amplification factor is determined as  $K_V = (R_9 + R_{10} + R_{11}) / R_9$  (if  $R_{10} = R_{11}$ ). Taking into account the above-mentioned advantages, the limitations imposed on the amplification factor of the output pseudo differential amplifier as a result of the exceeding the limits of the linear operation mode by the output voltage.

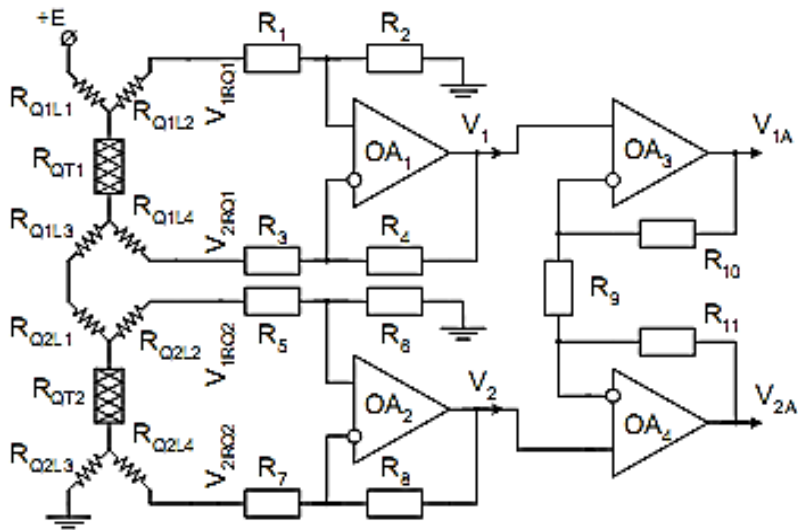


Fig. 6.27. Scheme of the signal converter #1

Model circuit and method of formation of the output characteristics of the signal converter #1 is shown in Fig. 6.28, the results of the research are shown in Fig. 6.29.

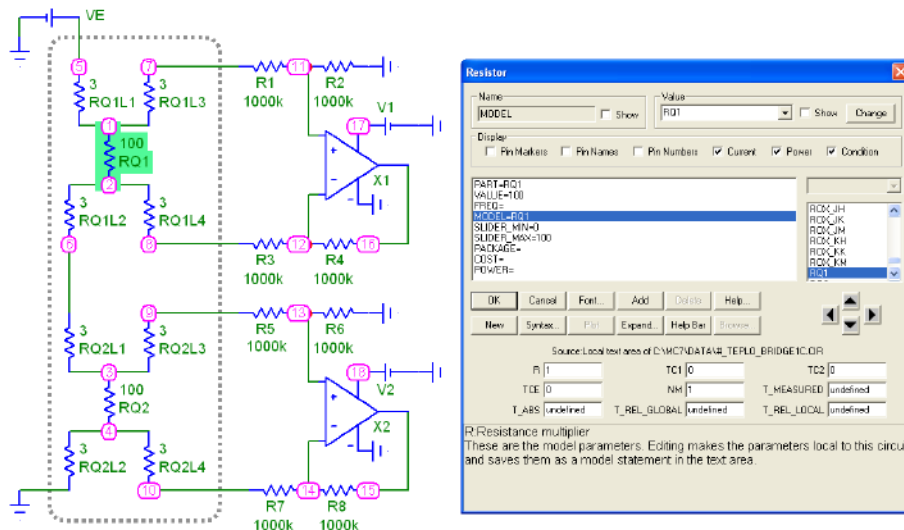


Fig. 6.28. Model diagram and method of the formation of the output characteristics of the signal converter #1

Method uses the possibility of scaling in the preset limits of one of the model parameters. In this case, scale coefficient NM of the thermoresistive element  $R_{Q1}$  is used, this coefficient in the process of model research changed from 0,95 to 1,05, that corresponds to the change of the resistance of the thermoresistive element  $R_{Q1}$  at  $\pm 5\%$ .

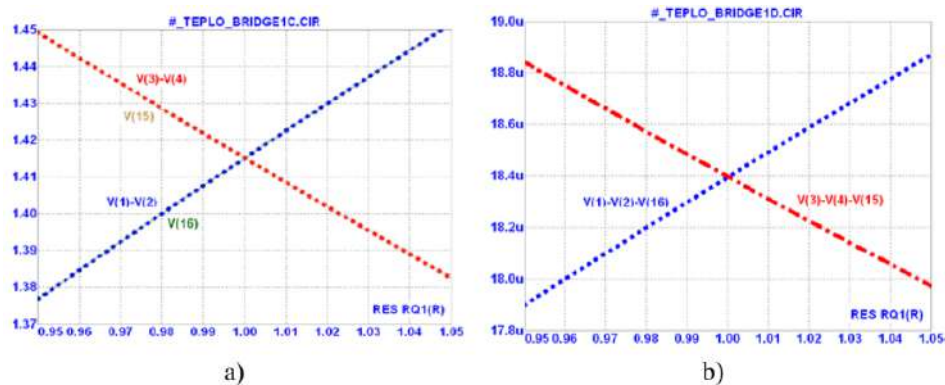


Fig. 6.29. Results of the modeling studies of the signal converter #1

As it can be seen in Fig. 6.29 if the resistances of the thermoresistive elements of the converter  $R_{Q1} = R_{Q2}$  (the flow in the flowmeter is not available) that occurs if  $RES RQ1(R) = 1$ , first, the output voltages of the differential amplifiers are mutually equal  $V(15) = V(16)$  and, secondly, half supply voltages are approximately equal (supply voltage 3 V, and output voltage of the amplifiers is 1,415 V). If the flow rate increases the relation between the resistances of the thermoresistive elements of the converter increases  $NM = R_{Q1}/R_{Q2}$ , this stipulates the disbalance – the voltage  $V(16)$  increases, and the voltage  $V(15)$  decreases, correspondingly.

The example of the result of the conversion accuracy study is seen in Fig. 6.29 b, where the discrepancy between the output voltage of the differential amplifiers and voltage drop at thermoresistive elements  $R_{Q1}, R_{Q2}$  of the converter is shown:  $[V(1)-V(2)]-V(16)$  and  $[V(3)-V(4)]-V(15)$ , correspondingly. As it is seen, at the set parameters of the element base such discrepancy does not exceed 0,005%, and circuit engineering completely meets the requirements to the precision signal converters.

Another variant of the signal converter (#2), which is optimized for the differential integral thermoresistive converters, the design of which enables to neglect (minimize) the stray resistance between these converters (for instance, if the latter are manufactured in the integral realization) is shown in Fig. 6.30.

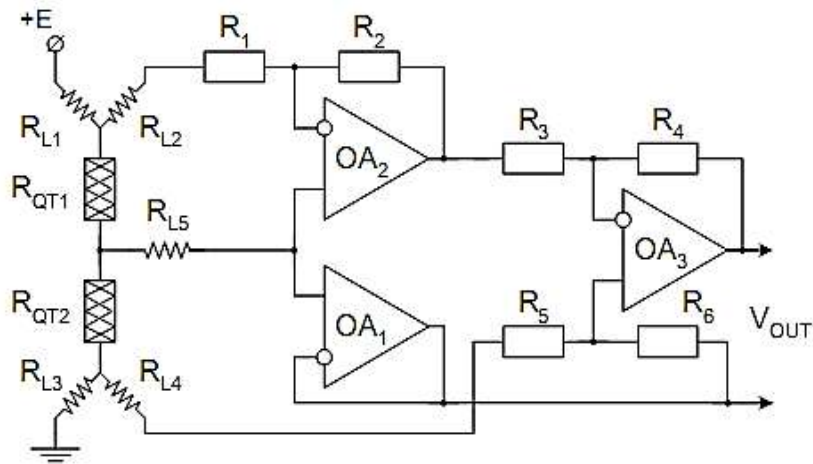


Fig.6.30. Diagram of the signal converter #2

Such realization enables us to simplify the circuit engineering solution of the signal converter. The circuit consists of the follower on  $OA_1$ , inverter on  $OA_2$ ,  $R_1$ ,  $R_2$  and differential amplifier on  $OA_3$ ,  $R_3$ – $R_6$ . The common point of the output signal  $V_{REF}$  is located approximately in the middle of the supply voltage. The potential of this common point that numerically equals the potential between the integrated thermoresistive converters  $R_{QT1}$ ,  $R_{QT2}$  is eliminated across the line  $L_5$  (taking into account the limiting small values of the input currents of the operation amplifiers  $OA_1$ ,  $OA_2$  voltage drop at the stray resistance  $R_{L5}$  of the line  $L_5$  may be neglected) and is formed by the voltage follower at  $OA_1$ :  $V_{REF} = V_{+OA1} = V_{+OA2} = V_{OUTOA1}$ . Minimization of the voltage drop at the stray resistances of the potential outputs (signal lines)  $R_{L2}$   $R_{L4}$  is provided by currents minimization across them, for this purpose the resistances  $R_1$ ,  $R_2$ ,  $R_5$ ,  $R_6$  must be maximally large (typically  $10^4$ ... $10^5$  Ohm).

If the above-mentioned requirements are met and if the resistances of the feedback of the inverter  $R_1 = R_2$  are equal, the voltage  $V_{OUTOA2} = V_{REF} - V(R_{QT1})$ , is formed at its output, further this voltage is sent to the inverting input of the differential amplifier. Instead, the voltage  $V_{REF} - V(R_{QT2})$  is sent to the non-inverting input of this amplifier. Thus, the output voltage of the signal converter  $V_{OUT}$  is determined by the difference of the voltage drop at the thermoresistive converters  $R_{QT1}$ ,  $R_{QT2}$ , does not depend on the stray resistances of the signal lines and numerically is  $V_{OUT} = (V(R_{QT1}) - V(R_{QT2})) K_V$ , where  $K_V = R_4 / R_3 = R_6 / R_5$  – is signal amplification coefficient.

We will show the possibility of the controlled heating of the differential pair of functionally integrated thermal resistive converters.

As it was already noted such controlled heating provides the possibility to minimize energy consumption, widening of the range of flow rate measurement and, from the point of view of biomedical flow sensors, heating temperature limitation in order to avoid thermal degradation of the flow substance.

Information value regarding the temperature in the controlled heating mode is the total resistance of the differential pair of functionally integrated thermoresistive converters, and the information value regarding the flow rate- is the difference of the resistances of this pair. Signal converter that performs the formation of the corresponding information values of voltages, is shown in Fig. 6.31.

The circuit combines two converters – temperature mode controller (see Fig.6.11) and signal converter #2 (see Fig.6.30).

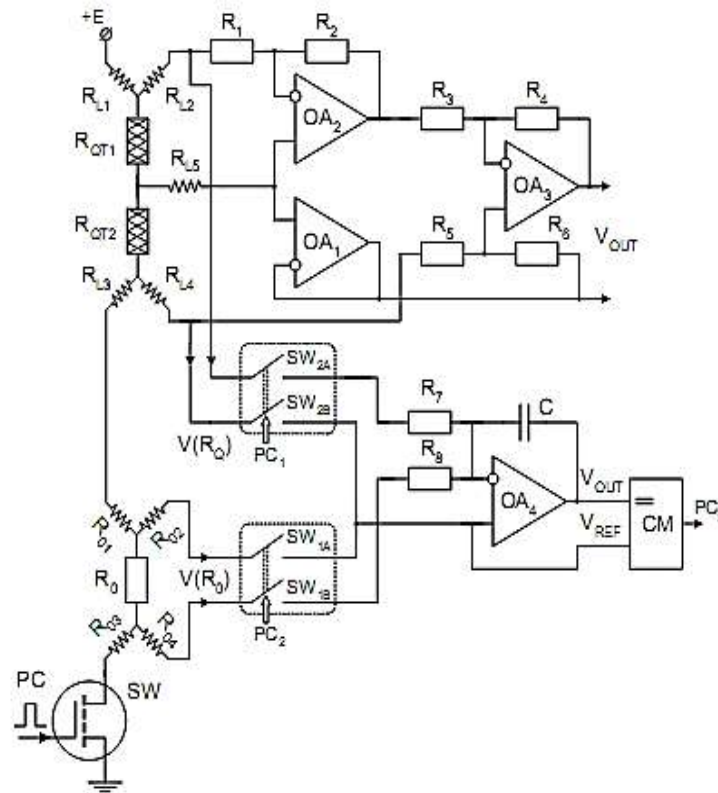


Fig. 6.31. Diagram of the signal converter #3

Principles of operation and the components of this circuit coincide with the above-considered converters, that is why, they do not require separate consideration.

Instead, we consider the problem of the signal converters development and selection of the element base in the circuit of the current supply of the thermoresistive measuring converters. The detailed analysis and the advantages of the measuring converters in the process of the transition from the bridge or half bridge circuits to independent current supply of the thermoresistive measuring converters of thermal flow sensors were considered in the Section 3. The problem to be considered is circuit engineering realization of the precision current sources, voltage drop at their control circuits, as compared with the voltage drop on load, is minimized. It enables: first, to increase the sensitivity of the flow sensor, secondly, maximally use the energy of the supply voltage source and third, minimize the heating of the control elements of the current sources, the integral realization of the flow sensor prevents the impact of the temperature of these control elements on the temperature gradient in the structure of the thermoresistive measuring converters.

The first stage of the development of the current supply sources is the selection of the element base. As it is shown in Fig.6.32, it is necessary to provide minimal voltage drop in the output circuit of the operational amplifier  $OA_1$  – voltage  $V_{OUT}$  on the load  $R_{LOAD}$  must maximally approach to the voltage of the supply source  $E$ . It is obvious, that such approaching has certain limits.

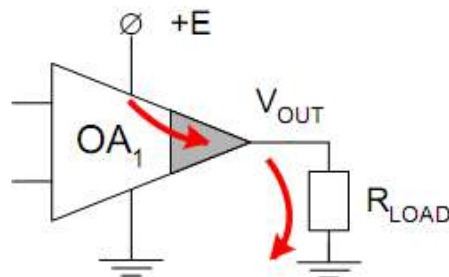


Fig. 6.32. Distribution of voltages in the loading circuit of the operational amplifier (output circuit of OA is emphasized in order to draw the attention to its parameters)

First, it is necessary to have the information regarding the current dependence of the voltage drop at the output transistors of the operation amplifiers, used in the current source circuits. Second, when the speed of the measuring flow changes, the resistances of the thermoresistive converters, i.e., load resistance, change. That is why, the availability of a certain reserve of voltage is necessary and the calculation of the operation modes of the circuit is necessary to perform for maximum value of the thermoresistive converter resistance.

In particular, Fig. 6.33 shows the experimental results of the current dependences of the voltage drop at the output stages of the operational amplifiers AD8551/2/4 and AD8051/2/4 (the number of OA in one housing of

the integrated circuit is given across the fraction) . We can see that when current increases, the voltage drop at the output stage AD8552 drastically increases, making the selection of this OA only at load currents not greater than 10 mA. Instead, AD8052 provides rather low voltage drops to the current of 50 mA. If it is necessary to provide greater currents of the warming circuits of the thermoresistive converters it is necessary to use operational amplifiers with more powerful output or, as it will be shown below, the control elements of the output circuit of the current sources on the discrete transistors.

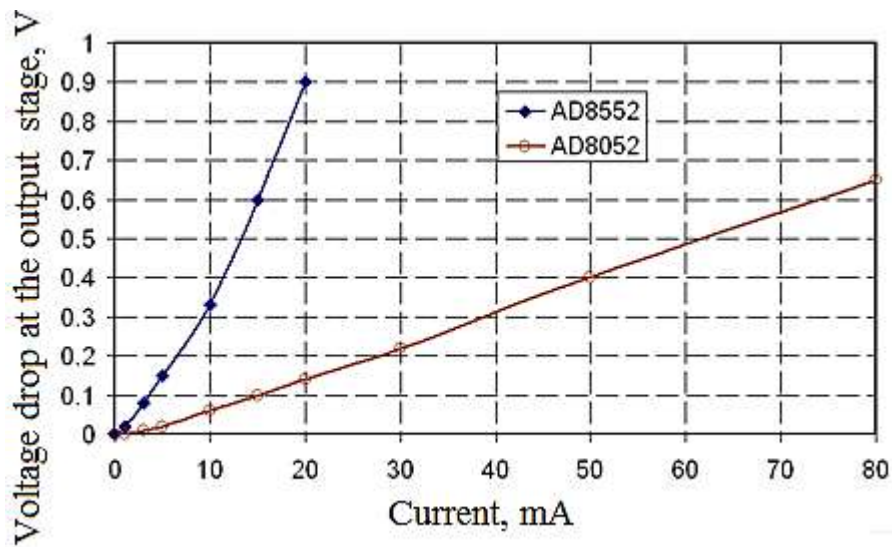


Fig. 6.33. Experimental results of the current dependence of the voltage drop at the output stages of the operation amplifiers AD8551/2/4 and AD8051/2/4

The example of the circuit engineering realization of the signal converter with the current supply is shown in Fig. 6.34. Sources of current are realized on the operation amplifiers  $OA_1$ ,  $OA_2$  with the feedback reference resistors  $R_{01}$ ,  $R_{02}$ . On the noninverting inputs of  $OA_1$ ,  $OA_2$  the reference voltage  $V_0$  is sent, that forms the source  $E_{REF}$ . According to the given circuit, if the input currents of the operation amplifiers are neglected, we can assume that the currents across the thermoresistive converters  $R_{QT1}$ ,  $R_{QT2}$  are fixed  $I(R_{QT1}) = V_0/R_{01}$ ,  $I(R_{QT2}) = V_0/R_{02}$ .



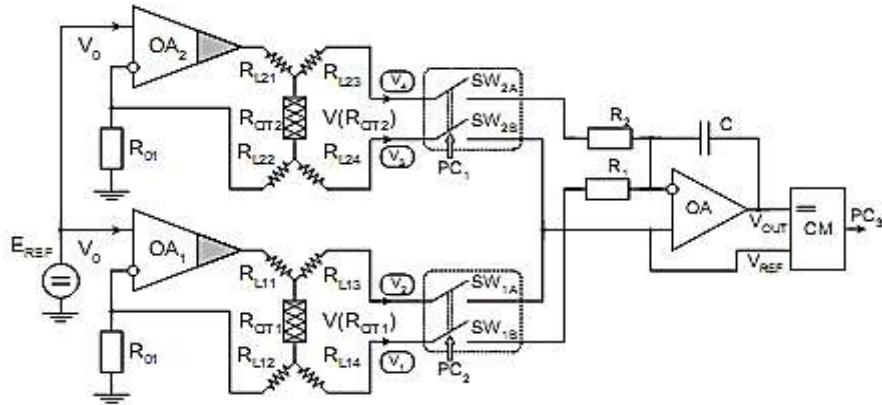


Fig. 6.34. Circuit of the signal converter #4

Maximum efficiency of the circuit is provided at the voltages of the thermoresistive converters  $V(R_{OT1})$ ,  $V(R_{OT2})$ , values of which are maximally close to the supply voltage of the circuit. For this purpose voltage drop at the output circuits of  $OA_1$ ,  $OA_2$  and on feedback resistors  $R_{O1}$ ,  $R_{O2}$  are minimized. Proceeding from these requirements the selection of the corresponding operation amplifiers is performed, knowing the parameters of its shift voltage instability, the reference voltage  $V_0$  is determined. For greater parts of cases the value of this voltage does not exceed 0,5 V.

The formation of the output signal of the differential pair of functionally integrated thermoresistive converters may be analogous to the above-considered solutions, in particular, using the integrator, shown in Fig. 6.11.

It is obvious that the parameters of the source  $E_{REF}$  of the reference voltage must meet the requirements of the low-voltage energy saving electronic equipment. That is why, it is not efficient to use the conventional stabilitrans on the avalanche effect of p-n junction break – from the point of view of voltage temperature coefficient and differential resistance of the avalanche break optimal is the value of the voltage of approximately 7 V, it is inadmissible in low voltage, in particular 3 V, equipment. Instead, integrated circuits of the reference sources, constructed on the principle of the voltage formation, numerically equals the Bandgap References, in particular REF19X series (Analog Devices), which, as compared with the stabilitrans, successfully operate, using the supply voltages, starting from 2 V, are characterized by considerably better stability and less energy consumption [206].

In case, when the heating power of the thermoresistive measuring converters must be great (flowmeters for measurements of large volumes of fluids and gases), minimization of the voltage drop at the control elements of the output circuits is provided by means of using the discrete transistors, in particular, as it

is shown in Fig.6.35. To prevent the transistors saturation mode (as it is shown on the diagram of the bipolar n-p-n transistors), that might be the reason of the worsening of the current stabilization accuracy, the voltage drop on these bipolar transistors must not be less than 0,2 V.

Usage of the modern HEXFET® Power MOSFET field-effect transistors is the matter of priority, in particular IRLML2803 [202], if necessary, the voltage drop on them may be decreased to 0,01 V.

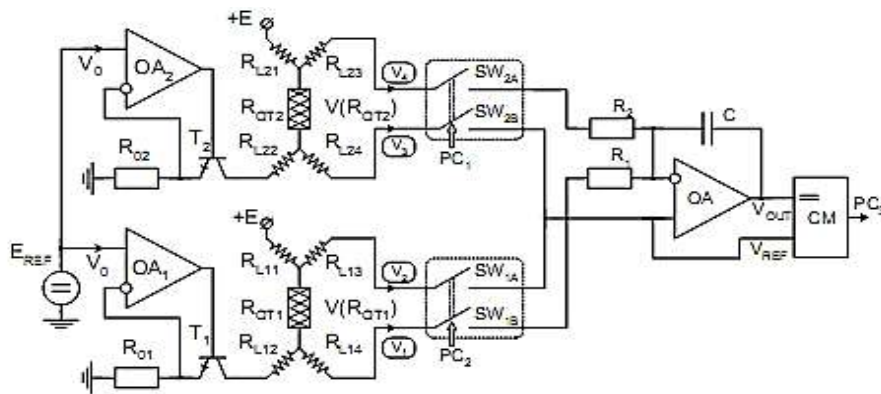


Fig. 6.35. Diagram of the signal converter #5

According to the calculations, performed in Section 3, if 90 % usage of the supply voltage, in particular, if the voltage drop on the thermoresistive converter is not less than 4,5V in the circuit with 5 V single pole supply, the application of the signal converters with the current supply of the thermoresistive converters (see Fig 6.34, 6.35) as compared with the conventional bridge or half bridge circuits enables to increase the efficiency of the signal conversion  $S_{QT1} / S_{QTR} \approx 7$  times.

The developed and considered above signal converters were experimentally studied in a number of devices, used for measurement of fluids and gasses flow rate. As the primary converters, miniature copper thermoresistors and integrated MEMS structures of the thermal flow sensors, manufactured within the frame of scientific cooperation at the Institute of Sensor Systems (IMOS) of Otto von Guericke Universitat (Magdeburg, Germany) were used. The photograph of such a structure is shown in Fig. 6.36.

MEMS structure contains a central heater and four thermoresistive elements, distributed over the periphery of the crystal. The size of the semiconductor crystal of such a structure is  $3 \times 3$  mm.

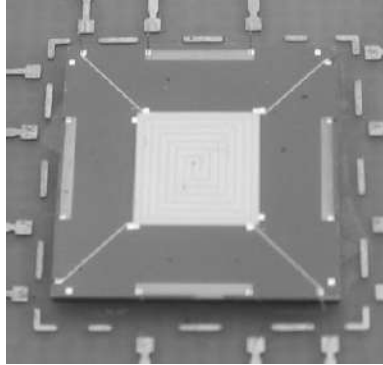


Fig. 6.36. External view of the integrated MEMS structure of the thermal flow sensor

Photographs of the sample of the sensor device for flow measurement and its unit of primary converter, on the base of which the testing of the results obtained was carried out, are shown in Fig. 6.37.



Fig. 6.37. External view: a) sensor device for flow measurement ; b) block of the primary converter

Universal components of the device, developed for measurement of the flow speed are analog-to-analog converter (ADC), supply voltage stabilizer and the interface with PC. The realization of the analog-to-analog converter depends on the requirements regarding the accuracy from the point of view of the cost, 12-digit ADC are selected, for the unique high precision sensors- 24-digit devices , in particular, microconverters ADuC824 or ADuC834, considered above [205]. Voltage stabilizer must meet the requirements of low voltage electronics and be based on the circuit of voltage formation, numerically equal to the value of band gap ( $V_{REF}=1.2\text{ V}$ ) – it is the integrated circuit of the stabilizer with the low voltage drop on the control element ADP3367AR. For the realization of the

interface, a universal serial USB microcontroller FT232R manufactured by the company FTDI, is selected.

Taking into account the fact that problems of the engineering realization of the universal components of the flow sensor device do not contain any novelty, they are rather universal for the greater part of modern microelectronic sensors, that is why their detailed consideration is not expedient.

The important aspect is the stress on the signal converters, which determine the specific features of the developed flow devices and are the subject of the study. The selection of a certain type of the considered signal converters depends on the specific designation of the flow sensor. In such sensors, in particular, if there are no requirements to the extended range of measuring flows, the selection of the signal converters #1 or #2 is expedient.

Signal converter #3 is expedient if it is necessary to realize sensors for wide range of flow speed measurement, provided by the controlled warming up of the thermoresistors. This type of the converter is expedient in the sensors of biomedical designation if the maximum warming up temperature of the flow is limited and energy consumption limitation is actual.

This is realized by a wide range of the pulse, in particular Sleep Mode [101], operation modes. Signal converters #4 and #5 are actual if there exists the necessity to provide high sensitivity of the flow sensor and minimize the stray heating circuit.

In general, signal converters, presented in the given study are the result of the complex approach to the solution of the problem, dealing with the improvement of technical characteristics of the thermal flow sensors, and these converters are suitable both for the realization microflows sensors (units of the milliliters of the fluid per minute) and flow sensors with large mass transfer (up to hundreds of liters per minute), and meet the requirements of modern energy saving low-voltage electronics.

#### **6.4. Circuit functional organization of the push-pull d.c. amplifiers, characteristics of which correspond to system requirements**

It is well known that all the necessary analog blocks, such as, voltage buffers, normalizing amplifiers, current voltage and voltage-current converters, difference amplifiers and others can be realized on the base of the amplifiers [122,123]. The best indices for the construction of the high linear analog devices have PPDC with the distributed amplification channels which allow to considerably reduce the level of uncorrectable errors. At the same time, the construction of such PPDC requires the exact setting of the working point current [134]

The generalized structural diagram of PPDC may have the view, shown in Fig.6.38. The Principal scheme of PPDC is shown in Fig.6.39 [207]. Characteristics of the circuit, in particular, AFC, PFC and non-linearity are shown in Fig. 6.40

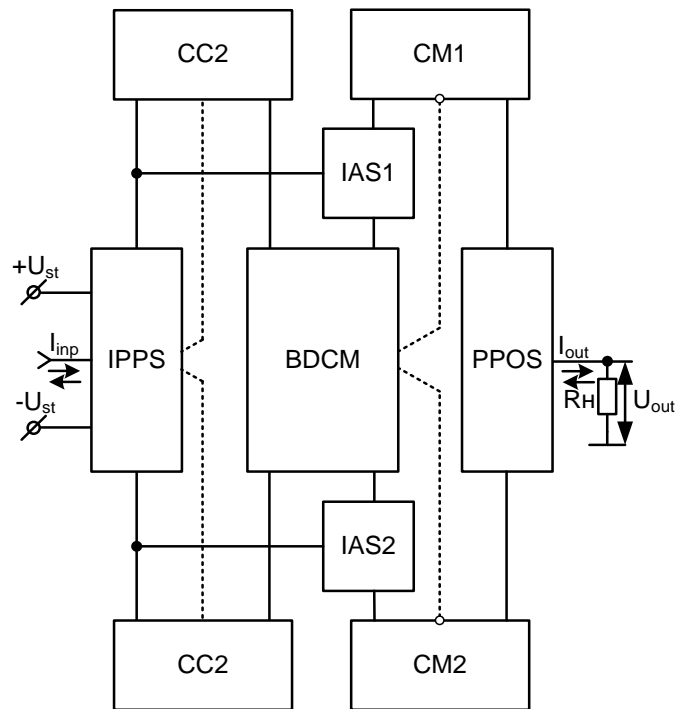


Fig. 6.38. Generalized structural diagram of PPDC

The amplifier contains IPPS, constructed on VT6–VT9 transistors. Working point of this stage is set by the current sources  $I_1$  and  $I_2$ , and transistors VT1–VT4. For d.c. mode setting of the transistors VT7, VT8 and VT18,VT21 of IAS BDCM is used, built on the transistors VT14, VT15, VT19,VT20, and CC, built on the transistors VT5, VT11, VT13 and VT10, VT12, VT16 correspondingly. Transistors VT17, VT23, VT25, VT26 and VT22, VT24, VT27, VT28 form complex Wilson reflectors that provide the decoupling of IAS with the output of the circuit.

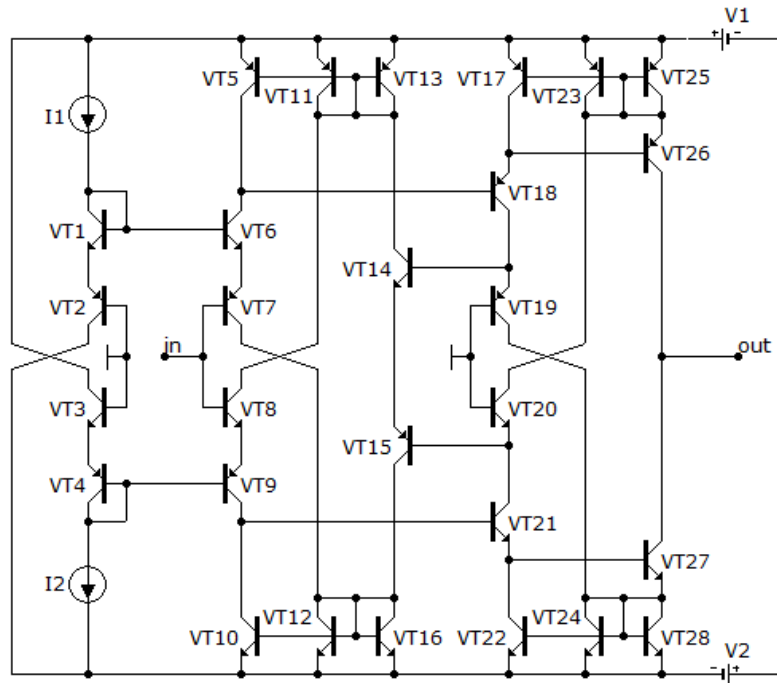


Fig. 6.39. Principal scheme of PPDCA

Current amplification factor in Fig. 6.39 can be determined by the formula (4.31). Channels amplification factors are determined:

$$K'_i = K'_{iinp} \cdot K'_{IAS} \cdot K'_{iout};$$

$$K''_i = K''_{iinp} \cdot K''_{IAS} \cdot K''_{iout},$$

where  $K'_{iinp}$ ,  $K''_{iinp}$  – IPPS current amplification factor in the upper and low channels correspondingly, determined by the formulas (4.30);  $K'_{IAS}$ ,  $K''_{IAS}$  – current amplification factor of IAS, determined:

$$K'_{IAS} = \frac{\beta^{p-n-p}}{\sqrt{1 + \left(\frac{f}{f_p}\right)^2}}; \quad K''_{IAS} = \frac{\beta^{n-p-n}}{\sqrt{1 + \left(\frac{f}{f_p}\right)^2}};$$

$K'_{iout}, K''_{iout}$  – current amplification factors of Wilson mirrors in the upper and low channels correspondingly  $K'_{iout} \approx K''_{iout} \approx 1$ .

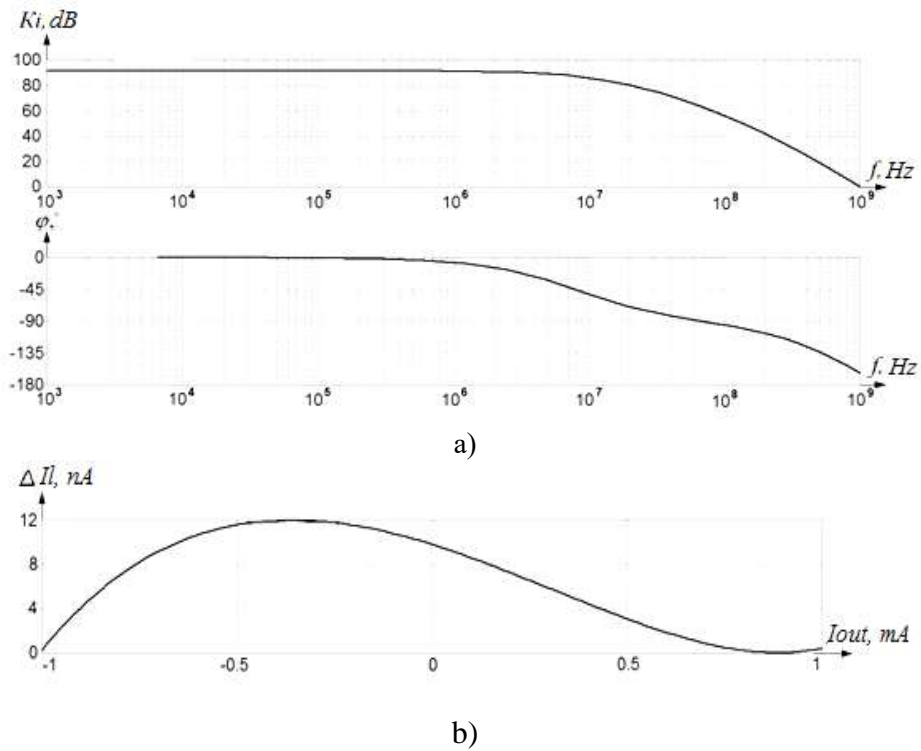


Fig. 6.40. Results of PPDCA modeling: a) AFC i PFC; b) non-linearity of the transfer characteristic

PPDCA provides such characteristics:

- - amplification factor  $K_i$  – 95 dB;
- linearity error  $\delta_l = 0,0006\%$  ;
- zero shift current – 5 mA;

- range of the output current –  $\pm 1$  mA;
- range of the output voltage –  $\pm 10$  V;
- input resistance – 3,6 k $\Omega$ ;
- frequency of full undistorted power – 850 kHz;
- unity gain frequency – 980 MHz.

PPDCA were constructed according to the considered structural functional organization, these PPDCA are protected by the Patents of Ukraine [183, 207–289].

### 6.5. High-linear current-voltage and voltage-voltage converters with the parametric correction of the zero-shift

Construction of CVC and VVC is realized using an operational amplifier, connected according to the circuit with deep feedback (DF) [133, 198]. It is known that the application of the current amplifier with low-resistance input has certain advantages and enables to considerably decrease the impact of the capacity of the input signal source and construct multiple digit fast acting current DAC as well as ADC on their base [167, 195].

In [197, 199] it was proved that for the construction of high linear CVC it is expedient to use PPDCA with low input resistance  $r_{in}$ , their structural functional organization is shown in Fig. 6.41. Principle diagram is shown in Fig. 6.42 [268]. Characteristics of the circuit, in particular, AFC, PFC, non-linearity are shown in Fig. 6.43.

The amplifier contains IPPS, built on the transistors VT11 and VT12. The working point of this stage is set by the current source I1, and transistors VT1–VT8. For d.c. mode setting of the transistors VT20 and VT23 of IAS BDCM is used, built on the transistors VT16, VT17, VT21, VT22, and CC, built on the transistors VT9, VT10, VT15 and VT13, VT14, VT18 correspondingly. Transistors VT19, VT24–VT28, VT31, VT32 form Wilson mirrors and provide the decoupling of IAS with PPOS, which is built on the transistors VT29, VT30, VT33, VT34.



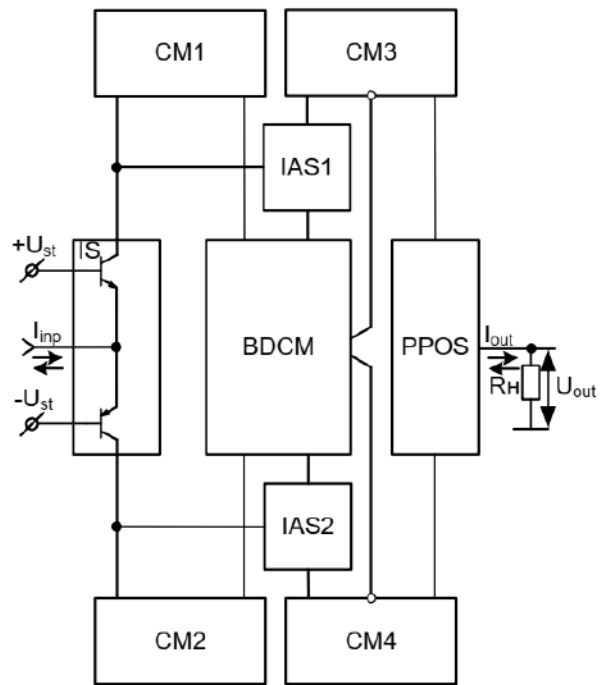


Fig. 6.41. Structural-functional organization of PPDCA with low input resistance for CVC

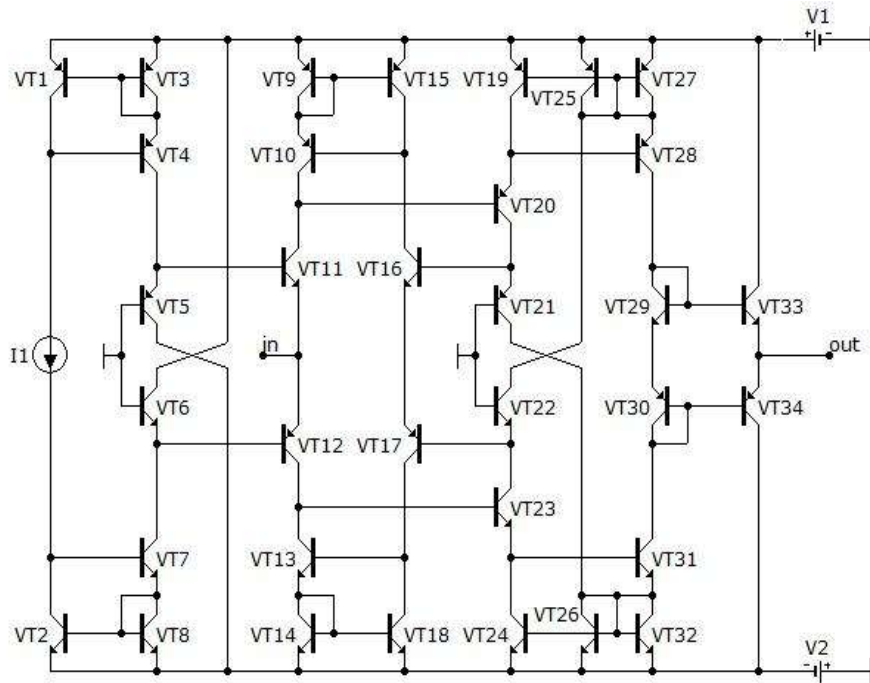
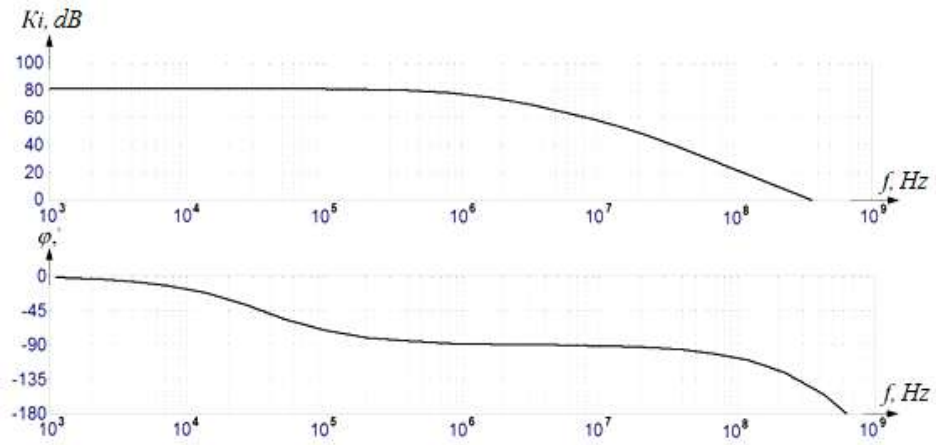
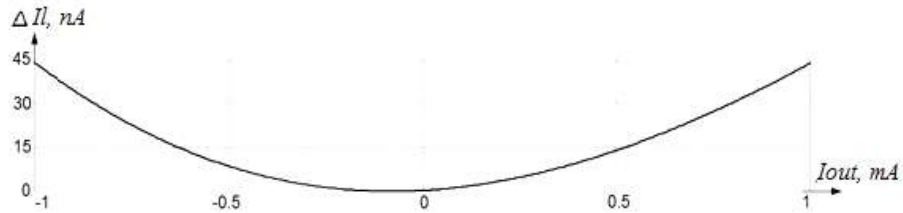


Fig. 6.42. Block diagram of PPDCA with low input resistance for CVC



a)



b)

Fig 6.43. Results of modeling of PPDCA with low input resistance for CVC: a)AFC and PFC; b) non-linearity of the transfer characteristic

Characteristic feature of PPDCA on the bipolar transistors is non-zero input current, that leads to the emerging of zero shift error  $\Delta U_{sh0}$ , and

$$\Delta U_{sh0} = \Delta I_{sh0} \cdot R_M, \text{ if } I_{in} = 0.$$

To decrease zero shift error, the method of the structural-functional organization of PPDCA with auto correction of zero-shift is suggested, its diagram is shown in Fig. 6.44.

Unit of zero auto correction (UZA), which consists of the simulator of the input stage (ISS), currents converter (CC1, CC2), current mirrors (CM1, CM2) and transistors VT1–VT10, provides auto correction of the current  $I_{sh0}$  by parametric method, so that  $\Delta I_{sh0} \rightarrow 0$ . This, in its turn, enables to decrease the error of current shift by 1–2 orders.

BDCM together with CM3–CM6, provide automatic balancing of the amplification in the upper and low amplification channels, built on BK, ПK1, ПK2 and PPOS.

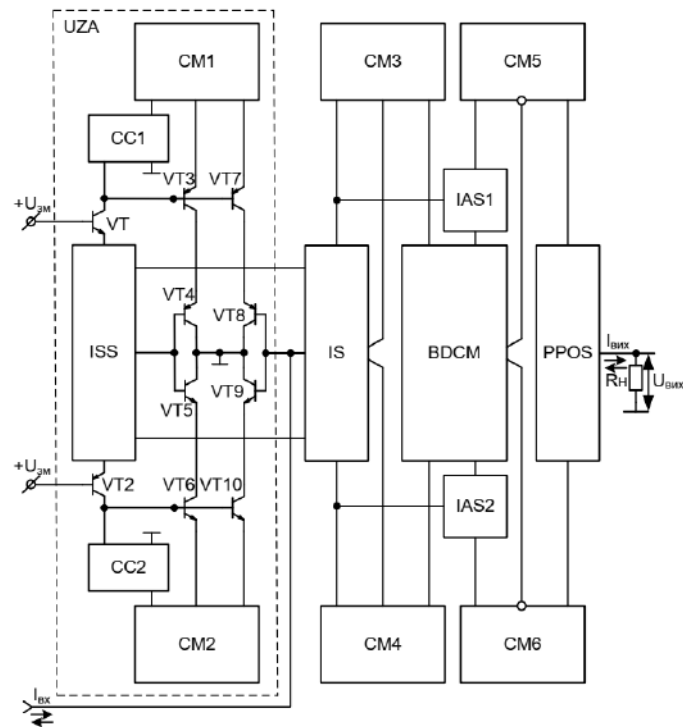


Fig. 6.44. Structural functional organization of PPDCA with auto correction of zero shift

PPDCA, built according to the considered structural functional organization, provides the following characteristics:

- amplification factor  $K_i$  – 125 dB;
- linearity error  $\delta_l = 0,000016\%$  ;
- zero shift current – 90 nA;
- range of the output current –  $\pm 1$  mA;
- range of the output voltage –  $\pm 10$  V;
- input resistance – 3,4 k $\Omega$ ;
- frequency of the complete non-distorted power – 600 kHz;
- unity gain frequency – 800 MHz.

According to the considered structural- functional organization PPDCA were built, they are protected by the patents of Ukraine [183, 207–289].

## 6.6. High linear fast acting buffer voltage devices with push-pull organization

Buffer devices are used for matching the input signal from highohmic source with low ohmic input of the amplifier [170] and are also called voltage repeaters and have the following properties [177]:

- amplification factor is rather close to 1;
- input resistance is high;
- output resistance is low.
- Buffer devices are used in case of matching of:
  - input of the high linear ADC with the current signal source;
  - input of the high linear ADC with the voltage signal source;
  - output of the capacitor DAC.

Structural-functional organization of the high linear-buffer devices on the base of the push-pull symmetric structures (PPSS) [195, 290] is suggested; these structures are shown in Fig. 6.45, where  $K'_i, K''_i$  – amplifying stages; CM1, CM2 – current mirrors; BS – balancing circuit. Depending on the usage in case of matching, the input circuits can be constructed both on bipolar and field-effect transistors.

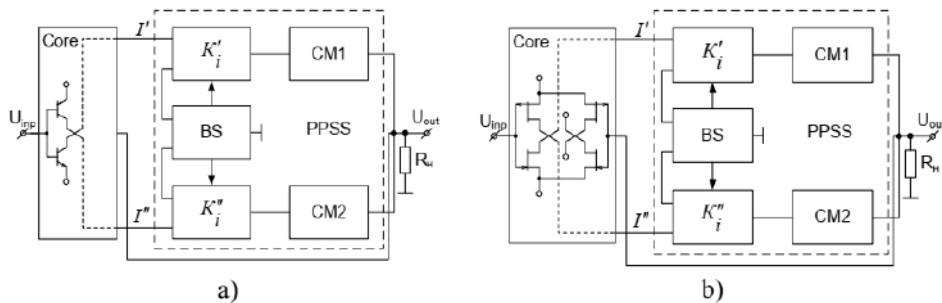
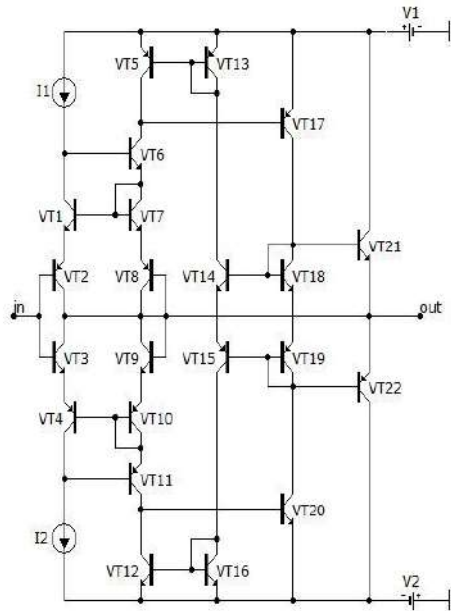
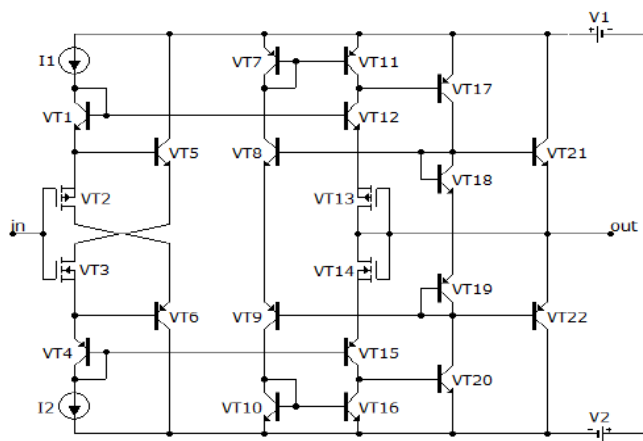


Fig. 6.45. Structural-functional organization of the high-linear buffer devices on the base of PPSS with the input stages on: a) bipolar transistors; b) field-effect transistors

The base of the device is a core, which, in its turn, is also built on the base of PPSS. Usage of PPDCA enables to increase the loading capacity and maintain the set linearity of the circuit core. Principle diagrams, constructed according to the proposed structural-functional organization, is shown in Fig.6.46 [291, 292]. The errors of the transfer characteristics are given in Fig. 6.47.

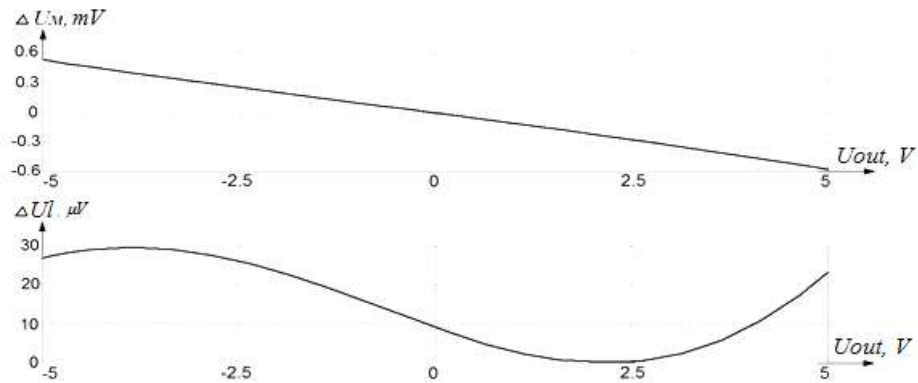


a)

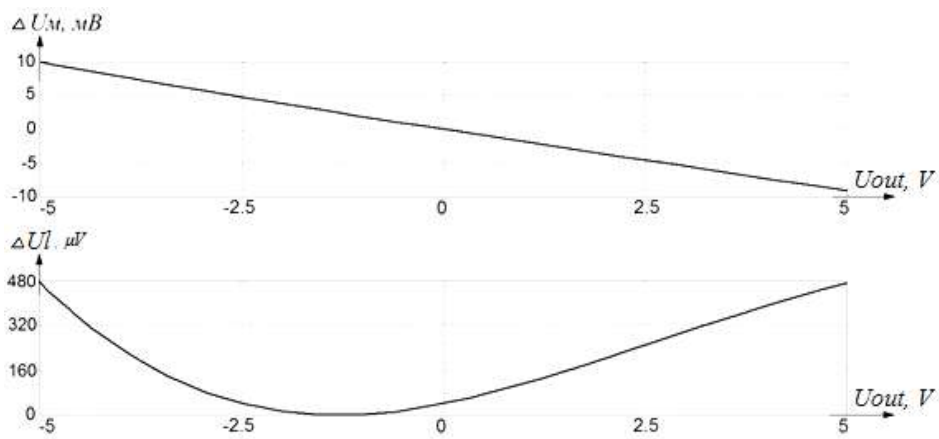


b)

Fig 6.46. Principle diagrams of the buffer devices on the base of PPSS with the input stages on: a) bipolar transistors; b) field-effect transistors



a)



b)

Fig. 6.47. Errors of the transfer characteristics of the buffer devices with the input stages on: a) bipolar transistors; b) field-effect transistors

High linear buffer devices, constructed according to the structural-functional organization on the base of PPSS, provide such characteristics:

- range of the input signal  $-\pm 5\text{V}$ ;
- output current  $-\pm 5\text{ mA}$ ;
- zero shift error  $\Delta U_{sh0} \leq 10\text{ mV}$ ;
- scale error  $\delta_{\mathcal{M}} \leq 0,0001\%$ ;

- linearity error  $\delta_l = 0,000005\%$  .

Buffer devices, protected by the patents of Ukraine [291–309] are constructed according to the considered structural functional organizations.

### 6.7. Amplifier of the difference currents for high sensitive comparators

To provide the operation of the comparison circuit (CC) it is necessary to limit the amplitude of the input signal, because the exceedance of the acceptable level may lead to the failure of CC mode. Simultaneously, in case of a small input signal the CC will not function. That is why, it is necessary to use the amplifier of the current differences, its structural functional organization is shown in Fig. 6.48.

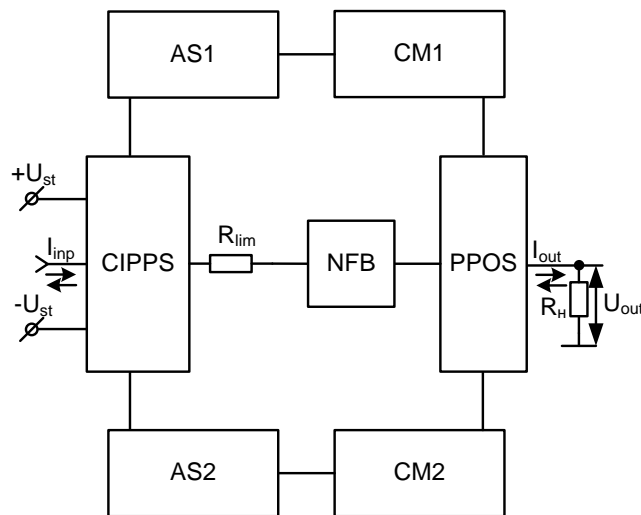


Fig. 6.48. Structural-functional organization of current difference amplifier for the high sensitive comparator

In Fig: CIPPS- compound input push pull stage, NFB- nonlinear: feedback; PPOS- output stage,  $R_{lim}$  – resistor, limiting the impact of NFB on IPPS. Principal diagram of the difference currents amplifier for the high sensitive comparator is shown in Fig. 6.49 [310]. The characteristics of the circuit are presented in Fig. 6.50, 6.51. According to the considered structural- functional organization, a number of devices are constructed; they are protected by the patents of Ukraine [310–316].



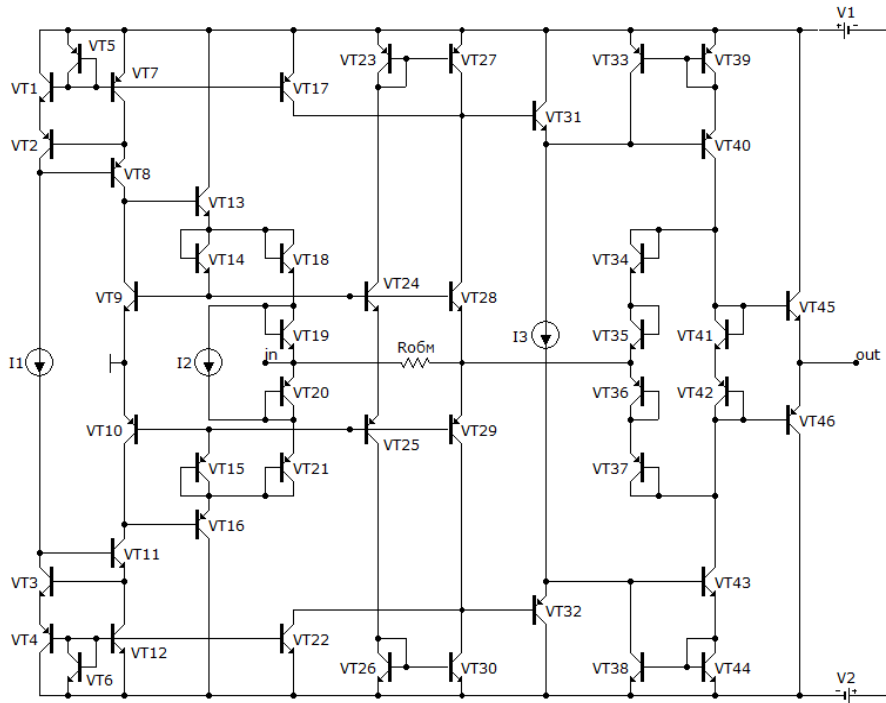


Fig. 6.49. Circuit diagram of the current difference amplifier for high-sensitive comparator

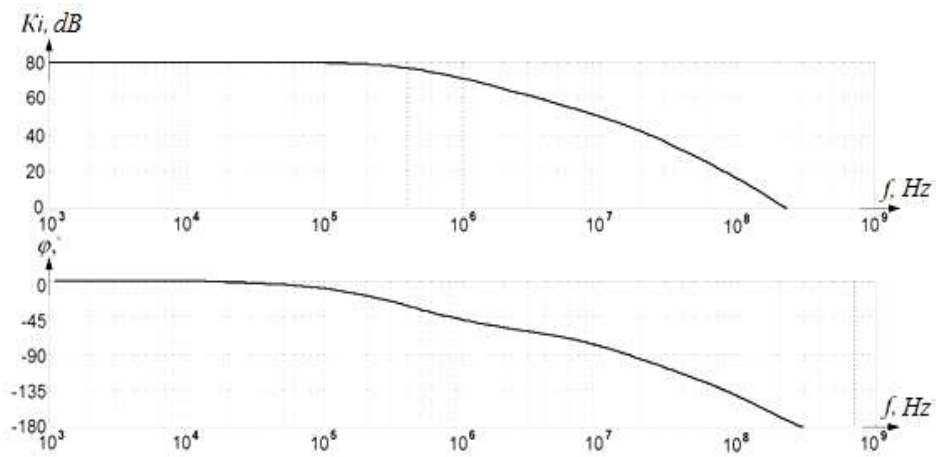


Fig.6.50. AFC and FAC of the amplifier of the current difference for the high-sensitive comparators

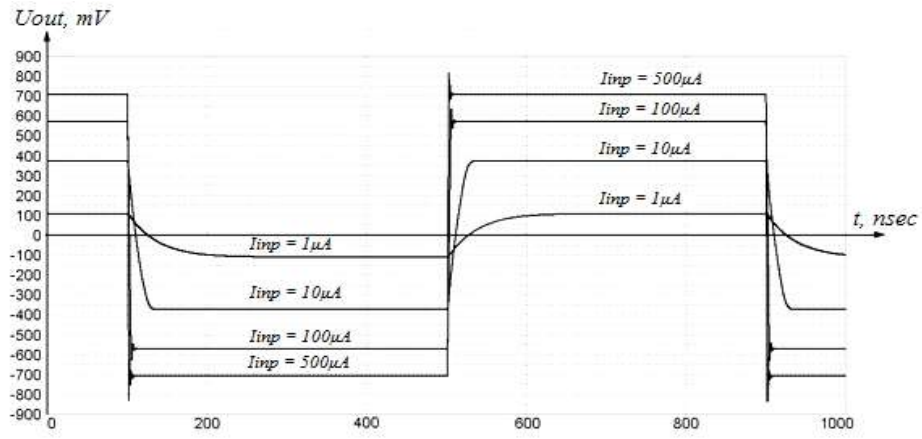


Fig 6.51. Transient characteristic of the currents difference for the high-sensitive comparators

## 7. References

- [1] Mohamed Gad-el-Hak. Flow Control: Passive, Active, and Reactive Flow Management. – Cambridge University Press. 2000.
- [2] E. L. Upp, Paul J. LaNasa. Fluid flow measurement: a practical guide to accurate flow measurement. – Gulf Professional Publishing, 2002.
- [3] David W. Spitzer. Flow Measurement: Practical Guides for Measurement and Control. – The Instrumentation, Systems, and Automation Society. 2001.
- [4] Richard Miller. Flow Measurement Engineering Handbook. – McGraw-Hill Professional. 1996.
- [5] Кремлевский П. П. Расходомеры и счетчики количества веществ / П. П. Кремлевский. – Изд. Политехника, 2004.
- [6] Fleming W.J. Overview of automotive sensors // Sensors Journal, IEEE. – 2001. – Vol. 1, No. 4. – P. 296–308.
- [7] P. Gravesen, J. Branebjerg, O.S. Jensen. Microfluidics – a review // J. Micromech. Microeng. – 1993. – No. 3. – P. 168–182.
- [8] P. Norlin, O. Öhman, B. Ekström, L. Forssen. A chemical microanalysis system for the measurement of pressure, flow rate, temperature, conductivity, UV-absorption and fluorescence // Sensors and Actuators: B. – 1998. – No. 49. – P. 34–39.
- [9] N.T. Nguyen. Micromachined flow sensors – a review // Flow Meas. Instrum. – 1997. No. 8. – P. 7–16.
- [10] N.T. Nguyen, R. Kiehnscherf. Low-cost silicon sensors for mass flow measurements of liquids and gases // Sens. Actuators A: Phys. – 1995. – No. 49. – P. 17–20.
- [11] J. Chen, Z.F. Fan, J. Zou, J. Engel, C. Liu. Two-dimensional micromachined flow sensor array for fluid mechanics studies // J. Aerospace Eng. – 2003. – No. 16. – P. 85–97.
- [12] J. VanKuijk, T.S.J. Lammerink, H.-E. de Bree, M. Elwenspoek, J.H.J. Fluitman. Multi-parameter detection in fluid flows // Sensors and Actuators A: Phys. – 1995. – No. 47. – P. 369–372.
- [13] Jungkyu Kim, Bruce K. Gale. Rapid prototyping of microfluidic systems using a PDMS/polymer tape composite // Lab. Chip. – 2009. – Vol. 9. – P. 1290–1293.
- [14] Rebecca L. Rich, Adam R. Miles, Bruce K. Gale, David G. Myszka.

- Detergent screening of a GPCR using serial and array biosensor technologies // *Anal. Biochem.* – 2009.– Vol. 386, No. 1. – P. 98–104.
- [15] Kathryn A. Smith, Bruce K. Gale, John C. Conboy. Micropatterned fluid lipid bilayer array // *Anal. Chem.* Vol. 80, No. 21. – P. 7980–7987.
- [16] Niel Crews, Timothy A. Ameel, Carl Wittwer, Bruce Gale. Flow- Induced Thermal Effects on Spatial DNA Melting // *Lab. Chip.* – 2008. – Vol. 8. – P. 1922–1929.
- [17] Mark A. Eddings, Michael A. Johnson, Bruce K. Gale. Determin- ing the optimal PDMS–PDMS bonding technique for microfluidic devices // *J. Micromech. Microeng.* – 2008. – Vol. 18. – P. 1–4.
- [18] Niel Crews, Carl Wittwer, Bruce Gale. Continuous-Flow Thermal Gradient PCR // *Biomed. Microdevices.* – 2008. – Vol. 10, No. 2. – P. 13–19.
- [19] Bruno Frazier, Karin D. Caldwell, Bruce K. Gale, Ian Papautsky. Integrated micromachined components for biological analysis systems // *Journal of Micromechatronics.* – 2000. – Vol. 1, No. 1. – P. 67–84.
- [20] Bruce K. Gale. Novel Techniques and Instruments for Field Flow Fractionation of Biological Materials // *Proc. 225th ACS National Meeting, New Orleans, LA, March 23–27, 2003.* – P. 107–109.
- [21] Electronic Encyclopedia Wikipedia. [Web resource]: [http:// wikipedia.org](http://wikipedia.org).
- [22] Sensors of electric magnetic radiation for bioengineering research / G. S. Tymchyk; V. I. Skytsiuk, M. A. Waintraub, T. R. Klochko. – K. : S.E. Lesia, 2004.
- [23] Web-resource Fluidic Flowmeters. – Access mode : <http://www.fluidicflow-meters.com>.
- [24] Web-resource Pentagon Reports. – Access mode : <http://www.stormingmedia.us>.
- [25] George Mon. Advanced Fluidic Temperature Studies // Storming Media. Pentagon Reports. [Web-resource] – Access mode : <http://www.stormingmedia.-us/89/8987 /D898700.html>.
- [26] Robert W. Young, Leonard D. Dansbury. Fluidic Interface Means // Storming Media. Pentagon Reports. – Access mode : <http://www.stormingmedia. us/95/9527/ D952700.html>.
- [27] Allen B. Holmes. Electro Fluidic Actuator // Storming Media. Pentagon Reports. [Web-resource] – Access mode : <http://www.stormingmedia.us/28/2898/D289800.html>.

- [28] Walter M. Posingies. Advanced Fluidic Temperature Studies. // Storming Media. Pentagon Reports. [Web-resource] – Access mode : <http://www.stormingmedia.us/74/7413/A741360.html>.
- [29] Leonard M. Sieracki. Handbook of Fluidic Sensors // Storming Media. Pentagon Reports. [Web-resource] – Access mode : <http://www.stormingmedia.us/54/5411/A541140.html>.
- [30] Carl J. Campagnuolo; Harold S. Duff; Henry C. Lee; Frank E. Blodgett; Leon Scheinine. A Fluidic Generator as an Environmental and Safety Device for the SUU53/A Cartridge Dispenser // Storming Media. Pentagon Reports. [Web-resource] – Access mode : <http://www.stormingmedia.us/02/0218/A021830.html>.
- [31] E. Meng, S. Gassmann, Y.-C. Tai. A MEMS body fluid flow sensor // Micro Total Analysis Systems. – 2001. Monterey, CA. – P. 167–168.
- [32] S. Wu, Q. Lin, Y. Yuen, Y.-C. Tai. MEMS flow sensors for nanofluidic applications // Sensors and Actuators A : Phys. – 2001. – No. 89. – P. 152–158.
- [33] E. Meng, Y.-C. Tai. A Parylene MEMS flow sensing array // Transducers 2003. Boston, MA, June 8–12, 2003. – P. 686–689.
- [34] C.Q. Yang, H. Soeberg. Monolithic flow sensor for measuring milliliter per minute liquid flow // Sensors and Actuators A : Phys. – 1992 – No 33. – P. 143–153.
- [35] Y. Itoh and K. Takahashi. Nano thermal sensor for micro fluidic devices // Proc. 22nd Sensors Symposium. – 2005. – P. 171–174.
- [36] Compact portable ultrasonic fluid flow meters PORTAFLOW. [Web resource] – Access mode : <http://www.energotest.ru/fm.html>.
- [37] Arshak Poghosian, Lars Berndsen, Michael J. Schöning. Chemical sensor as physical sensor: ISFET-based flow-velocity, flowdirection and diffusion-coefficient sensor // The 16th European Conference on Solid-State Transducers September 15-18, – 2002. TP33 – P.649–650.
- [38] D. Lee, X. Sun, E. Quevy, R. T. Howe, T.-J. King. WetFET-Novel Fluidic Gate-Dielectric Transistor for Sensor Applications // IEEE VLSI-TSA Meeting Technical Digest. – 2007. – P. 124–125.
- [39] P. Bergveld. Thirty years of ISFETology: what happened in the next 30 years and what may happen in the next 30 years // Sensors and Actuators B. – 2003. – No. 88. – P. 1–20.
- [40] B.W. van Oudheusden. Silicon thermal flow sensors // Sensors and

- Actuators A: Phys. – 1992. – No. 30. – P. 5–26.
- [41] M. Ashauer, H. Glosch, F. Hedrich, N. Hey, H. Sandmaier, W. Lang. Thermal flow sensor for liquids and gases based on combinations of two principles // Sensors and Actuators A. – 1999. – Vol. 73. – P. 7–13.
- [42] F. Jiang, Y.-C. Tai, C.-M. Ho, R. Karan, M. Garstener. Theoretical and experimental studies of micromachined hot-wire anemometers // International Electron Devices Meeting (IEDM), San Francisco, December, 11–14. – 1994. – P. 139–142.
- [43] J.J. van Baar, R.W. Wiegerink, T.S.J. Lammerink, G.J.M. Krijnen, M. Elwenspoek. Micromachined structures for the thermal measurements of fluid and flow parameters // J. Micromech. Microeng. – 2001. – No. 11. – P. 311–318.
- [44] T. S. T. Lammerink, N. R. Tas, M. Elwenspoek, J. H. J. Fluitman. Micro-liquid flow sensor // Sensors and Actuators A. – 1993. – P. 45–50.
- [45] P.M. Handford, P. Bradshaw. The pulsed-wire anemometer // Exp. Fluids 7. – 1989. – P. 125–132.
- [46] Ellis Menga, Po-Ying Li, Yu-Chong Tai. A biocompatible Parylene thermal flow sensing array // Sensors and Actuators A. – 2008. – No. 144. – P. 18–28.
- [47] Bartsch de Torres, C. Renschb, T. Thelemannc, J. Müller, M. Hoffmann. Fully Integrated Bridge-type Anemometer in LTCCbased Microfluidic Systems Advances [Web-resource] // Science and Technology. – 2008. – Vol. 54. – P. 401–404. – Access mode : <http://www.scientific.net>.
- [48] Margelov A. Gas-consumption sensors of the Honeywell company [Web resource] / A. Margelov // Chip News. – 2005. – № 9 (102). – C. 56–58. – Access mode to the journal: [www.chip-news.ru](http://www.chip-news.ru).
- [49] N.-T. Nguyen, W. Dotzel. Asymmetrical locations of heaters and sensors relative to each other using heater arrays: a novel method for designing multi-range electrocaloric mass-flow sensors // Sensors and Actuators: A Phys. – 1997. – Vol. 62. – P. 506–512.
- [50] N. Sabate, J. Santande, L. Fonseca, I. Gracia, C. Cane. Multi-range silicon micromachined flow sensor // The 16th European Conference on Solid-State Transducers. – 2002. – P. 202–205.
- [51] Ihsan Hariadi, Hoc-Khiem Trieu, Wilfried Mokwa, Holger Vogt. M. Integrated MFlow Sensor with Monocrystalline Silicon Membrane Operating in Thermal Time-of-Flight Mode // The 16th European

- Conference on Solid-State Transducers. – 2002. – P. 115–116.
- [52] ELDRIDGE PRODUCTS INC Thermal Gas Mass Flow Measurement and Control Instrumentation. [Web-resource] – Access mode : <http://www.cmctechnologies.com.au/index.htm>.
- [53] Hot-wire air flow meters Testo 405, Testo 425. [Web resource] – Access mode : <http://www.inducr.com.ua> .
- [54] Y. Fang and W. W. Liou. Computations of the Flow and Heat Transfer in Microdevices Using DSMC With Implicit Boundary Conditions // J. Heat Transfer. – 2002. – Vol. 124. – P. 338–345.
- [55] W.W. Liou and Y. Fang. Implicit Boundary Conditions for Direct Simulation Monte Carlo Method in MEMS Flow Predictions // CMES. – 2000. – Vol. 1, No. 4, – P. 119–128.
- [56] Y. Weiping, L. Chong, L. Jianhua, M. Lingzhi and N. Defang. Thermal distribution microfluidic sensor based on silicon // Sensors and Actuators B. – 2005. – Vol. 108. – P. 943–946.
- [57] Koji Takahashi, Taku Higuchi, Yohei Ito, Tatsuya Ikuta, Kunihiro Nagayama. Study on Local Heat Transfer of Nano Fluidic Sensor // Proceedings of the 23rd sensor symposium. – 2006. – P. 279–282.
- [58] Knauss H., Gaisbauer U., Wagner S., Buntin D., Maslov A., Smorodsky B., Betz J. Calibration experiments of a new active fast response heat flux sensor to measure total temperature fluctuations. Part I. Introduction to the problem // Intern. Conf. on the Methods of Aerophys. Research.: Proc. Pt. III. Novosibirsk. – 2002. – P. 85–91.
- [59] Knauss H., Gaisbauer U., Wagner S., Buntin D., Maslov A., Smorodsky B., Betz J. Calibration experiments of a new active fast response heat flux sensor to measure total temperature fluctuations. Part III. Heat flux density determination in a short duration wind tunnel // Intern. Conf. on the Methods of Aerophys. Research. : Proc. Pt. III. Novosibirsk. – 2002. – P. 102–112.
- [60] G. Kaltsas, D. Goustouridis, A. G. Nassiopoulou, D. Tsoukalas, S. Chantzandroulis. Flow study in both turbulent and laminar flow with a system of thermal flow and capacitive pressure sensors. – Access mode : <http://www.imel.demokritos.gr>.
- [61] G. Kaltsas, A. A. Nassiopoulos and A. G. Nassiopoulou. Characterization of a Silicon Thermal Gas-Flow Sensor With Porous Silicon Thermal Isolation // IEEE Sensors Journal. – 2002. – № 5. – P. 22–29.

- [62] Y. Mo, Y. Okawa, K. Inoue and K. Natukawa, Low-voltage and lowpower optimization of micro-heater and its on-chip drive circuitry for gas sensor array // *Sensor and Actuators A*. – 2002. – Vol. 100. – P. 94–101.
- [63] Characteristic features of thermal calculation of pulse power stages. Components and technologies [Web resource] – Access mode : <http://www.compitech.ru>.
- [64] Tsydelko V. D. Uncertainty of measurement. Data processing and measurement results submitting / Tsudelko V.D., Yaremchuk N.A. – K.: IVT Polytechnica, 2002.
- [65] Program of thermal calculation SEMISEL 3.1 [Web resource] – Access mode : <http://www.tsdrive.com.ua>.
- [66] Calandra E. F. Introduction to PSPICE Using ORCAD for Circuits and Electronics // *Circuits and Devices Magazine, IEEE*. – 2005. – Vol. 21, No. – P. 26–27.
- [67] Micro-Cap 7.0, 8.0, 9.0 Electronic Circuit Analysis Program. Reference Manual. Spectrum Software. 2001, 2005, 2008. [Web resource] – Access mode : [www.spectrum-soft.com](http://www.spectrum-soft.com).
- [68] Desing J., Lindgren P. Sensor communication technology towards ambient intelligence // *Measurement Science and Technology*. – 2005. – Vol. 16. – P. 37–46.
- [69] Desing J. Sensor communication technology for the ambient intelligence creation / J. Desing, P. Lindgren // *Sensors and system* – 2005. – № 12. – C. 63–74
- [70] Dusad S., Diggavi S.N., Al-Dhahir N., Calderbank A. R. Diversity Embedded Codes: Theory and Practice // *IEEE Journal of selected topics in signal processing*. – 2008. – Vol. 2, No. 2. – P. 202–219.
- [71] Naffziger S. Microprocessors of the future: Commodity or engine growth? // *Solid-State Circuits Magazine, IEEE*. – 2009. – Vol. 1, No. 1. – P. 76–82.
- [72] Intelligent instrumentation products. The Handbook of Personal Computer. Instrumentation for Data Acquisition. Test. Measurement and Control. – Burr-Brown Corp. and Intelligent Instrumentation Inc, 1989.
- [73] John Brignell, Neil While. Intelligent Sensor System. – Institute of Physics Publishing Bristol and Philadelphia. IOP Publishing. 1996.
- [74] Lunze J. Notion of the state in systems theory and artificial intelligence //



- Intelligent Systems Engineering. – 1994. – Vol. 3, No. 4. – P. 201–210.
- [75] Wang Fei-Yue. Intelligent Systems in a Connected World // Intelligent Systems Engineering. 2009. – Vol. 24, No. 1. – P. 2–4.
- [76] Ivanov S. Yu. Analysis of the data processing algorithms for the intelligent pressure sensors / S. Yu. Ivanov, G. E. Kartalov // Measuring engineering – 1990. – № 3. – C. 26–29.
- [77] Xiao Fan Wang, Guanrong Chen. Complex networks: small-world, scale-free and beyond // Circuits and Systems Magazine, IEEE. – 2003. – Vol. 3, No. 1. – P. 6–20.
- [78] Ayazifar B. Can we make signals and systems intelligible, interesting, and relevant? // Circuits and Systems Magazine, IEEE. – 2009. – Vol. 9, No. 1. – P. 16–18.
- [79] Collins Luke. Cut the cord // Electronics. – 2007. – Vol. 5, No. 6. – P. 42–46.
- [80] Song E.Y.; Kang Lee. Understanding IEEE 1451-Networked smart transducer interface standard What is a smart transducer? // Instrumentation & Measurement Magazine, IEEE. – 2008. – Vol. 11, No. 2. – P. 11–17.
- [81] Leens F. An introduction to I2C and SPI protocols // Instrumentation & Measurement Magazine, IEEE. – 2009. – Vol. 12, No. 1. – P. 8–13.
- [82] Gorod A., Sauser B., Boardman J. System-of-Systems Engineering Management: A Review of Modern History and a Path Forward // Systems Journal, IEEE. – 2008. – Vol. 2, No. 4. – P. 484–499.
- [83] Azarov O. D. High linear digit wise ADC with weight redundancy for the system of registration and processing of signals: monograph / O. D. Azarov, O. A. Arkhipchuk, S. M. Zakharchenko. – Vinnytsia: UNIVERSUM - Vinnytsia, 2005.
- [84] Ivanov V. S. New solution of Freescale Semiconductor for the embedded control systems and data collection [Web resource] / V.S. Ivanov, I. N. Chepurin // Access mode : [www.freescale.com/files/abstract/global/RUSSIA\\_ART\\_3.doc](http://www.freescale.com/files/abstract/global/RUSSIA_ART_3.doc).
- [85] Rabaey J., Ammer J., Otis B.; Burghardt F., Chee Y.H.; Pletcher N., Sheets M., Qin H. Ultra-low-power design // Circuits and Devices Magazine, IEEE. – 2006. – Vol. 22, No. 4. – P. 23–29.
- [86] Kwong Joyce, Chandrakasan Anantha. Advances in Ultra-LowVoltage Design // Solid-State Circuits Newsletter, IEEE. – 2008. – Vol. 13, No. 4.

– P. 20–27.

- [87] Alippi C., Anastasi G., Di Francesco M., Roveri M. Energy management in wireless sensor networks with energy-hungry sensors // *Instrumentation & Measurement Magazine, IEEE*. – 2009. – Vol. 12, No. 2. – P. 16–23.
- [88] Jianyong Lin; Wendong Xiao; Lewis F.L.; Lihua Xie. EnergyEfficient Distributed Adaptive Multisensor Scheduling for Target Tracking in Wireless Sensor Networks. *Instrumentation and Measurement, IEEE*. – 2009. – Vol. 58, No. 6. – P. 1886–1896.
- [89] Vittoz Eric A. The Electronic Watch and Low-Power Circuits // *Solid-State Circuits Newsletter, IEEE*. – 2008. – Vol. 13, No. 3. – P. 7–23.
- [90] Chang-Tzu Wang; Ming-Dou Ker. Design of Power-Rail ESD Clamp Circuit With Ultra-Low Standby Leakage Current in Nanoscale CMOS Technology // *Journal of Solid-State Circuits, IEEE*. – 2009. – Vol. 44, No. 3. – P. 956–964.
- [91] Lhermet H., Condemine C., Plissonnier M., Salot R., Audebert P., Rosset M. Efficient Power Management Circuit: From Thermal Energy Harvesting to Above-IC Microbattery Energy Storage // *Journal of Solid-State Circuits, IEEE*. – 2008. – Vol. 43, No. 1. – P. 246–255.
- [92] Khorovits P. Art of circuit engineering: in 2 volumes / P. Khorovits W. Hill. – M.: MIR, 1984.
- [93] Smolov V. B. Functional converters of information / V.B. Smolov. – L.: Energy Publishing House, 1981.
- [94] Alekseenko A. Z. Application of the precision analog microcircuits / A. G. Alekseenko, E. A. Kolombet, G. I. Starodub. – M.: Radio and Communication, 1985.
- [95] Brinali K. Measuring converters. Handbook: Translated from English /K. Brinali. – M.: MIR, 1991.
- [96] Gutnikov V. S. Integral electronics in measuring devices / V.S. Gutnikov. – L.: Energoatom Publishing House Leningrad Division, 1988.
- [97] Kolombet E. A. Microelectronic devices for the analog signals processing / E. A. Kolombet. – M.: Radio and communication, 1991.
- [98] Osadchuk O. V Microelectronic frequency converters on the base of the transistor structures with negative resistance / O. V. Osadchuk. – Vinnytsia: UNIVERSUM- Vinnytsia, 2000.
- [99] Kuprianov M. S. Engineering support of digital processing of signals. Reference book / M. S. Kuprianov, B. D. Matiushkin, V. E. Ivanova. – St.

Petersburg: Science and Engineering, 2000.

- [100] Barmena X. Applied laser medicine / X. Barmena, G. Muller. – M.: Interexpert, 1997.
- [101] Analog microcircuit engineering of measuring and sensor devices / [under the Editorship of Z. Gotra, R. Goliaka]. – Lviv: Publishing House of State University «Lvivska Polytechnica», 1999.
- [102] Schmalzel J.L., Rauth D.A. Sensors and signal conditioning // Instrumentation & Measurement Magazine, IEEE. – 2005. – Vol. 8, No. 2. – P. 48–53.
- [103] Ziegler S.; Woodward R.C.; Iu H., Borle, L.J. Current Sensing Techniques: A Review // Sensors Journal, IEEE. – 2009. – Vol. 9, No. 4. – P. 354–376.
- [104] Dvorkind T. G.; Eldar Y. C. Robust and Consistent Sampling // Signal Processing Letters, IEEE. – 2009. – Vol. 16, No. 9. – P. 739–742.
- [105] Candes E.J., Wakin M.B. An introduction to compressive sampling // Signal Processing Magazine, IEEE. – 2008. – Vol. 25, No. 2. – P. 21–30.
- [106] Treichler J. Signal processing: A view of the future, part 1 // Signal Processing Magazine, IEEE. – 2009. – Vol. 26, No. 2. – P. 116–120.
- [107] Treichler J. Signal processing: A view of the future, part 2 // Signal Processing Magazine, IEEE. – 2009. – Vol. 26, No. 3. – P. 83–86.
- [108] Rapuano S., Daponte P., Balestrieri E., De Vito L.; Tilden S.J., Max S.; Blair J. ADC parameters and characteristics // Instrumentation & Measurement Magazine, IEEE. – 2005. – Vol. 8, No. 5. – P. 44–54.
- [109] Fujimoto Y., Kanazawa Y., Re P.L.; Iizuka K.A. 100 MS/s 4 MHz Bandwidth 70 dB SNR Delta Sigma ADC in 90 nm CMOS // Journal of Solid-State Circuits, IEEE. – 2009. – Vol. 44, No. 6. – P. 1697–1708.
- [110] Sevenhans Jan, Craninckx Jan. Europe's Analog Design Experts Convened at 16th AACD Workshop // Solid-State Circuits Newsletter, IEEE. – 2007. – Vol. 12, No. 3.
- [111] Nauta Bram. Analog IC Design at the University of Twente // Solid-State Circuits Newsletter, IEEE. – 2007. – Vol. 12, No. 1. – P. 5–10.
- [112] Gang Liu, Haldi P., Tsu-Jae King Liu, Niknejad A.M. Fully Integrated CMOS Power Amplifier With Efficiency Enhancement at Power Back-Off // Journal of Solid-State Circuits, IEEE. – 2008. – Vol. 43, No. 3. – P. 600–609.
- [113] Ferreira L., Pimenta T., Moreno, R. CMOS implementation of precise

- sample-and-hold circuit with self-correction of the offset voltage // Circuits, Devices and Systems, IEE Proceedings. – 2005. – Vol. 152. No. 5. – P. 451–455.
- [114] Chih-Wen Lu. A Rail-To-Rail Class-AB Amplifier With an Offset Cancellation for LCD Drivers // Journal of Solid-State Circuits, IEEE. – 2009. – Vol. 44, No. 2. – P. 525–537.
- [115] Rashidzadeh R.; Muscedere R.; Ahmadi M.; Miller W. C. A Delay Generation Technique for Narrow Time Interval Measurement // Instrumentation and Measurement, IEEE. – 2009. – Vol. 58, No. 7. – P. 2245–2252.
- [116] Lin B.R., Huang C.L. Analysis and implementation of a novel softswitching pulse-width modulation converter // Power Electronics, IET. – 2009. – Vol. 2, No. 1. – P. 90–101.
- [117] Zero-Drift Single-Supply Rail-to-Rail Input/Output Operational Amplifier AD8551/52/54. Data sheet. [Web-resource] – Access mode : [www.analog.com](http://www.analog.com).
- [118] General-Purpose CMOS Rail-to-Rail Amplifiers AD8541/42/44. Data sheet. [Web-resource] – Access mode : [www.analog.com](http://www.analog.com).
- [119] R. Kersjes, F. Lienscher, E. Spiegel, Y. Manoli, W. Mokwa. An invasive catheter flow sensor with on-chip CMOS readout electronics for the on-line determination of blood flow // Sensors and Actuators A: Phys. – 1996. – Vol. 54. – P. 563–567.
- [120] Metrology. Terms and definitions: SSTU 2681–94. – Valid since 01.01.1995. – K.: Statestandard of Ukraine, 1995.
- [121] Krupelnytskyi L. V. Analog-digital devices of the self-correcting systems, for measurements and processing of low-frequency signals: monograph/ L. V. Krupelnytskyi, O. D. Azarov. – Vinnytsia: UNIVERSUM–Vinnytsia, 2005.
- [122] Walt Kester. ANALOG-DIGITAL CONVERSION / Walt Kester. – ADI: Central Application Department, March 2004.
- [123] Romanov V. A. Theory, methods of construction technical realization of the microprocessor-based convertors of the information form with higher reliability and performance: Extended abstract of Sc. (Eng.) Dissertation: 05.13.05 / V.A. Romanov. – K., 1994.
- [124] Ornatskyi P. P automatic measurements and devices (analog and digital) / P. P. Ornatskyi. 5<sup>th</sup> edition, revised and enlarged. – K.: Vyscha Shkola,

- 1986.
- [125] High performance converters of the information form / [A. I. Kondalev, V. A. Bagatskyi, V. A. Romanov, V. A. Fabrichev]. – K.: Naukova Dumka, 1987.
  - [126] Gudina F. New areas of application of the analog-to-digital converters with high resolution / F. Gudina // *Electronics*. – 1991. – №7. p 39-42.
  - [127] Azarov O. D. Fundamentals of the theory of analog-to-digital conversion, based on the redundant position computation systems: monograph / O. D. Azarov. – Vinnytsia: UNIVERSUM–Vinnytsia, 2004.
  - [128] Walter G. Jong. Op Amp applications handbook / Walter G. Jong. – Analog Devices series, 2004.
  - [129] Sokolov S. Analog integrated circuits / Sidney Sokolov; translated from English by A. B. Perezentsev. – M.: MIR, 1988.
  - [130] Alekseev A. G. Operation amplifiers and their application / A. G. Alekseev, G. V. Voishvillo. – M.: Radio and communication, 1989.
  - [131] Titse W. Semiconductor circuit engineering / W. Tilse, K. Shenk; translated from German. DMK Press. – M.: DMK Press, 2008. – Vol. 1.
  - [132] Kiarlone F. Voltage to current converted on the base of two measuring amplifiers / F. Kiarlone // *Electronic components and systems*. – 2010. – № 7. – P. 40–41.
  - [133] Folkenberry L. Application of the operation amplifiers and linear IC. I. L. Folkenberry; translated from English by L. M. Noimark. – M.: MIK, 1985.
  - [134] Azarov O. D. Push-pull d. c. amplifiers for multidigit converters of the information form: monograph / O. D. Azarov, V. A. Garnaga. – Vinnytsia: VNTU, 2011.
  - [135] Smith K. C. The Current-Conveyor – A New Circuit Building Block / K. C. Smith, A. Sedra // – *IEEE Proc.* – 1968. – №56. – P. 1368–1369.
  - [136] Sedra A. A second Generation Current-Conveyor and its Applications / A. Sedra, K. C. Smith // – *IEEE Trans.* – 1970. – CT-17. – P. 132–134.
  - [137] Lidgley F. J. Current-followers and a universal operational amplifier / F. J. Lidgley, C. Toumazou // – *Electronics World and Wireless World*. – 1984. – № 90(1577). – P. 40–43.
  - [138] Toumazou C. Novel Current-Mode Instrumentation Amplifier / C. Toumazou, F. J. Lidgley // – *Electron. Lett.* – 1985. – №21(15). – P. 640–642.

- [139] Toumazou C. Extending Voltage-Mode op-amps to Current-Mode Performance / C Toumazou, F. J. Lidgley, C.A. Makris // – IEE Proc. – 1990. – № 137(2). – P. 116–130.
- [140] Toumazou C. Novel Current-Mode Instrumentation Amplifier / C. Toumazou, F. J. Lidgley // – Electron. Lett. – 1989. – № 25(3). – P. 228–230.
- [141] Bruun E. Current-conveyor Based EMG Amplifier with Shutdown Control / E. Bruun, E. U. Haxthausen // – Electron. Lett. – 1990. – № 27(23). – P. 2172–2174.
- [142] Yodprasit U. High-precision CMOS current conveyor / U. Yodprasit // – Electron. Lett. – 2000. – Vol. 36, № 27(23). – P. 609–610.
- [143] Patent 3986134 USA, H 03 F 3/16. Push-pull amplifier circuitry / Kenji Yokoayama, Nippon Gakki Seizo Kabushiki Kaisha. – № 605172; filed 15.08.75; issued 12.10.76.
- [144] Patent 3852678 USA, H 03 F 3/26. Push-pull amplifier with current mirrors for determining the quiescent operating point / George Joseph Frye. – № 358152 ; filed 07.05.73 ; issued 12.10.76.
- [145] Patent 4031481 USA, H 03 F 3/16. Transistor amplifier / Tadao Yoshida assignor to Sony Corporation. – № 578195 ; filed 16.05.75 ; issued 21.06.77.
- [146] Technical description AD810: Low Power Video Op Amp with Disable / Analog Devices // Official site. – Access mode : [http://www.analog.com/static/importedfiles/data\\_sheets/AD810.pdf](http://www.analog.com/static/importedfiles/data_sheets/AD810.pdf)
- [147] Technical description AD811: High Performance Video Op Amp / Analog Devices // Official site. – Access mode : [http://www.analog.com/static/importedfiles/data\\_sheets/AD811.pdf](http://www.analog.com/static/importedfiles/data_sheets/AD811.pdf).
- [148] Technical description AD812: Dual, Current Feedback Low Power Op Amp / Analog Devices // Official site. – Access mode : [http://www.analog.com/static/importedfiles/data\\_sheets/AD812.pdf](http://www.analog.com/static/importedfiles/data_sheets/AD812.pdf).
- [149] Technical description AD813: Single Supply, Low Power Triple Video Amplifier / Analog Devices // Official site. – Access mode : [http://www.analog.com/static/importedfiles/data\\_sheets/AD813.pdf](http://www.analog.com/static/importedfiles/data_sheets/AD813.pdf).
- [150] Technical description AD815: High Output Current Differential Driver / Analog Devices // Official site. – Access mode : [http://www.analog.com/static/importedfiles/data\\_sheets/AD815.pdf](http://www.analog.com/static/importedfiles/data_sheets/AD815.pdf).

- [151] Technical description EL5160, EL5161, EL5260, EL5261, EL5360: 200MHz Low-Power Current Feedback Amplifiers / Intersil // Official site. – Access mode :<http://www.intersil.com/content/dam/Intersil/documents/fn73/fn7387.pdf>.
- [152] Technical description EL5162, EL5163, EL5262, EL5263, EL5362: 500MHz Low Power Current Feedback Amplifiers with Enable / Intersil // Official site. – Access mode : <http://www.intersil.com/content/dam/Intersil/documents/fn73/fn7388.pdf>.
- [153] Technical description EL5164, EL5165, EL5364: 600MHz Current Feedback Amplifiers with Enable / Intersil // Official site. – Access mode : <http://www.intersil.com/content/dam/Intersil/documents/fn73/fn7389.pdf>.
- [154] Technical description NCS2501: 1.1 mA 200 MHz Current Feedback Op Amp with Enable Feature / On semiconductor // Official site. – Access mode : <http://www.chipfind.ru/datasheet/pdf/onsemi/ncs2501.pdf>.
- [155] Technical description NCS2502: 650 A 110 MHz Current Feedback Op Amp with Enable Feature / On semiconductor // Official site. – Access mode : <http://www.chipfind.ru/datasheet/pdf/onsemi/ncs2502.pdf>.
- [156] Technical description NCS2510: 1.4 GHz Current Feedback Op Amp / On semiconductor // Official site. – Access mode : <http://www.chipfind.ru/datasheet/pdf/onsemi/ncs2510.pdf>.
- [157] Technical description NCS2511: 1 GHz Current Feedback Op Amp / On semiconductor // Official site. – Access mode : <http://www.chipfind.ru/datasheet/pdf/onsemi/ncs2511.pdf>.
- [158] Technical description NCS2530: Triple 1.1 mA 200 MHz Current Feedback Op Amp with Enable Feature / On semiconductor // Official site. – Access mode : <http://www.chipfind.ru/datasheet/pdf/onsemi/ncs2530.pdf>.
- [159] Technical description NCS2535: Triple 1.4 GHz Current Feedback Op Amp with Enable Feature / On semiconductor // Official site. – Access mode : <http://www.chipfind.ru/datasheet/pdf/onsemi/ncs2535.pdf>.
- [160] Polonikov D. E. Operation amplifiers: principles of construction theory circuit engineering / D. E. Polovnikov. – M.: Energiatomizdat, 1983.
- [161] Prokopenko N. N. Architecture and circuit engineering of fast acting operation amplifiers / N. N. Prokopenko. A. S. Budiakov. – Shakhty: Publishing House of SRSUES, 2006.

- [162] Prokopenko N. N. Non-linear active correction in the precision analog micro-circuits / N. N. Prokopenko. – Rostov-On-Don: Publishing House of North Caucasian Scientific Center of Higher Education, 2000.
- [163] Prokopenko N. N. Non-linear correcting circuits based on current voltage switches in analog microcircuits / N. N. Prokopenko, N. N. Nikulichev, – Shakhty: Publishing House of SRSUES, 2006.
- [164] Budiakov S. A. Architecture and circuit engineering of the operation amplifiers with limiting values of the dynamic parameters: Extended abstract of Cond. Sc. (Eng) Dissertation: 05.13.05 / S. A. Budiakov. – Taganrog, 2008.
- [165] Analysis of the transfer characteristic of push-pull symmetric d. c. amplifier / O. D. Azarov, S. V. Bogomolov, V. A. Garnaga, O. O. Reshetnik // scientific works of VNTU. – 2007. – № 1. – P. 1–8. – Access mode : <http://www.nbu.gov.ua/e-journals/VNTU/2007-1/vyp1.html>.
- [166] Bogomolov S. V. Push- pull d. c. amplifiers with symmetrical structure / O. D. Azarov, S. V. Bogomolov, V.A Garnaga // Bulletin of Khmelnytskyi National University. – 2008. – № 4. – P. 20–24.
- [167] Win Palmer. Fast acting precision amplifier-converter of the resistances / Win Palmer // Electronics. Series: methods, circuits, equipment. – 1988. – № 1. – P. 77–82.
- [168] Bogomolov S. V. High linear analog devices for multidigital analog-to-digital systems / O. D. Azarov, S. V. Bogomolov // Problems of IT based management and control. National aviation University. – 2011. – № 4(36). – P. 6–18.
- [169] Azarov O. D. Multidigital ADC and DAC with weight redundancy, parametric failures resistant: monograph / O. D. Azarov, O. V. Kaduk. – Vinnytsia, 2010.
- [170] Bakhtiarov G. D. Analog-to-digital converters / G. D. Bakhtiarov, V. V. Malinin, V. P. Shkolin. – M.: Soviet Radio, 1980.
- [171] Ornatskyi P. P. Theoretical fundamentals information-measuring instrumentation / P. P. Ornatouskyi. – 2<sup>nd</sup> revised and corrected edition. – K.: Vyshcha Shkola, 1983.
- [172] Provision of the heating conditions of electronic engineering products / A. A. Chernyshov, V. I. Ivanov, A. I. Aksenov, D. N. Glushkova. – M.: Energy, 1980.
- [173] Microelectronic sensors of physical values [3 volumes] [under the



- editorship of Z. Gotra]. – Lviv: League-Press.[Volume 1 – 2002, volume 2 – 2003, volume 3 – 2004].
- [174] Sensors. Reference book [under the editorship of Z. Yu. Gotra, O. I. Chaikoskyi]. – Lviv: Kameniar, 1995.
- [175] Photoplethysmographic technologies of cardiovascular system control: monograph / S. V. Pavlov, V. P. Kozhemiako, V. R. Petruk, P. F. Kolsnyk, – Vinnytsia: Universum Vinnytsia, 2007.
- [176] Sah C.-T. Fundamentals of solid-state electronics // C.-T. Sah. World Scientific. – 1991.
- [177] Stepanenko I. P. Fundamentals of microelectronics: manual for graduate students – 2<sup>nd</sup> revised and corrected edition / I. P. Stepanenko. – M.: Laboratory of Basic Knowledge, 2003.
- [178] Bogomolov S. V. Circuit organization of the input complementary stage of the push-pull symmetric d. c. amplifier / O. D. Azarov, S. V. Bogomolov // Problems of computerization and control. National aviation university – 2009. – № 3(27). – P. 6–13.
- [179] Models of AFC and PFC of the integrated bipolar transistors on the base of the equivalent circuits with the controlled current generators / O. D. Azarov. S. V. Bogomolov, S. Sh. Katsiv, et al. Problems of computerization and control. National aviation University. – 2009. – №4(28). – P. 5-15.
- [180] Bogomolov S. V. ADC with weight redundancy for scrambling of linguistic signals / O. D. Azarov, S. V. Bogomolov // XXXVII scientific engineering conference of the teacher's staff, researchers, students of the university with the participation of the representatives of research institutions and enterprises of Vinnytsia and Vinnytsia Region., March 17-18: Proceedings. – Vinnytsia, 2008.
- [181] Greban A. B. Design of the analog integrated circuits / A. B. Greban. – M.: Energy, 1976.
- [182] Bogomolov S. V. Linearity error of the transfer characteristic of the input stage of the push-pull current amplifier / O. D. Azarov, S. V. Bogomolov, V. Ja. Steiskal // Information technologies and computer engineering. – 2010. – № 3(19). – P. 4–12.
- [183] Useful model Patent 41316 Ukraine, IPC (2009) H 03 F 3/26. Direct current amplifier / Azarov O. D., Bogomolov S. V., Krupenlnytskyi L. V., claimer and owner of the patent Vinnytsia National Technical University.

- № u200900492; claimed 23.01.2009; Published 12.05.2009; Bulletin № 9.
- [184] Bogomolov S. V. Nonlinear distortion of the input stages of the push-pull current amplifiers / O. D. Azarov, S. V. Bogomolov, I. V. Abramchuk // Problems of computerization and control. National aviation university. – 2011. – № 2(34).
- [185] Bogomolov S.V. Analog-to-digital components of the computer systems of digital teleradiobroadcasting channels with the protected channels monitoring / O. D. Azarov, S. V. Bogomolov // XXXVIII scientific engineering conference of the teacher's staff, reseachers and studnts of the university with participation of scientific-research institutions, engineers and researchers of the enterprises of Vinnytsia and Vinnytsia Region., March 17-20: Proceedings. – Vinnytsia, 2009. P. 21.
- [186] Azarov O.D. Fundamentals of the theory of lineal integrated circuits / O. D. Azarov, V. V. Baiko, M. P. Obertiukh. – Vinnytsia: Vinnytsia VSTU, 1999.
- [187] Abramovits M. Reforence book on special functions / M. Abramovits, I. Shigan. – M.: Nauka, 1979.
- [188] Jahnke E. Special functions: Formulas, graphs, tables / E. Jahnke, F. Emdl, F. Lesch; translated from German by L. I. Sedov. – M.: Nauka, 1977. – p. 92-111.
- [189] Sato Yu. Signals processing. First acquaintance / Yu. Sato: under the editorship of E. Ameniya. – M.: Publishing House «DODEKA», 2002.
- [190] Bogomolov S. V. Dynamic characteristics of the input complimentary stage of push-pull d. c. amplifier / O. D. Azarov, S. V. Bogomolov, V. A. Garnaga // Problems of computerization and control. National aviation university – 2010. – №3(31). – P. 5–13.
- [191] Zeveke G. V. Fundamentals of the circuits theory: manual for graduate students / G. V. Zeveke, P. A. Ionkin, A. V. Netushil, S. V. Strakhov. – 5<sup>th</sup> edition, revised. – M.: Energoatomizdat, 1989.
- [192] Kasatkin A. S. Electric Engineering: manual for graduate students / A. S. Kasatkin, M. Y. Nemlsov. – 4<sup>th</sup> edition revised. – M.: Energoatomizdat, 1983.
- [193] Lungu K. N. Higher mathematics: Guide book for problems solution / K. N. Lungu, E. V. Makarov. – 2<sup>nd</sup> edition, updated and revised. – Part 1. – M.: PHIZMATLIT, 2010.

- [194] Vygodskiy M. Ya. Reference book on higher mathematics / M. Ya. Vygodskiy, – M.: ACT: Astrakhan, 2005.
- [195] Bogomolov S. V. Precision buffer devices on the base off push-pull symmetric structures / O. D. Azarov, S. V. Bogomolov // Information technologies and computer engineering. – 2011. – №3(22). – P.4–12.
- [196] Useful model Patent 51011. Ukraine, IPC (2009) H 03 K 5/22, G 05 B 1/00. Buffer stage / Azarov O. D. Dudnyk O. V., Bogomolov S. V., Kaduk O. V.; claimer and owner of the patent-Vinnytsia National Technical University. – № u201000934; claimed 29.01.10 ; published 25.06.10, Bulletin № 12.
- [197] Bogomolov S. V. Current-voltage and voltage-current converters on the base of push-pull current amplifiers / O. D. Azarov, S. V. Bogomolov // Information technologies and computer engineering. – 2011. – № 2(21). – P. 4–11.
- [198] Peiton A. J. Analog electronics on operational amplifiers / A. J. Peiton, V. Volsh. – M.: BINOM, 1994.
- [199] Bogomolov S. V. Linearity errors of the precision current-voltage and voltage-current converters on the base push-pull current amplifiers / O. D. Azarov, S. V. Bogomolov // Information technologies and computer engineering. – 2012. – №1(23). – P.24–30.
- [200] Makarenko V. Operation amplifiers with super small distortions for the high quality audio applications / V. Makarenko // Electronic components and systems. – 2011. – №12(172). – P.34–38.
- [201] CMOS 3V/5V Wide Bandwidth Quad 2:1 Mux ADG774. [Electronic resource] – Access mode : [www.analog.com](http://www.analog.com).
- [202] IRLML2803 HEXFET® Power MOSFET. International Rectifier. [Electronic resource]: [www.irf.com](http://www.irf.com).
- [203] Differential Thermometer Testo922. [Electronic resource] – Access mode : [www.testo.com](http://www.testo.com).
- [204] SBIR Model 104 – High Resolution Differential Thermometer 0,01 °C. [Electronic resource] – Access mode : <http://www.sbir.com/thermometers.htm>.
- [205] ADuC824. MicroConverter, Dual-channel 16-/24-Bit ADCs with Embedded FLASH MCU.. Analog Devices, Inc. [Electronic resource] – Access mode : <http://www.analog.com>.
- [206] References: bandgap, low dropout. [Electronic resource] – Access mode :

www.analog.com.

- [207] Useful model patent 70131 Ukraine IPC (2012.01) H 03 K 5/22 (2006.01), G 05 B 1/00. Direct current amplifier / Azarov O. D., Bogomolov S. V., Kyrylenko D. O., Krupelnytskyi L. V.; claimer and owner of the patent Vinnytsia National Technical University – №u201113981; claimed 28.11.2011; published 25.05.2012, Bulletin № 10.
- [208] Useful model patent 22671 Ukraine IPC (2006) H 03 K 5/22, G 05 B 1/00. Push-pull symmetric current amplifier / Azarov O. D., Koduk O. V., Lukashchuk O. O., Bogomolov S. V., Krupelnytskyi V. B.; claimer and owner of the patent Vinnytsia National Technical University – №u200613036; claimed 11.12.2006; published 25.04.2007, Bulletin № 5.
- [209] Useful model patent 23607 Ukraine IPC (2006) H 03 K 5/22, G 05 B 1/00. Push-pull symmetric current amplifier / Azarov O. D., Bogomolov S. V., Lukashchuk O. O. Krupelnytskyi L. V.; claimer and owner of the patent Vinnytsia National Technical University – № a200612459; claimed 27.11.2006; published 11.06.2007, Bulletin № 8.
- [210] Useful model patent 23989 Ukraine IPC (2006) H 03 K 5/22, G 05 B 1/00. Push-pull symmetric current amplifier / Azarov O. D., Bogomolov S. V., Lukashchuk O. O. Tarasova O. M.; claimer and owner of the patent Vinnytsia National Technical University – № a200701145; claimed 05.02.2007; published 11.06.2007, Bulletin № 8.
- [211] Useful model patent 23989 Ukraine IPC (2006) H 03 K 5/22, G 05 B 1/00. Push-pull symmetric current amplifier / Azarov O. D., Bogomolov S. V., Krupelnutskyi L. V.; claimer and owner of the patent Vinnytsia National Technical University – № u200701969; claimed 11.06.2007; published 11.06.2007, Bulletin № 8.
- [212] Useful model patent 24001 Ukraine IPC (2006) H 03 K 5/22, G 05 B 1/00. Push-pull symmetric current amplifier / Azarov O. D., Bogomolov S. V., Krupelnutskyi L. V., Tarasova O. M.; claimer and owner of the patent Vinnytsia National Technical University – № u200702065; claimed 26.02.2007; published 11.06.2007, Bulletin № 8.
- [213] Useful model patent 25609 Ukraine IPC (2006) H 03 K 5/22, G 05 B 1/00. Push-pull symmetric current amplifier / Azarov O. D., Bogomolov S. V., Krupelnutskyi L. V.; claimer and owner of the patent Vinnytsia

- National Technical University – № u200704477; claimed 23.04.2007; published 10.08.2007, Bulletin № 12.
- [214] Useful model patent 26413 Ukraine IPC (2006) H 03 K 5/22, G 05 B 1/00. Push-pull symmetric current amplifier / Azarov O. D., Kaduk O. V., Bodomolov S. V., Garnaga V. A., Reshetnik O. O.; claimer and owner of the patent Vinnytsia National Technical University – № u200702063; claimed 26.02.2007; published 25.09.2007, Bulletin № 15.
- [215] Useful model patent 26493 Ukraine IPC (2006) H 03 K 5/22, G 05 B 1/00. Ukraine IPC (2006) H 03 K 5/22, G 05 B 1/00. Push-pull symmetric current amplifier / Azarov O. D., Bodomolov S. V., Reshetnik O. O., Garnaga V. A.; claimer and owner of the patent Vinnytsia National Technical University – № u200705169; claimed 11.05.2007; published 25.09.2007, Bulletin № 15.
- [216] Useful model patent 26495 Ukraine IPC (2006) H 03 K 5/22, G 05 B 1/00. Push-pull symmetric current amplifier / Azarov O. D., Bodomolov S. V., Reshetnik O. O., Garnaga V. A.; claimer and owner of the patent Vinnytsia National Technical University – № u200705196; claimed 11.05.2007; published 25.09.2007, Bulletin № 15.
- [217] Useful model patent 26771 Ukraine IPC (2006) H 03 K 5/22, G 05 B 1/00. Push-pull symmetric current amplifier / Azarov O. D., Bodomolov S. V., Krupelnutskyi L. V., Reshetnik O. O., Garnaga V. A.; claimer and owner of the patent Vinnytsia National Technical University – № u200704476; claimed 23.04.2007; published 10.10.2007, Bulletin № 16.
- [218] Useful model patent 34462 Ukraine IPC (2006) H 03 K 5/22, G 05 B 1/00. Push-pull symmetric current amplifier / Azarov O. D., Bodomolov S. V., Krupelnutskyi L. V., Volkov V. P.; claimer and owner of the patent Vinnytsia National Technical University – № u200803598; claimed 21.03.2008; published 11.08.2008, Bulletin № 15.
- [219] Useful model patent 36692 Ukraine IPC (2006) H 03 K 5/22, G 05 B 1/00. Push-pull symmetric current amplifier / Azarov O. D., Shabatura M. Yu., Bodomolov S. V., Garnaga V. A.; claimer and owner of the patent Vinnytsia National Technical University – № u200802987; claimed 07.03.2008; published 10.11.2008, Bulletin № 21.
- [220] Useful model patent 39796 Ukraine IPC (2006) H 03 K 5/22, G 05 B 1/00. Push-pull symmetric current amplifier / Azarov O. D., Teplytskui M. Yu., Reshetnik O. O., Bogomolov S. V.; claimer and owner of the

- patent Vinnytsia National Technical University – № u200812467; claimed 23.10.2008; published 10.03.2009, Bulletin № 5.
- [221] Useful model patent 41318 Ukraine IPC (2006) H 03 K 5/22, G 05 B 1/00. Ukraine IPC (2006) H 03 K 5/22, G 05 B 1/00. Push-pull symmetric current amplifier / Azarov O. D., Bogomolov S. V., Krupelnutskyi L. V.; claimer and owner of the patent Vinnytsia National Technical University – № u200900494; claimed 23.01.2009; published 12.05.2009, Bulletin № 9.
- [222] Useful model patent 41857 Ukraine IPC (2009) H 03 K 5/22, G 05 B 1/00. Push-pull symmetric current amplifier / Azarov O. D., Shabatura M. Yu., Bogomolov S. V.; claimer and owner of the patent Vinnytsia National Technical University – № u200900487; claimed 23.01.2009; published 10.06.2009, Bulletin № 11.
- [223] Useful model patent 42149 Ukraine IPC (2009) H 03 F 3/26, G 05 B 1/00. Push-pull symmetric current amplifier / Azarov O. D., Melnyk S. O., Bogomolov S. V., Khodzhanijazov I. K.; claimer and owner of the patent Vinnytsia National Technical University – № u200900503; claimed 23.01.2009; published 25.06.2009, Bulletin № 12.
- [224] Useful model patent 42150 Ukraine IPC (2009) H 03 F 3/26. Push-pull symmetric current amplifier / Azarov O. D., Khodzhanijazov I. K., Bogomolov S. V., Melnyk S. O.; claimer and owner of the patent Vinnytsia National Technical University – № u200900504; claimed 23.01.2009; published 25.06.2009, Bulletin № 12.
- [225] Useful model patent 42946 Ukraine IPC (2009) H 03 F 3/26. Push-pull symmetric current amplifier / Azarov O. D., Khodzhanijazov I. K., Bogomolov S. V., Melnyk S. O.; claimer and owner of the patent Vinnytsia National Technical University – № u200902267; claimed 16.03.2009; published 27.07.2009, Bulletin № 14.
- [226] Useful model patent 42951 Ukraine IPC (2009) H 03 F 3/26. Push-pull symmetric current amplifier / Azarov O. D., Melnyk S. O., Bogomolov S. V., Khodzhanijazov I. K.; claimer and owner of the patent Vinnytsia National Technical University – № u200902293; claimed 16.03.2009; published 27.07.2009, Bulletin № 14.
- [227] Useful model patent 45749 Ukraine IPC (2009) H 03 F 3/26, G 05 B 1/00. Push-pull symmetric current amplifier / Azarov O. D., Melnyk S. O., Bogomolov S. V., Khodzhanijazov I. K.; claimer and owner of the patent

- Vinnitsia National Technical University – № u200905593; claimed 01.06.2009; published 25.11.2009, Bulletin № 22.
- [228] Useful model patent 48143 Ukraine IPC (2009) H 03 K 5/22. Push-pull symmetric current amplifier / Azarov O. D., Bogomolov S. V., Krupelnutskyi L. V.; claimer and owner of the patent Vinnitsia National Technical University – № u200909018; claimed 31.08.2009; published 10.03.2010, Bulletin № 5.
- [229] Useful model patent 49814 Ukraine IPC (2009) H 03 F 3/26. Push-pull symmetric current amplifier / Azarov O. D., Melnyk S. O., Bogomolov S. V., Khodzhanijazov I. K.; claimer and owner of the patent Vinnitsia National Technical University – № u200912323; claimed 30.11.2009; published 11.05.2010, Bulletin № 9.
- [230] Useful model patent 50244 Ukraine IPC (2009) H 03 K 5/22, G 05 B 1/00. Push-pull symmetric current amplifier / Azarov O. D., Dudnik O.V., Bogomolov S. V.; claimer and owner of the patent Vinnitsia National Technical University – № u200913620; claimed 25.12.2009; published 25.05.2010, Bulletin № 10.
- [231] Useful model patent 50245 Ukraine IPC (2009) H 03 K 5/22, G 05 B 1/00. Push-pull symmetric current amplifier / Azarov O. D., Dudnik O.V., Bogomolov S. V.; claimer and owner of the patent Vinnitsia National Technical University – № u200913621; claimed 25.12.2009; published 25.05.2010, Bulletin № 10.
- [232] Useful model patent 50845 Ukraine IPC (2009) H 03 F 3/26, G 05 B 1/00. Push-pull symmetric current amplifier / Azarov O. D., Bogomolov S. V., Sologub I. V.; claimer and owner of the patent Vinnitsia National Technical University – № u200913550; claimed 25.12.2009; published 25.06.2010, Bulletin № 12.
- [233] Useful model patent 50846 Ukraine IPC (2009) H 03 K 5/22, G 05 B 1/00. Push-pull symmetric current amplifier / Azarov O. D., Bogomolov S. V., Rososhchuk A. V.; claimer and owner of the patent Vinnitsia National Technical University – № u200913551; claimed 25.12.2009; published 25.06.2010, Bulletin № 12.
- [234] Useful model patent 50861 Ukraine IPC (2009) H 03 K 5/22, G 05 B 1/00. Push-pull symmetric current amplifier / Azarov O. D., Bogomolov S. V., Sentiabov E. S.; claimer and owner of the patent Vinnitsia National

- Technical University – № u200913622; claimed 25.12.2009; published 25.06.2010, Bulletin № 12.
- [235] Useful model patent 50876 Ukraine IPC (2009) H 03 K 5/22, G 05 B 1/00. Push-pull symmetric current amplifier / Azarov O. D., Teplitsky M. Yu., Bogomolov S. V.; claimer and owner of the patent Vinnytsia National Technical University – № u200913704; claimed 28.12.2009; published 25.06.2010, Bulletin № 12.
- [236] Useful model patent 51958 Ukraine IPC (2009) H 03 K 5/22, G 05 B 1/00. Push-pull symmetric current amplifier / Azarov O. D., Bogomolov S. V., Garnaga V. A., Kyrylenko D.O.; claimer and owner of the patent Vinnytsia National Technical University – № u201000906; claimed 29.01.2010; published 10.08.2010, Bulletin № 15.
- [237] Useful model patent 51963 Ukraine IPC (2009) H 03 K 5/22, G 05 B 1/00. Push-pull symmetric current amplifier / Azarov O. D., Dudnik O.V., Bogomolov S. V.; claimer and owner of the patent Vinnytsia National Technical University – № u201000930; claimed 29.01.2010; published 10.08.2010, Bulletin № 15.
- [238] Useful model patent 52704 Ukraine IPC (2009) H 03 F 3/26. Push-pull symmetric current amplifier / Azarov O. D., Khodzhanijazov I. K., Bogomolov S. V., Melnyk S. O.; claimer and owner of the patent Vinnytsia National Technical University – № u201001031; claimed 01.02.2010; published 10.09.2010, Bulletin № 17.
- [239] Useful model patent 52717 Ukraine IPC (2009) H 03 K 5/22, G 05 B 1/00. Push-pull symmetric current amplifier / Azarov O. D., Dudnik O.V., Bogomolov S. V.; claimer and owner of the patent Vinnytsia National Technical University – № u201001305; claimed 08.02.2010; published 10.09.2010, Bulletin № 17.
- [240] Useful model patent 52764 Ukraine IPC (2009) H 03 K 5/22, G 05 B 1/00. Push-pull symmetric current amplifier / Azarov O. D., Bogomolov S. V. Kyrylenko D. O.; claimer and owner of the patent Vinnytsia National Technical University – № u201002045; claimed 25.02.2010; published 10.09.2010, Bulletin № 17.
- [241] Useful model patent 52770 Ukraine IPC (2009) H 03 K 5/22, G 05 B 1/00. Push-pull symmetric current amplifier / Azarov O. D., Bogomolov S. V., Kyrylenko D. O.; claimer and owner of the patent Vinnytsia



- National Technical University – № u201002055; claimed 25.02.2010; published 10.09.2010, Bulletin № 17.
- [242] Useful model patent 52786 Ukraine IPC (2009) H 03 K 5/22, G 05 B 1/00. Push-pull symmetric current amplifier / Azarov O. D., Dudnik O.V., Bogomolov S. V.; claimer and owner of the patent Vinnytsia National Technical University – № u201002330; claimed 01.03.2010; published 10.09.2010, Bulletin № 17.
- [243] Useful model patent 52787 Ukraine IPC (2009) H 03 K 5/22, G 05 B 1/00. Push-pull symmetric current amplifier / Azarov O. D., Dudnik O.V., Bogomolov S. V.; claimer and owner of the patent Vinnytsia National Technical University – № u201002331; claimed 01.03.2010; published 10.09.2010, Bulletin № 17.
- [244] Useful model patent 52800 Ukraine IPC (2009) H 03 F 3/26. Push-pull symmetric current amplifier / Azarov O. D., Khodzhanijazov I. K., Bogomolov S. V., Melnyk S. O.; claimer and owner of the patent Vinnytsia National Technical University – № u201002590; claimed 09.03.2010; published 10.09.2010, Bulletin № 17.
- [245] Useful model patent 52801 Ukraine IPC (2009) H 03 F 3/26. Push-pull symmetric current amplifier / Azarov O. D., Melnyk S. O., Bogomolov S. V., Khodzhanijazov I. K.; claimer and owner of the patent Vinnytsia National Technical University – № u201002593; claimed 09.03.2010; published 10.09.2010, Bulletin № 17.
- [246] Useful model patent 52802 Ukraine IPC (2009) H 03 F 3/26, G 05 B 1/00. Push-pull symmetric current amplifier / Azarov O. D., Bogomolov S. V., Sologub I. V.; claimer and owner of the patent Vinnytsia National Technical University – № u201002596; claimed 09.03.2010; published 10.09.2010, Bulletin № 17.
- [247] Useful model patent 52803 Ukraine IPC (2009) H 03 K 5/22, G 05 B 1/00. Push-pull symmetric current amplifier / Azarov O. D., Bogomolov S. V., Rososhchuk A. V.; claimer and owner of the patent Vinnytsia National Technical University – № u201002597; claimed 09.03.2010; published 10.09.2010, Bulletin № 17.
- [248] Useful model patent 53415 Ukraine IPC (2009) H 03 K 5/00, G 05 B 1/00. Push-pull symmetric current amplifier / Azarov O. D., Teplytskyi M. Yu., Bogomolov S. V.; claimer and owner of the patent Vinnytsia

- National Technical University – № u201002875; claimed 15.03.2010; published 11.10.2010, Bulletin № 19.
- [249] Useful model patent 53416 Ukraine IPC (2009) H 03 F 3/26. Push-pull symmetric current amplifier / Azarov O. D., Khodzhanijazov I. K., Bogomolov S. V., Melnyk S. O.; claimer and owner of the patent Vinnytsia National Technical University – № u201002880; claimed 15.03.2010; published 11.10.2010, Bulletin № 19.
- [250] Useful model patent 53917 Ukraine IPC (2009) H 03 K 5/22, G 05 B 1/00. Push-pull symmetric current amplifier / Azarov O. D., Bogomolov S. V., Krupelnutskyi L. V.; claimer and owner of the patent Vinnytsia National Technical University – № u201003899; claimed 06.04.2010; published 25.10.2010, Bulletin № 20.
- [251] Useful model patent 58787 Ukraine IPC H 03 F 3/26(2011.01). Push-pull symmetric current amplifier / Azarov O. D., Melnyk S. O., Bogomolov S. V., Shabature M. Yu.; claimer and owner of the patent Vinnytsia National Technical University – № u201011637; claimed 30.09.2010; published 26.04.2011, Bulletin № 8.
- [252] Useful model patent 58951 Ukraine IPC (2011.01) H 03 K 5/22(2011.01), G 05 B 1/00. Push-pull symmetric current amplifier / Azarov O. D., Bogomolov S. V., Kyrylenko D. O.; claimer and owner of the patent Vinnytsia National Technical University – № u201012866; claimed 29.10.2010; published 26.04.2011, Bulletin № 8.
- [253] Useful model patent 58952 Ukraine IPC (2011.01) H 03 K 5/22, G 05 B 1/00. Push-pull symmetric current amplifier / Azarov O. D., Bogomolov S. V., Kyrylenko D. O.; claimer and owner of the patent Vinnytsia National Technical University – № u201012867; claimed 29.10.2010; published 26.04.2011, Bulletin № 8.
- [254] Useful model patent 59964 Ukraine IPC (2011.01) H 03 K 5/22 (2006.01), G 05 B 1/00. Push-pull symmetric current amplifier / Azarov O. D., Bogomolov S. V., Kyrylenko D. O.; claimer and owner of the patent Vinnytsia National Technical University – № u201012849; claimed 29.10.2010; published 10.06.2011, Bulletin № 11.
- [255] Useful model patent 63661 Ukraine IPC (2011.01) H 03 K 5/22 (2006.01), G 05 B 1/00. Push-pull symmetric current amplifier / Azarov O. D., Bogomolov S. V., Rososhchuk A. V.; claimer and owner of the

- patent Vinnytsia National Technical University – № u201106600; claimed 26.05.2011; published 10.10.2011, Bulletin № 19.
- [256] Useful model patent 63948 Ukraine IPC (2011.01) H 03 K 5/22, G 05 B 1/00. Push-pull symmetric current amplifier / Azarov O. D., Bogomolov S. V., Rososhchuk A. V., Tarasova O. M.; claimer and owner of the patent Vinnytsia National Technical University – № u201103779; claimed 29.03.2011; published 25.10.2011, Bulletin № 20.
- [257] Useful model patent 63949 Ukraine IPC (2011.01) H 03 K 5/00, G 05 B 1/00. Push-pull symmetric current amplifier / Azarov O. D., Krupelnytskyi L. V., Kyrylenko D. O., Bogomolov S. V.; claimer and owner of the patent Vinnytsia National Technical University – № u201103780; claimed 29.03.2011; published 25.10.2011, Bulletin № 20.
- [258] Useful model patent 63951 Ukraine IPC (2011.01) H 03 K 5/00, G 05 B 1/00. Push-pull symmetric current amplifier / Azarov O. D., Bogomolov S. V., Kyrylenko D. O., Steiskal V. Ja.; claimer and owner of the patent Vinnytsia National Technical University – № u201103783; claimed 29.03.2011; published 25.10.2011, Bulletin № 20.
- [259] Useful model patent 63952 Ukraine IPC (2011.01) H 03 K 5/22, G 05 B 1/00. Push-pull symmetric current amplifier / Azarov O. D., Bogomolov S. V., Rososhchuk A. V.; claimer and owner of the patent Vinnytsia National Technical University – № u201103784; claimed 29.03.2011; published 25.10.2011, Bulletin № 20.
- [260] Useful model patent 63955 Ukraine IPC (2011.01) H 03 K 5/22 (2006,01), G 05 B 1/00. Push-pull symmetric current amplifier / Azarov O. D., Bogomolov S. V., Khodzhanijazov I. K.; claimer and owner of the patent Vinnytsia National Technical University – № u201103791; claimed 29.03.2011; published 25.10.2011, Bulletin № 20.
- [261] Useful model patent 63956 Ukraine IPC (2011.01) H 03 K 5/22 (2006.01), G 05 B 1/00. Push-pull symmetric current amplifier / Azarov O. D., Bogomolov S. V., Rososhchuk A. V., Krupelnytskyi L. V claimer and owner of the patent Vinnytsia National Technical University – № u201103792; claimed 29.03.2011; published 25.10.2011, Bulletin № 20.
- [262] Useful model patent 63959 Ukraine IPC (2011.01) H 03 K 5/22 (2006.01), G 05 B 1/00. Push-pull symmetric current amplifier / Azarov O. D., Bogomolov S. V., Khodzhanijazov I. K.; claimer and owner of the

- patent Vinnytsia National Technical University – № u201103795; claimed 29.03.2011; published 25.10.2011, Bulletin № 20.
- [263] Useful model patent 65056 Ukraine IPC H 03 K 3/26 (2006.01). Push-pull symmetric current amplifier / Azarov O. D., Melnyk S. O., Bogomolov S. V.; claimer and owner of the patent Vinnytsia National Technical University – № u201105250; claimed 26.04.2011; published 25.10.2011, Bulletin № 22.
- [264] Useful model patent 65267 Ukraine IPC (2011.01) H 03 K 5/22 (2006.01), G 05 B 1/00. Push-pull symmetric current amplifier / Azarov O. D., Bogomolov S. V., Kyrlyenko D. O., Pavlov S. V.; claimer and owner of the patent Vinnytsia National Technical University – № u201107992; claimed 24.06.2011; published 25.11.2011, Bulletin № 22.
- [265] Useful model patent 65785 Ukraine IPC (2011.01) H 03 K 5/22 (2006.01), G 05 B 1/00. Push-pull symmetric current amplifier / Azarov O. D., Bogomolov S. V., Kyrlyenko D. O., Krupelnutskyi L. V.; claimer and owner of the patent Vinnytsia National Technical University – № u201107984; claimed 24.06.2011; published 12.12.2011, Bulletin № 23.
- [266] Useful model patent 66944 Ukraine IPC (2011.01) H 03 K 5/22 (2006.01), G 05 B 1/00. Push-pull symmetric current amplifier / Azarov O. D., Bogomolov S. V., Rososhchuk A. V.; claimer and owner of the patent Vinnytsia National Technical University – № u201108118; claimed 29.06.2011; published 25.01.2012, Bulletin № 2.
- [267] Useful model patent 69741 Ukraine IPC (2012.01) H 03 K 5/22 (2006.01), G 05 B 1/00. Push-pull symmetric current amplifier / Azarov O. D., Pavlov S. V., Bogomolov S. V., Rososhchuk A. V.; claimer and owner of the patent Vinnytsia National Technical University – № u201112873; claimed 02.11.2011; published 10.05.2012, Bulletin № 9.
- [268] Useful model patent 69743 Ukraine IPC (2012.01) H 03 K 5/22 (2006.01), G 05 B 1/00. Push-pull symmetric current amplifier / Azarov O. D., Bogomolov S. V., Rososhchuk A. V.; claimer and owner of the patent Vinnytsia National Technical University – № u201112877; claimed 02.11.2011; published 10.05.2012, Bulletin № 9.
- [269] Useful model patent 69746 Ukraine IPC (2012.01) H 03 K 5/22 (2006.01), G 05 B 1/00. Push-pull symmetric current amplifier / Azarov O. D., Zakharchenko S. V., Boiko O. V., Bogomolov S. V., Tarasova O. M.; claimer and owner of the patent Vinnytsia National Technical

- University – № u201112882; claimed 02.11.2011; published 10.05.2012, Bulletin № 9.
- [270] Useful model patent 70121 Ukraine IPC (2012.01) H 03 K 5/22 (2006.01), G 05 B 1/00. Push-pull symmetric current amplifier / Azarov O. D., Bogomolov S. V., Jatsyk V. E., Murashchenko O. G.; claimer and owner of the patent Vinnytsia National Technical University – № u201113956; claimed 28.11.2011; published 25.05.2012, Bulletin № 10.
- [271] Useful model patent 70320 Ukraine IPC (2012.01) H 03 K 5/22 (2006.01), G 05 B 1/00, H 03 F 3/26 (2006.01). Push-pull symmetric current amplifier / Azarov O. D., Bogomolov S. V., Rososhchuk A. V., Sdeiskal V. Ja.; claimer and owner of the patent Vinnytsia National Technical University – № u201112862; claimed 02.11.2011; published 11.06.2012, Bulletin № 11.
- [272] Useful model patent 70362 Ukraine IPC (2012.01) H 03 K 5/22 (2006.01), G 05 B 1/00. Push-pull symmetric current amplifier / Azarov O. D., Zakharchenko S. M., Boiko O. V., Bogomolov S. V.; claimer and owner of the patent Vinnytsia National Technical University – № u201113218; claimed 09.11.2011; published 11.06.2012, Bulletin № 11.
- [273] Useful model patent 91923 Ukraine IPC (2009) H 03 K 5/22, H 03 F 3/26. Push-pull symmetric current amplifier / Azarov O. D., Bogomolov S. V., Garnaga V. A.; claimer and owner of the patent Vinnytsia National Technical University – № a200900486; claimed 23.01.2009; published 10.09.2010, Bulletin № 17.
- [274] Useful model patent 92648 Ukraine IPC (2009) H 03 F 3/26, H 03 K 5/22, G 05 B 1/00. Push-pull symmetric current amplifier / Azarov O. D., Bogomolov S. V., Garnaga V. A., Zakharchenko S. M.; claimer and owner of the patent Vinnytsia National Technical University – № a200900484; claimed 23.01.2009; published 25.11.2010, Bulletin № 22.
- [275] Useful model patent 93124 Ukraine IPC (2011.01) H 03 F 3/26 (2011.01), G 05 B 1/00. Push-pull symmetric current amplifier / Azarov O. D., Bogomolov S. V.; claimer and owner of the patent Vinnytsia National Technical University – № a200906388; claimed 19.06.2009; published 10.01.2011, Bulletin № 1.
- [276] Useful model patent 94131 Ukraine IPC H 03 K 5/22, G 05 B 1/00, H 03 F 3/26 (2006.01). Push-pull symmetric current amplifier / Azarov O. D., Bogomolov S. V.; claimer and owner of the patent Vinnytsia National

- Technical University – № a200906399; claimed 19.06.2009; published 11.04.2011, Bulletin № 7.
- [277] Useful model patent 96650 Ukraine IPC H 03 K 5/22 (2006.01), G 05 B 1/01(2006.01). Push-pull symmetric current amplifier / Azarov O. D., Bogomolov S. V.; claimer and owner of the patent Vinnytsia National Technical University – № a201002056; claimed 25.02.2010; published 25.11.2011, Bulletin № 22.
- [278] Useful model patent 97686 Ukraine IPC H 03 K 5/22 (2006.01), G 05 B 1/01 (2006.01), H 03 F 3/34 (2006/01). Measuring push-pull symmetric current amplifier / Azarov O. D., Bogomolov S. V.; claimer and owner of the patent Vinnytsia National Technical University – № a201003869; claimed 06.04.2010; published 12.03.2012, Bulletin № 5.
- [279] Useful model patent 19728 Ukraine IPC (2006) H 03 K 5/22, G 05 B 1/00. Push-pull symmetric current amplifier / Azarov O. D., Lukashchuk O. O., Bogomolov S. V., Garnaga V. A., Reshetnik O. O.; claimer and owner of the patent Vinnytsia National Technical University – № u200608586; claimed 31.07.2006; published 15.12.2006, Bulletin № 12.
- [280] Useful model patent 23999 Ukraine IPC (2006) H 03 K 5/22, G 05 B 1/00. Push-pull symmetric current amplifier / Azarov O. D., Bogomolov S. V., Garnaga V. A., Reshetnik O. O.; claimer and owner of the patent Vinnytsia National Technical University – № u200702059; claimed 26.02.2007; published 11.06.2007, Bulletin № 8.
- [281] Useful model patent 26530 Ukraine IPC (2006) H 03 F 3/26. Push-pull symmetric current amplifier / Azarov O. D., Bogomolov S. V., Zakharchenko S. M., Kusiuk D. V., Ornev V. G.; claimer and owner of the patent Vinnytsia National Technical University – № u200705515; claimed 21.05.2007; published 25.09.2007, Bulletin № 15.
- [282] Useful model patent 26533 Ukraine IPC (2006) H 03 F 3/26. Push-pull symmetric current amplifier / Azarov O. D., Kusiuk D. V., Bogomolov S. V.; claimer and owner of the patent Vinnytsia National Technical University – № u200705532; claimed 21.05.2007; published 25.09.2007, Bulletin № 15.
- [283] Useful model patent 52763 Ukraine IPC (2009) H 03 K 5/22, G 05 B 1/00. Push-pull symmetric current amplifier / Azarov O. D., Bogomolov S. V., Rososhchuk A. V.; claimer and owner of the patent Vinnytsia

- National Technical University – № u201002043; claimed 25.02.2010; published 10.09.2010, Bulletin № 17.
- [284] Useful model patent 52769 Ukraine IPC (2006) H 03 K 5/22, G 05 B 1/00. Push-pull symmetric current amplifier / Azarov O. D., Bogomolov S. V., Sentiabov E. S.; claimer and owner of the patent Vinnytsia National Technical University – № u201002053; claimed 25.02.2010; published 10.09.2010, Bulletin № 17.
- [285] Useful model patent 63660 Ukraine IPC (2011.01) H 03 F 3/26 (2006.01), G 05 B 1/00. Push-pull symmetric current amplifier / Azarov O. D., Bogomolov S. V., Rososhchuk A. V.; claimer and owner of the patent Vinnytsia National Technical University – № u201106585; claimed 26.05.2011; published 10.10.2011, Bulletin № 19.
- [286] Useful model patent 63950 Ukraine IPC (2011.01) H 03 K 5/00, G 05 B 1/00. Push-pull symmetric current amplifier / Azarov O. D., Pavlov S. V., Kyrylenko D. O., Bogomolov S. V.; claimer and owner of the patent Vinnytsia National Technical University – № u201103782; claimed 29.03.2011; published 25.10.2011, Bulletin № 20.
- [287] Useful model patent 70122 Ukraine IPC H 03 K 5/24 (2006.01), G 05 B 1/01 (2006.01). Push-pull symmetric current amplifier / Azarov O. D., Bogomolov S. V., Jatsyk V. E.; claimer and owner of the patent Vinnytsia National Technical University – № u201113959; claimed 28.11.2011; published 25.05.2012, Bulletin № 10.
- [288] Useful model patent 70130 Ukraine IPC (2012.01) H 03 K 5/22 (2006.01), G 05 B 1/00. Push-pull symmetric current amplifier / Azarov O. D., Bogomolov S. V., Kyrylenko D. O., Steiskal V. Ja.; claimer and owner of the patent Vinnytsia National Technical University – № u201113980; claimed 28.11.2011; published 25.05.2012, Bulletin № 10.
- [289] Useful model patent 70321 Ukraine IPC H 03 F 3/26 (2006.01). Push-pull symmetric current amplifier / Azarov O. D., Bogomolov S. V., Rososhchuk A. V., Krupelnutskyi L. V.; claimer and owner of the patent Vinnytsia National Technical University – № u201112863; claimed 02.11.2011; published 11.06.2012, Bulletin № 11.
- [290] Bogomolov S. V. Linearity errors of the transfer characteristics of the complementary stage of the push-pull current amplifiers / O. D. Azarov, S. V. Bogomolov S. V. // XL. scientific-engineering conference of the teachers staff, researchers and students of the university with the

participation of the researchers of scientific with the participation of the researchers of scientific research institutions and engineering staff of enterprises of the Vinnytsia and Vinnytsia Region, March 9–11 : Proceedings.– Vinnytsia, 2010,–P. 26.

- [291] Useful model patent 21954 Ukraine IPC (2006) H 03 K 5/22. Buffer element // Azarov O. D., Bogomolov S. V., Garnaga V. A., Lukashchuk O. O., Reshetnic O. O.; claimer and owner of the patent Vinnytsia National Technical University – № u200611431; claimed 30.10.06; published 10.04.07, Bulletin № 4.
- [292] Useful model patent 49578 Ukraine IPC (2009) H 03 F 3/26. Buffer stage/ Azarov O. D., Khadzhanijazov I. K., Bogomolov S. V., Melnyk S. O.; claimer and owner of the patent Vinnytsia National Technical University – № u200912325; claimed 30.11.09; published 26.04.10, Bulletin № 8.
- [293] Useful model patent 21553 Ukraine IPC (2006) H 03 F 3/26. Buffer stage / Azarov O. D., Lukashchuk O. O., Bogomolov S. V.; claimer and owner of the patent Vinnytsia National Technical University – № u200610927 claimed 16.10.06; published 15.03.07, Bulletin № 3.
- [294] Useful model patent 22794 Ukraine IPC (2006) H 03 F 3/26. Buffer stage / Azarov O. D., Bogomolov S. V., Lukashchuk O. O., Krupelnutskyi L. V.; claimer and owner of the patent Vinnytsia National Technical University – № u200613722; claimed 25.12.06; published 25.04.07, Bulletin № 5.
- [295] Useful model patent 24882 Ukraine IPC (2006) H 03 F 3/26. Buffer stage / Azarov O. D., Bogomolov S. V., Lukashchuk O. O., Krupelnutskyi L. V., Tarasova O. M.; claimer and owner of the patent Vinnytsia National Technical University – № a200701203; claimed 05.02.07; published 25.07.07, Bulletin № 11.
- [296] Useful model patent 27750 Ukraine IPC (2006) H 03 F 3/26. Buffer stage / Azarov O. D., Bogomolov S. V., Krupelnutskyi L. V.; claimer and owner of the patent Vinnytsia National Technical University – № u200708022; claimed 16.07.07; published 12.11.07, Bulletin № 18.
- [297] Useful model patent 30183 Ukraine IPC (2006) H 03 F 3/26. Buffer stage / Azarov O. D., Bogomolov S. V., Krupelnutskyi L. V.; claimer and owner of the patent Vinnytsia National Technical University – № u200712818; claimed 19.11.07; published 11.02.08, Bulletin № 3.



- [298] Useful model patent 34470 Ukraine IPC (2006) H 03 F 3/26. Buffer stage / Azarov O. D., Bogomolov S. V., Krupelnutskyi L. V.; claimer and owner of the patent Vinnytsia National Technical University – № u200803626; claimed 21.03.08; published 11.08.08, Bulletin № 15.
- [299] Useful model patent 42148 Ukraine IPC (2009) H 03 K 5/22, G 05 B 1/00. Buffer stage / Azarov O. D., Bogomolov S. V., Krupelnutskyi L. V.; claimer and owner of the patent Vinnytsia National Technical University – № u200900502; claimed 23.01.09; published 25.06.09, Bulletin № 12.
- [300] Useful model patent 51224 Ukraine IPC (2009) H 03 K 5/22, G 05 B 1/00. Buffer stage / Azarov O. D., Dudnik O.V., Bogomolov S. V.; claimer and owner of the patent Vinnytsia National Technical University – № u200913561; claimed 25.12.09; published 12.07.10, Bulletin № 13.
- [301] Useful model patent 51345 Ukraine IPC (2009) H 03 F 3/26. Buffer stage / Azarov O. D., Khodzhanijazov I. K., Bogomolov S. V. Melnyk S. O.; claimer and owner of the patent Vinnytsia National Technical University – № u201001032; claimed 01.02.10; published 12.07.10, Bulletin № 13.
- [302] Useful model patent 51370 Ukraine IPC (2009) H 03 K 5/22. Buffer stage / Azarov O. D., Bogomolov S. V., Rososhchuk A. V.; claimer and owner of the patent Vinnytsia National Technical University – № u201001289; claimed 08.02.10; published 12.07.10, Bulletin № 13.
- [303] Useful model patent 51959 Ukraine IPC (2009) H 03 K 5/22, G 05 B 1/00. Buffer stage / Azarov O. D., Bogomolov S. V., Kyrilenko D. O.; claimer and owner of the patent Vinnytsia National Technical University – № u201000910; claimed 29.01.10; published 10.08.10, Bulletin № 15.
- [304] Useful model patent 52715 Ukraine IPC (2009) H 03 K 5/22, G 05 B 1/00. Buffer stage / Azarov O. D., Bogomolov S. V., Sentiabov E. S.; claimer and owner of the patent Vinnytsia National Technical University – № u201001301; claimed 08.02.10; published 10.09.10, Bulletin № 17.
- [305] Useful model patent 52716 Ukraine IPC (2009) H 03 F 3/26, G 05 B 1/00. Buffer stage / Azarov O. D., Bogomolov S. V., Sologub I. V.; claimer and owner of the patent Vinnytsia National Technical University – № u201001303; claimed 08.02.10; published 10.09.10, Bulletin № 17.
- [306] Useful model patent 57896 Ukraine IPC H 03 K 5/22 (2011.01). Buffer stage / Azarov O. D., Rososhchuk A. V., Bogomolov S. V.; claimer and owner of the patent Vinnytsia National Technical University – № u201014274; claimed 29.11.10; published 10.03.11, Bulletin № 5.

- [307] Useful model patent 59352 Ukraine IPC H 03 K 5/22 (2006.01). Buffer stage / Azarov O. D., Rososhchuk A. V., Bogomolov S. V.; claimer and owner of the patent Vinnytsia National Technical University – № u201013024; claimed 02.11.10; published 10.05.11, Bulletin № 9.
- [308] Useful model patent 59353 Ukraine IPC H 03 K 5/22 (2006.01). Buffer stage / Azarov O. D., Rososhchuk A. V., Bogomolov S. V.; claimer and owner of the patent Vinnytsia National Technical University – № u201013025; claimed 02.11.10; published 10.05.11, Bulletin № 9.
- [309] Useful model patent 92963 Ukraine IPC (2009) H 03 F 3/34. Buffer stage / Azarov O. D., Bogomolov S. V.; claimer and owner of the patent Vinnytsia National Technical University – № a200903013; claimed 30.03.09; published 27.12.10, Bulletin № 24.
- [310] Useful model patent 24003 Ukraine IPC (2006) H 03 K 5/22, G 05 B 1/00. Input device of the currents comparison circuit / Azarov O. D., Bogomolov S. V., Lukashcuk O. O., Krupelnytskyi L. V.; claimer and owner of the patent Vinnytsia National Technical University – № u200702068; claimed 26.02.2007; published 11.06.2007, Bulletin № 8.
- [311] Useful model patent 19379 Ukraine IPC (2006) H 03 K 5/22, G 05 B 1/00. Input device of the currents comparison circuit / Azarov O. D., Lukashcuk O. O., Zakharchenko S. M., Bogomolov S. V., Tarasova O. M.; claimer and owner of the patent Vinnytsia National Technical University – № u200606595; claimed 13.06.2006; published 15.12.2006, Bulletin № 12.
- [312] Useful model patent 20246 Ukraine IPC (2006) H 03 K 5/00, G 05 B 1/00. Input device of the currents comparison circuit / Azarov O. D., Lukashcuk O. O., Bogomolov S. V., Garnaga V. A., Reshetnik O. O.; claimer and owner of the patent Vinnytsia National Technical University – № u200607987; claimed 17.07.2006; published 15.01.2007, Bulletin № 1.
- [313] Useful model patent 25471 Ukraine IPC (2006) H 03 K 5/22, G 05 B 1/00. Input device of the currents comparison circuit / Azarov O. D., Kaduk O. V., Bogomolov S. V., Garnaga V. A., Reshetnik O. O.; claimer and owner of the patent Vinnytsia National Technical University – № u200703563; claimed 02.04.2007; published 10.08.2007, Bulletin № 12.
- [314] Useful model patent 27019 Ukraine IPC (2006) H 03 K 5/00, G 05 B 1/00. Input device of the currents comparison circuit / Azarov O. D.,

- Bogomolov S. V., Krupelnutskyi L. V.; claimer and owner of the patent Vinnytsia National Technical University – № u200706811; claimed 18.06.2007; published 10.10.2007, Bulletin № 16.
- [315] Useful model patent 28375 Ukraine IPC (2006), G 05 B 1/00, H 03 K 5/22. Input device of the currents comparison circuit / Azarov O. D., Bogomolov S. V., Krupelnutskyi L. V., Garnaga V. A., Reshetnik O. O.; claimer and owner of the patent Vinnytsia National Technical University – № u200707425; claimed 02.07.2007; published 10.12.2007, Bulletin № 20.
- [316] Useful model patent 53517 Ukraine IPC (2009) H 03 K 5/22, G 05 B 1/00. Input device of the currents comparison circuit / Azarov O. D., Bogomolov S. V., Krupelnutskyi L. V.; claimer and owner of the patent Vinnytsia National Technical University – № u201003926; claimed 06.04.2010; published 11.10.2010, Bulletin № 19.
- [317] Wójcik, W., Pavlov, S., Kalimoldayev, M. (2019). Information Technology in Medical Diagnostics II. London: Taylor & Francis Group, CRC Press, Balkema book. – 336 Pages, <https://doi.org/10.1201/9780429057618>, eBook ISBN 9780429057618.
- [318] Pavlov S. V. Information Technology in Medical Diagnostics //Waldemar Wójcik, Andrzej Smolarz, July 11, 2017 by CRC Press - 210 Pages. <https://doi.org/10.1201/9781315098050>, eBook ISBN 9781315098050.
- [319] Pavlov Sergii, Avrunin Oleg, Hrushko Oleksandr, and etc. System of three-dimensional human face images formation for plastic and reconstructive medicine // Teaching and subjects on bio-medical engineering Approaches and experiences from the BIOART-project Peter Arras and David Luengo (Eds.), 2021, Corresponding authors, Peter Arras and David Luengo. Printed by Acco cv, Leuven (Belgium). - 22 P. ISBN: 978-94-641-4245-7.
- [320] Kukharchuk, Vasyl V., Sergii V. Pavlov, Volodymyr S. Holodiuk, Valery E. Kryvonosov, Krzysztof Skorupski, Assel Mussabekova, and Gaini Karnakova. 2022. "Information Conversion in Measuring Channels with Optoelectronic Sensors" *Sensors* 22, no. 1: 271. <https://doi.org/10.3390/s22010271>
- [321] Avrunin, O.G.; Nosova, Y.V.; Pavlov, S.V.; Shushliapina, N.O.; and etc. Research Active Posterior Rhinomanometry Tomography Method for Nasal Breathing Determining Violations. *Sensors* **2021**, *21*, 8508. doi: 10.3390/s21248508, <https://www.mdpi.com/1424-8220/21/24/8508>
- [322] Avrunin, O.G.; Nosova, Y.V.; Pavlov, S.V.; and etc. Possibilities of Automated Diagnostics of Odontogenic Sinusitis According to the

- Computer Tomography Data. *Sensors* 2021, 21, 1198.  
<https://doi.org/10.3390/s21041198> (Q2).
- [323] Vasyl V. Kukharchuk, Sergii V. Pavlov, Samoil Sh. Katsyv, and etc. “Transient analysis in 1st order electrical circuits in violation of commutation laws”, *PRZEGLĄD ELEKTROTECHNICZNY*, ISSN 0033-2097, R. 97 NR 9/2021, p. 26-29, doi:10.15199/48.2021.09.05 (Q3)